

Doctoral Thesis

Engineering Geological Appraisal of Tendaho Dam Project, Tectonics & Risk; Afar Depression, NE Ethiopia

Author:

Nehemia Solomon BEYENE

Reviewers:

Franz-Josef BROSCH, *Ao. Univ.-Prof., Dr. phil*

Institute of Applied Geosciences, Graz University of Technology, Austria

Walter KURZ, *Univ.-Prof., Mag.rer.nat., Dr.rer.nat.*

Institute of Earth Sciences, University of Graz, Austria



Graz University of Technology

Institute of Applied Geosciences

Graz, December 2009

Acknowledgements

I would like to thank God who made possible for me to begin and finish this work successfully.

I do not have adequate words to express my feelings of gratitude to Prof. Kurt Klima whose kind guidance and constant encouragement during the present study could help me to complete my work. He is the person who has always helped me. His constant encouragement made me strong enough to face every ups and down with confidence. So, I express my feeling of profound gratitude to him.

I would like to express my sincere gratitude to Prof. Franz-Josef Brosch, Institute of Applied Geosciences, Graz University of Technology and Prof. Walter Kurz, Institute of Earth Sciences, University of Graz for reviewing the Thesis, constructive comments, suggestions and helping me to give the final shape of the Thesis.

I am grateful to Prof. Martin Dietzel and Prof. Scott Kieffer, Institute of Applied Geosciences, Graz University of Technology and members of the Institute for their help, encouragement and cooperation which gave me the strength for carrying out the research.

I also would like to extend my gratitude to Prof. Aberra Mogessie, Institute of Earth Sciences, University of Graz for his constant support, encouragement and sharing ideas. I have special thanks to Dr. Tarun K. Raghuvanshi, Department of Earth Sciences, Addis Ababa University for reviewing the Thesis, comments, constant encouragement, and unconditional friendship.

Great thanks to Mr. Gerald Pischner, a PhD candidate who assisted me for the fielding mapping of tectonic features in the Afar Depression; Dr. Christina Latal helped me how to use the thin section laboratory; Mr. Gerald Lauk prepared the rock samples for thin section analysis; Dr. Stephan Köhler, Mr. Peter Schriben, and Mrs. Anna Pendle, for their constant encouragement and support which helped me during the course of this work.

I am thankful to the following institutions: Austrian Development Cooperation – North South Dialogue Scholarship Program (ÖAD) for providing me full scholarship; Department of Earth Sciences - Addis Ababa University, my home institution; Ethiopian Ministry of Water Resources, Afar Regional Government and Tendaho Dam and Irrigation Project Authorities.

I have special thanks to my friends, Engdawork Mulatu (Engdu) Hailu Zenebe (Ajaju), Tewodros Teklu (Teddy-Graz), Sara Asefa (Azeb), Medhanye Beidebirhan (Meda), Tewodros Alemayehu (Teddy), Tigist Teame (Titi), Henok Gidey, Felimon Megerssa and many others for their constant encouragement and help.

Special thanks to Dr. Abraham Abebe and Sara G/Medhin family for their constant encouragement.

Especially, I express my feeling of deep gratitude to my wife Bitiya Ali Yesuf (Biti), for her constant encouragement and caring support. She is my sweetie!

Declaration

I hereby declare that the Doctoral Thesis, entitled “Engineering Geological Appraisal of Tendaho Dam Project, Tectonics & Risk; Afar Depression, NE Ethiopia”, represents my own work. To the best of my knowledge and belief, it contains neither material previously published or written by another person nor material which has been previously submitted for the award of any other degree, diploma or other qualification of the university or other institute of higher learning, except where due acknowledgements has been made in the text.

Signature:

Name: Nehemia Solomon BEYENE

Date: December 2009

Place: Graz, Austria

Abstract

The Tendaho Dam and Irrigation project is located, 570 Km NE of Addis Ababa, in the center of Afar Depression where the Main Ethiopian Rift (MER), the Red Sea Rift and the Gulf of Aden Rift join at the extensional triple junction. As per the project plan, 90,000 hectare of land will be irrigated with the proposed 1.8 billion m³ reservoir capacity of the Tendaho reservoir.

The main objective of the present study was to study the tectonic situation and associated risk to Tendaho Dam and Irrigation project. In order to understand the tectonic situation of the area interpretation of remote sensing and DEM datasets, and field mapping of tectonic features were undertaken. The study showed the Gesye Graben was formed during the propagation of the Main Ethiopian Rift structures towards the Afar Depression. Later on the Graben was bisected by the magmatic dyke intrusion at the center and crosscut by the NW-SE trending Red Sea Rift propagation structures. Further, scan line mapping of the lacustrine deposit, about 1.5 Km E of the Tendaho dam axis, indicates the spreading of the Tendaho Graben in the 1 – 12k.a. with NE-SW extension direction.

Furthermore, the rifting hazards were estimated based on published tectonic model of the area, seismological records, field mapping of historical evidences and the recent formation of the Dabbahu, 2005 and Karbahri, 2007 rifting episodes. Three assumptions were considered for the prediction of potential occurrence of the active rifting hazards in the Tendaho Graben. Based on these assumptions Tendaho Graben (50 - 60km wide) was opened by the Manda Hararo and Tendaho rifting (i) with a constant spreading rate; (ii) with a number of violent rifting episodes and magma injection; and (iii) with both events alternatively. Based on the above assumptions, the average potential occurrence of the active rifting hazards during the lifetime of the schemes were estimated as 0.6 and 1.8% from the Manda Hararo and Tendaho rifts, respectively. If the rifting is supplied with sufficient magmatic injection, the horizontal and vertical ground deformation along the rifting axis may reach up to 15 – 20km buffer zone.

Ten parameters were considered for the risk assessment of the tectonic structures related to the reservoir leakage are; Tectonic Parameters – tectonic status T_s , tectonic regime T_{rr} , tectonic history T_h , aerial extent of the structure Ex , cross cut index Cci ; and External Parameters – hydrogeology G , proximity P , relative position P_s , Elevation difference Ed and hydraulic pressure Hp . Semi-quantitative approaches of simple averaging AVE, pairwise comparison PWC and analytic hierarchy process AHP were applied to analyze the risk level of the tectonic structures. Study showed that tectonic structures, which are very close to the proposed reservoir, formed by the extensional tectonic activities, larger aerial extent and cross cut termination index have potential high risk to the reservoir leakage. The overall risk for reservoir leakage for worst and modest scenarios is estimated to be $25.4m^3/s$ and $2.4m^3/s$, respectively.

Key words: Tectonics, Risk, Afar Depression, Tendaho Graben, Active rifting, Ethiopia

Kurzfassung

Das Tendaho Bewässerungsprojekt mit dem Tendaho Damm liegt ca. 570 km nordöstlich von Addis Ababa im Zentrum der Afar - Depression, wo das Main Ethiopian Rift (MER), das Red Sea Rift und das Gulf of Aden Rift einen Tripelpunkt bilden. Nach den Projektplänen ist vorgesehen, aus dem 1,8 Mio m³ großen Speicher eine Fläche von 90.000 zu bewässern.

Ziel der Arbeit ist, die tektonische Situation im Projektbereich und die damit verbundenen Risiken für das Projekt zu untersuchen. Zur Klärung der Tektonik wurden Satelliten und Luftbildauswertungen sowie eine geologische Kartierung im Gelände durchgeführt. Als Ergebnis dieser Arbeiten zeigt sich, dass sich der Gesye Graben während des Fortschreitens der MER-Strukturen in Richtung der Afar-Depression entwickelte. Später wurde der Graben durch eine zentrale Dyke-Intrusion geteilt und von NW-SE streichenden Strukturen des fortschreitenden Red Sea Rifts durchschnitten. Durch Scan-line mapping in den etwa 1,5 km östlich des Tendaho - Dammes liegenden lakustrinen Sedimenten wurden Hinweise auf das NE-SW Spreading des Tendaho Grabens vor 12.000 bis 1.000 Jahren gefunden.

Die Gefahr für das Projekt durch aktives Rifting wurde auf Basis des tektonischen Modells unter Verwendung von seismischen Daten, Kartierung von historischen Ereignissen und den rezenten Riftingepisoden von Dabbahu (2005) und Karbahri (2007) abgeschätzt. Zur Abschätzung einer Gefahr durch aktives Rifting im Tendaho-Graben wurden drei Annahmen getroffen: (1) Der 50 – 60 km breite Graben öffnete sich durch das Manda Hararo und das Tendaho Rifting; (2) Die Spreading-Rate war konstant, es kam zu einzelnen heftigen Rifting-Episoden mit Magmenaktivität; (3) Zeiten hoher Aktivität und geringer Aktivität wechselten einander ab. Aufgrund dieser Annahmen wird das Potential für das Eintreten eines aktiven Rifting - Ereignisses in der Lebenszeit des Bewässerungsprojektes mit 0,6% für das Manda Hararo und 1,8% für das Tendaho Rift ermittelt. Wenn das Rifting mit nennenswerten Magmaaktivitäten einhergeht, kann die horizontale und vertikale Bodendeformation entlang der Rifting Achse eine 15 – 20 km breite Zone betreffen.

Zur Ermittlung des Risikos einer Umläufigkeit des Speichers durch tektonische Strukturen wurden zehn Parameter herangezogen: Der tektonische Status (Ts), das tektonische Regim (Trr), die tektonische Vorgeschichte (Th), Ausdehnung einer Struktur (Ex), Veschneidungsindex (Cci), Hydrogeologie (G), Abstand (P), relative Position (Ps), Höhendifferenz (Ed) und hydraulischer Druck (Hp). Folgende Methoden wurden zur Abschätzung des Risikos durch tektonische Strukturen angewandt: Semiquantitative einfache Mittelwertbildung (AVE), Paarweiser Vergleich (PWC) und Analytischer Hirarchischer Prozess (AHP). Es zeigt sich, dass tektonische Strukturen die nahe dem Speicher liegen, die durch Dehnungsvorgänge gebildet wurden, eine große Ausdehnung haben und häufig geschnitten werden, ein hohes Potential für Umläufigkeit haben. Die Höhe möglicher Wasserverluste aus dem Speicher wurde für ein ungünstiges Szenario mit $25,4 \text{ m}^3/\text{s}$ und für ein mittleres Szenario mit $2,4 \text{ m}^3/\text{s}$ ermittelt.

Schlagwörter: Tektonische, Risikos, Afar Depression, Tendaho Graben, Aktive rifting, Äthiopien

Dedications

To my wife, Bitiya Ali YESUF (Biti), it would have been impossible to complete the work without your love and support.

To my father, Solomon Beyene

To my mother, Terefech Ayana

Table of Contents

1	Introduction.....	1
1.1	Preamble.....	1
1.2	Tendaho dam and irrigation site.....	4
1.3	Research Objectives	5
1.4	Research Methodologies	6
1.4.1	<i>Literature Reviews.....</i>	6
1.4.2	<i>Field studies.....</i>	7
1.4.3	<i>Data Analysis and Interpretation</i>	7
1.5	Significance of study.....	8
1.6	Thesis Outline/structure	9
2	Literature Review	10
2.1	Introduction	10
2.2	The Afar Depression	10
2.2.1	<i>Geological and Tectonic Settings.....</i>	11
2.2.2	<i>Seismicity and Recent Tectonic Activities.....</i>	13
2.2.3	<i>Tendaho Graben.....</i>	15
2.3	Risk Assessment.....	16
2.3.1	<i>Risk Assessment of Natural Hazards.....</i>	17
2.3.2	<i>Geological Risk Assessment</i>	18
3	Interpretation of Remote sensing and DEM for Geological Mapping	20
3.1	Introduction	20
3.2	Remote sensing data and methods	21
3.2.1	<i>Aerial Photograph.....</i>	22
3.2.2	<i>Landsat ETM+.....</i>	22
3.2.3	<i>SRTM (Shuttle Radar Topography Mission)</i>	23
3.2.4	<i>TIN (Triangular Irregular Network)</i>	23
3.3	Result.....	24
3.3.1	<i>Gayderu Ridge.....</i>	24
3.3.2	<i>Gesye Plain.....</i>	27
3.3.3	<i>Megenta Ridge.....</i>	27
3.3.4	<i>Tendaho Graben.....</i>	28
3.4	Discussion	29
4	Tectonic Structures of Gesye and part of Tendaho Graben	33
4.1	Introduction	33
4.2	Geology	33
4.3	Structural settings.....	36
4.3.1	<i>West of the Proposed Tendaho Reservoir.....</i>	36
4.3.2	<i>Within the Proposed Tendaho Reservoir and at the dam axis.....</i>	37
4.3.3	<i>East of the Proposed Tendaho Reservoir</i>	40

4.3.4	<i>Irrigation Canal & Manda Hararo Rift Segment</i>	41
4.4	Result.....	44
4.4.1	<i>Gesye Graben</i>	44
4.4.2	<i>Tendaho Graben</i>	48
4.5	Discussion	51
5	Active Rifting Hazards	54
5.1	Introduction	54
5.2	Assumptions of Rift Development.....	56
5.2.1	<i>Constant Spreading Rate</i>	57
5.2.2	<i>Violent Rifting Episodes</i>	58
5.2.3	<i>Both Assumptions Alternatively</i>	59
5.3	Hazard Analysis	60
5.4	Interpretation	63
6	Risk Assessment of Tectonic Structures - Related to Reservoir Leakage	65
6.1	Introduction	65
6.2	Risk Parameters.....	66
6.2.1	<i>Tectonic Parameters</i>	66
6.2.2	<i>External Parameters</i>	69
6.3	Risk Analysis	70
6.3.1	<i>Simple weighting (Average)</i>	73
6.3.2	<i>AHP – Analytical Hierarical Process</i>	77
6.3.3	<i>PWC – Pairwise Comparison</i>	81
6.4	Risk Estimation	83
6.5	Discussion	88
7	Conclusion	90
7.1	Conclusion.....	90
7.2	Future research direction.....	91
8	References	93
9	List of Figures	104
10	List of Tables	108
11	Appendices	i
11.1	Appendix A	i
11.2	Appendix B	xiii
11.3	Appendix C	xxvi

Chapter One

Introduction

1.1 Preamble

The need of engineering geological involvements in day to day life enormously increases as the scope of the discipline has widened to environmental problems in addition to the traditional engineering geology which deals with ‘the application of geology in construction practice’ (Paige, 1950). The International Association for Engineering Geology and the Environment (IAGE, 2000) define the disciplinary as *“a science devoted to the investigation, study and solution of engineering and environmental problems which may arise as the result of the interaction between geology and the works or activities of man, as well as the prediction and development of measures for the prevention or remediation of geological hazards”*.

Even though the environmental problems like natural and anthropogenic hazards are started to be addressed by engineering geological field too, there are a number of issues/limitations which still need further scientific efforts to the application of geology in engineering work. The known Engineering Geologist, Evert Hoek, 1999 said *“assigning numbers to geology requires a delicate balance between the commonly held opinion that geology cannot be quantified and the overoptimistic view that every physical quantity can be described in precise mathematical terms. In reality, many geological characteristics cannot be quantified precisely and intelligent guesses based upon experience and logical arguments are the best that can be hoped for”*.

The difficulties of ‘putting numbers to geology’ come from the heterogeneity of the geology structures and the dynamics of environmental parameters. The heterogeneity of the geology

and the environment depend on the past and current geological conditions of the given area, respectively (Knill, 2003). In 1970's, Knill and Price expressed the engineering behaviour of the ground by three verbal equations (Price, 2009):-

Material properties + mass fabric = mass properties

Mass properties + environment = the engineering geological situation

The engineering geological situation + changes produced by the engineering work = the engineering behaviour of the ground

Fig 1.1 illustrates the simplified verbal equations of the engineering behaviour of the ground (Price, 2009) with the consideration of tectonic structures and activities as past and ongoing geological conditions for two types of engineering works (tunnel and reservoir). If the engineering properties of the tectonic structures (mass fabric) and its activities (environmental – dynamic load) are not considered at the feasibility stage of the project, the risk of failure of the engineering work increases as shown in the figure. Brittle tectonic deformations have significant influences on the civil engineering structures that can be considered as a problem (hydrogeological, residual stress and geotechnical weakness).

Geological conditions are the main challenges for large scale engineering works within and nearby the Main Ethiopian Rift system. To mention some: the 26 Km tunnel construction of Gilgel Gibe II hydropower project, SW Ethiopia, delayed by more than two years from its time schedule because of unforeseen geological conditions (tectonic structures and weathering effect) during the feasibility stages (EEPCO, 2004 and 2007). Koka reservoir which is located within the Main Ethiopian Rift (MER) system faced leakage problems through the normal fault at the right side of the reservoir (Mamo and Yokota, 1998). The Kesem – Kebena dam and irrigation project is being constructed in the same area, MER. According to the design, the dam axis is located near to the normal fault. MacDonald, 1987 and Halcrow 1989 discussed the presence of high pressure artesian hot spring under the dam foundation and how difficult will be to confront with nature. During the grouting stage of the dam abutments and river bed, the contractors were not able to grout the dam foundation to prevent excessive water leakage.

Uncertainties in ground engineering are common because of the high diversity of geological processes which are responsible for the current geological situation of one particular area. It is not possible for the engineering geologist to come up with 100% certainties about the

ground and its respond to the engineering induced load. But advanced and excellent knowledge of the geological processes/conditions in the past and present and the ability or capability of a person to develop a better geological model (physical, numerical, conceptual or other), could drag the required certainties level/percentage to reliability (Knill, 2003; Bock, 2006).

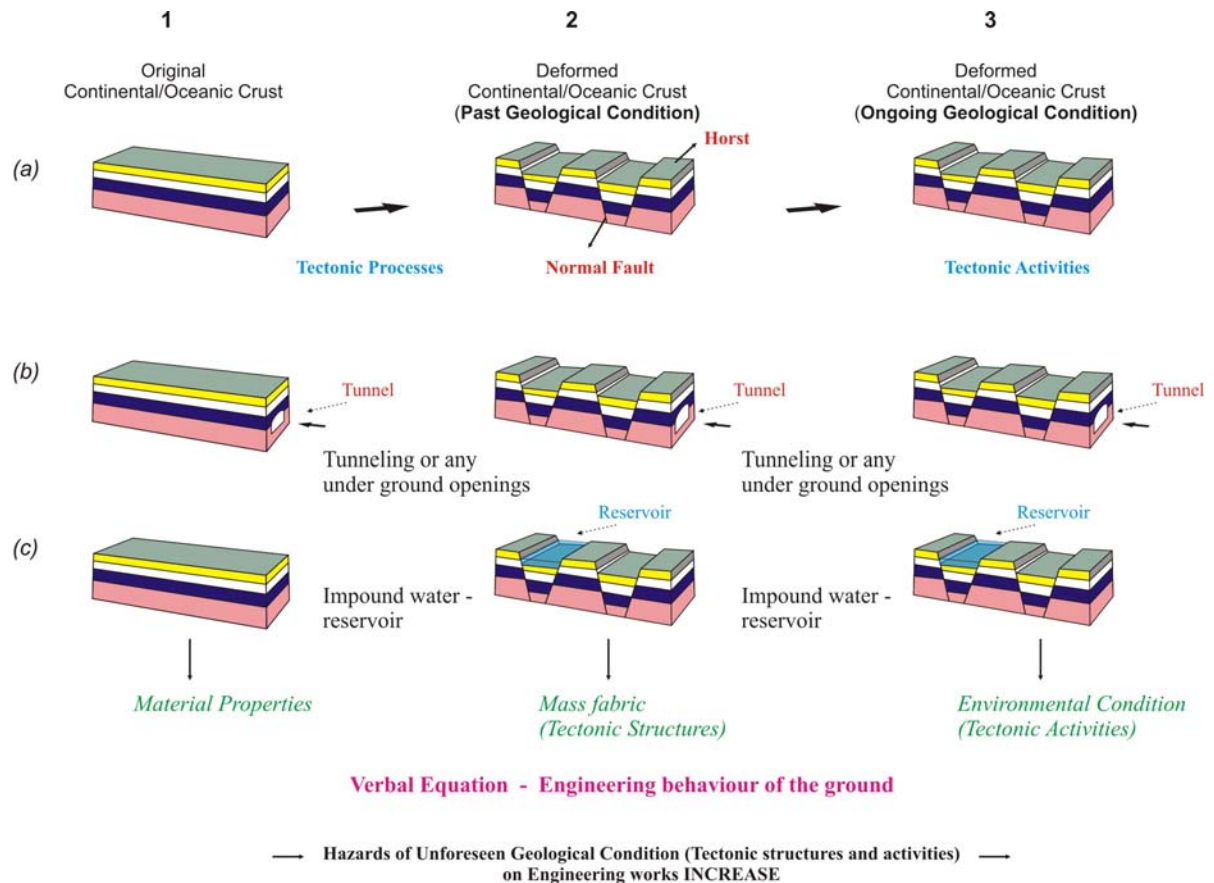


Fig 1.1: Schematic illustration for verbal equation of *engineering geological behaviors of the ground* (Price, 2009): (a) Stages of tectonic processes 1 - 3 (b) & (c) tunneling and reservoir impoundment through different tectonic conditions, respectively. The graben drawing is taken from USGS.

The so called ‘reliability and/or certainty’ of ground engineering can be achieved based on a quality investigation of data collection, analysis or interpretation. Quality investigation can be a measure of assessment in terms of its geotechnical relevancy, statistically representative, state of the art, economically accessibility and transparency, decisiveness and meaningfulness. So, well organized engineering geological investigations will lead for the better achievement of certainty in addition to the above aspects.

According to the International Institute for Geo-Information Science and Earth Observatory (ITC-Netherlands, 2009), risk is defined as “*the expected losses as a result of potentially damaging phenomena within a given time period, and within a given area. It can be*

analyzed by assessing three major components: the probability of the event with a certain magnitude, the vulnerability of the elements at risk (building stock, lifelines, critical facilities, population, and economic activities) exposed to the event with a certain magnitude and the amount or costs of these elements at risk”.

However, risk is not only generated from some source of hazard event/phenomena but poor engineering geological investigation of geological conditions (*unforeseen*) may induce unexpected risk on human and/or property.

1.2 Tendaho Dam and Irrigation Site

The study site is located in the Afar Depression, Afar Regional State, NE Ethiopia (**Fig 1.4**). It is 570km NE from the capital city, Addis Ababa and accessible through Addis Ababa – Samara asphalt road; The area is defined by co-ordinates 700000 - 730000E and 1260000 - 1312000N, UTM Zone 37. Low land, hot climatic conditions, no vegetation cover, active geological processes and nomad’s life are typical expression of the area.

The “Tendaho Dam” is a very important dam, as it forms a part of “Tendaho Dam and Irrigation Project”, which aims to harness the inflow of river Awash and provide irrigation to sugar cane plantation covering a total area of 90,000 hectares. The irrigation through Tendaho Dam project will facilitate a high yield of sugar cane in the area and a total production of about more than 500,000 tone of sugar per annum (WWDSE-WPCS (I), 2005). The success of this project will entirely depends on its safe functioning and to meet out the irrigation needs of the command area.

In the late 1960’s, feasibility studies of the Tendaho Dam and Irrigation project started by Sogreah – FAO (1965) with a special support from Imperial Haile Silase administration. Before the ‘Water Works Design & Supervision Enterprise’ in association with Water & Power Consultancy Service India Ltd, (2005) finalized the current detail project design, three other organizations investigated and studied the feasibility and detail design of the project, namely; Gibbs (1975), UZBEK (1985) and Haldrow (1989). All investigations/studies are focused on the dam foundation, construction materials of the embankment and the command area. However, recently during 2007 investigations on reservoir leakage potential were carried out by an Italian company (Studio Petran Gelli, 2007).

1.3 Research Objectives

Tendaho dam and irrigation project has numbers of gaps in the ground engineering aspect which needs a further and detail investigation tasks to avoid any unpredicted risk in terms of time and money in addition to the unforeseeable natural hazards risk. The present research area motivates to study ‘how hazardous or risk-full are the tectonics structures and activities for manmade structures which were formed in the past and severely weakened the geo-material’.

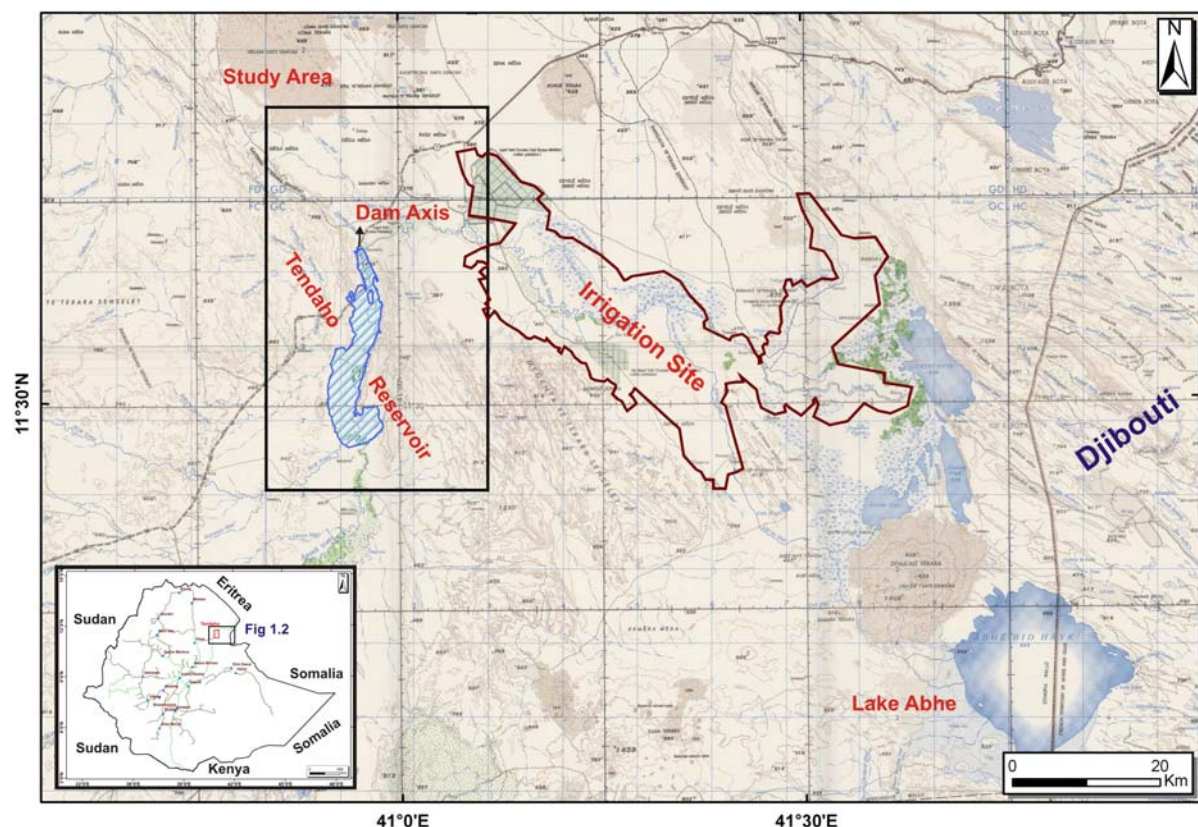


Fig 1.2: Location map of Tendaho reservoir and irrigation site (the base map is clipped from 1:250,000 scale Serdo NC 37-4, 1972 topographic map).

Long, 1974 published a paper entitled “Seismicity investigations at dam sites”. In this paper, he presented the Tendaho dam project as case study and predicted the seismicity risk based on the 1969 Serdo earthquake and the tectonic activities of the Afar depression. In another paper, Lane, 1974 discussed the problem of reservoir induced seismicity of the project and recommended further studies. The active geological processes and a construction of a dam along Awash River attract engineering geologist too to study the risk of existing tectonic structure effects on water tightness of the reservoir and tectonic activities. It is an ideal place

to spend time and resource for the upgrading of knowledge on tectonic processes and civil structure relation in addition to other adverse geological processes (hazards/phenomena).

A. Main objectives

- To understand the tectonic situation and,
- To assess the tectonic related risk at the Tendaho reservoir and irrigation site

B. Specific Objectives

- To develop Tectonic model of the area,
- To assess active rifting hazard,
- To assess risk of tectonic structures (*unforeseen geological condition during the feasibility stage*) related to reservoir seepage.

1.4 Research Methodologies

In order to achieve the above-mentioned objectives the following systematic methodology (**Fig. 1.3**) has been adopted;

1.4.1 Literature review

In order to learn from the previous research results and acquire the state of the art in brittle tectonics and geological and related risk assessments, literatures were reviewed. It helped the research to formulate and bound the scope of the contribution to the scientific realm within a limited and tight time table. The main objectives of the literature reviews in the present study were as follow:

- To develop a clear engineering geological research methodology which is required in the entire work progress,
- To understand the regional geological and tectonic setting of Afar depression, its past and present geological processes and zones of active tectonics,
- To learn about the basics and advanced research finding in the brittle tectonics subject,
- To grasp the recent state of the art approaches in natural (geohazards) and anthropogenic hazards and geological risk assessment.

1.4.2 Field Studies

With the objectives of understanding the tectonic situation of the Tendaho reservoir and its vicinity; and their unexpected risks, the study area was visited two times for a total of four and half months; **1st** March 23, 2007 – July 3, 2007 and **2nd** March 21, 2008 – May 06, 2008. During these times data related to the objectives were collected systematically with a consideration of basic principles of geological mapping and engineering geological field data collection. **Fig 1.4** shows the time break down of the major field activities.

Limitations on time and resources, harsh climatic conditions, poor accessibilities to area of interest and restriction of freedom to work alone were the main challenges encounter during the field study program for the present research study. However, continuous dedicated efforts resulted into reliable and sufficient data/information which made it possible to achieve the proposed objectives of the present study.

1.4.3 Data Analysis and Interpretation

Analysis and interpretation of field, remote sensing, DEM and published data were conducted in GIS, thin section and water chemistry tests were conducted in Lab of the Institute of Applied Geosciences, Graz, Austria and partly at the petrography Lab of the Department of Earth Sciences, Addis Ababa University, Ethiopia. Free to use and download ETH+ Land-Sat 7 satellite image with 9 bands including the panchromatic image of P168 R052 were clipped with a boundary of interest area and pre-processed before the first field visit to Afar Depression. Tectonic features which were collected during the first and second field visit to the study area were analyzed with the help of available software and interpreted for the development of tectonic/geological modeling of Tendaho reservoir and its vicinity. Petrography data analysis (thin section) of different rock samples, joint filling and spring water examination for possible mineral precipitations contribute reasonable information for the development of the model. Mainly, ArcGIS 9.1 with full extension package, ERDAS 8.6, AutoCAD Map 2000, AutoCAD 2006 – 08, Mathematica 6.1 and Tectonics FP software were used for the analysis of remote sensing, tectonics data and risk assessment of brittle tectonic structures – related to reservoir leakage. Finally, all the analyzed data were organized and entered into the ArcGIS database system for the assessment of tectonic related risk.

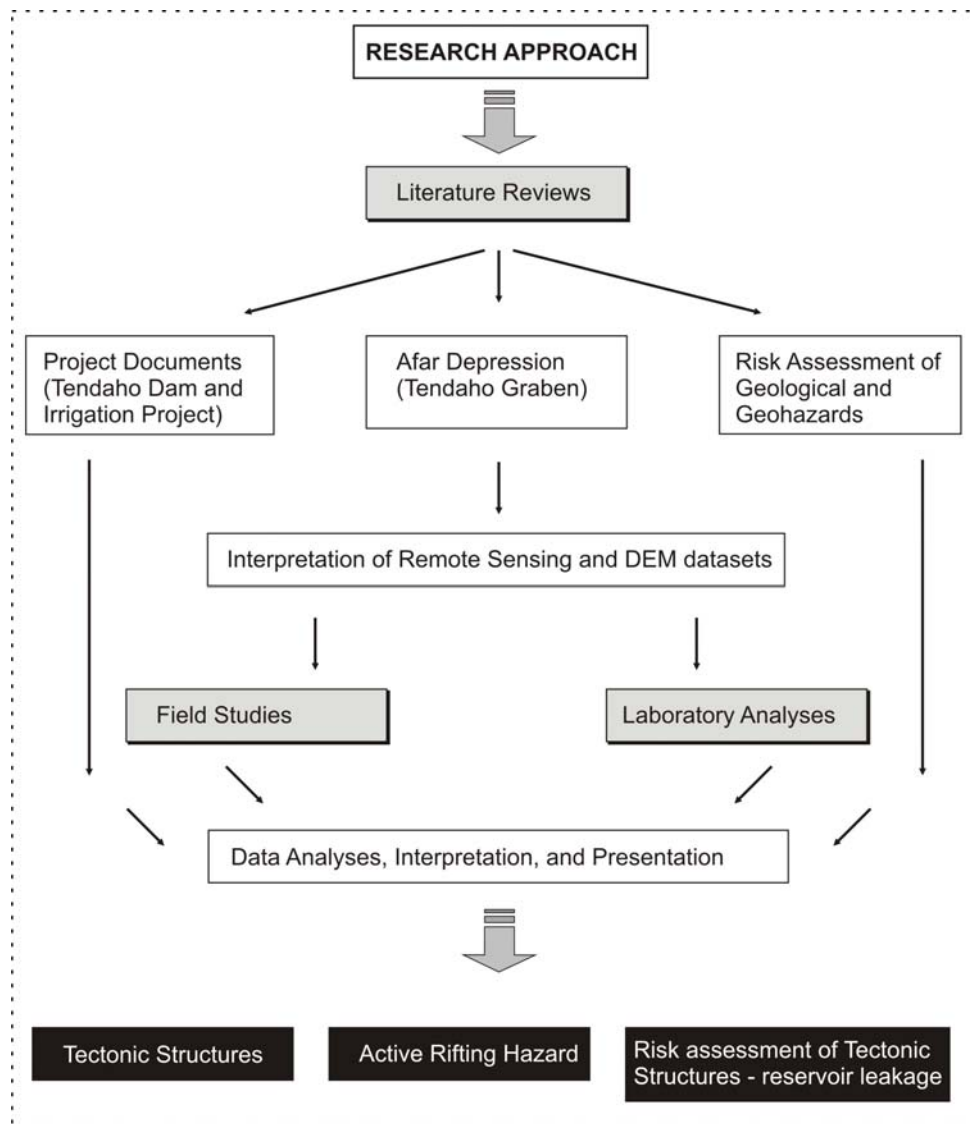


Fig 1.3: Flow Chart of adopted research methodology.

1.5 Significance of study

In the coming years, the government and private agencies have planned many development projects such as; dam, irrigation, road and building within the main Ethiopian rift system. The present study may help the decision makers and professional to deal with such geological hazardous conditions/ situations. The study may also be used to assess the feasibility condition of a particular engineering project with some modification for example; reservoir water tightness. Moreover, related to the new understanding of the tectonic situation of the present study area, the later researchers may adopt the similar methodology for similar projects elsewhere.



Fig 1.4: The first 'a' and second 'b' field visit to Afar Depression, NE Ethiopia.

1.6 Chapter outline/structure

Chapter 1: Introduction, research objectives, methodology and description of the study area,

Chapter 2: Literatures were reviewed on topics related to regional geological and tectonic settings of the Afar depression; and state of the art of natural hazards (geohazards) and geological risk assessment,

Chapter 3: Integration of satellite, aerial photography, SRTM and TIN datasets for the lithological and structural mapping of the Tendaho reservoir and its vicinity,

Chapter 4: Extensional tectonic features which were collected and documented from the field; and laboratory analysis of rocks, filling materials and water samples helped to understand the tectonic situation of the Tendaho reservoir and its vicinity,

Chapter 5: Assessment of probable occurrence of active rifting hazard within the life time of Tendaho dam and irrigation schemes,

Chapter 6: Risk assessment of tectonic structures related to reservoir leakage has been discussed in this chapter with a consideration of proximity, tectonic regime, aerial extent, dip direction, termination index, tectonic status, previous tectonic history, geology, relative position and hydraulic pressure as key risk parameters,

Chapter 7: Summarizes the conclusions drawn from this research and outlines future directions.

Chapter Two

Literature Review

2.1 Introduction

With the objective of learning from the previous research results and to acquire the state of the art about the risk assessment of geohazards, published and unpublished literatures were reviewed. Under this chapter, mainly two topics will be discussed; the Afar Depression and Risk Assessment. Other related literatures will be raised adjoining with the topics of the chapters. Geological & tectonic settings, seismicity & recent tectonic activities and the Tendaho graben are the sub topics which are covered in the topic of the Afar Depression. Further, risk assessment of natural hazards and geological risk assessments are the parts of the risk assessment literature review.

2.2 The Afar Depression

The Afar depression has a total of 200,000 km² area span (Beyene & Abdelsalam, 2005) and surrounded by western plateau of the Ethiopian highland in the west and south; southeastern or the Somalian plateau in the southeast; Red Sea in the northeast and the Gulf of Aden in the east (Kazmir, 1973; Abbate, 1995; Tesfaye et al., 2003). It is one of the broadly classified major physiographical regions of Ethiopia and known as low land and its hot climatic condition (Tefera, 1996; see **Fig 2.1**). The lowest elevation in the depression is found at Dallol with 127 m below sea level and the adjoining plateaus rise greater than 1500 meter above sea levels (Thurmond, 2006). The current physiographical settings are gained as result of subsequent tectonic processes including rifting, faulting, cracking or ground opening, volcanic eruption and magma injection along the opened rifts axis.

2.2.1 Geological and Tectonic Settings

According to (Reference), the depression has six major tectonics elements namely; the Danakil block, the Ali – Sabieh block, the East – Central block (ECB), the Manda Hararo – Gobbad rift, the Asal – Manda Inakle rift and the Sabure Hartale Adado rift. Due to a far field stress exerted as a result of the Eurasian and the Arabian Plates convergence along the Zagros Orogenic Front and upwelling mantle plume since 30 million year ago, Afar depression had formed.

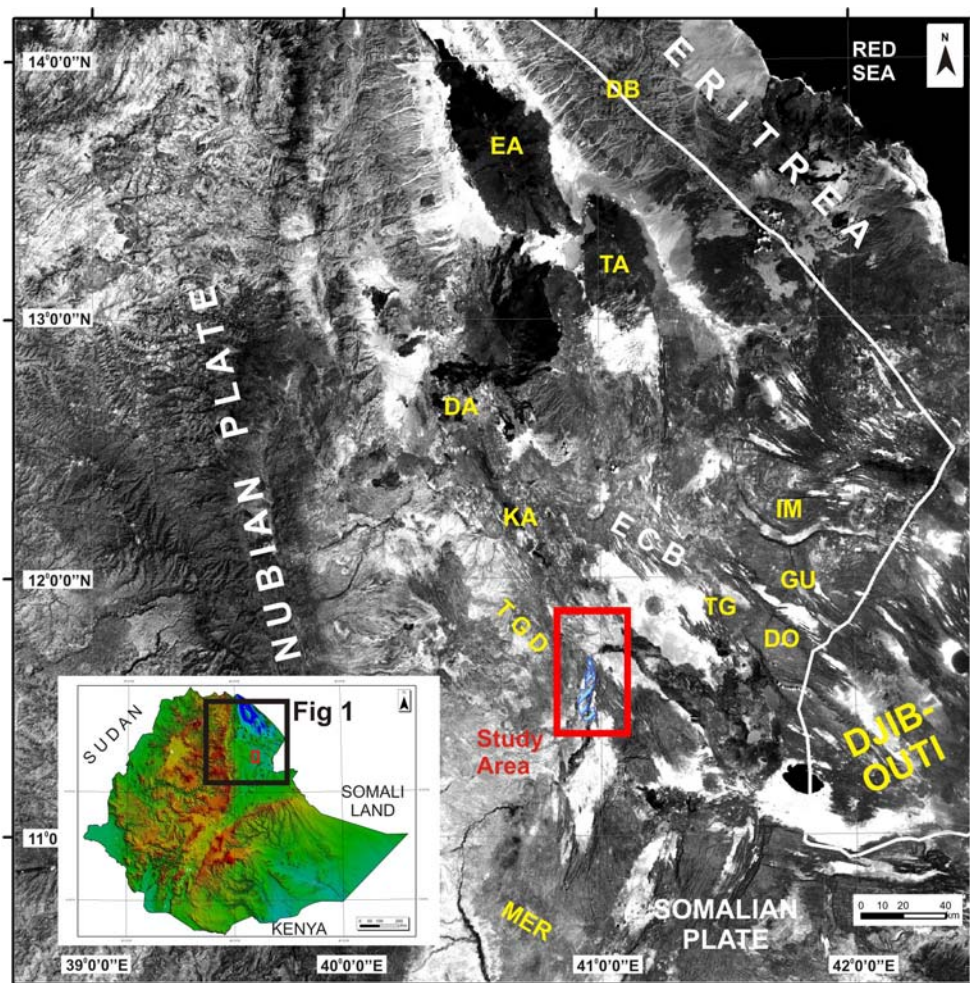


Fig 2.1: Satellite image (panchromatic image of Landsat Enhanced Thematic Mapper Plus) of Afar Depression, NE Ethiopia; Tenahdo Dam and Reservoir site is located at the center of the depression. Abbreviations: DA Dabbahu rifting, DB Danakil block, DO Dobi graben, EA Erta' Ale, ECB East Central Block GU Guma graben, IM Immino graben, KA Karbahri graben, MER Main Ethiopian Rift, TA Tat 'Ale, TG Tendaho graben, TGD Tendaho Goba'ad Discontinuity.

It commenced with the separation of Arabian-Nubian plate, Arabian-Somalian plate and Nubian-Somalian plate. Then rifting of Red Sea propagate towards the center of the Afar depression by cross cutting the Main Ethiopian Rifting structures and rifting of Gulf of Aden propagate towards NW direction along Asal – Manda Hararo rifting axis. Recently the

tectonics activities are concentrated at the East Central Block (ECB) and it is referred as the third order tectonics structures (Beyene & Abdelsalam, 2005).

Fig 2.2 represents the different tectonic elements in the depression and the tectonic orders.

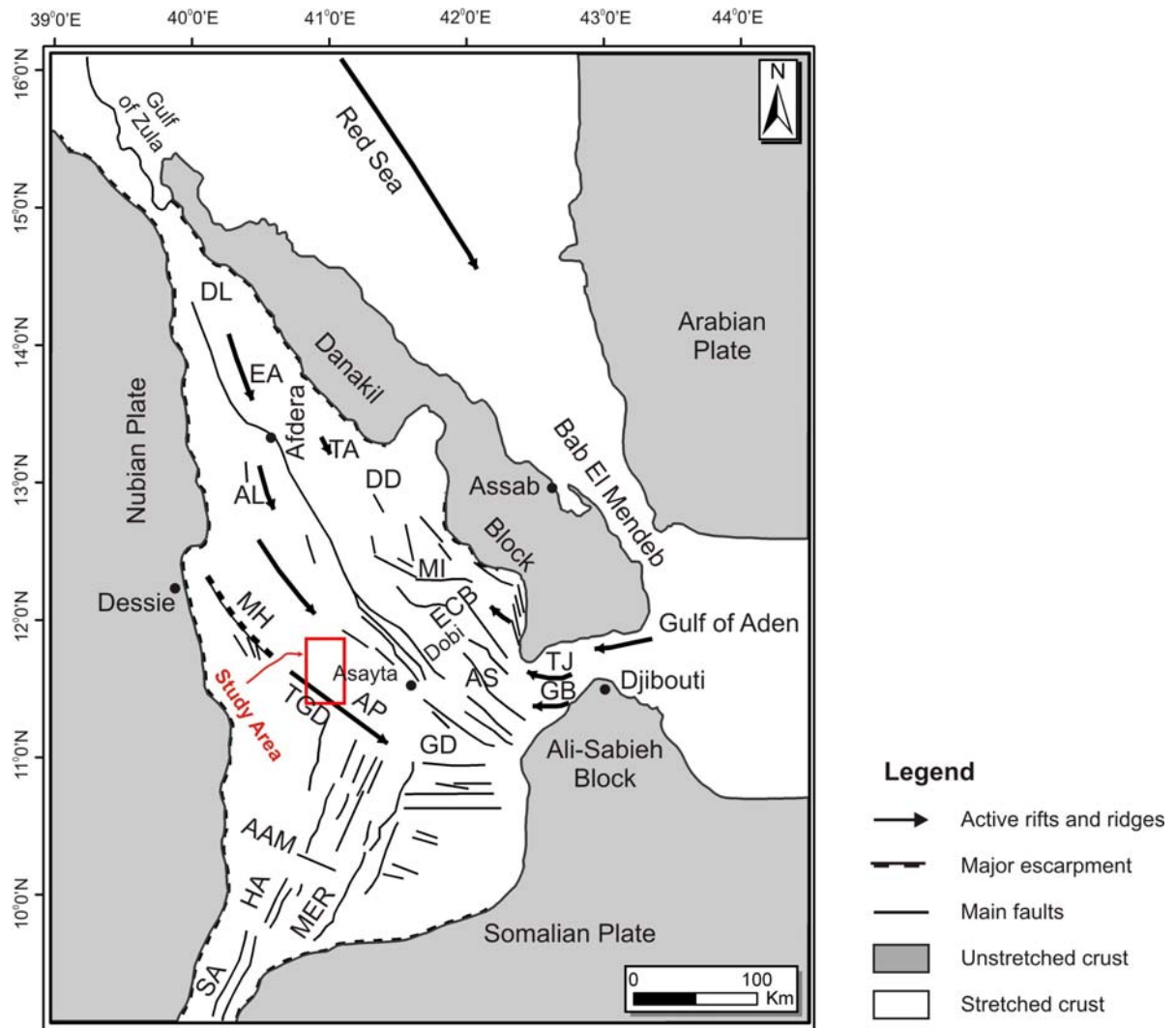


Fig 2.2: Tectonic map the Afar Depression (after Manighetti et al., 1998, 2001; Beyene & Abdelsalam, 2005). AAM Ayelu Amoissa; AL Alayata; AP Awsa plain; AS Asal; DD Dadar graben; DL Dallol; ECB East Central Block; EA Erta Ale; GB Ghoubbet; HA Herta Ale; GD Goba'ad; TA Tat Ale; MER Main Ethiopian Rift; MH Manda Hararo; MI Manda Inakir; SA Sabure; TGD Tendaho Goba'ad Discontinuity; TJ Tajura.

The geological units of the Afar Depression and marginal areas can be divided into four broad groups (**Fig. 2.3**; Varet, 1978): (1) Neoproterozoic basement, Mesozoic sedimentary rocks, and Eocene–Miocene basalts; (2) Miocene igneous rocks; (3) Pliocene volcanic rocks; and (4) Quaternary volcanic and sedimentary rocks. The unstretched crust (**Fig 2.2**) of Neoproterozoic basement (Nubain and Somalian plate, Danakil and Ali-Sabieh block) surround the most dominating Pliocene – Pleistocene stratoid basalt. Miocene volcanic

series at the marginal line of the depression and quaternary volcanic and sedimentations are part of the geological setting of East Central Block (Beyene & Abdelsalam, 2005).

2.2.2 Seismicity and recent tectonic activities

There are five regional broad-band stations near the Afar Depression, namely; ATD and AGD in Djibouti, SODA in Saudi Arabia, FURI and AAE in Ethiopia. Seismic activities of the Afar Depression were discussed by several authors (Gouin, 1979; Kebede et al., 1980; Gresta et al., 1997; and Ayele et al., 2006). Ayele, 1995 compiled the earthquake catalogue of the Horn of Africa for the years 1960-1993 based on the International Seismic Center (ISC) and National Earthquake Information Service (NEIS).

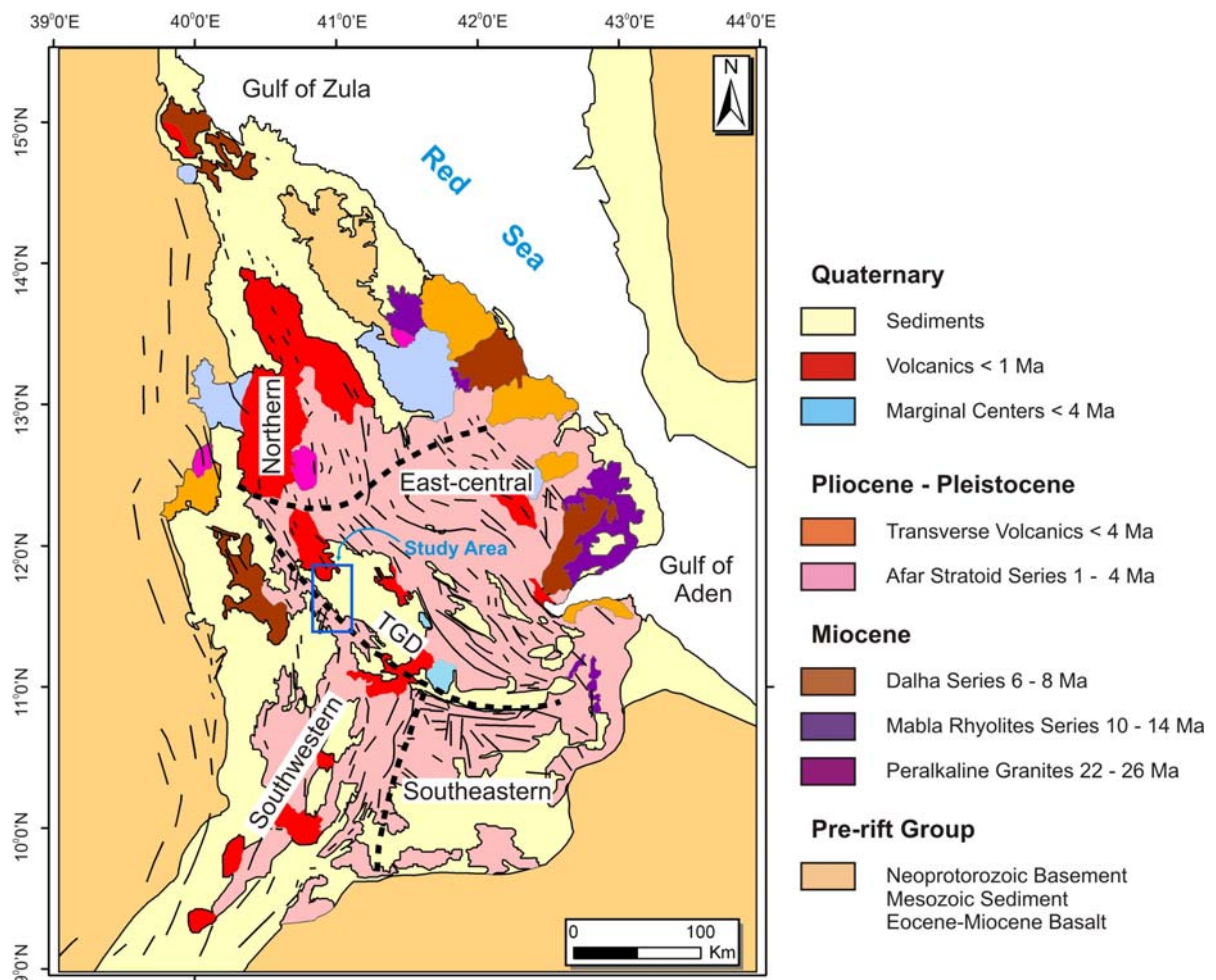


Fig 2.3: Geological Settings of the Afar Depression (after Varet, 1978; Acton et al., 1991; Beyene, 2004).

Hofstetter & Beyth, 2003 classified the depression into seven seismological regions based on the geological, tectonic and seismological data. **Fig 2.4a** shows the different seismological regions and earthquake magnitudes (body wave magnitude) greater than $3m_B$

(1960 – 2000). According to the result, region 4 is the most active region in the recent period. The calculation of seismic moment and sources parameters for the intermediate and strong earthquakes indicates that the strike-slip and normal sense of movement are originating from fault planes striking NW-SE. The 2001 – 2009 years earthquake events are shown in **Fig 2.4b**. During this time the activities of the depression was mostly concentrated in region IV and V. The seismic activities in the other regions were less or minimum as III, I, II, VI and VII, respectively.

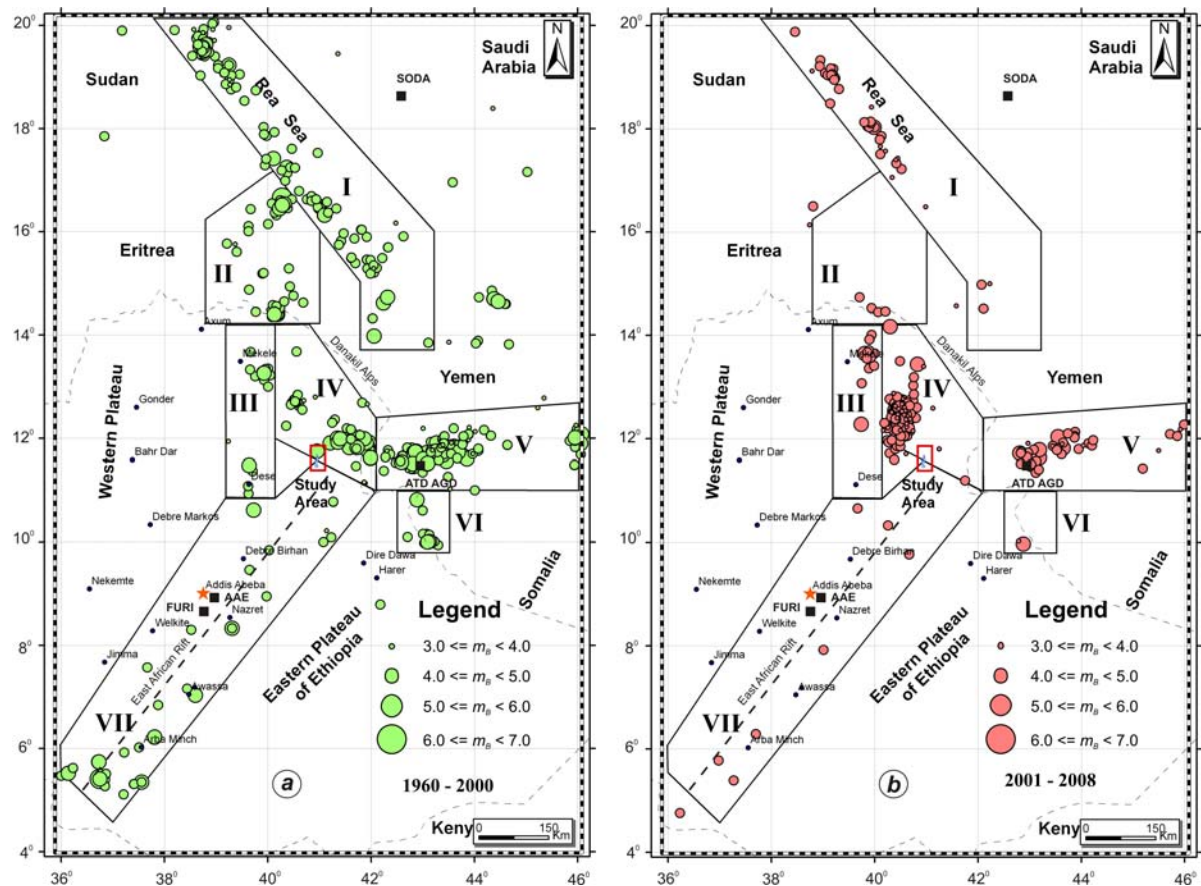


Fig 2.4: Seismicity in the Afar Depression during (a) the 1960 – 2000 (green circle) and (b) 2001 – 2009 (deep pink – see **Appendix B-1** for the data) (modified after Hofstetter and Beyth, 2003). Broad band stations are represented by a solid square. The dimensions of the circle are related to the magnitude of the earthquake and boxes are referred in the text as region I-VII. See **Appendix A-1** for higher resolution.

In September 2005, a violent ground cracking, earthquake and injection of magmatic material occurred at Dabbahu area, North of ECB, Afar depression. The event had resulted with 60 km long rifting, maximum of 8 m ground opening, 2-4 m vertical and 10-15 km lateral ground deformation along the rifting axis.

The presence of high quality and precise satellite technology of interferometric radar imaging helped to record the ground deformation at higher accuracy (Rowland, 2007;

Wright, 2006; BBC news, 2007, 2008; Keir, 2009). Such violent episodes continued at Karbahi graben in August 2007 and February and April 2008; indicate that the present tectonic activities are concentrated within region 4 of seismological regions (Hofsteller & Beyth, 2003) and NE-SW rifting extension (**Fig 2.5**).

2.2.3 Tendaho Graben

The propagation of the Red Sea rifting along the Manda Hararo – Gobbad rift axis and the Gulf of Aden rifting along the Asal – Manda Inakle rift axis form 15,000km² wide overlapping zones called East Central Block (Courtilot et al. 1984; Acton & Stein 1991; Beyene & Abdelsalam 2005) (**Fig 2.1, 2.2, 2.3**). This block includes Tendaho, Dabbahu, Dobi, Karbahi, Immino, and Guma grabens tectonic elements which show the recent tectonic activities in the depression and it is stated as the third order tectonic structures of the Afar depression (Beyene, 2004). **Fig 2.6** shows the tectonic elements of ECB.

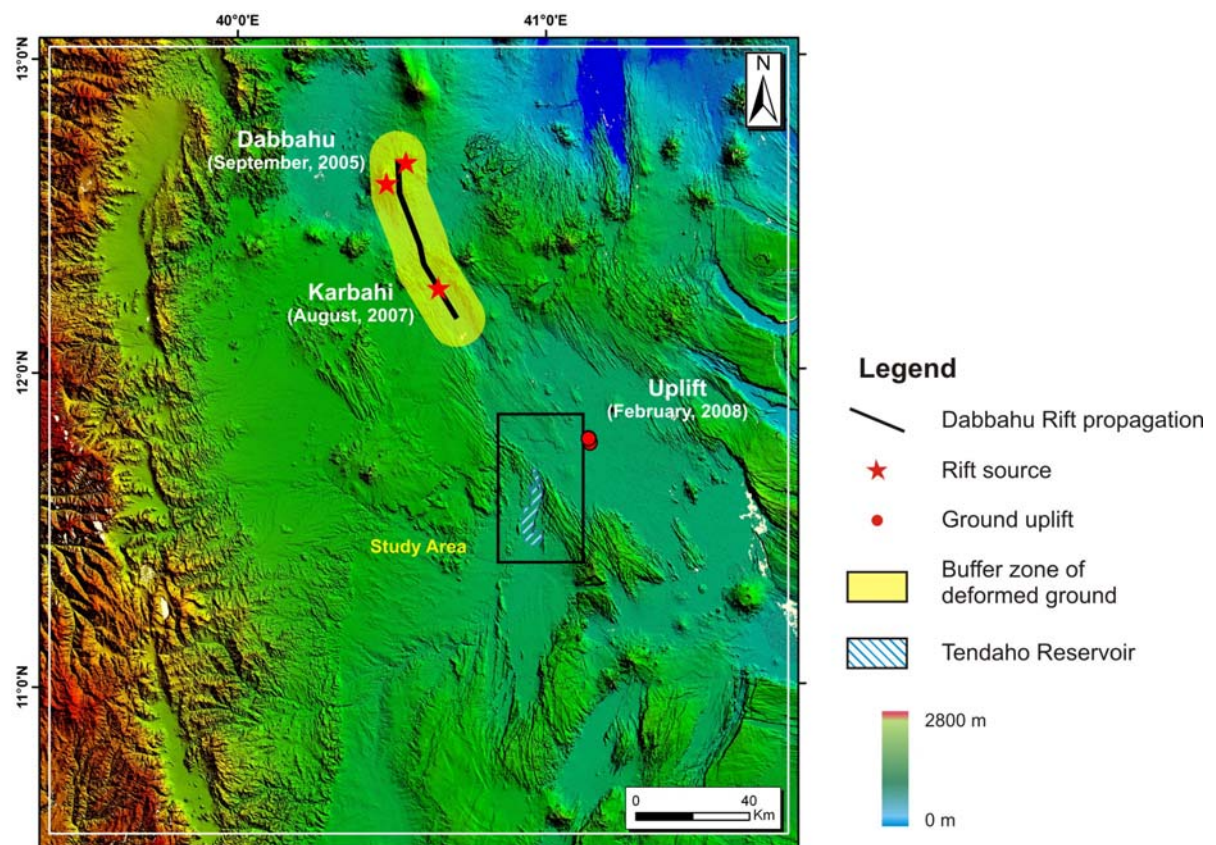


Fig 2.5: Recent Tectonic Activities at North of East Central Block ECB, Afar Depression. Shuttle Radar Tomography Mission (SRTM) elevation model (90m resolution) is used here as base map to locate the September, 2005 Dabbahu rifting episode (after Rowland, 2007); August, 2007 Karbahi rifting (report of the Afar Rift Consortium, 2007); and the February, 2008 ground uplift (documented during the second field studies time in Spring 2008).

Tendaho graben is one of the most stretched graben within the ECB with a rate of 2-3 mm/year (Sigmundsson 1992; Acocella et al., 2008). Lacustrine deposition, fissural basalt, volcanics and NW – SE oriented structures are the main geological features of the graben. The recent seismological data, rifting activities and field examination of tectonic features indicate the propagation of Red Sea rifting towards the graben with an extension of the far field stress in NE – SW direction and magmatic intrusion along the rifting cracks.

In **Fig 2.6**, two active rifting axes are shown close to the Tendaho reservoir and irrigation site, Tendaho and Manda Hararo rifting axes.

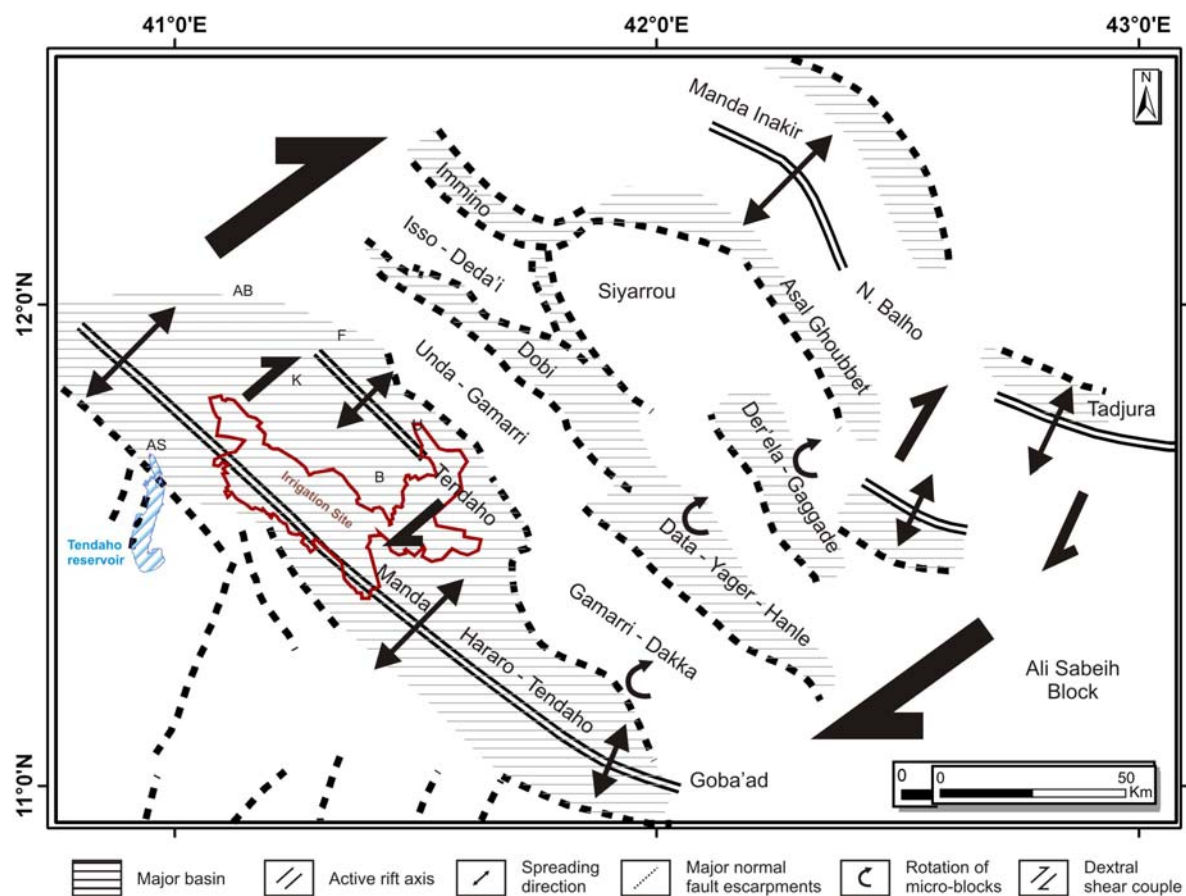


Fig 2.6: After Thurmond, 2007; Schematic representation of major tectonic elements acting within the East Central Block (ECB): AB = Abana, AS = Asgura, B = Borwali, F = Finini, K=Kurub Koma, U=Unda Gamari.

2.3 Risk Assessment

ITC Netherlands, School for Disaster Geo-Information Management (ITC-SDGIM), 2007 define risk as *the expected losses as a result of potentially damaging phenomena within a given time period, and within a given area*. Numbers of natural hazards are affecting the day to day human activities in different perspectives.

According to Asfaw, 2007 risk to an object of interest is a product of hazard and the vulnerability of the object of interest, and the risk could result from a variety of hazards and their higher order effects. The sources of hazards can be natural hazards (earthquake, volcano, landslide, draught and hurricanes) and/or human induced hazards (emission of GHG, toxic chemical, coal dust). The element of at risk or object of interest can be population, buildings and engineering works, infrastructure, environmental features and economic activities in the area affected by a hazard.

2.3.1 Risk Assessment of Natural Hazards

After a tremendous loss of human life and properties due to natural and human induced hazards, interventions of scientific effort and researches have been extremely accepted by most groups. Risk assessment of natural and human induced hazards can be analyzed in *quantitative*, *qualitative* and/or *semi-quantitative* approaches. ITC-SDGIM, 2007 expresses risk as a product of the magnitude of the hazard, the vulnerability of the element at risk and the cost/amount.

$$\text{Risk} = \text{Hazard} * \text{Vulnerability} * \text{Amount}$$

Based on the International Society of Soil Mechanics and Geotechnical Engineering (ISSMGE) Technical Committee on Risk Assessment and Management (TC32), 2005; *risk* is a measure of the probability and severity of an adverse effect to life, health, property, or the environment and *hazard* is probability that a particular danger (threat) occurs within a given period of time. Quantitatively it is expressed as -

$$\text{Risk} = \text{Hazard} * \text{Potential Worth of Loss}$$

And it can also be expressed as 'Probability of an adverse event times the consequences if the event occurs'. In addition, the ISSMGE define *risk analysis* as the use of available information to estimate the risk to individuals or populations, property or the environment, from hazards. Risk analyses generally contain the following steps (**Fig 2.7**): definition of scope, danger (threat) identification, estimation of probability of occurrence to estimate hazard, evaluation of the vulnerability of the element(s) at risk, consequence identification, and risk estimation.

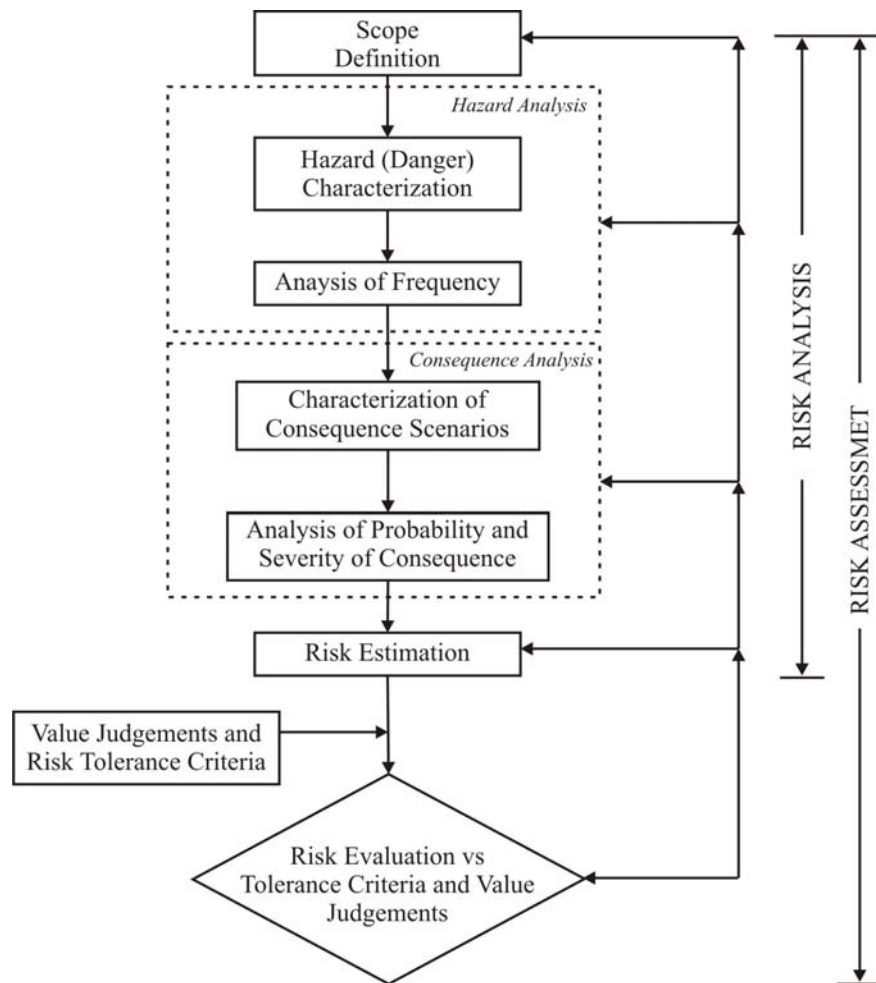


Fig 2.7: Flow chart for landslide risk assessment (ISSMGE, 2005).

Risk assessment is the processes of making a decision recommendation on whether existing risks are tolerable and present risk control measures are adequate, and if no, whether alternative risk control measures are justified or will be implemented. It incorporates the risk analysis and risk evaluation phases.

2.3.2 Geological Risk Assessment

Geology or Geological materials are not homogeneous like engineering products therefore it is difficult to give number to geology. This heterogeneity is a result of various geological processes in extreme different magnitudes and time span (Hoek, 1999). In the beginning of 1960's, (by John 1962 and Müller 1963) rock mass classification techniques were discussed briefly to explain the strength of intact rock and jointing intensity under the engineering geological field. Then after, many researches and new ideas were contributed to the science from all over the world. Coates, 1964; Deere et al., 1968 (RQD Rock Quality Designation); Wickham et al., 1972 (RSR Rock Structure Rating); Rocha, 1976 (MR Rock Mass

Parameter); Barton et al., 1974 (Q Rock Mass Quality); Beiniawski, 1976 (RMR Rock Mass Rating); Romana, 1985 (SMR Slope Mass Rating); Palmstrom, 1996 (RMi Rock Mass Index) can be mentioned as a prominent findings in the geological risk assessment approaches for engineering practices. Although, most of these empirical approaches are used to make estimation for the rock mass characterization for various purposes but indirectly these approaches may correlate to geological risk assessment. For instance if Beiniawski's RMR classifies rock mass as poor quality it reflects indirectly to the risk for the engineering structure to be constructed in such poor quality rock mass.

The above classification systems do not much consider the geological processes which are responsible for the formation of the rock mass. Riedmüller et al., 2001 classify fault rocks in terms of engineering practices and properties. This classification system considers special geological processes which are responsible for the development of brittle deformation. Fault rocks have different geotechnical properties compare to other rock masses. Unless a proper care is taken, the geological risk level can be increased due to the unforeseen conditions.

In addition, Anbalagan, 1992a and 1992 came with a new technique and possibilities to estimate the potential landslide hazard zones by putting numbers to different influencing/governing parameters of landslide and rate them accordingly. Since then others researches were also employed to assess the risk of geological and geomorphological conditions (Turrini and Visintainer, 1998). Sanchez, et al, 2007 also proposed geological risk assessment index by taking Altamira Cave, Spain as a case study.

Chapter Three

Interpretation of Remote Sensing and DEM data for Geological Mapping

3.1 Introduction

For over a century remotely captured images of aerial photography and satellite imagery are used for mapping of geological and geomorphological features. The remote sensing technology is still advancing since its earlier commencement of panchromatic image capturing of aerial photography to multi-spectral satellite images of high degree of resolution. In a similar way the techniques and approaches of image interpretation have evolved from the simple image analysis of tonal variation to the present achievements of image integration, fusion and/or merging.

Currently, it is possible to get different types of remote sensing data from various sources with higher resolution and accuracy as per the research or study objectives. However, the image interpretation task plays an important role to extract high reliable information/result from the given sets of remote sensing data of one particular area of interest (Rees, 2001; Richards and Jia, 2006).

Field methods of geological and geomorphological mapping should have very specific objectives to address limited area of extents otherwise lots of time and resources might be required to cover the entire area of interest. To have first hand impression and prioritize or select sites for field mapping, geologists are practiced to analysis the remotely sensed image before their first field visit to the area. Such approach is well tested and proved how important is for the better visualization of the different possible geological features that might be encountered and their extents in advance in addition to vital contribution for the final interpretation (Gupta, 2004).

3.2 Remote sensing data and methods

In the present study data from different sources representing remote sensing systems and TIN model are used; (1) Landsat Enhanced Thematic Mapper Plus (ETM+); (2) Aerial photography with 1:50000 resolution; (3) DEMs – extracted from the Shuttle Radar Topography Mission (SRTM); (4) Triangular Irregular Network (TIN) with 20 m contour interval.

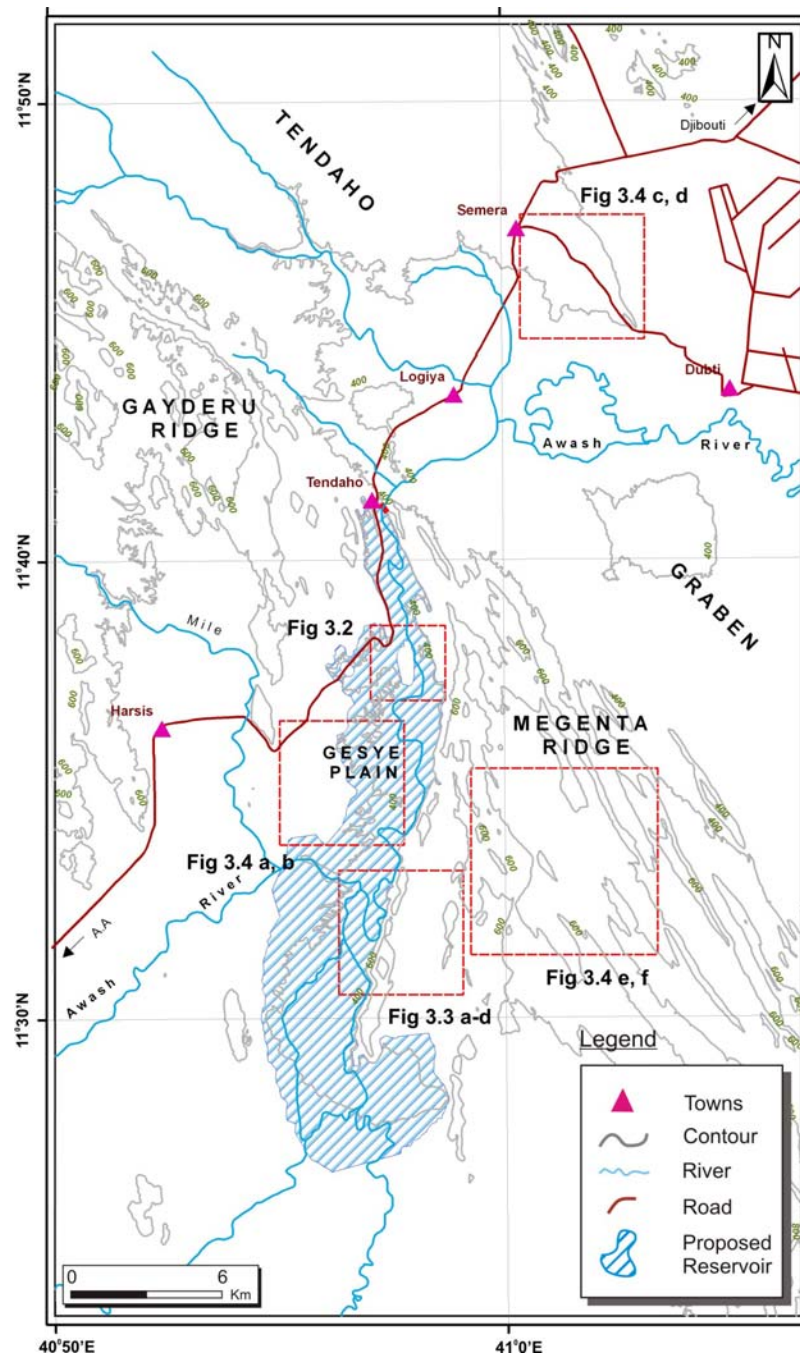


Fig 3.1: Location map of the study area including the proposed maximum level of Tendaho Reservoir; the red rectangles show the locations of **Fig 3.2, 3.3** and **3.4**.

Band combinations of ETM+ Landsat imagery were used for lithological mapping of the current study area (**Fig 3.1**). The spatial resolutions of the 8 bands were enhanced by the panchromatic band of 15 m resolution. About 35 aerial photos were used to delineate lithological boundaries of different rock types within the reservoir area and geomorphological data extraction (**Fig 3.1**). SRTM, TIN and Landsat ETM+ imagery (with edge enhancement and Principal Component Analysis [PCA] techniques) data sets were combined to delineate morphologically defined structures. The Landsat ETM+ imagery had dragged on TIN data set for advanced lineament interpretation and better visualization of morphologically defined features and additional measurements.

3.2.1 Aerial Photograph

It is the oldest and most widely used method of remote sensing. In a simplified expression, it is the taking of photographs of the ground from an elevated position. For this study, vertical photographs (Scale 1:50,000) which were taken by the Ethiopian Mapping Agency in 1994 were used to delineate lithological boundaries and lineaments at the center of the proposed Tendaho reservoir (**Fig 3.2a, b**).

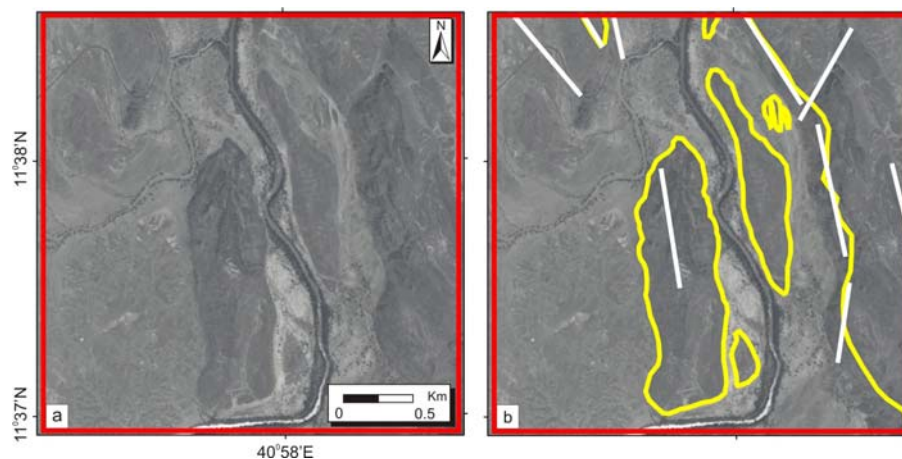


Fig 3.2: (a) Aerial Photo at the center of a proposed maximum level of Tendaho Reservoir (b) lineaments and lithological boundaries are delineated with white and yellow lines, respectively, see **Fig 3.1** for the location.

3.2.2 Landsat ETM+

For the present study, Landsat ETM+ image which was taken on March 20, 2001 with a path and row number of P167 and R052, respectively were used (**Fig 3.4a-f**). Band combination (**Fig 3.4a, b**), principal component analysis (**Fig 3.4c, d**) and Intensity-Hue-Saturation (**Fig**

3.4e, f) image enhancement techniques were employed to delineate lithological boundaries and lineaments.

3.2.3 *SRTM (Shuttle Radar Topography Mission)*

Space Shuttle Endeavour with Shuttle Radar Topographic Mission (SRTM) payload launched into space on February 11, 2000. Within ten days of operation, the most complete near-global high-resolution database of the earth's topography (from 60⁰N to 56⁰S) was obtained. As Thurmond, 2006 explained *SRTM is capable of producing DEMs with an X–Y resolution of 1 arcsecond (approximately 30 m) and a vertical resolution (Z) of 6–16 m (90% confidence)*. Interferometry technique is used by SRTM to generate topographic (elevation) data of the earth. In this technique, two images are taken from different fixed points of the same area. The slight difference in the two images allows to determine the height of the same area. The SRTM data is available for the US at full resolution and degraded to 3 arcseconds (90 m) for the rest of the world (SRTM Project Office, 2006; Thurmond, 2006; Reuter et al., 2007 See **Fig 3.3c-d**).

3.2.4 *TIN (Triangular Irregular Network)*

Triangulated irregular network (TIN) model was developed in the early 1970's as a simple way to build a surface from a set of irregularly spaced points (Reuter et al., 2007). *It is a vector based representation of the physical land surface or sea bottom with three dimensional coordinates (x, y and z) that are arranged in a network of non-overlapping triangles¹*.

For the present study, TIN model was generated from 1:50000 scale topographical map of Ethiopia; Sheet number **Loma 1140 B2, Semera 1141 A1, Logiya 1140 B4, Dubti 1141 A3, Mile 1140 D2** and **Deneba 1141 C1** (see **Fig 3.3a-b**).

¹ http://en.wikipedia.org/wiki/Triangulated_irregular_network accessed on February 19, 2009.

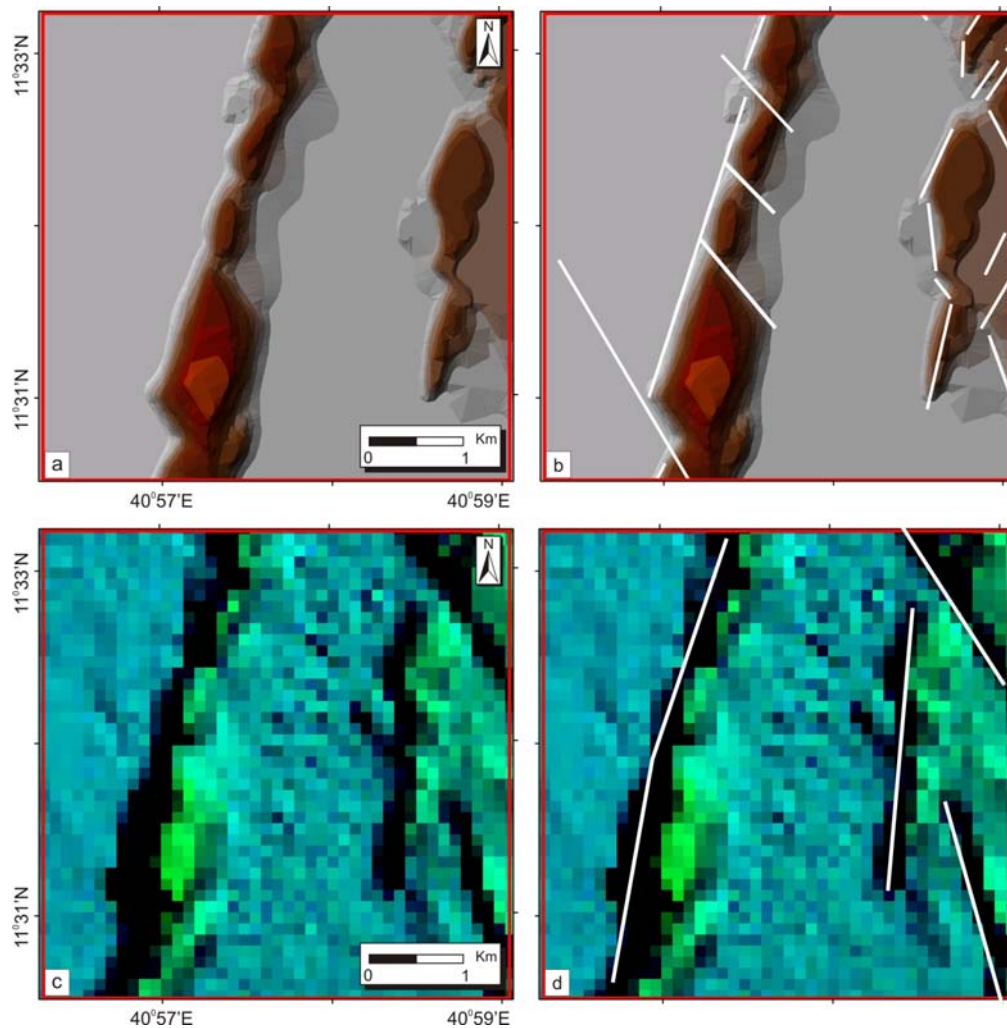


Fig 3.3: Compare TIN and SRTM topographic models; *(a)* Triangular Irregular Network (TIN), *(b)* lineaments are delineated with white lines from the TIN topographic model, *(c)* Shuttle Radar Topographic Mission (3-arc, 90 meter resolution) and *(d)* lineaments are delineated with white lines from the SRTM topographic model, see **Fig 3.1** for the locations.

3.3 Results

The result of remote sensing data sets and TIN analysis are classified into four major areas based on the Tendaho reservoir position and analysis techniques (see **Fig 3.5**); (1) **GD** Gayderu Ridge – Left (East) of Tendaho Reservoir, (2) **GP** Gesye plain, (3) **MR** Megenta Ridge – Right (West) side of Tendaho Reservoir and (4) **TG** Tendaho Graben.

3.3.1 Gayderu Ridge – West of the proposed Tendaho Reservoir

It is the extension of Tendaho Gobbad Discontinuity ridge in the southeastern part, **Fig 3.5**. The Main Ethiopian Rift and the propagation of Red Sea rift structures are the only regional tectonic settings found on the ridge. Stratoid basalt, ignimbrite and quaternary deposition of

lake, alluvial, coluvial and eluvial sedimentation are mapped from the remote sensing data sets. The different lithological boundaries were easily delineated from the Landsat ETM+ image (band combination, Intensity-Hue-Saturation [IHS], RGB and edge enhancement techniques) and aerial photographs.

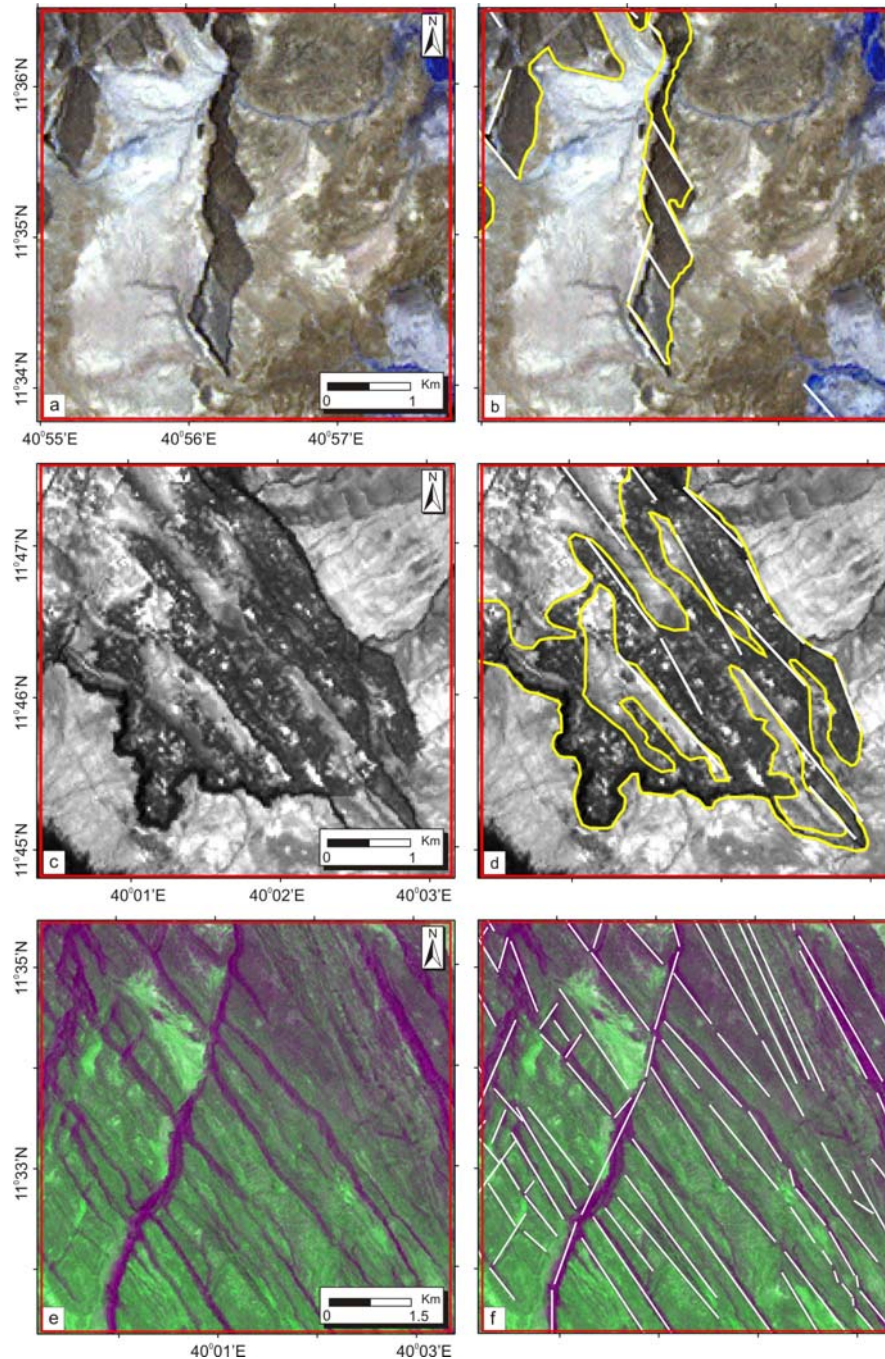


Fig 3.4: (a) Band combination (4-5-3) of Landsat ETM+ image, (b) lineaments and lithology boundaries are delineated with white and yellow lines, respectively from the Landsat ETM+ image, (c) Principal Component Analysis (PCA) image (d) lineaments and lithology boundary are delineated with white and yellow lines, respectively from PCA, (e) Intensity-Hue-Saturation (IHS of band combination 2-1-2) image, and (f) lineaments are delineated with white lines from IHS, see **Fig 3.1** for the locations.

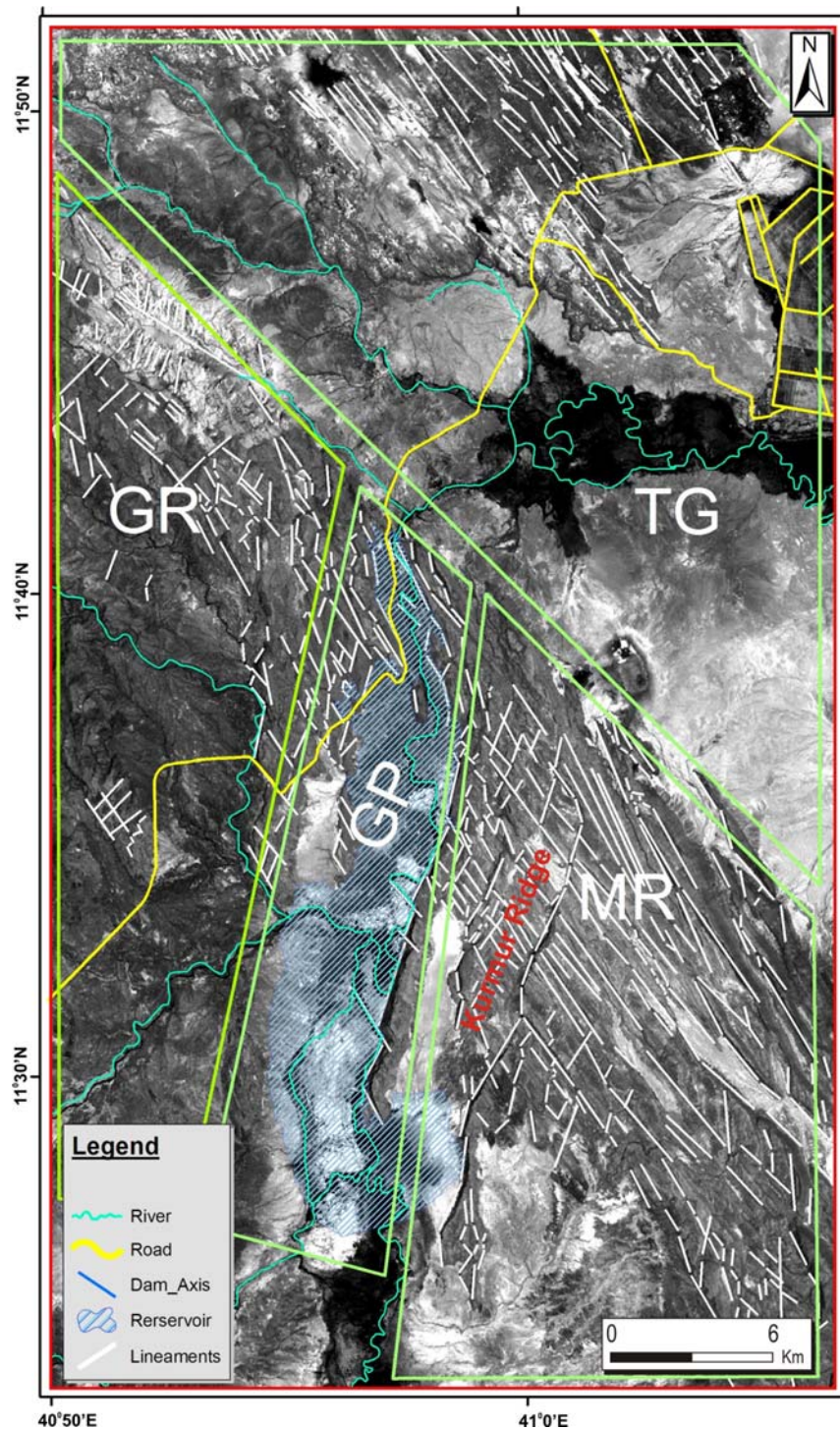


Fig 3.5: Panchromatic image (Band 8) of Landsat ETM+ with delineated lineaments (white color). **GR** Gayderu Ridge – NW to W of the proposed maximum level of Tendaho Reservoir; **GP** Gesye Plain – center of the proposed maximum level of Tendaho reservoir; **MR** Megenta Ridge – E to SE of the proposed maximum level of Tendaho Reservoir; and **TG** Tendaho Graben. See **Appendix A-2** for higher resolution.

Edge enhancement and band combination of IHS techniques helped to trace the possible tectonic structures in addition to the SRTM data set of remote sensing type and the 20 meter interval TIN model. NW-SE structures (**Fig 3.6b**) are the most dominant tectonic features along the stratoid basalt formation and NE-SW structures (**Fig 3.6b**) also found on the

stratoidal ignimbrite (felsic volcanic material). Lattice, 2003 used the ignimbrite as a cursor indicator for Tendaho graben separation/opening and age estimation (dating).

The NE-SW structures are not the dominating tectonic features along the Gayderu ridge (**Fig 3.6b**). This shows the influence of the Main Ethiopian rift which was limited towards the center of the Tendaho reservoir. The morphological defined structures were not prominent to identify their relationship to the tectonic setting because of high ridge weathering and reformation of the ground due to different extensional direction. Moreover, **Table 3.1** and **Fig 3.7** show the lineament distribution within the Gayderu region.

3.3.2 Gesye Plain – within the proposed Tendaho Reservoir

Quaternary sedimentation of fluvial and lacustrine deposition covers most of the Tendaho reservoir area except the area covered by basaltic dyke intrusion (2.4 km²). Digital aerial photographs were geo-referenced with the help of well known ground control points and used to delineate the different lithological boundaries and lineaments (probable tectonic structures) within the reservoir. The previous researches focused on the regional tectonic settings of TGD ridge in a glance and it was not possible to figure out and map the geological features within the reservoir area. NNE-SSW striking basaltic dyke is aligned within the proposed Tendaho reservoir. The TIN model in this area was used to delineate morphologically defined and sharp edged morphological features as probable tectonic structures. Both the Red Sea rift and the Main Ethiopian rift structures with NW-SE and NNE-SSW striking, respectively are traced at the opposite flanks of the reservoir (**Fig 3.5** and **3.6c**). In addition, **Table 3.1** and **Fig 3.7** show the lineament distribution within the Gesye Plain.

3.3.3 Megenta Ridge – East of the proposed Tendaho Reservoir

This ridge is the left side of host structure of the Tendaho graben. The active Tendaho Gobbad discontinuity fault passes in between the ridge and graben with a maximum of 350 meter vertical down. The ridge has the maximum elevation point as of the total study area at the marginal end of eastern part. Alternative sequences of scoriaceous, vesicular, theolitic basalt and scoria (the Pleistocene – Pliocene stratoidal basalt) are the dominate lithology mapped from the Landsat ETM+ imagery. A simple band combination technique was employed to identify the boundaries comparing with the different electromagnetic wave

reflection result of its adjoining quaternary deposition. Moreover, edge enhancement and PCA image interpretation techniques were deployed to trace the possible tectonic structures. NNE-SSW striking of the main Ethiopian rift structures is concentrated up to the first 15-20 km of the lateral distance from the maximum reservoir level at the Kurmur ridge (**Fig 3.5**). However, most of the tectonic structures have striking direction of NW-SE which is the result of Red Sea Rift propagation along the TGD ridge (**Fig 3.6d**). Moreover, **Table 3.1** and **Fig 3.7** show the lineament distribution within the Megenta region.

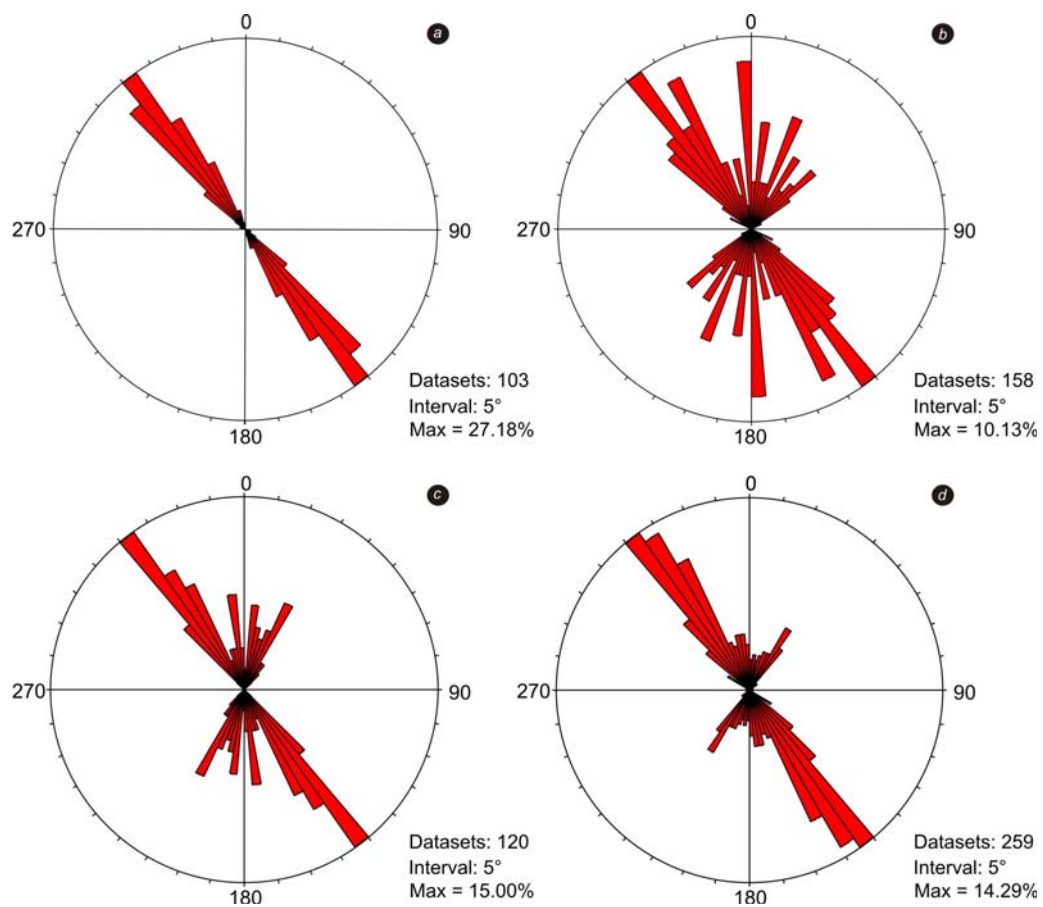


Fig 3.6: Rose diagrams of lineaments at (a) Tendaho Graben TG, (b) Gayderu Ridge GR, (c) Gesye Plain GP and (d) Megenta Ridge MR, see **Fig 3.5** for the locations.

3.3.4 Tendaho Graben

Part of the Tendaho graben was included in the present study to understand the tectonic settings and activities around the Tendaho dam and reservoir area. This graben is one of the most stretched/opened tectonic structures within ECB (Stimmungsdson, 1992): Similar data sets were employed to delineate the different lithological boundaries and tectonic features. Recent quaternary fissural basalt is concentrated along the active Tendaho rifting axis. Lake

sediments (sandstone, mudstone, siltstone and conglomerates) of 1-12 k.y (Lattice et al., 2003) and alluvial depositions are the main lithological formation found in the graben. NW-SE (**Fig 3.6a**) striking tectonic structures are the only tectonic features which were mapped with the help of aerial photography and Landsat ETM+ image analysis. In addition, **Table 3.1** and **Fig 3.7** show the lineament distribution within the Tendaho graben.

Fig 3.8 shows the final result of the interpretation of the remote sensing and DEM data sets for geological mapping.

Table 3.1: Summary of lineaments distribution at Tendaho Graben (TG), Gayderu Ridge (GR), Gesye Plain (GP) and Megenta Ridge (MR).

	Number of Lineament	Min (m)	Max (m)	Mean	Std	Total Length (m)	Total Area (km ²)
TG	103	214	4635	1472	813	151621	522.5
GR	158	170	7309	956	706	150857	333.5
GP	120	124	3384	943	634	113170	213.4
MR	259	138	6567	1273	1053	329664	368.6

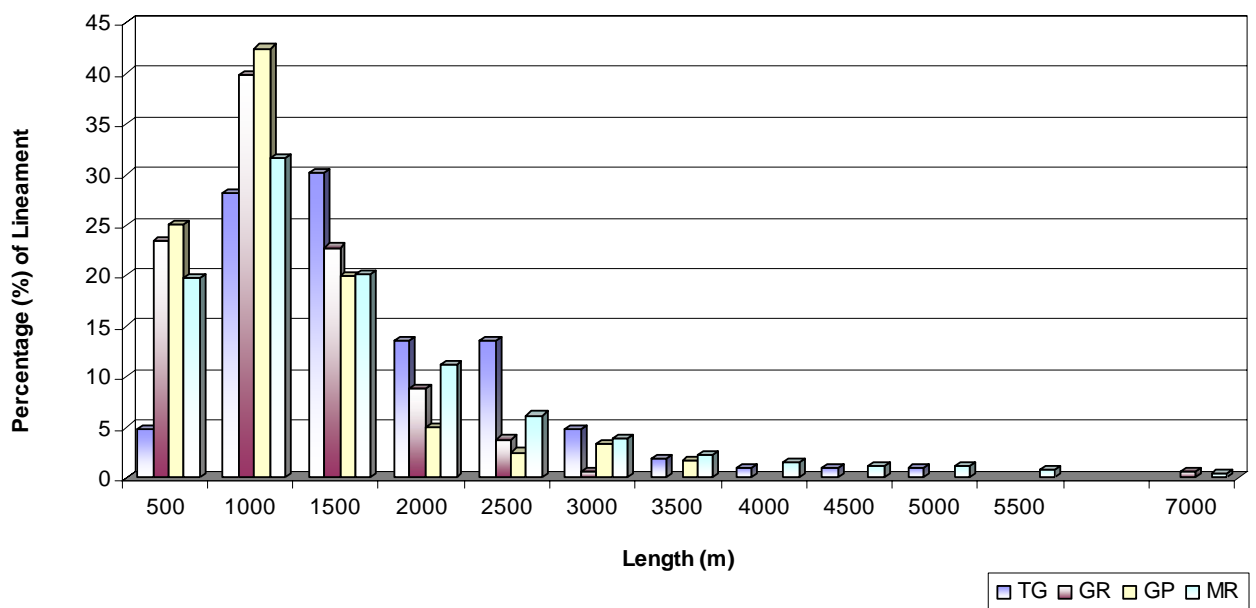


Fig 3.7: Distribution of lineaments length at Tendaho Graben (TG), Gayderu Ridge (GR), Gesye Plain (GP) and Megenta Ridge (MR).

3.4 Discussion

In the previous studies of Abdelsalam et al., 2000 & Thurmond et al., 2006, the integration of Optical-Radar-SRTM remote sensing data sets were shown as it had a power to delineate morphologically defined structures and lithological boundaries. In the present study, the

integration of the Landsat ETM+ image, aerial photograph, SRTM DEM and TIN helped to delineate lithological boundaries and morphologically pronounced structures with higher resolution. The dragged image of ETM+ Landsat satellite imagery on TIN model gave a much better visualization, advanced interpretation and measurements of tectonic structures.

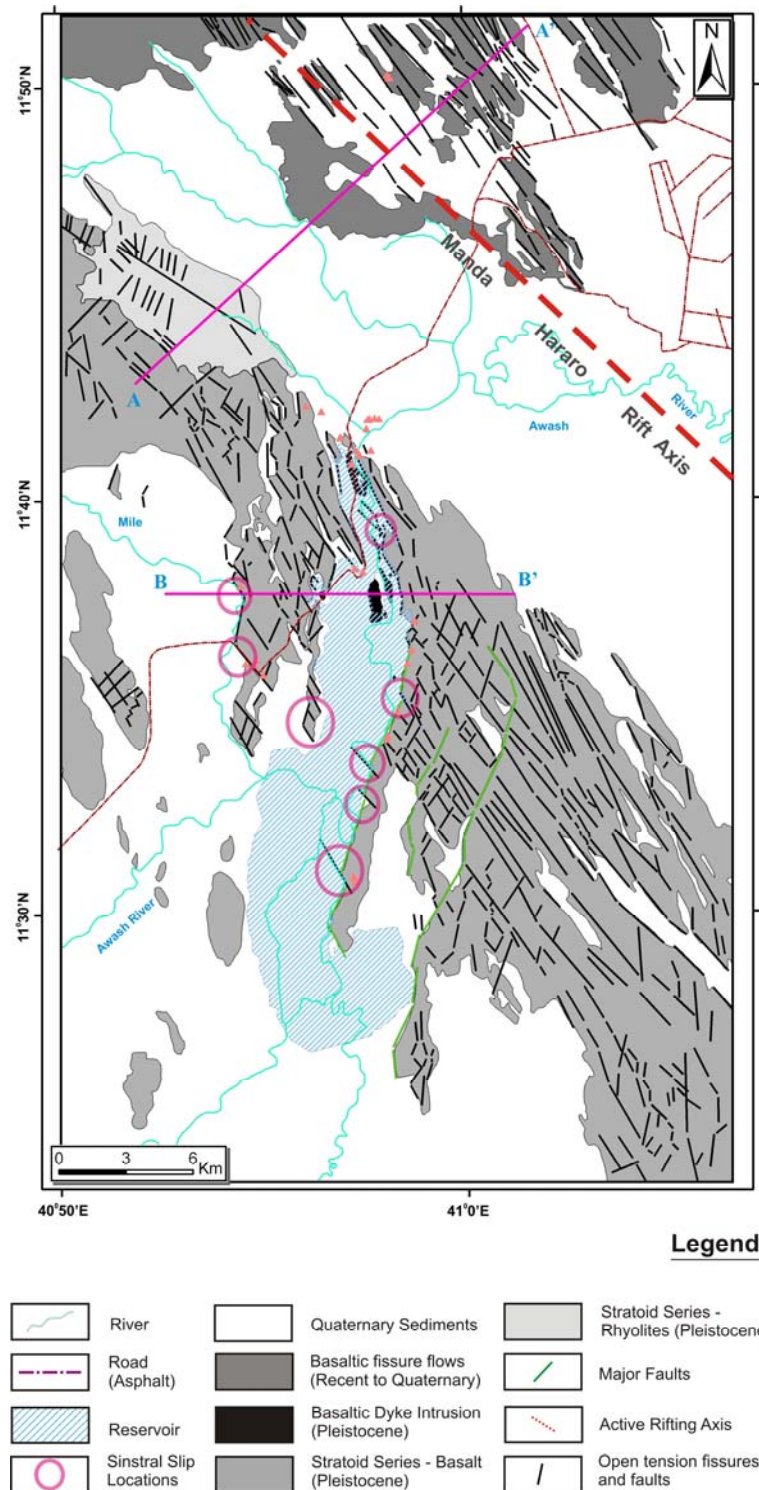


Fig 3.8: Geological map of the proposed Tendaho Reservoir and its vicinity; Modified after Varet, 1978; Manighetti et al., 1998, 2001; & Thurmond et al., 2006 with the interpretation of Landsat ETM+ image, aerial photograph, SRTM and TIN model. See **Appendix A-5** for higher resolution.

Fig 3.9 compares the SRTM and TIN datasets for the visualization of tectonic structures. Because of its higher resolution, the TIN datasets pronounced more the geomorphological defined structures (**Fig 3.8** – *sinstral slip locations*) than the SRTM (3 arc second resolution). Further more, the higher resolution of the aerial photograph helped to delineate the elongated dyke intrusion at the middle of the reservoir.

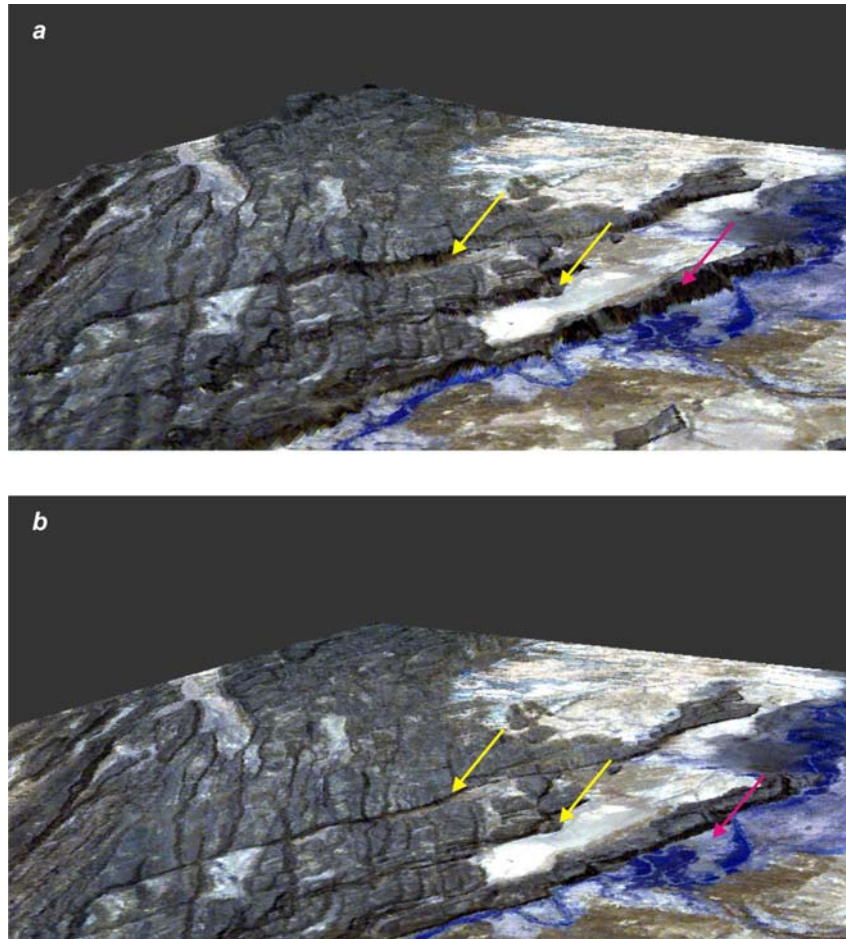


Fig 3.9: Landsat ETM+ image (band combination 4-5-3) dragged on; **A** TIN model and **B** SRTM (2x vertical exaggeration) to compare the SRTM and TIN elevation models for visualization of morphologically defined structures and extraction of risk parameters (structural).

Lineaments are highly concentrated at NW and SW of the proposed reservoir area. The reservoir bed and most of the Tendaho graben have very less lineament density except areas NE of the Tendaho dam axis (**Fig 3.10**). The local and regional groundwater flow direction and the hydraulic conductivity behavior of the rock mass may be influenced by the lineament density zone and pattern.

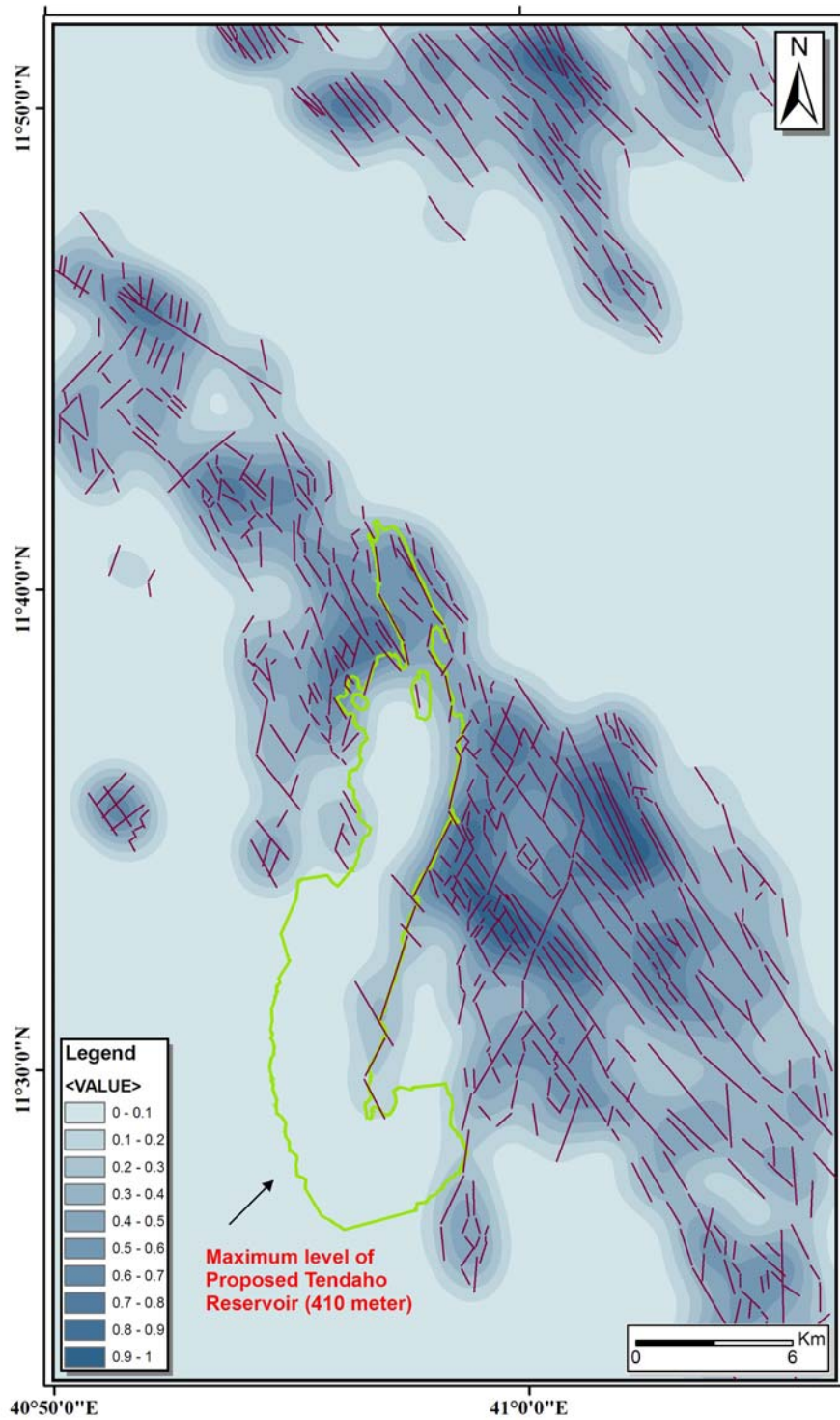


Fig 3.10: Lineament density zones using Kernel density analysis method² (Arc GIS) with approximately 120 meter pixel size and 2 Km radius. The classification was normalized by dividing the class boundaries with the maximum value – 0.002692875. See **Appendix A-3** for higher resolution.

²<http://webhelp.esri.com/arcgisdesktop/9.1/index.cfm?id=2961&pid=2960&topicname=Density%20calculation> s, accessed on December 15, 2009

Chapter Four

Tectonic Structures of Gesye Graben and part of Tendaho Graben

4.1 Introduction

The proposed Tendaho reservoir lies at the center of the Gesye plain and the entire irrigation scheme is built within the Tendaho Graben. As it was discussed in the previous chapter (*Chapter two*), the famous active tectonic regime (Redfield et al., 2003) – the Afar Depression is consisted of six major tectonic elements (Beyene, 2004). The East Central Block (ECB) is one of the most recently active regions within the depression. The current study area (partially the Tendaho Graben) is component of the ECB and the Gesye plain is found along the Tendaho Goba’ad Discontinuity (TGD) ridge.

Brittle tectonic structures are structures which are formed as the result of tectonic activities/processes at the upper crust (Kearey & Vine, 1990; Twiss & Moores, 1992; and Tarbuck & Lutgens, 1996). To reconstruct the past tectonic events, understand the current situation and predict the future tectonic activity, many approaches have been practiced so far (remote sensing data analysis, field mapping, outcrop description, laboratory analysis of rock samples etc). One could generate data from regional to microscope scale to study the tectonic settings of a given area. The understanding of the tectonic situation of the particular place increases with the integration of observations of the tectonics’ data at all scales (Moores & Twiss, 1995).

4.2 Geology

The Afar depression consists of mainly volcanic and quaternary sediments (Beyene, 2005), where two third of the depression is covered by the stratoidal basalt flow and the lower part of the Tendaho graben is mainly covered by the quaternary depositions.

A. Stratoidal basalt

Both flanks of the proposed Tendaho reservoir ridges are covered with stratoidal basalt flows (**Fig. 4.12**). The different flow sequences include amygdaloidal, vesicular, scoracious, porphoritic, aphanitic and theollitic (rich with sodium) basalts(WWDSE-WPCS-I, 2005). **Fig 4.1a, b, & d** show the thin section analysis of basaltic rock samples. The basalts were exposed to physical (rock fragmentation) and chemical weathering (decomposed to soil) due to the past and current climatic condition and presence of water. Along the left flank of the proposed reservoir side (E & SE of the reservoir), the stratoidal basalts form higher cliff with columnar joint sets.

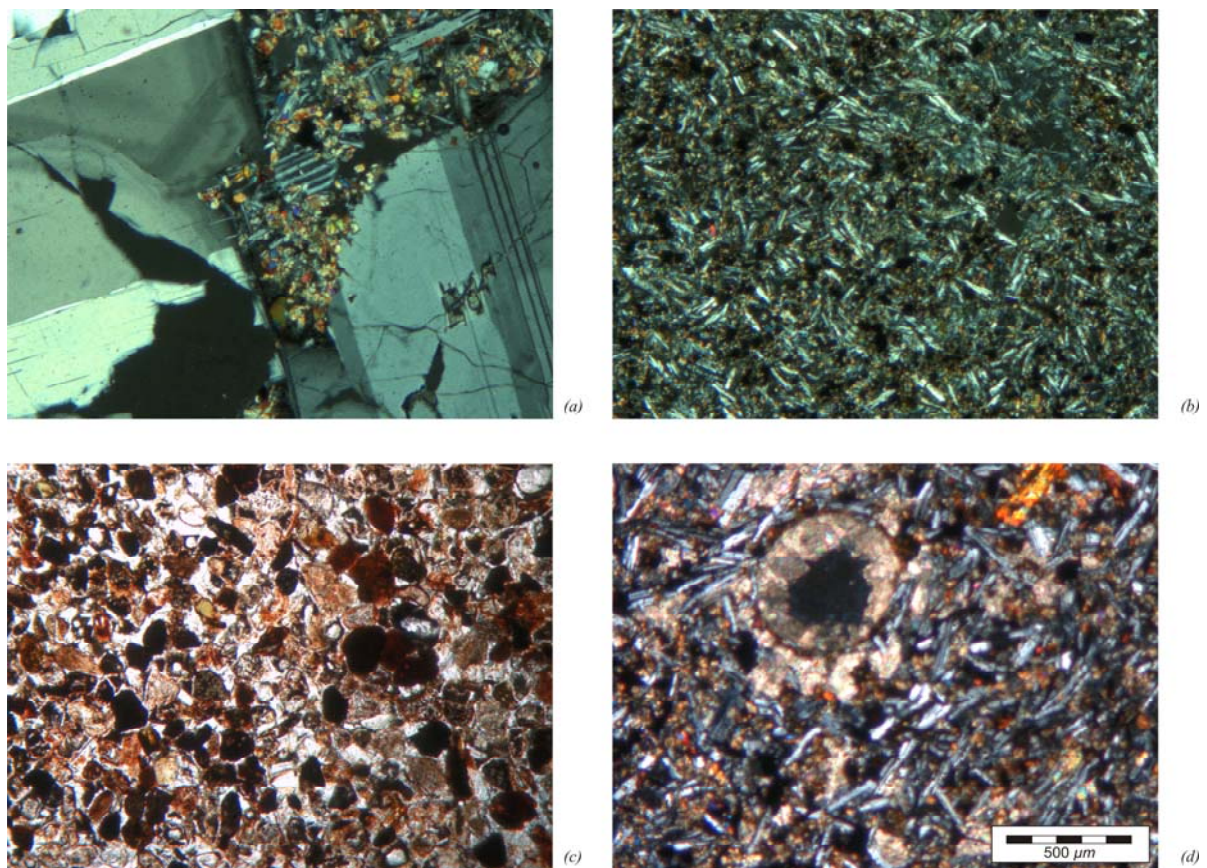


Fig 4.1: Petrographic thin section analysis with polarized and 4x resolution: (a) LR 022/1, Fresh coarse grained plagioclase crystal with ground mass olivine, pyroxene and plagioclase – called fresh porphoritic basalt; (b) RR 032/1, Fine grained basalt with plagioclase (very fine), rich in feldspar and opaque minerals; (c) IC 023/1, Coarse grained sandstone with oolitic material, quartz and feldspar; and (d) RR 032/2 (0-2); Coarse grained Amygdaloidal basalt, mainly plagioclase, pyroxene, feldspar & secondary mineral growth - carbonate. For the location of the samples, see **Fig 4.2**.

B. Quaternary deposit

The quaternary depositions are commonly found in the Afar depression within the lower elevation basins like the Tendaho graben. The proposed reservoir bed and the irrigation site

are covered with the lacustrine (lake and river) depositions (**Fig. 4.12**). Along the irrigation canal cut, alternative sequences of the sediments; mudstone, claystone, siltstone, sandstone, conglomerate, carbonates and chert were observed. The thin section analysis of the rock samples from the quaternary deposition show the presence of oolitic materials, rock fragment, quartz and feldspar (**Fig 4.1c**).

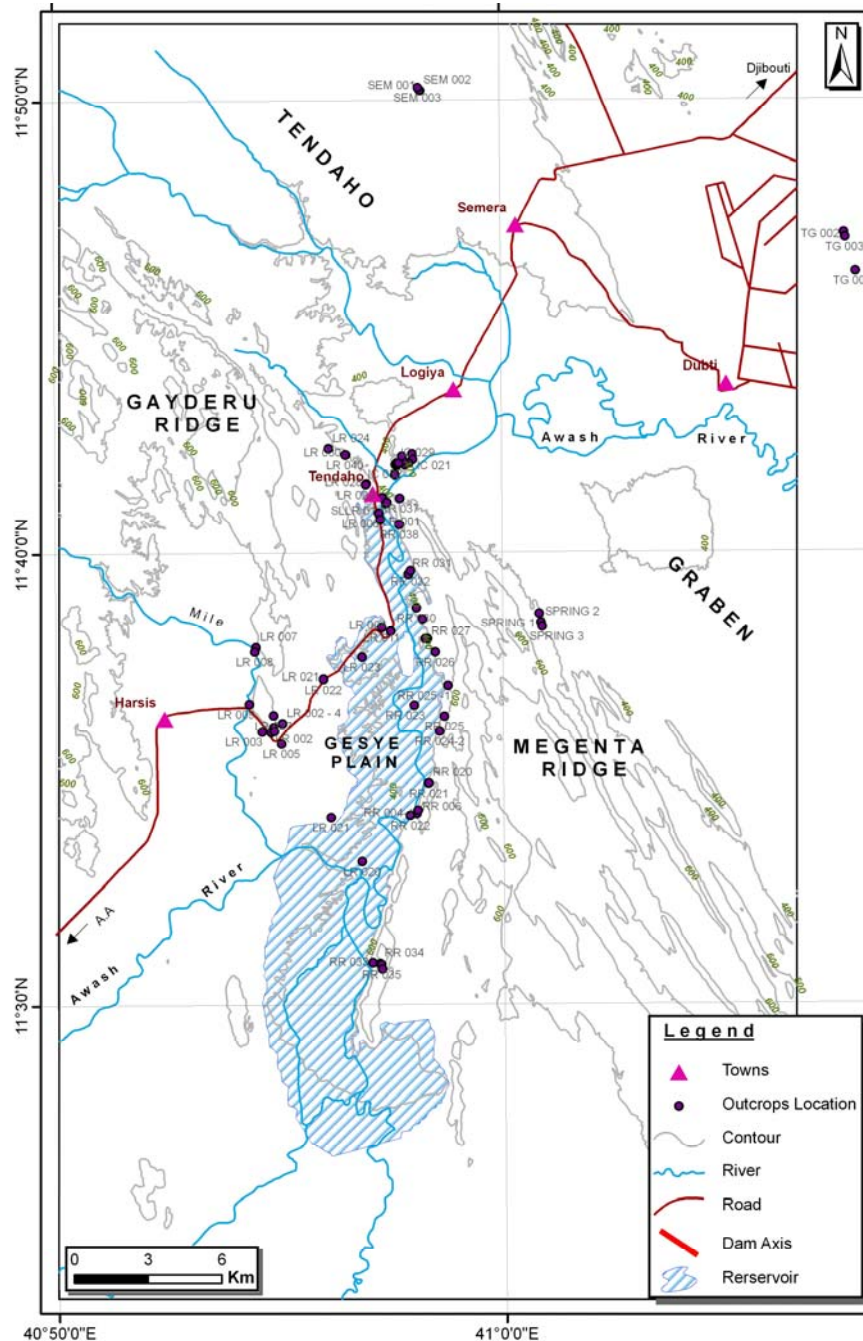


Fig 4.2: Outcrop locations of faults, regional joint settings, scan line mapping; and sample location of rocks, water and filling materials. Where *IC* Irrigation Canal, *RR* Right Reservoir, *RDX* Right dam axis, *LR* Left Reservoir, *LDX* Left dam axis, *SLLR* Scanline Left reservoir, *SLIC* Scanline Irrigation canal, *SEM* Semera Fissure, *TG* Tendaho Graben and *SPRING* Alalobeda Thermal Spring. See **Appendix A-4** for higher resolution.

4.3 Structural settings

With the objective of understanding the tectonic situation of the Tendaho reservoir and irrigation site, a total of 69 outcrops were examined. Faults and sense of slip features, regional joint sets, outcrop sketches (inclination of basaltic flow direction, block rotation) and scan line mapping of regional joint sets in the lacustrine deposition and stratoidal basalt were collected and analyzed. In order to avoid any ambiguity, care was taken during the field mapping to distinguish the origin of the structures (tectonic, erosion, cooling and/or lava flow pattern) of the outcrops. Summary of the outcrops locations and types of identified tectonic features are presented in four sub sessions; *west of the proposed Tendaho Reservoir, within the proposed Tendaho Reservoir and along the dam axis, east of the proposed Tendaho Reservoir and irrigation canal & Manda Hararo rift segment*. **Fig 4.2** shows the location map of the outcrops with respect to the reservoir position.

4.3.1 West of the Proposed Tendaho Reservoir

The west side of the proposed Tendaho reservoir area includes the Gayderu ridge and the road side outcrops on the way towards Harsis town from Logiya. Six outcrops of regional joint sets and three fault planes were identified and data were analyzed. The summarized data are presented in **Table 4.1 & 4.2** for the regional joint sets and fault planes, respectively.

Regional joint sets: to differentiate the tectonic originated fractures with the others, a 2 meter minimum persistency was considered. In this particular area, tectonic fractures (extensional and shear joints) mainly have striking orientations of NW-SE and NE-SW direction (**Fig 4.3**) with a minimum and maximum opening of 0 and 29 mille meters, respectively. Moreover, the fractures are filled with carbonates, quartz, sands and silts.

Faults: at three locations (LR 002, LR 002-2 & LR 005 – **Table 4.2**) fair, bad and excellent quality of faults were identified. From the fault sense features of the LR 005 normal fault (NE-SW striking direction), it was possible to analyze the paleostress direction. **Fig 4.4** shows photo of exposed normal fault plane and results of paleostress analysis. The other faults are normal conjugated fault (NE-SW striking direction) with fair fault sense features and sinistral strike slip fault (NW-SE striking direction) with bad fault sense features.

4.3.2 Within the Proposed Tendaho Reservoir and nearby the dam axis

This area will be entirely flooded by the proposed Tendaho reservoir which mainly includes the Gesye plain near to the Tendaho town. Four outcrops of regional joint sets, three fault planes and 90 meter wide exposure for scanline mapping were identified and data were analyzed accordingly. The summarized data are presented in **Table 4.3, 4.4 & 4.5** for the regional joint sets, fault planes, and scanline mapping, respectively.

Table 4.1: Regional joint sets located west of the proposed Tendaho reservoir.

Sample ID	Location		Sets	Mean Orientation		Aperture (mm)		Persistency (m)		Filling Material	Remarks
	Northing	Easting		Dir	Dip	Min	Max	Min	Max		
LR 003	1283117	708263	Set 1	043	87	1	20	2	3	S, St	Sh
			Set 2	121	80	3	18	2	Cont	St	Sh
LR 007	1286553	708013	Set 1	030	77	1	14	2	Cont	S	Sh
			Set 2	112	80	2	26	2	Cont	St	Sh
LR 024	1294652	710952	Set 1	170	67	0	12	2	4	St, S	Ex
			Set 2	047	89	4	17	2	Cont	Co	Sh
			Set 3	119	68	1	21	2	Cont	Q	Ex
LR 028	1293243	712495	Set 1	161	83	2	24	2	3	Co, Q	Ex
			Set 2	259	89	2	29	2	Cont	Co	Ex
LR 029	1293209	712464	Set 1	322	85	1	13	2	Cont	Co	Ex
			Set 2	068	80	1	19	2	4	Co	Ex
LR 040	1294403	711634	Set 1	333	72	3	23	2	Cont	Co	Ex
			Set 2	064	67	1	11	2	Cont	Co	Ex

Ex - Extensional joint; Sh - Shear joint; Cont - Continuous; Cl - Clay; S - Sand; St - Silt; G - Gravel; Co - Carbonate; Q - Quartz; and N - None

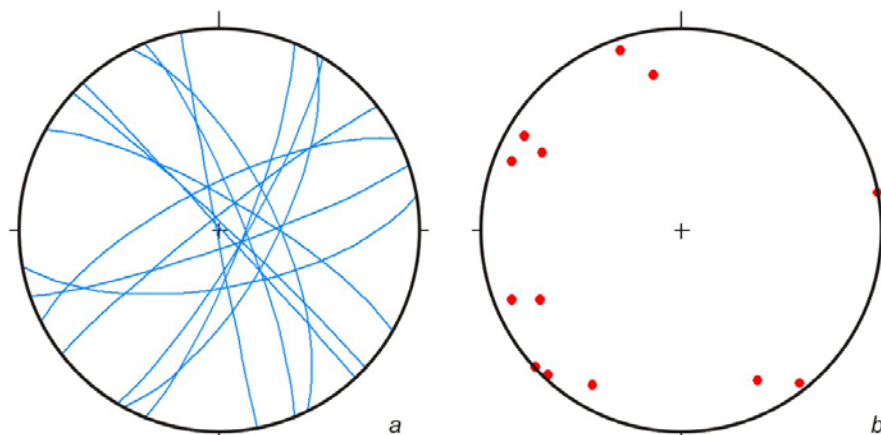


Fig 4.3: Regional joint sets of tectonic structures located at west of the proposed Tendaho Reservoir area; (a) great circle and (b) Pi-Plot.

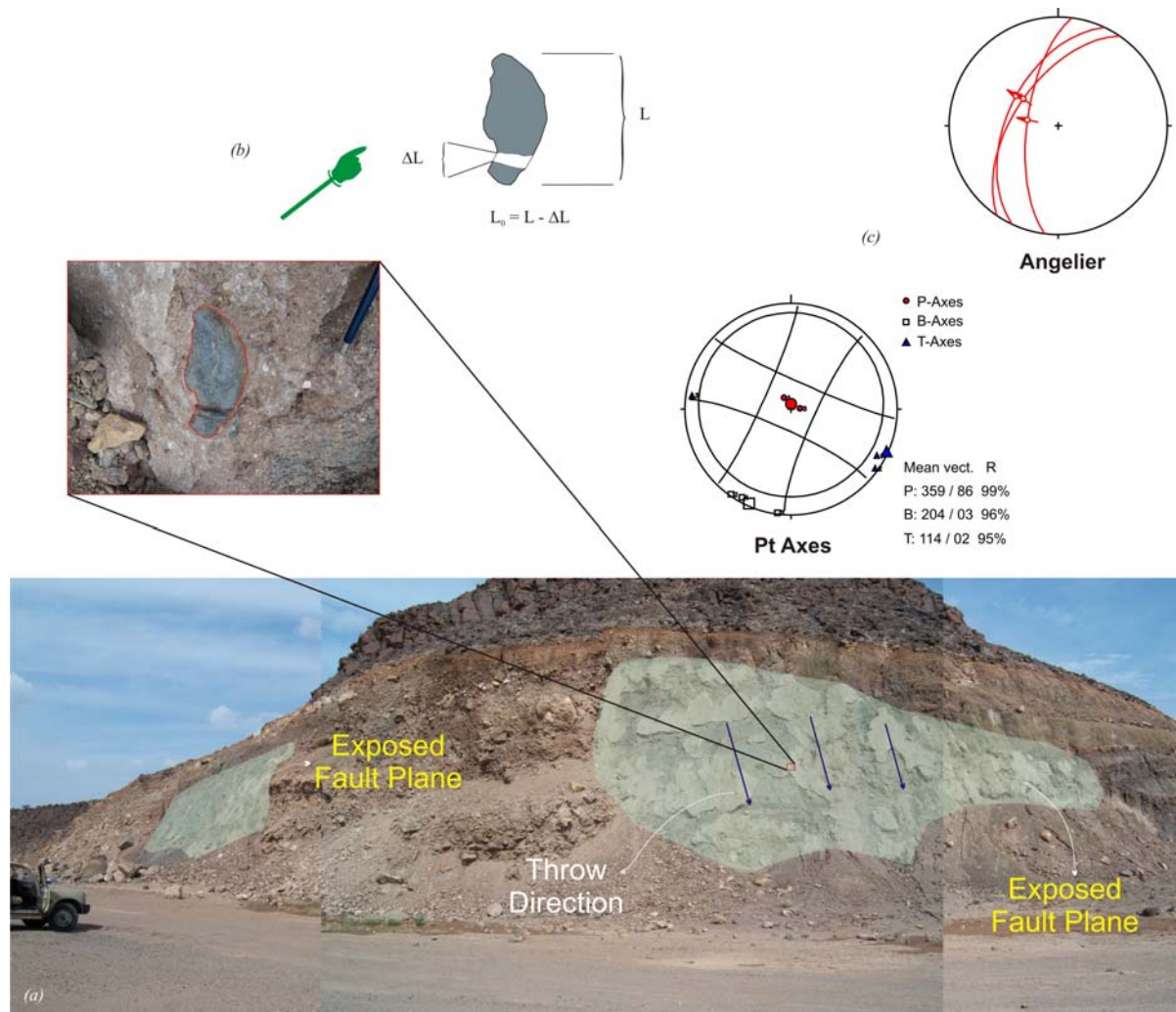


Fig 4.4: Field mapping of LR 005 fault plane (LR left reservoir - Fig 4.2): (a) Landscape shows more than 800 m lateral extent and 40 m vertical displacement; (b) stretched boulder along the sliding plane. It can be used to estimate the magnitude of the applied tectonic stress in the area; (c) paleostress analysis of fault plane using Angelier and Pt Axes methods (Angelier, 1994).

Table 4.2: Faults located west of the proposed Tendaho reservoir.

Sample ID	Location		Dip Direction	Dip Angle	Azimuth	Plunge	Sense	Quality	Remarks
	Northing	Easting							
LR 002	1283090	708634	137	80	117	81	N	F	FS
			247	89	182	83	N	F	FS,CF
			139	63	185	49	N	F	FS,CF
			203	68	179	68	N	F	FS,CF
LR 002 - 2	1283295	708733	203	68	179	65	SF	B	
			011	59	9	60	SF	B	
			137	80	117	81	SF	B	
			247	89	182	83	SF	B	
			139	63	185	49	SF	B	
LR 005	1282623	709052	295	51	304	45	N	E	FS
			304	57	308	57	N	E	FS
			277	67	281	65	N	E	FS

FP - Fault Plane; FS - Fault Striation; CF - Conjugate Fault; N - Normal Fault; DF - Dextral Slip Fault; SF - Sinistral Slip Fault; E - Excellent; G - Good; F - Fair; B - Bad

Regional joint sets: in a similar way with the previous section (*Section 4.3.1*), 2 meter minimum persistency was considered to differentiate the tectonic originated fractures with others. In this particular area, tectonic fractures (extensional and shear joints) mainly have striking orientations of NW-SE, NE-SW and few NNW-SSE direction (**Fig 4.5**) with a minimum and maximum opening of 0 and 26 mille meters, respectively. In addition, the fractures are filled with silt, sand, and few quartz, and carbonates.

Faults: at three locations (LR 001, LR 004 & LR 011 – **Table 4.4**) fair, good and bad qualities of faults were examined. Normal conjugated faults (NNE-SSW, NE-SW striking direction) with good and bad fault sense features are mapped during the field study. Moreover, sinstral strike slip fault (NNE-SSW striking direction) with bad fault sense features was also mapped.

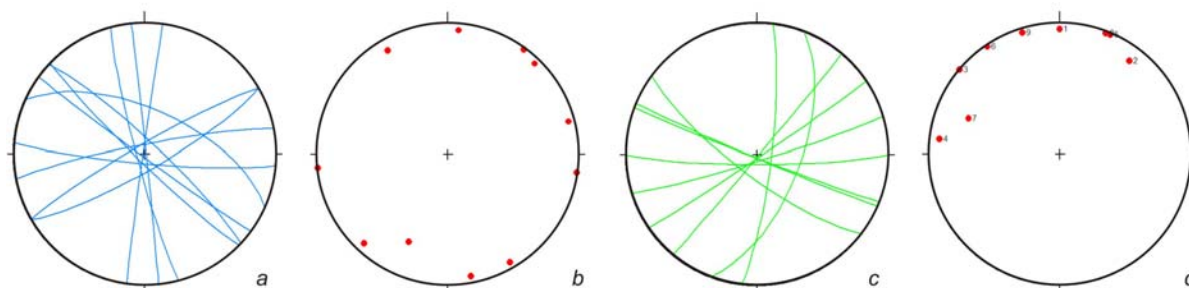


Fig 4.5: Regional joint sets (*a & b*) and scanline mapping (*c & d*) of tectonic structures located within the proposed Tendaho Reservoir area and nearby the dam axis; (*a, c*) great circle and (*b, d*) Pi-Plot.

Table 4.3: Regional joint sets located within the proposed Tendaho reservoir and nearby the dam axis.

Sample ID	Location		Sets	Mean Orientation		Aperture (mm)		Persistency (m)		Filling Material	Remarks
	Northing	Easting		Dir	Dip	Min	Max	Min	Max		
LDX 001	1292661	713185	Set 1	330	84	0	18	2	Cont	St, S	Sh
			Set 2	216	88	3	22	2	Cont	St	Ex
			Set 3	278	90	1	11	2	3	S	Ex
			Set 4	255	85	2	15	2	Cont	St	Sh
LR 006	1292039	712997	Set 1	150	80	1	26	2	Cont	Co	Sh
			Set 2	24	62	1	19	2	4	Q	Sh
RDX 001	1292445	713289	Set 1	349	84	3	17	2	Cont	St	Ex
			Set 2	43	82	5	23	2	Cont	St, S	Ex
RDX 002	1292480	713330	Set 1	84	89	1	18	2	3	S, St	Ex
			Set 2	224	85	2	12	2	Cont	St	Ex
			Set 3	185	84	1	15	2	Cont	St	Ex

Ex - Extensional joint; Sh - Shear joint; Cont - Continuous; Cl - Clay; S - Sand; St - Silt; G - Gravel; Co - Carbonate; Q - Quartz; and N - None

Scanline mapping: scanline mapping of an outcrop is used to characterize rock mass in terms of discontinuity frequency, density and spacing (Priest and Hudson, 1976, 1979, 1981). However, other parameters of discontinuity were also collected along the scanline direction. For the present study, this method was used to study the tectonic situation of the proposed Tendaho reservoir area and irrigation site. The site was selected for the scanline mapping because of its accessibility, closeness to the dam axis and wider exposure (the project authorities excavated the site for the quarry purpose). The data show the presence of two major joint sets (extensional) with striking orientation of NE-SW and NW-SE. The maximum and minimum openings were observed on either of the sets, 2 and 70 mm, respectively. Moreover, the fractures were filled with silt and sands.

4.3.3 East of the Proposed Tendaho Reservoir

East of the proposed Tendaho reservoir area includes the Megenta ridge which has approximately 18 km marginal contact with the reservoir (**Fig 4.2**). Three outcrops of regional joint sets and six fault planes were identified and data were analyzed accordingly. The summarized data are presented in **Table 4.6, & 4.7** for the regional joint sets and fault planes, respectively.

Table 4.4: Faults located within the proposed Tendaho reservoir.

Sample ID	Location		Dip Direction	Dip Angle	Azimuth	Plunge	Sense	Quality	Remarks
	Northing	Easting							
LR 001	1292041	712997	99	73	153	50	SF	F	FS
			99	77	14	62	SF	F	
			119	82	158	81	SF	F	
			122	80	182	68	SF	F	
LR 004	1287237	713492	295	76	295	76	N	G	CF
			332	88	247	64	N	G	CF
			174	86	257	68	N	G	CF
LR 011	1287383	713125	259	38	-	-	N	B	FP
			280	31	-	-	N	B	FP
			289	69	-	-	N	B	FP

FP - Fault Plane; FS - Fault Striation; CF - Conjugate Fault; N - Normal Fault; DF - Dextral Slip Fault; SF - Sinstral Slip Fault; E - Excellent; G - Good; F - Fair; B - Bad

Regional joint sets: as it was discussed in the previous section (*Section 4.3.1 & 4.32*), 2 meter minimum persistency was considered to differentiate the tectonic originated fractures with others. In this particular area, tectonic fractures (extensional and shear joints) mainly have striking orientations of NW-SE and few NE-SW direction (**Fig 4.6**) with a minimum

and maximum opening of 1 and 30 mm, respectively. Moreover, the fractures are filled with quartz, carbonates and few silt, and sand.

Table 4.5: Scanline mapping of tectonic structures located within the proposed Tendaho reservoir.

Scanline Interval (m)	Sets	Mean Orientation		Aperture (mm)		Persistency (m)		Filling Material	Remarks
		Dir	Dip	Min	Max	Min	Max		
0 - 30	Set 1	180	84	2	40	2	Cont	St	Ex
	Set 2	217	77	2	50	2	Cont	S	Ex
	Set 3	130	89	2	60	2	Cont	St	Ex
30 - 60	Set 1	097	80	1	5	2	Cont	Co	Ex
	Set 2	203	89	1	70	2	3	Q	Ex
	Set 3	146	89	2	20	2	Cont	St	Ex
60 - 90	Set 1	111	62	10	31	2	Cont	St, S	Ex
	Set 2	201	88	2	30	2	Cont	S, St	Ex
	Set 3	163	86	2	30	2	Cont	St	Ex

Ex - Extensional joint; Sh - Shear joint; Cont - Continuous; Cl - Clay; S - Sand; St - Silt; G - Gravel; Co - Carbonate; Q - Quartz; and N - None

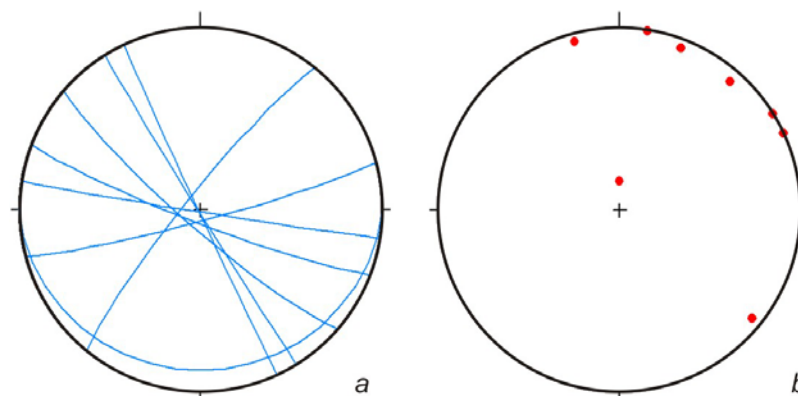


Fig 4.6: Regional joint sets of tectonic structures located east of the proposed Tendaho Reservoir area; (a) great circle and (b) Pi-Plot.

Faults: are located along the Megenta ridge which have higher cliff compare with the other flanks of the proposed Tendaho reservoir (RR 020, RR 021, RR 024, RR 025, RR 025-1 & RR 034 – **Table 4.7**). The quality of the fault sense features (normal fault) vary from bad, fair, and good with striking directions of NNE-SSW, NNW-SSE, NE-SW and NW-SE. From the fault sense features of the RR 021 normal fault, it was possible to analyze the paleostress direction (**Fig 4.12**).

4.3.4 Irrigation Canal & Manda Hararo Rift Segment

The irrigation canal and Manda Hararo rift segment are located at the margin and center of the Tendaho graben, respectively. Seven outcrops of regional joint sets and 270 meter wide

exposed outcrop for scanline mapping were identified and data were analyzed accordingly. The summarized data are presented in **Table 4.9 & 4.8** for the regional joint sets and scanline mapping.

Regional joint sets and open fractures: as it was discussed in the previous section (*Section 4.3.1, 4.3.2 & 4.3.3*), 2 meter minimum persistency was considered to differentiate the tectonic originated fractures with the others. In this particular area, tectonic fractures (extensional) mainly have striking orientations of NW-SE, and some has NE-SW, E-W and N-S direction (**Fig 4.7**) with a minimum and maximum opening of 1 and 30 mm, respectively. The fractures are filled with carbonates, quartz, clay and few silt and sand.

Moreover, open fracture was mapped along the Manda Hararo rift segment (**Fig 4.8**). The fractures have up to 3.5 meter opening and more than 4 meter depth. **Fig 4.9** shows the recent activities of the Manda Hararo rift segment near to the Dubti town. The ground was uplifted by magmatic mud pressure with 1.5 meter height and continuous geothermal vapor release was also observed.

Table 4.6: Regional joint sets located east of the proposed Tendaho reservoir.

Sample ID	Location		Sets	Mean Orientation		Aperture (mm)		Persistency (m)		Filling Material	Remarks
	Northing	Easting		Dir	Dip	Min	Max	Min	Max		
RR 004-J	1279775	714560	Set 1	201	84	2	23	2	3	Co, Q	Ex
			Set 2	245	89	1	14	2	Cont	St, S	Ex
			Set 3	180	13	1	11	2	Cont	St	Ex
RR 035	1273595	713128	Set 1	309	83	1	20	2	Cont	Co	Ex
			Set 2	238	89	4	19	2	3	Q	Ex
			Set 3	189	89	3	26	2	Cont	N	Ex
RR 036	1273411	713158	Set 1	221	82	2	27	2	Cont	N	Ex
			Set 2	165	85	1	30	2	Cont	N	Ex

Ex - Extensional joint; Sh - Shear joint; Cont - Continuous; Cl - Clay; S - Sand; St - Silt; G - Gravel; Co - Carbonate; Q - Quartz; and N - None

Scanline mapping: this method was applied along the lacustrine deposition with the objective to study the rifting activities in the past 1-10 ky. The data show the presence of one major joint set (extensional) with striking orientation of NW-SE and three minor joint sets N-S, NE-SW and E-W. The maximum openings were observed on the major joint set about 200 mm and the minimum openings were concentrated along the minor joint sets. Moreover, the fractures were mainly filled with carbonates, quartz, clay and some silt and sands (**Fig 4.10**).

Table 4.7: Faults located east of the proposed Tendaho reservoir.

Sample ID	Location		Dip Direction	Dip Angle	Azimuth	Plunge	Sense	Quality	Remarks
	Northing	Easting							
RR 020	1281026	715031	90	77	167	62	N	F	FS
			268	89	187	73	N	F	
			114	84	23	68	N	F	
			294	87	25	80	N	F	
			266	89	350	81	N	F	
RR 021	1281021	715042	281	82	10	77	N	G	FS
			276	77	5	70	N	G	FS
			300	86	29	70	N	G	FS
			285	86	357	73	N	G	FS
			282	79	9	69	N	G	FS
			283	80	4	73	N	G	FS
			288	84	22	73	N	G	FS
RR 034	1273629	713078	191	68	156	41	N	B	
			221	76	112	59	N	B	
			198	77	126	58	N	B	
RR 024	1283161	715478	286	73	351	68	N	B	
			282	71	9	68	N	B	
RR 025	1283772	715680	287	71	-	-	N	F	FP
			291	73	-	-	N	F	FP
			295	75	-	-	N	F	FP
RR 025 -1	1285035	715824	240	89	149	71	N	F	
			242	87	151	73	N	F	

FP - Fault Plane; FS - Fault Striation; CF - Conjugate Fault; N - Normal Fault; DF - Dextral Slip Fault; SF - Sinistral Slip Fault; E - Excellent; G - Good; F - Fair; B - Bad

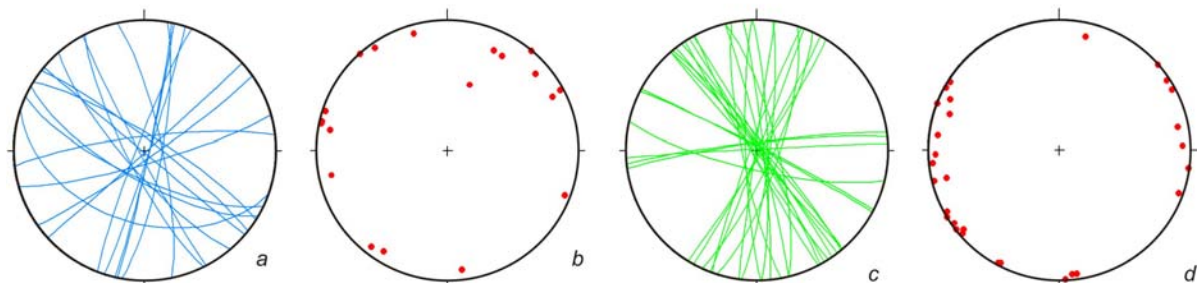


Fig 4.7: Regional joint sets (a & b) and scanline mapping (c & d) of tectonic structures located within the irrigation canal, 1.5km west of the Tendaho dam axis; (a, c) great circle and (b, d) Pi-Plot.



Fig 4.8: SEM 003, Extension fracture at the center of Tendaho Graben. **Fig 4.12** for the location of the site.

Table 4.8: Scanline mapping of tectonic structures located within the irrigation canal, 1.5km west of the Tendaho dam axis.

Scanline Interval (m)	Sets	Mean Orientation		Aperture (mm)		Persistency (m)		Filling Material	Remarks
		Dir	Dip	Min	Max	Min	Max		
0 - 30	Set 1	108	76	1	18	2	3	Co	Ex
	Set 2	193	78	1	34	2	3	Co	Ex
	Set 3	50	84	1	81	2	Cont	Co, Q	Ex
	Set 4	259	81	1	35	2	Cont	Co, Q	Ex
30 - 60	Set 1	290	86	0	10	2	Cont	Cl	Ex
	Set 2	61	87	0	63	2	Cont	Q	Ex
60 - 90	Set 1	111	89	0	29	2	Cont	Q, Co	Ex
	Set 2	242	87	3	82	2	Cont	Co	Ex
90 - 120	Set 1	354	85	1	-	2	Cont	Cl	Ex
	Set 2	278	89	1	-	2	Cont	Q	Ex
	Set 3	59	89	5	83	2	Cont	N	Ex
120 - 150	Set 1	97	82	20	70	2	Cont	N	Ex
	Set 2	88	83	21	-	2	Cont	Co	Ex
	Set 3	352	85	0	60	2	Cont	Co, Q	Ex
	Set 4	237	87	0	100	2	3	Co	Ex
150 - 180	Set 1	357	89	3	20	2	Cont	Q	Ex
	Set 2	268	83	2	30	2	Cont	Co	Ex
	Set 3	119	88	1	13	2	Cont	Co, Q	Ex
	Set 4	229	89	1	35	2	Cont	Q	Ex
180 - 210	Set 1	115	80	1	-	2	Cont	Co	Ex
	Set 2	27	87	1	9		Cont	Co	Ex
	Set 3	76	77	1	25	2	3	Co, Q	Ex
	Set 4	55	87	1	150	2	Cont	Co, Q	Ex
210 - 240	Set 1	76	87	4	10	2	Cont	Cl	Ex
	Set 2	49	87	5	200	2	Cont	N	Ex
240 - 270	Set 1	122	87	18	65	2	Cont	N	Ex
	Set 2	28	88	1	125		Cont	Co	Ex
	Set 3	84	86	1	75	2	Cont	Co, Q	Ex
	Set 4	52	89	1	180	2	Cont	Co	Ex

Ex - Extensional joint; Sh - Shear joint; Cont - Continuous; Cl - Clay; S - Sand; St - Silt; G - Gravel; Co - Carbonate; Q - Quartz; and N - None

4.4 Result

Based on the above conventional methods, data and interpretation of remote sensing and DEM datasets in the previous chapter (*Chapter 3*), the study area is classified into two major tectonic *elements*; (1) Gesye Graben and (2) Tendaho Graben.

4.4.1 Gesye Graben

The name, Gesye Graben is derived from the wide flat plain called Gesye plain. It is found at the center of the Tendaho reservoir. In the previous studies (Acton et al., 2000; Thurmond

et al., 2007; Acocella et al., 2008), this plain was considered as part of the Tendaho Goba'ad Discontinuity TGD ridge, in general. However, during the present study, based on the result of adopted methodologies and data used, it is interpreted as a graben structure. It has a wider opening and NE orientation at the Gesye plain (about 9 km) and it narrows (3km) and slightly turned to NNW orientation near to the Tendaho dam axis. This is due to the propagation of Red Sea structures in sinistral sense of movement.

Table 4.9: Regional joints sets located within the irrigation canal, 1.5km west of the Tendaho dam axis.

Sample ID	Location		Sets	Mean Orientation		Aperture (mm)		Persistency (m)		Filling Material	Remarks
	Northing	Eastings		Dir	Dip	Min	Max	Min	Max		
IC 001	1293622	713653	Set 1	210	72	2	26	2	Cont	Q	Ex
			Set 2	100	79	2	30	2	3	Co	Ex
			Set 3	138	90	3	15	2	Cont	Co, Q	Ex
			Set 4	78	79	1	20	2	Cont	Q	Ex
IC 002	1294101	714016	Set 1	38	83	1	19	2	Cont	Co	Ex
			Set 2	145	85	1	27	2	Cont	Co	Ex
IC 022	1294068	714212	Set 1	102	87	4	15	2	Cont	Co, Q	Ex
			Set 2	229	78	2	26	2	3	Co, Q	Ex
			Set 3	164	82	1	12	2	Cont	Cl	Ex
IC 028	1294036	713697	Set 1	353	81	1	17	2	Cont	Q	Ex
			Set 2	32	80	3	21	2	Cont	Q, Co	Ex
			Set 3	103	87	3	24	2	Cont	Co	Ex
IC 031	1294052	713740	Set 1	291	85	1	29	2	Cont	Cl	Ex
			Set 2	242	87	3	13	2	3	Q	Ex
			Set 3	199	44	1	19	2	3	N	Ex
IC 032	1294070	713809	Set 1	243	79	1	23	2	Cont	N	Ex
			Set 2	205	73	1	11	2	Cont	Co	Ex
			Set 3	108	87	1	19	2	Cont	Co, Q	Ex
RR 037	1292653	713854	Set 1	220	89	2	16	2	Cont	Co	Ex

Ex - Extensional joint; Sh - Shear joint; Cont - Continuous; Cl - Clay; S - Sand; St - Silt; G - Gravel; Co - Carbonate; Q - Quartz; and N - None



Fig 4.9: A Ground uplifted in February, 2008 by 1.5 m height with continued release of geothermal vapors along the active Tendaho Rift Axis (TG 001); and B new geothermal spot (TG 002, TG 003). See Fig 4.2 for the location of the site.

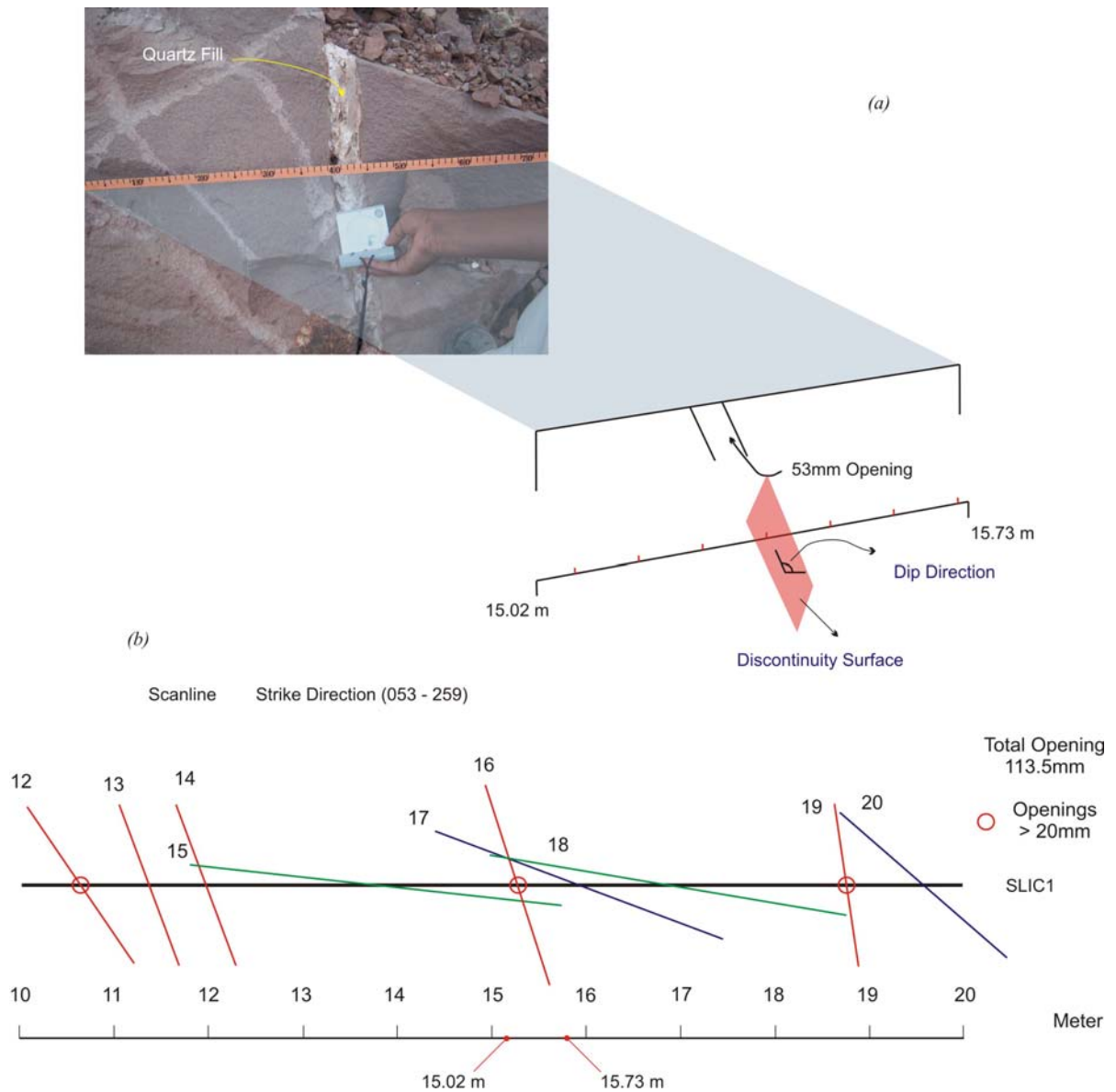


Fig 4.10: Scanline Mapping of lacustrine deposit along irrigation canal: (a) photo shows scanline alignment and how to collect data of tectonic feature (dip direction, filling material and aperture width); (b) SLIC1 (Scanline Irrigation canal 1) between 10 – 20m and their discontinuity parameters.

The graben was formed during the propagation of the Main Ethiopian Rift structures into the Afar depression. This followed magmatic basalt injection at the center of the graben and later, the propagation of the Red Sea Rift structures crosscut the graben with NW-SE striking oblique strike slip structures. **Fig 4.11** shows topographic profile of Gesye graben from point B to B' (**Fig 4.12**).

A total of twelve faults, six at the left side (East) and the remaining six along the right side (West) of the proposed Tendaho reservoir, have been identified. The faults have a normal sense of movement except the RR 034 FP which is an oblique strike slip. The exposed outcrops of fault surface vary in aspects related to sense of slip features. A clear striation

type of sense of slip features found only at three of the mapped faults. On the other surface, the slip features couldn't be able to differentiate very well because of the effect of weathering and quaternary deposition.

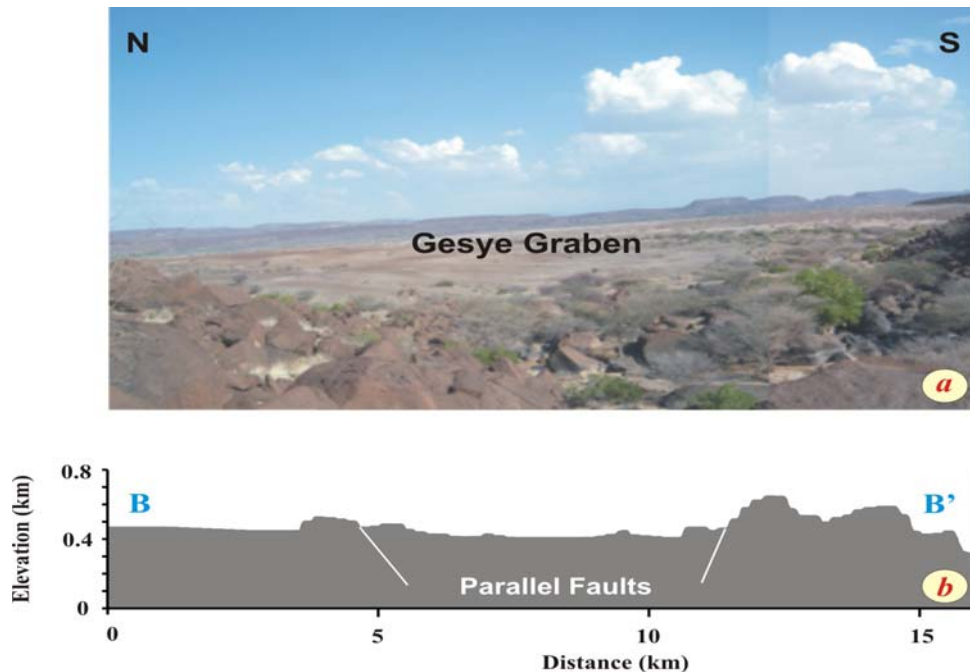


Fig 4.11: Gesye Graben: A Photo shows the Tendaho Reservoir which lay at the center of the Gesye Graben, B Topographic profile of the graben from point B to B'. **Fig 4.12** shows the location of the profile BB'.

Paleostress analysis of outcrops LR 004, LR 005 and RR 021 were conducted with Angelier approach (Angelier, 1994). The first two outcrops are located at the left side (East) of the proposed Tendaho reservoir about 13 km far from the Tendaho dam axis to the south. Based on the applied approach for LR 004 & LR 005, the paleostress analyses of the outcrops indicate that the normal faults (NE-SW striking orientation) are formed due to the NW-SE oriented extensional forces. Moreover, the analyses for the RR 021 outcrop also indicate the same extensional direction (NW – SE). Most of the other fault planes have an orientation of NNE/NE – SSW/SW striking direction. And the RR 034FP outcrop has NW-SE orientation and its sense of movement show an oblique strike slip fault. **Fig 4.4** shows the LR 005 outcrop and its sense of slip analysis. And **Fig 4.12** shows the result of outcrop analysis.

Mostly, two sets of regional joint settings (NW-SE & NE-SW) were identified from the field study of the Gesye graben. The outcrops are located at the left(East) and right (West) side of the reservoir, along the irrigation canal and within the Tendaho graben. The joint sets have striking direction of NE – SW and NW – SE directions especially outcrops which are located at the opposite sides of the reservoir (see **Fig 4.12**). At two sites (about 10km south of the Tendaho dam axis) RR 004FP and RR 006FP, blocks are rotated because of the

tectonic activities. The orientations of the basalt flow were collected to investigate the direction of block rotation and its implication. The result is presented at **Fig 4.12** and it is related with the formation of strike slip faults long the right flank of the reservoir.

Apart from the individual outcrop examination of joint settings, an attempt was made to study the dominant joint sets and find extensional indicators within the Gesye graben. With this objective, scanline mapping of an outcrop (SLLR 001) of 90 meter long which is located 1.5 km southwest far from the dam axis was conducted. The result indicates three joint sets with striking orientation of NE –SW, E –W and NW – SE (**Fig 4.5**). But the joint opening doesn't show any systematic extensional indicators (**Table 4.5**).

4.4.2 Tendaho Graben

According to Beyene & Abdelsalam, 2005, the Tendaho graben is a part of the third order tectonic events in the Afar depression. It is the youngest event in the study area when compared to the Main Ethiopian Rift and Red Sea Rift structures. The interpretation of remote sensing and DEM data sets show the dominant NW-SE striking structures and the quaternary deposition and volcanoes. As it was discussed in the previous chapters (*Chapter 2, 3*), the graben is one of the most stretched/opened graben within the ECB (Eastern Central Block). The proposed Tendaho irrigation structures are built within the graben near to the active Manda Hararo and Tendaho rifting axis.

Because of the geothermal resources, the 1969 earthquake event at Serdo, the existing Tendaho irrigation scheme and its accessibility to the capital city of Afar (Asayta – *the old* and Semera – *the new*), the Tendaho graben is studied in the past by some scientists from different aspect (Aquater, 1996; Kebede et al., 1989; Acocella et al., 2008). Keeping all published and unpublished research results; effort was made to understand the tectonic activities of the graben from the lacustrine deposition, extension fractures and uplift of ground near to the geothermal spot.

In the first and second field study time, Spring season of 2007 and 2008 extension fractures and uplift of ground were documented. The extension fractures are located at 4 km northeast far from the Semera town in the north direction. Parallel fractures with 3.5 meters wide and 4 meters deep have NW – SE striking directions (see **Fig 4.12**). At some places the fractured blocks are slightly rotated as it is shown in **Fig 4.8**. Ground uplift was observed nearby the

assumed active Tendaho rifting axis (Manda Hararo Rift) (Sigmundson, 1992; Acocella et al., 2008). **Fig 4.9** shows the ground uplift and geothermal spot at the location of TG 001 and TG 002.

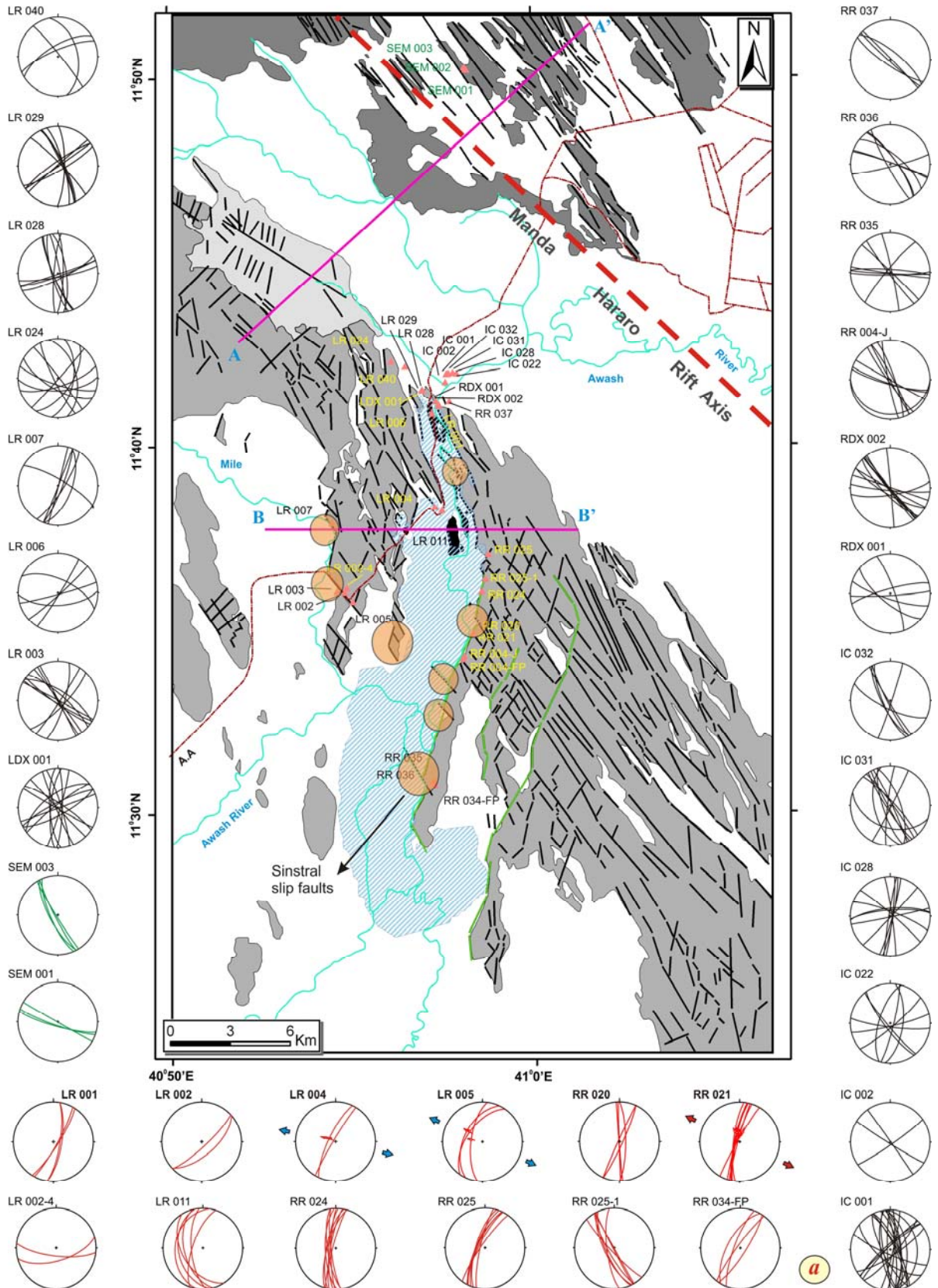


Fig. 4.12 Cont.....

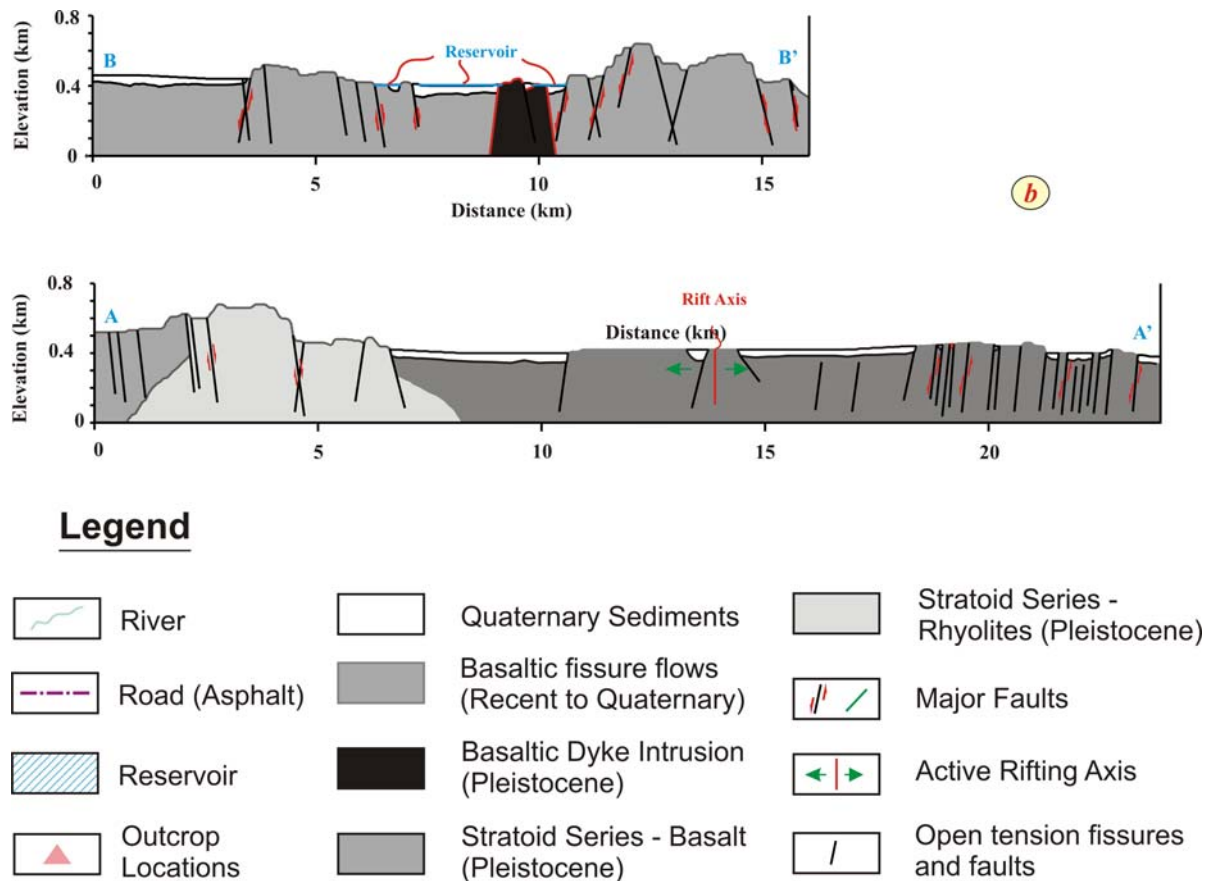


Fig 4.12: Tectonic structure of Gesye Graben: (a) Geological map of the Tendaho reservoir and its vicinity are presented with the stereonet projections of regional joint sets (black), fault planes (red), block rotation (blue) and fissure crack (green); (b) Geological cross sections along point AA' and BB' (borehole data are used from Aquater, 1996 and IPCC, 2005). See **Appendix A-5** for higher resolution.

During the first field studies in the graben (Spring 2007), scanline mapping of an outcrop located within the lacustrine deposit and 0.8km east of the Tendaho dam axis were conducted to study the tectonic activities in the Holocene time. A total of 270 m continuous mapping was done along the excavated irrigation canal line. The outcrop is close to dam axis and accessible from the project sites.

Along the scanline alignment; orientations, opening/aperture and filling materials of the joints were collected. Care was taken during the mapping of tectonic originated joints to avoid any ambiguities with others. It was only collected joints which have an extent of more than 2 meters. The data were organized and analyzed with the *Tectonics FP* software. The result shows that NW – SE striking joints are the dominant structures (**Fig 4.7**) along the irrigation canal. The joints have a maximum and minimum opening of 200mm and 1mm, respectively. The total sum of the joints opening is about 5.093 meters of the 270 meters long outcrop. **Fig 4.7** shows the result of scanline mapping along the irrigation canal.

4.5 Discussion

Based on the interpretation of remote sensing and DEM datasets, field mapping of tectonic features, laboratory examination of micro structures and previous research studies; the following tectonic situation of the site is understood. The most recent researches by Thurmond et al., 2007 and Acocella et al., 2008 repeated as the older Main Ethiopian rift structures are cross cut by the younger Red Sea rifting propagation structures along the Tendaho Goba'ad Discontinuity TGD ridges. However, in the present study, it is observed that during the propagation of the Main Ethiopian rift structures towards the Afar depression, Gesye graben was formed due to the NW-SE extension of the rift and a dyke was intruded at the center of the graben. Moreover, stretching indicators of the Tendaho graben in the Holocene series was observed from the lacustrine deposition. The schematic models of the tectonic events are illustrated at **Fig 4.13**.

A. *The Main Ethiopian Rift (MER) Structures (D1)*

Two major geologic events were happened during the time of the Main Ethiopian Rift structures propagate towards the Afar depression, particularly in the present study area. At the initially stage, the MER structures were formed due to NW-SE extension of tectonic forces and later on at the center of the rift, a basaltic dyke was intruded. Conjugate normal faults are formed at the either side of the Tendaho reservoir. From the geological map of Gesye graben (**Fig 4.9**), it is clearly seen that the MER structures are highly pronounced at the first 17 Km and then it decreases going further. This event is illustrated at **Fig 4.13** as tectonic events D1-1. Injections of magma are mostly found in the Afar depression as some authors discussed the situation (Rowland et al., 2007; Keir et al., 2009). In a similar way, at the center of the Tendaho reservoir a total of 2.3 km² exposed basaltic dyke is present. The petrographic thin section analysis show the basalt is composed of very fine grained plagioclase, rich in feldspar and opaque minerals. This situation is illustrated at **Fig 4.13** as tectonic event D1-2 which represents the intrusion of basaltic dyke at the center of Gesye graben or Tendaho reservoir.

B. *Propagation of the Red Sea Rift Structures (D2)*

The propagated Red sea rift structures cross cut the older MER structures almost at 90⁰ and it has NW – SE striking orientation. As it was observed by previous authors (Tapponier et

al., 1990; Sigmundson, 1992; and Manighetti et al., 2001, Tesfaye, 2005), similar bookshelf tectonic model is accepted for these structures along the TGD ridge. An oblique sinistral strike-slip faults are the dominate structures at the ridge and minor normal faults conjugate to the main structures are also observed from the interpretation of the remote sensing and DEM datasets. The structures are covered by the lacustrine deposition at the center of the Tendaho reservoir. However, at both side of the reservoir and along the intruded dyke, the structures are continued perfectly with the same orientation. At **Fig 4.13**, this tectonic event is presented as D-2 and its schematic model is also presented in the figure.

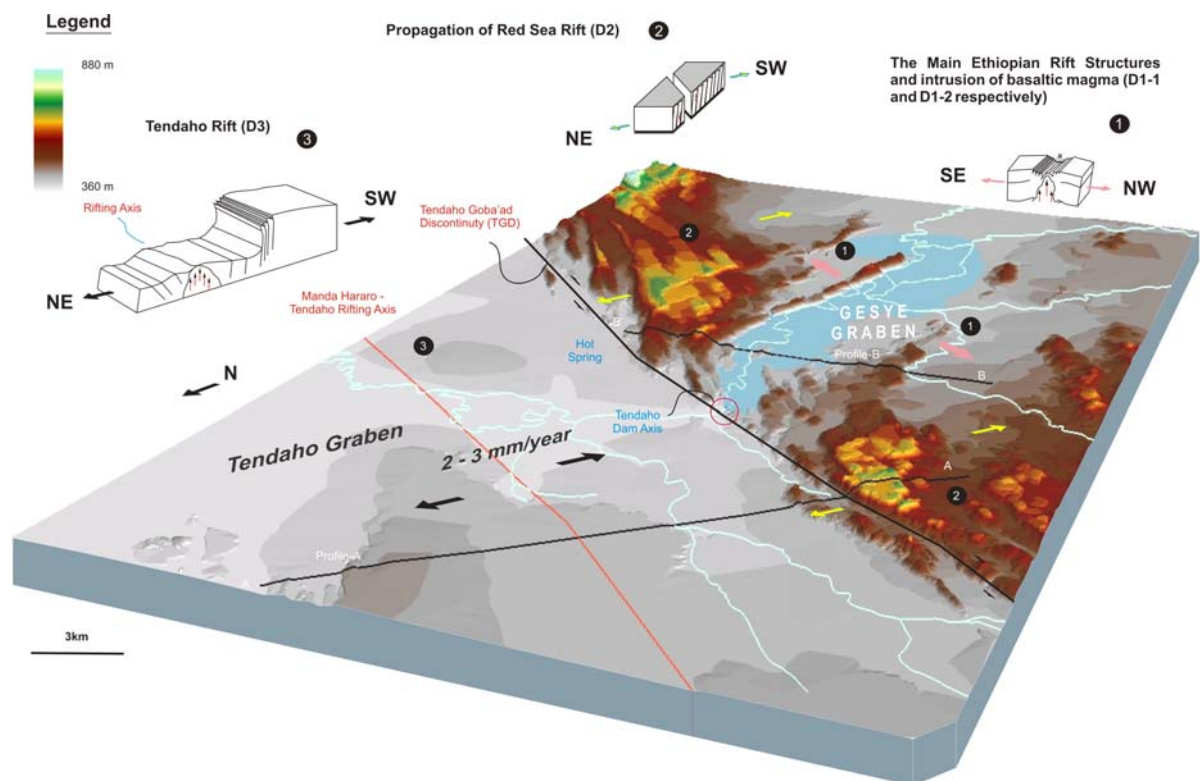


Fig 4.13: Schematic Model of Extensional Tectonics at Tendaho Dam and Irrigation Site (20 m contour interval) (Solomon et. al, 2008). (1) Main Ethiopian Rift MER (Normal Fault and uplift by dyke intrusion); (2) Propagation of Red Sea Rift and stretching to NE - SW direction; and (3) Tendaho Rift (Normal fault, fissure cracks and uplift). See **Appendix A-6** for higher resolution.

C. The Tendaho Graben Structures (D3)

The Tendaho graben is one of the most stretched and active graben structures within the East Central Block of the Afar depression (Beyene & Abdelsalam, 2005). The detail study of the graben is beyond the objective of the present study. However, as it was mentioned in the previous chapters, the graben was opened due to the NW – SE extensional forces of the far field stress regime. Acocella et al., 2008 explained the spreading rate of the graben from the known two rifting axis (Tendaho rifting 3.6 mm/year and Manda Hararo rifting 1.2

mm/year). For both spreading rates calculations, the authors main focus was on the stretching evidences which were available at the stratoid and fissure basalts. However, in the present study, it is observed that there was extension or stretching in the Holocene series. These data (regional joint sets) were found from the lacustrine deposition which is located near to the dam axis. This tectonic event is described as D-3 (deformation event 3) in **Fig 4.13**.

Chapter Five

Active Rifting Hazards

5.1 Introduction

There had been much debate in the past on the origin of the rift structures whether these are compressional or extensional. Nowadays, it is accepted that the extensional tectonics is the mode of development or mechanism of these formations (Olsen & Morgan, 1995). According to Olsen & Morgan, 1995 continental rift is defined as an elongate tectonic depression associated with which is the entire lithosphere which has been modified in extension. However, this definition excludes closely related extensional structures like simple graben, highly extended terrain and passive margins. In addition, pull apart basins, volcano-tectonic depressions and continental flood basalt provinces are described by the authors as “pseudorifts”.

Sengör in 1995 used three ways to classify the continental rift – *geometric*, *kinematic* and *dynamic* (Miall, 2002). Each classification has its own subdivision, like “active” and “passive” subdivisions which are parts of the dynamic way of continental rift classification. *Active rifting* is defined as rifting in response to a thermal upwelling of the asthenosphere, where the causative stresses for rifting are directly or indirectly associated with lateral thermal density variations in the lithosphere and the underlying asthenosphere. In *active rifting* the lithosphere is thermally thinned by heating and absorption into the asthenosphere, in addition to necking in response to extension, and hence the volume of asthenosphere rising into the lithosphere exceeds the volume of lithosphere displaced laterally by extension. *Passive rifting* is defined as rifting in response to a regional stress field, usually assumed to originate from remote plate boundary forces. In *passive rifting*, the lithosphere is

thinned only in response to extension. Fig 5.1 illustrates the two contrasting causative mechanisms (Sengör and Burke, 1978; Olsen and Morgen, 1995).

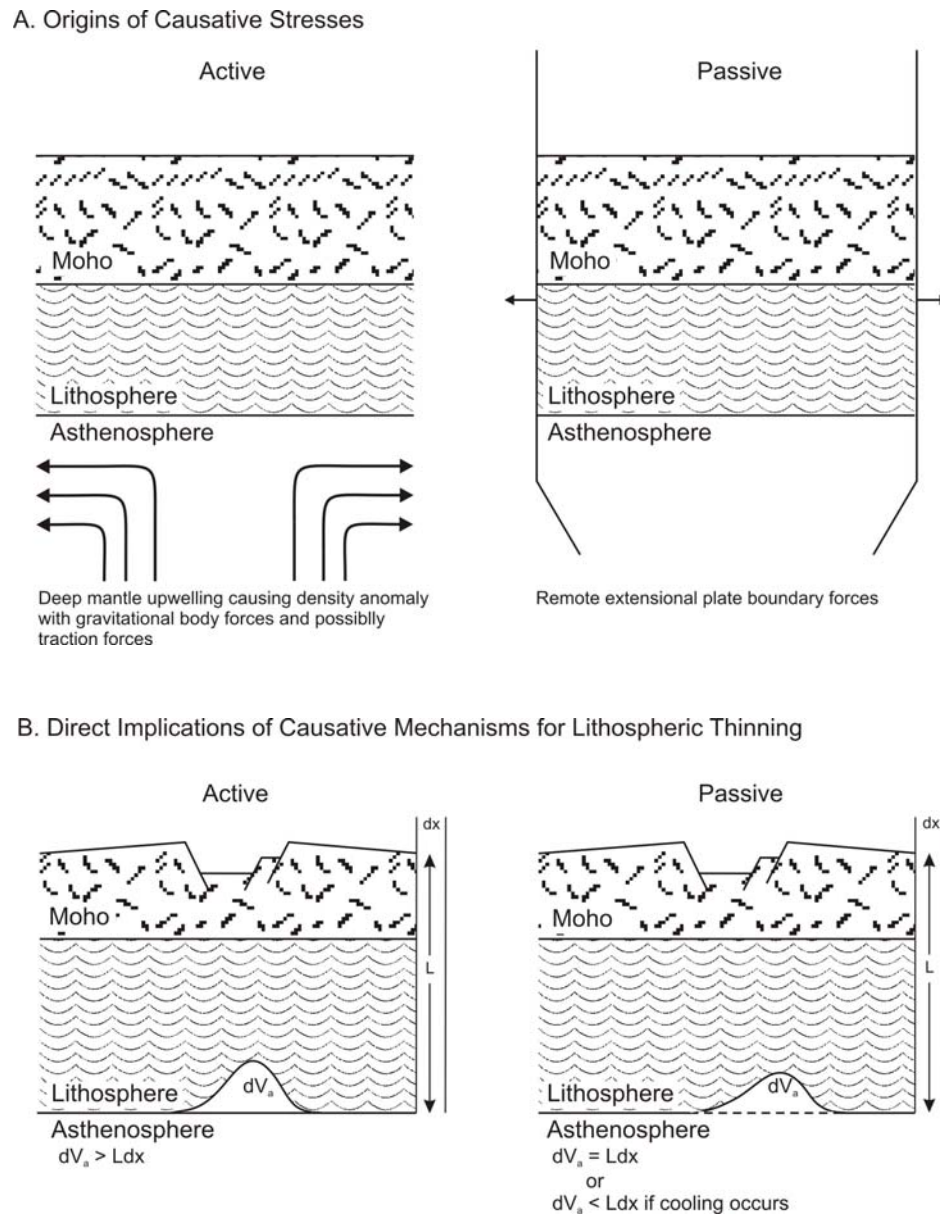


Fig 5.1: Highly simplified end-member models of the causative or initiating mechanisms of continental rifting (Olsen and Morgen, 1995).

One of the significant or important reason for studying rift zones and rifting processes is its potential natural hazards such as earthquakes, volcanism, crack, ground deformation and others. As it was discussed in the previous chapter (*Chapter two*), in order to estimate the risk of natural hazard phenomena, it is wise to know the nature of the hazard itself at the beginning. Because, the magnitudes of the hazard and the vulnerability of the site at risk determine the level of the risk. Under this chapter the potential occurrences of the active rifting hazards at the proposed Tendaho reservoir and irrigation site will be discussed.

The potential occurrence of seismic hazard at a particular site can be analyzed through statistical approaches. Depending on the nature of the available data a discrete or continue probability concepts can be used to predict the seismicity hazard. Klugel et al., 2006 proposed a scenario-based procedure for seismic risk analysis which is based on probabilistic interpretation of deterministic or scenario-based hazard analysis. Moreover, many authors (Wells and Coppersmith, 1994; Klügel et. Al., 2006) used the available data statistically to predict the potential occurrence and magnitude of seismic hazards. However, for geohazards, which had limited events of occurrence in the past, researchers have used simplified methods to predict the occurrence of their potential hazard. Crowe, 1986 considered the major variables (the structure of magma feeder system, the magma fragmentation and dispersal energy of eruption) which affect the volcanic hazards at the disposal site of high-level radioactive waste of the Hanford, south Washington and the Nevada test site, southern Nevada to assess the volcanic hazard. For the present study, the potential occurrence of active rifting hazard in the life time of the proposed Tendaho reservoir and irrigation scheme has been analyzed based on the assumptions of its formation/development.

5.2 Assumptions of Rift Development

As it was discussed in the previous chapters (*Chapter two & four*), the Tendaho graben is one of the most stretched graben in the Afar depression. Two forces are acting in the depression which opened/stretched the entire region; a far field stress exerted as a result of the Eurasian and the Arabian Plates convergence along the Zagros Orogenic Front and the upwelling mantle plume since 30 million years ago (Barbara, 1975; Variet, 1978; Beyene & Abdelsalem, 2005). **Fig 5.2** indicates the pattern of tectonic structures and lithological similarities considered as indicators to describe how long the graben is stretched by the Tendaho and Manda Hararo active rifting processes in the past 1.8Ma.

If the silicic lava – rhyolite (Lahitte, 2003) are taken as cursor indicator of the graben opening, the graben will have 50 km wide width. In a similar way, 60 km wide width could be measured if the inter fingered MER and the Red Sea rift structures, which are located at both side of the graben, are taken as stretching indicator. The active rifting hazard analysis is based on the ways of the graben opening; either with constant spreading rate or violent rifting episodes or both.

5.2.1 Constant Spreading Rate

With the extensional deformation mechanisms, rifts can be opened by a constant or average spreading rate due to remote extensional plate boundary forces and deep mantle upwelling causing density anomaly with gravitational body forces and possibly traction forces (Olsen & Morgen, 1995; Ebinger and Casey, 2001). Recently, Acocella et al., 2008 studied the extension or spreading rate of the Tendaho graben from remote sensing and field analysis.

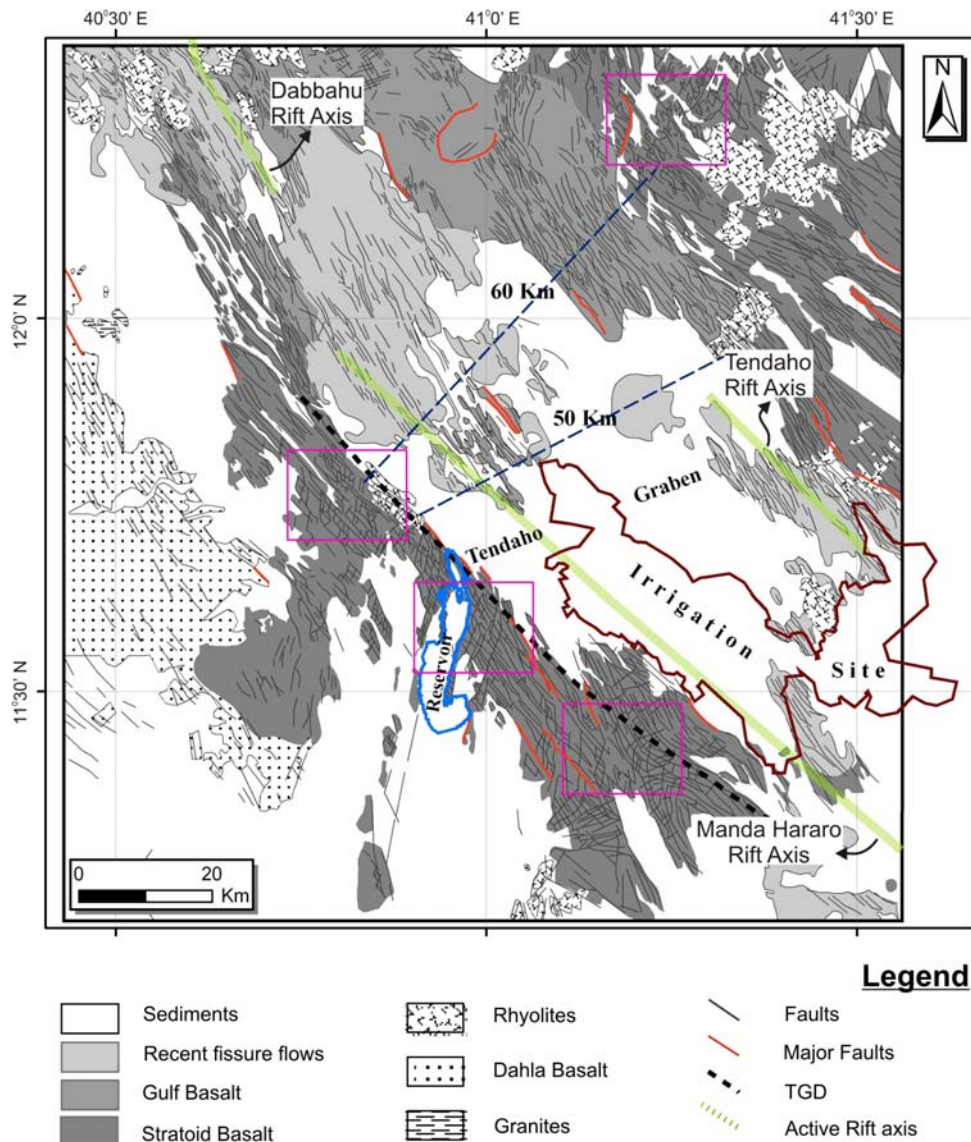


Fig 5.2: Geological Map of the Tendaho graben (after Thurmond, 2006). The purple rectangles indicate the inter-fingered MER and propagated Red sea rift structures. See **Appendix A-7** for higher resolution.

According to their findings, the Tendaho Graben has a stretching factor $\beta \sim 1.1$ and an extension rate of ~ 3.6 mm/yr with a total of 5km opening. It is mainly developed between 1.8 - 0.6 Ma, contemporaneously to the Afar Stratoids in the area, which become older toward the TGD sides. The Manda Hararo Rift marks the active site of extension within TG in

the last 0.2 Ma. Before terminating in the Dubti area, MHR has a stretching factor $\beta \sim 1.04$ and extension rate ~ 1.2 mm/yr with an average of 240m stretching.

$$\beta = \frac{\text{Stretched width of the graben}}{\text{Original width of the graben}} \dots\dots\dots (5.1)$$

Where β – stretching factor

5.2.2 Violent Rifting Episodes

Ebinger, 2006 said that “an average day in the life of an East African rift is tectonically boring: the African and Somalian plates separate at about the same rate as fingernail growth ~ 0.03 millimeters a day. But occasionally earthquakes and volcanic eruptions remind us of an immense force at work”. A violent rifting episode occurred at the Dabbahu rifting segment in September, 2005. It is located 95 km north of the present study area. This violent rifting episode is a part of the Red sea rift propagator structures (Manda Hararo Rift segment) which propagates towards the center of the Afar depression (*the study area*) along the SE direction. Results from InSAR, seismology and geodetic suggest that a rift segment of length > 60 km was activated in September 2005 with a maximum opening of 8 meters (Wright, 2006; Ayele, 2007a; Hamling et al., 2007; Ebinger, 2008; Keir, 2009) by a single violent rifting episodes. **Fig 5.3** shows photo of volcanic vent and the interferometric image of the Dabbahu near surface magmatic injection.

Fault dynamics research group, 2007 compared the Dabbahu rift to the nearby Dobi rift located to east of the present study site (Rowland, 2007). Surface rupture was measured only 1m during the 1989 Dobi rifting event. However, the maximum earthquake magnitude at Dabbahu and Dobi was 5.6 and 6.3, respectively.

The difference in the surface rapture came from the magma injection near the surface at the Dabbahu rifting. Similar situations were experienced at Krafl rifting episode in northern Iceland during 1975 – 1984 and the 1978 Asal-Ghoubbad diking event (Buck et al., 2006; Ebinger et al., 2008).

Similar to the Dabbahu rifting structures, extensional fractures are available within the Tendaho graben. During the field studies such structures were mapped and discussed in the previous chapter (**Fig 4.11 Chapter Four**). Acocella et al., 2008 mapped an extensional

fractures with an opening varying from 1 – 10m and near the Semera town an opening up to 4m was measured during the Spring 2008 field studies in the area.

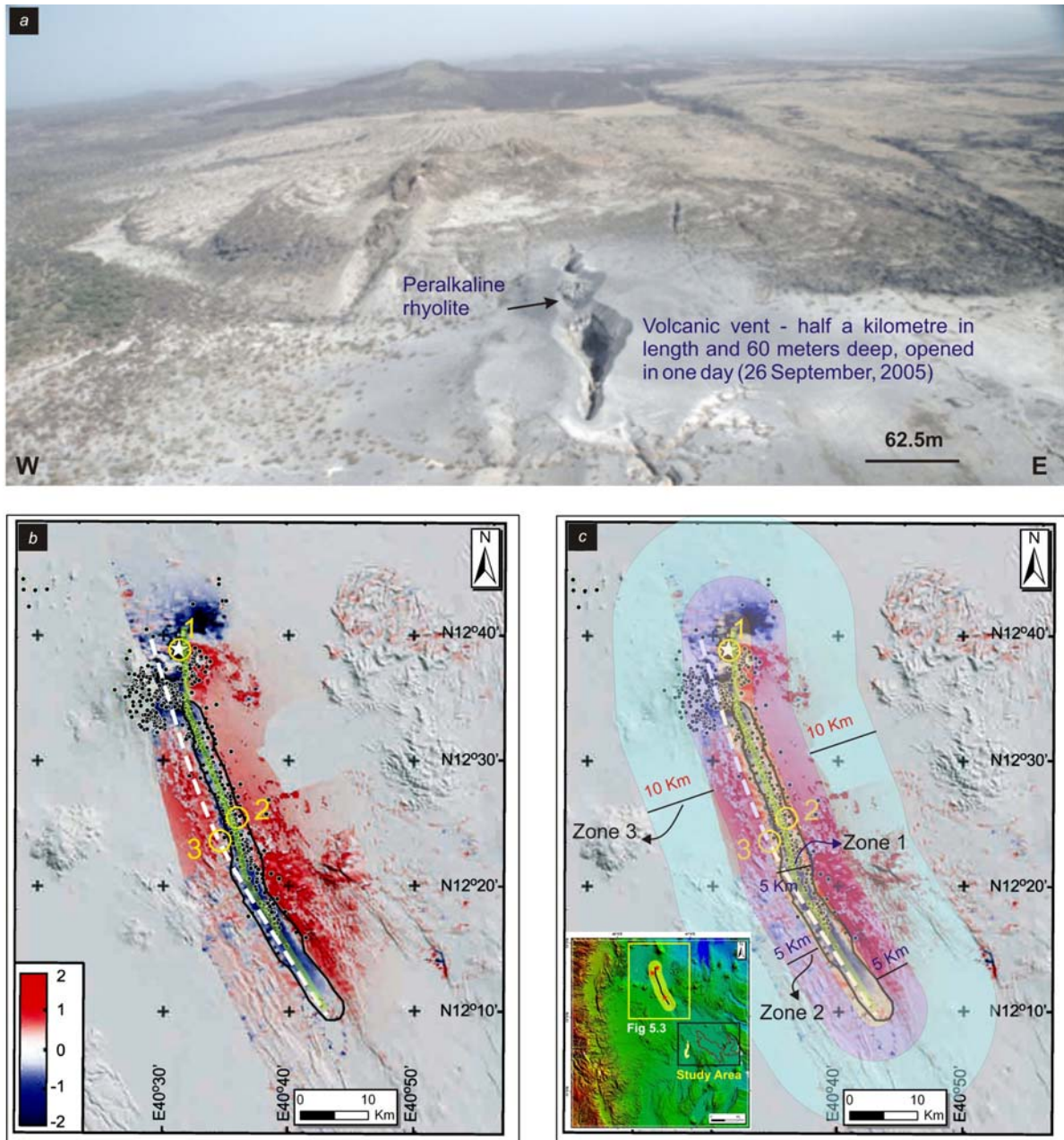


Fig 5.3: Radar interferometric image and aerial photograph of violent rifting episode of Dabbahu rifting – September, 2005 (Rowland, 2007). (a) Oblique aerial photograph of the vent area, viewed to the north. The photo was taken by Elizabeth Baker, Royal Holloway, University of London. (b) Initial subsidence during the major intrusive phase (blue area) inferred from satellite radar data (Wright *et al.* 2006) and the distribution of seismicity (Ebinger *et al.* 2006) associated with the post-intrusive phase (small black dots). (c) Zones of ground deformation due to magmatic injection. See **Appendix A-8** for higher resolution.

5.2.3 Combined Rifting Conditions

Even though 90% of the strain came from the magmatic force at the Dabbahu rift segment but also the geodetic data indicated that 10% was from the remote extensional plate

boundary force (Keir, 2009). Knowing that two types of forces are acting in the area, it is not wise to conclude the opening of the rift, graben or extensional structures only from one type of episode.

For the present study, the contribution of the constant spreading rate (CV) and violent rifting episodes (VR) to stretch the graben is considered with different combinations (1/3CV:2/3VR, 1/2CV:1/2VR and 2/3CV:1/3VR).

5.3 Hazard Analysis

The chances of the active rifting hazard occurrence in the life time of the Tendaho reservoir and irrigation scheme is analyzed based on the assumption discussed in the previous section and the tectonic record of the recent and past activities. Albert in 1996 said probabilities are generally hard to measure. It is easy to measure probabilities of events that are extremely rare or events that are extremely likely to occur. For example, your probability that the moon is made of green cheese (a rare event) is probably close to 0 and your probability that the sun will rise tomorrow (a sure event) is likely 1. According to Grinstead and Snell, 1997 the probability of getting T or H (tail or head of a coin) may be related to the number of occurrence of T or H in the previous tosses. The present study was analyzed based on the discrete probability concept.

$$P_i = A/B \quad \dots\dots\dots (5.2)$$

$$P_{LT} = LT \times P_i \quad \dots\dots\dots (5.3)$$

Where – P_i potential occurrence of violent rifting once in a year, A number of violent rifting events, B number of years, LT life time of the Tendaho Project and P_{LT} potential occurrence of violent rifting during the life time (50 years) of the Project .

Based on the above simplified combinations and assumptions of the rift formation, the probabilities of violent rifting occurrence in the life time of the Tendaho Project was analyzed. With the constant spreading condition, the potential occurrence of violent rifting is almost zero. Under this assumption, the rift will open constantly with smaller stretching rate. As per the previous research results (Sigmondal, 1992; Acocella et. Al, 2008), the Tendaho rift had a spreading rate of 3.6mm/yr whereas the recent active Manda Hararo rift has

1.2mm/yr spreading rate only. This rate (a total of 60 mm opening) may not have a very serious harm for the Tendaho reservoir and irrigation scheme. It is smaller than the expected consolidation settlement for the entire scheme due to the engineering load (WWDSE-WPCS-I, 2005). **Table 5.1** presents the summarized results for the potential occurrence of Manda Hararo and Tendaho rifting in the lifetime of the Tendaho Dam and Irrigation scheme.

From the field studies the spreading rate of the Manda Hararo rift (1.2mm/yr) was estimated by Acoccela et al., 2008. As it was discussed in section 5.2.2, the maximum and minimum stretching of the extensional fracture in the area are 10 and 1 meter, respectively. For the present potential occurrence analysis, 1, 5 and 10m were considered as a minimum, average and maximum opening of extensional fractures from a single rifting episode. The MH rift is active since 0.2Ma to present which means 240m was opened with the given spreading rate and activity time. Considering the average opening by a single rifting episode and the total opening width, the numbers of rifting episodes can be estimated as 48. If the rifting episodes were occurred randomly in the past years, the probability of the violent rifting episodes occurrence at anytime of the year and during the life time of the project can be estimated with *Equation 5.2* and *5.3*, respectively. Based on the given equation, the probability of MH active rifting episode is 1.2% if the violent rifting event is the only stretching for the rift formation. However, considering the contribution of both forces as equal, the probability becomes below 1% (**Table 5.1**).

Some researchers believe that the Tendaho rift is still active because of the Serdo 1969 earthquake event (Kebede et al., 1989; and Thurmond, 2007). The previous research results indicate that the rift was active from 1.8 – 0.6Ma. and during this time 5km wide opening occurred. In a similar way, 1, 5, and 10m of a minimum, average and maximum opening was considered from a single violent rifting episode. The probability results show three times greater rift occurrence than the MH rift in the life time of the project, 3.6 and 1.2% for violent rifting episode and both assumptions, respectively (**Table 5.1**). **Fig 5.4** shows the linear relationship between the numbers of violent rifting episodes in the past and potential occurrence of active rifting episode during the life time of the Tendaho dam and irrigation project (%) – 50 years.

Table 5.1: Summary of the potential occurrence of Manda Hararo and Tendaho rifting in the lifetime of the Tendaho Dam and Irrigation scheme.

No	Assumption	Rift Axis	Total Stretching (km)	Time (Ma)	Spreading Rate (mm/year)	Opening in a single rifting episode (m)			Number of rifting episodes			Potential occurrence of rifting (at anytime of a year) %			Potential occurrence of rifting (during in the life time of the project - 50yr) %		
1	CS	MH	0.24	0.2 – pre	1.2	0	0	0	0	0	0	0.00	0.00	0.00	0.00	0.00	0.00
2	VR				0				240	48	24	0.12	0.02	0.01	6.00	1.20	0.60
3	1/3 CS & 2/3 VR				1.2	1	5	10	160	32	16	0.08	0.02	0.01	4.00	0.80	0.40
4	1/2 CS & 1/2 VR				1.2	1	5	10	120	24	12	0.06	0.01	0.01	3.00	0.60	0.30
5	2/3 CS & 1/3 VR				1.2	1	5	10	80	16	8	0.04	0.01	0.00	2.00	0.40	0.20
6	CS	T	5	1.8 – 0.6 (pre)	3.6	0	0	0	0	0	0	0.00	0.00	0.00	0.00	0.00	0.00
7	VR				0				5000	1000	500	0.42	0.08	0.04	20.83	4.17	2.08
8	1/3 CS & 2/3 VR				3.6	1	5	10	3335	667	333	0.28	0.06	0.03	13.90	2.78	1.39
9	1/2 CS & 1/2 VR				3.6	1	5	10	2500	500	250	0.21	0.04	0.02	10.42	2.08	1.04
10	2/3 CS & 1/3 VR				3.6	1	5	10	1665	333	167	0.14	0.03	0.01	6.94	1.39	0.70

Where – MH – Manda Hararo Rift and T – Tendaho Rift

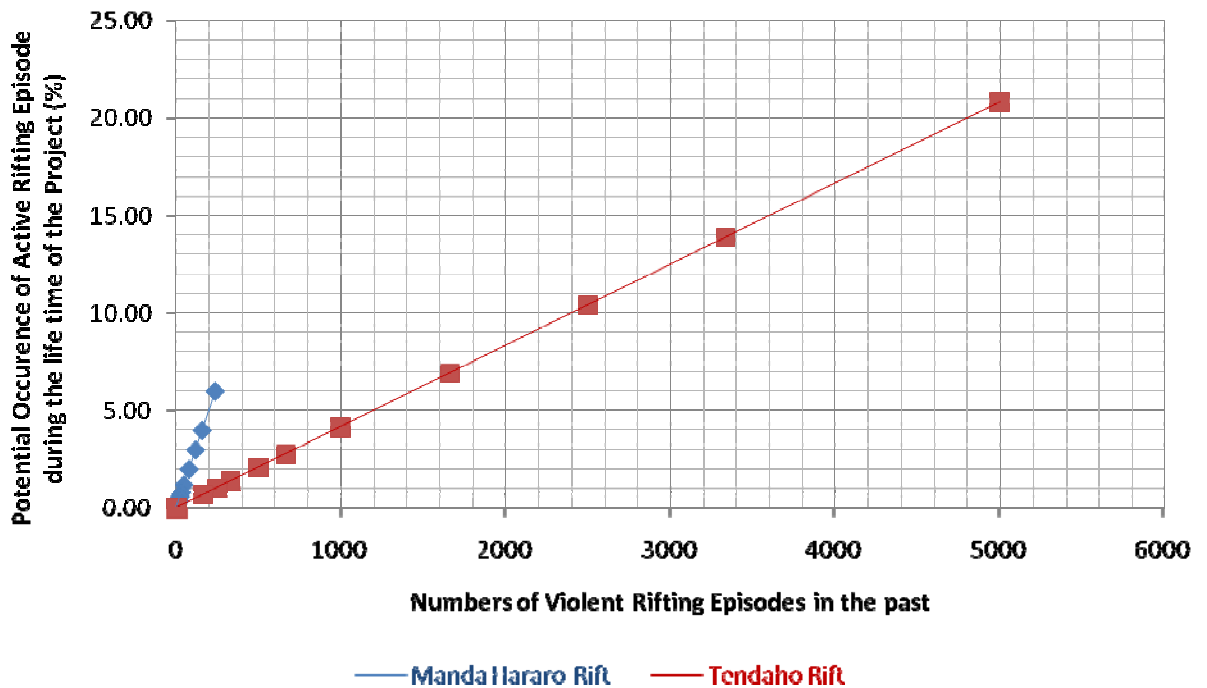


Fig 5.4: Linear relationship between the numbers of violent rifting episodes in the past and potential occurrence of active rifting episode during the life time of the Tendaho dam and irrigation project (%) – 50 years; Blue line – Manda Hararo Rift and Red line – Tendaho Rift.

5.4 Interpretation

The worst scenarios could happen if the Manda Hararo and Tendaho rift opens with violent rifting episode during the life time of the Project. From the recent Dabbahu rifting episode, it was observed that the violent rifting was supplemented by magmamtic injection. This source of rifting force deformed the ground up to 20km in lateral extension from the rift axis. The intensity of the ground deformation decreases away from the rift segment. The width of the ground deformation zones are estimated from the Dabbahu rifting observations.

$$W_{Zone(n)} = 2 * W_{Zone(n-1)} \dots\dots\dots (5.4)$$

Where $W_{Zone(n)}$ is width of Zone n. For instant according to the Dabbahu 2005 rifting episode, Zone 1 has 2.5km width for each side of the rift axis to the left and right side. The calculation of the width of Zone 2 will be two times the width of Zone 1 which is 5km. The same way Zone 3 has 10km width. **Fig 5.5** shows the probable extents of ground deformation zones due to the magmatic injection by the active rifting occurrence of the Manda Hararo and Tendaho rifts. Most of the reservoir, dam and irrigation schemes may be affected by the Manda Hararto rifting episode. However, less than 20% of the scheme could be affected by the Tendaho rifting episodes.

Any seismic activity in and around Tendaho dam project may not be that much destructive as far as water tightness of reservoir and irrigation scheme is considered. However, active rifting episodes may develop additional rock fractures and may change the characteristics of existing rock fractures in the reservoir area which may enhance the seepage potential thus resulting into more water losses from the reservoir.

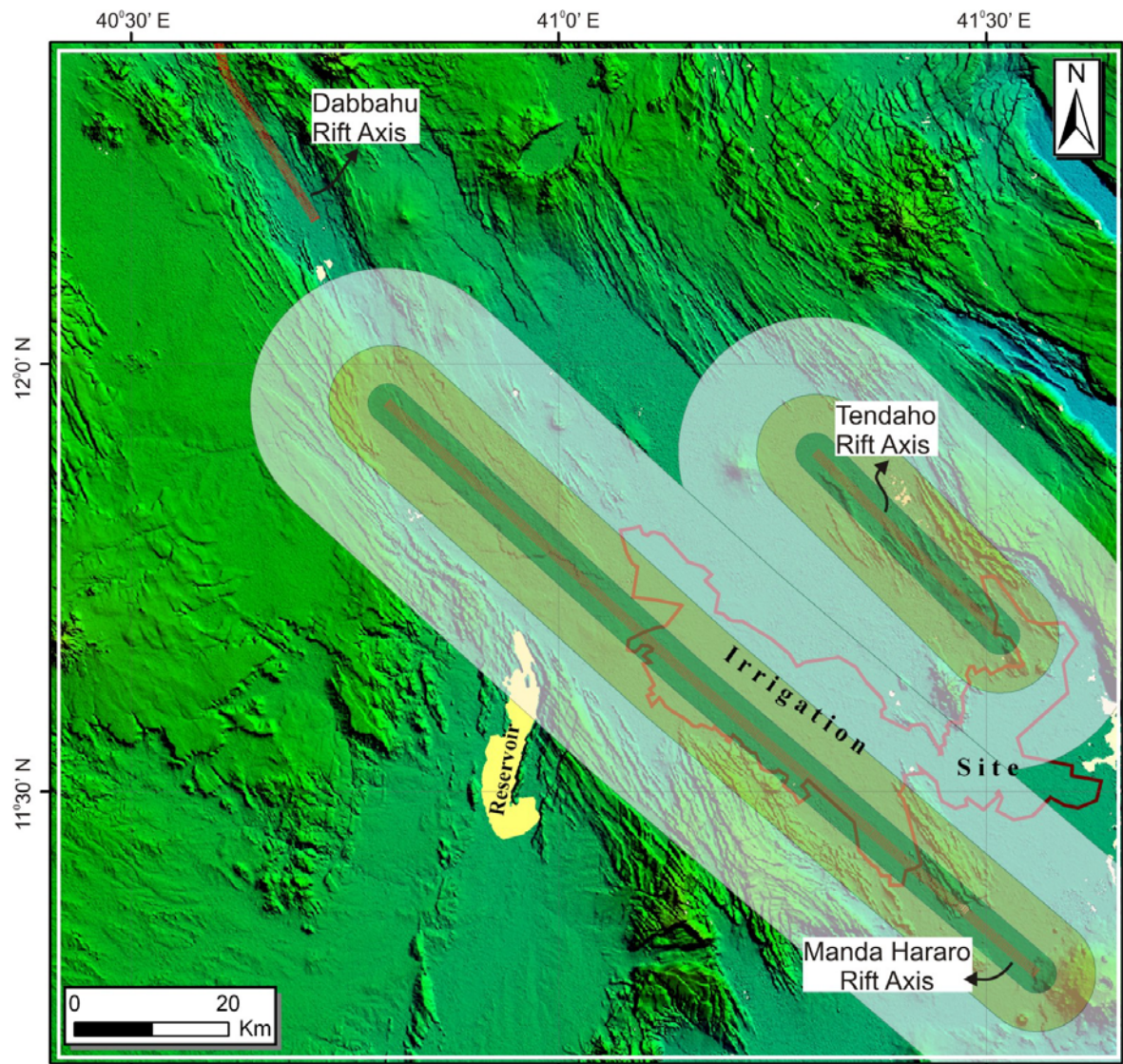


Fig 5.5: Potential extents of the ground deformation zones by the active rifting episodes of Manda Hararo and Tendaho rifting at the Tendaho reservoir and irrigation site.

Chapter Six

Risk Assessment of Brittle Tectonic Structures - Related to Reservoir Leakage

6.1 Introduction

According to the Darcy's Law, water flows through a geologic medium from higher to lower pressure, keeping the other influential factors constant. Among many other geological media which favor the flow of water, geological discontinuities can be taken as one of the essential feature. The water flow could occur in the geological medium of karstic environment, faulted or fracture ground, unconsolidated or permeable material and in general through porous geology (Wilson, 1986; Kalkani, 1997; Romanov et al., 2003; Li et al., 2007). All the above geological situations are favorable conditions in which water can pass through much faster than the other geological situations. For the investigation of reservoir water tightness brittle tectonic structures are important in the engineering practice because of their hydrogeological behavior. If these structures are not considered during the feasibility stage of the project, they may cause excessive loss of water from the reservoir.

The present date of reservoir water tightness investigation approaches depend on the different geological media which water is expected to pass through. Starting from the geological modeling of the reservoir area, permeability tests of geological samples in the laboratory and in-situ help to understand and identify the leakage zones of the reservoir (Al-Saigh et al., 1994; Mamo and Yokota, 1998; Heister et al., 2005; Unal et al., 2007 & 2008). In the present study, systematic approaches were adopted to assess the risk level of the tectonic structures related to reservoir leakage which were not considered in the feasibility stage of the project study.

Asfaw, 2007 proposed an integrated approach to study geohazards by considering a scenario studies. According to Asfaw, 2007, because of the earth's interior processes and/or solar-terrestrial interaction, there are possibilities of first order geohazards occurrences (**Fig 6.1a**). Such first order geohazards could probably trigger second order hazards and the second order phenomena trigger the third one and so on. The over all probability of geohazards on the object of interest (earth crust, engineering works, environmental features, human life) can be found with the sum of all scenarios and the vulnerability of the object of interest for those events.

For the present study, a parameter based geological risk assessment is proposed to assess the risk level of the brittle tectonic structures related to the proposed Tendaho reservoir leakage. The earth crust, foot prints of past geological processes, which were object of interest while assessing the geohazards can be now a source of potential hazards for the object of interest like engineering works. At one given site, there may be number of past geological processes which severely affect the earth crust. The risk assessment of past geological conditions, how severely was the processes, can be assessed based on the influencing parameters which explain the condition (**Fig 6.1b**). Finally, the total risk from both ongoing and past geological conditions could be summed up or weighted accordingly with the help of mathematical approaches.

6.2 Risk Parameters

There are number of parameters which explain the characteristics of the brittle tectonic structures. However, for the present study, parameters are selected based on their relevancy to the object of interest – ‘the proposed Tendaho Reservoir’ (**Fig 6.2**). Ten parameters were considered for the risk assessment of brittle tectonic structures related to the reservoir leakage which are mainly grouped into two, namely; **Tectonic Parameters** – tectonic status T_s , tectonic regime T_{rr} , multiple tectonic histories T_h , aerial extent of the structure Ex , dip direction Dir , and termination index T_i ; and **External Parameters** – hydrogeology G , proximity to the object of interest P , relative position P_s and hydraulic pressure Hp .

6.2.1 Tectonic Parameters

Under this sub topic, five parameters were considered, namely; tectonic status T_s , tectonic regime T_{rr} , tectonic history T_h , aerial extent of the structure Ex , and termination index T_i . See **Fig 6.2** and **Table 6.1**.

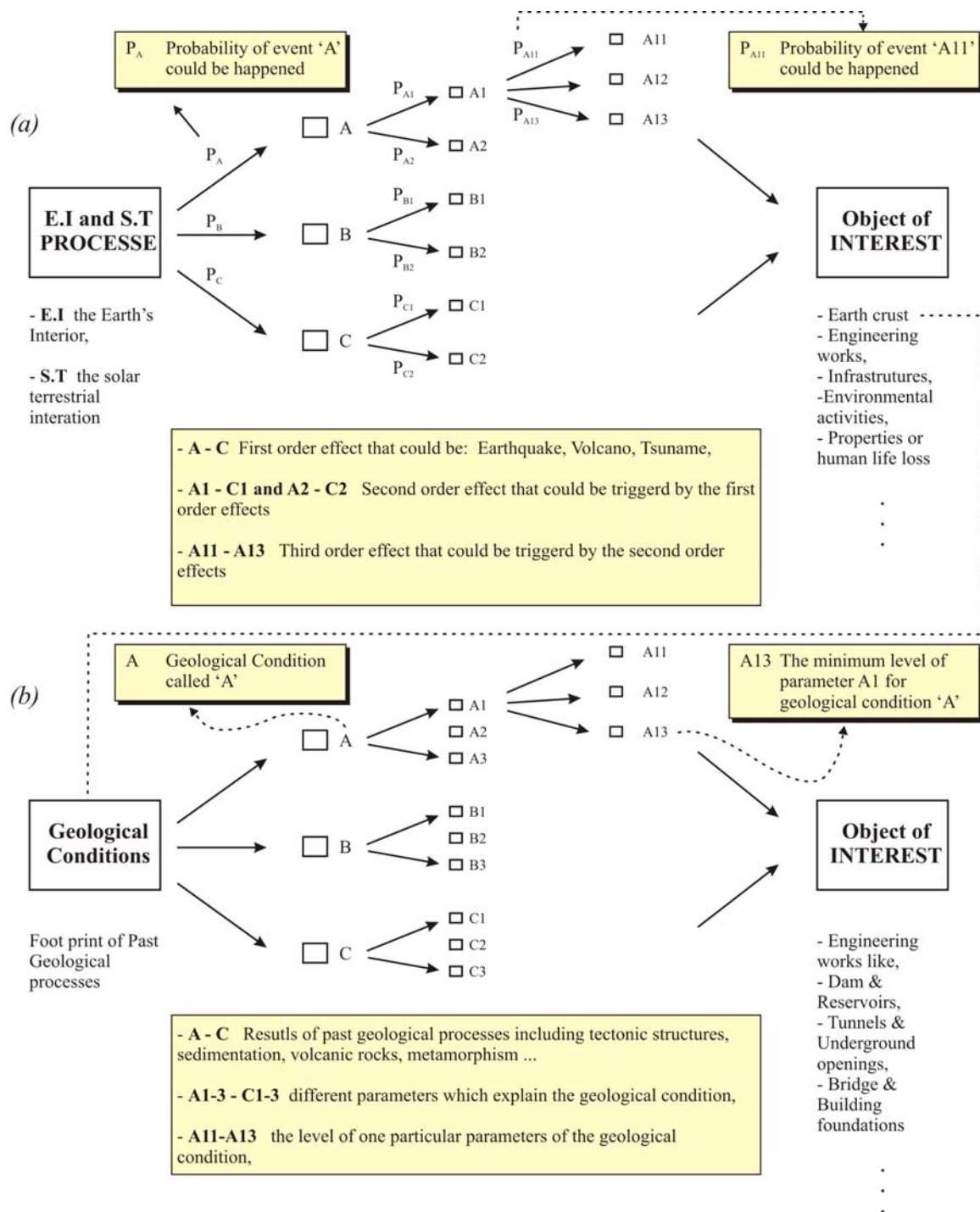


Fig 6.1: Risk assessment of natural hazards (geohazards) and geological conditions: **(a)** Asfaw, 2007; Chains of cause and effects for processes originating in the earth's interior (E.I.) or the solar–terrestrial (S–T) interaction. **(b)** Different geological conditions as a result of various geological processes can be source of risk for the object of interest.

Tectonic Status Ts: it is briefly the potential occurrence of tectonic activities like earthquake and rifting in the life time of the project. These activities may change the flow of water dramatically through the exiting tectonic structures. Wu et al., 2005 measure/s the fluctuation of the ground water flow because of the active fault displacement along the Golmud-Lhasa railway, Tibetan Plateau, China. In other studies, it is indicated that aggregates of fault zone can be rearranged due to the tectonic activities and such

rearrangement allow water to percolate through openings. In addition to the ground acceleration effects, rifting associated ground deformation could also play a significant role on rearranging the tectonic structures and water flow. Depending on how active is the area, the effect on the structures and ground water flow may vary. For these reason, the tectonic status was considered as one parameter for the risk assessment of tectonic structures related to 'Tendaho Reservoir leakage' with a wider range from *no indication of activity at all to the structure itself is an Active Fault*.

Tectonic Regime Trr: depending on the mode of development or mechanism of formation, the chances of water flow through the tectonic structures may vary. In the extensional tectonic regime, tectonic structures like normal faults are formed by extensional force. These extensional forces allow opening or stretching to compensate the applied stress. In contrast, the compressional tectonic regime compressed or shortened the earth body due to the applied contractional stress.

The amount of water flow increases from compressional to extensional tectonic regime. With these broad assumptions, tectonic regime was considered as one of the parameter for the risk assessment of tectonic structures related to reservoir leakage.

Multiple Tectonic Histories (Age) Th: the older brittle tectonic structures could be positively or negatively affected by the younger tectonic stress direction. Where positively means more opening or stretching and negatively means squeezing or closing of the tectonic structures. For example, the Main Ethiopian Rift structures subsequently affected negatively by the intrusion of magmatic dyke, propagation of the Red Sea Rift structures and extension of the Tendaho graben.

Areal extents of the structures Ex: is the structure regional or local or associated structure with the major one. It increases the chance of losing water through the structures if they have maximum contacts.

Cross cut index Cci: this parameter is common in the characterization of rock mass behavior since ISRM, 1978 (Priest; 1992). With the same idea by changing the scale of the discontinuities, the termination index concept can be used in the risk assessment of brittle tectonic structures. If the structure is isolated, the risk level would be less compared to the cross cut termination index.

6.2.2 External Parameters

In addition to the tectonic parameters geology G , proximity P , relative position Ps , Elevation difference Ed and hydraulic pressure Hp parameters would be discussed under this sub topic (**Fig 6.2** and **Table 6.1**).

Geology G : is considered as one of the parameter which influences the hydrogeological behavior of the site. Depending on the grain size, presence of additional structures; like cooling joints of volcanic rocks, fracture media and others, the permeability of similar lithology can vary. The conceptual hydrogeological model of the Tendaho reservoir and its vicinity has been developed from DT, 1973, regional hydrogeological model of Awash river basin (especially the lower Awash river basin model) prepared by Ayenew et al., 2008 and the lineament density (**Fig 3.10**). According to Ayenew et al., 2008, the groundwater in general, flows towards a northeast trending paleo-drainage channel. The main groundwater flow is towards Lake Abhe which is east of the present study area. **Fig 6.3** illustrates the highland rift groundwater flow and fault controlled major springs in the Awash River basin. **Fig 6.4** shows the conceptual hydrological model of the Tendaho reservoir.

From the permeability test results of the Tendaho reservoir by the project authorities, fractured basalts are considered to be permeable geology whereas, the lacustrine deposits are medium permeable geology.

Proximity P : is how close the structure is to the object of interest. Closeness of the brittle tectonic structures to the object of interest (in this case the Water Reservoir) is crucial. As the structure goes far and far from the object of interest, the risk level of the tectonic structures will decrease, no matter how the other parameters are. Therefore, this parameter can be considered as most important.

Relative position Ps : where is the tectonic structure positioned? Depending on the ground water flow direction and the drainage basin, the level of risk may vary.

Elevation difference Ed : the maximum level of the proposed Tendaho reservoir is about 410 meter. Depending on the elevation difference of the tectonic structures and maximum reservoir level, the risk class of the tectonic structures varies towards the reservoir leakage.

Water can easily pass through tectonic structures which are exposed to the physical weathering rather than structures which are found at depth.

Hydraulic pressure Hp: higher the hydraulic pressure higher will be the risk level to drive the water with pressure to percolate through the brittle tectonic structures. The risk level of hydraulic pressure at one particular area depends on the height of the water. The maximum water height will have maximum risk level.

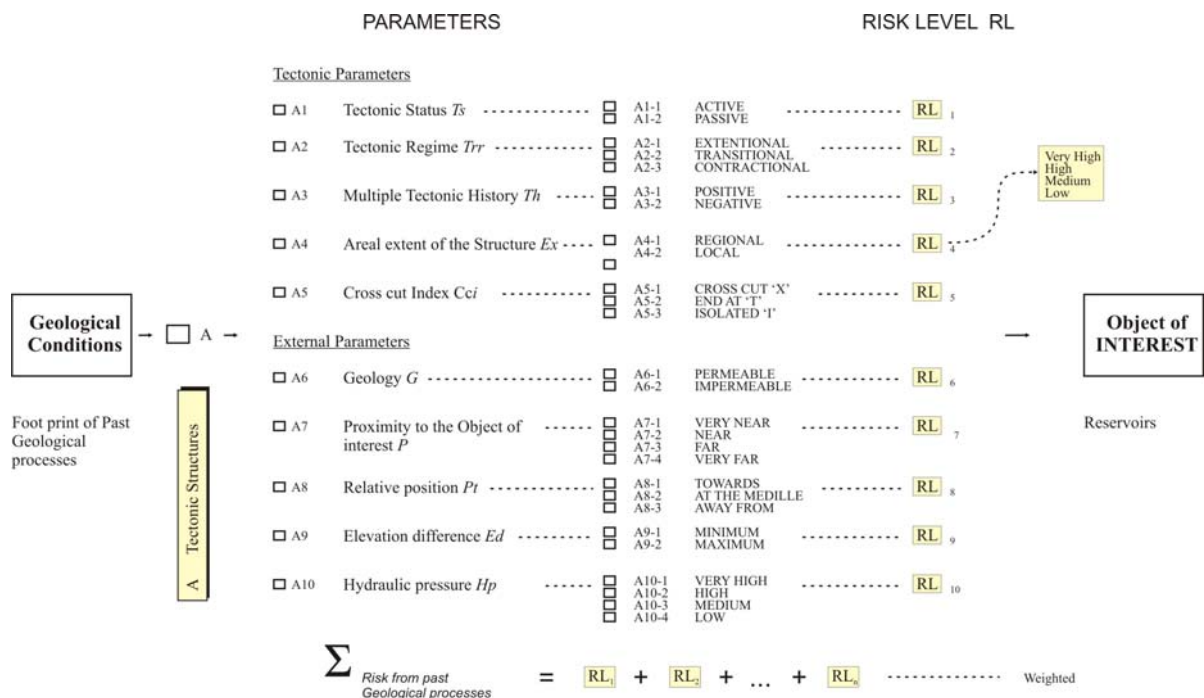


Fig 6.2: Key parameters for the risk assessment of brittle tectonic structures – related to ‘the proposed Tendaho Reservoir’.

6.3 Risk Analysis

For the present study semi-quantitative risk assessment of brittle tectonic structure has been carried out. The concept is adapted from the works of Sanchez, et al., 2007 on ‘*Geological risk assessment of the area surrounding Altamira Cave, Spain*’. They proposed Natural Risk Index and Safety Factor for protection of a prehistoric cave (object of interest). For the present study, ten parameters (**Table 5.1**) are considered to assess the tectonic risk related to ‘Tendaho Reservoir leakage’. Depending on their specific magnitude or level, a scale ranging from 0 to 10 is used to evaluate the risk level (Anbalagan, 1996; Sanchez, et al., 2007).

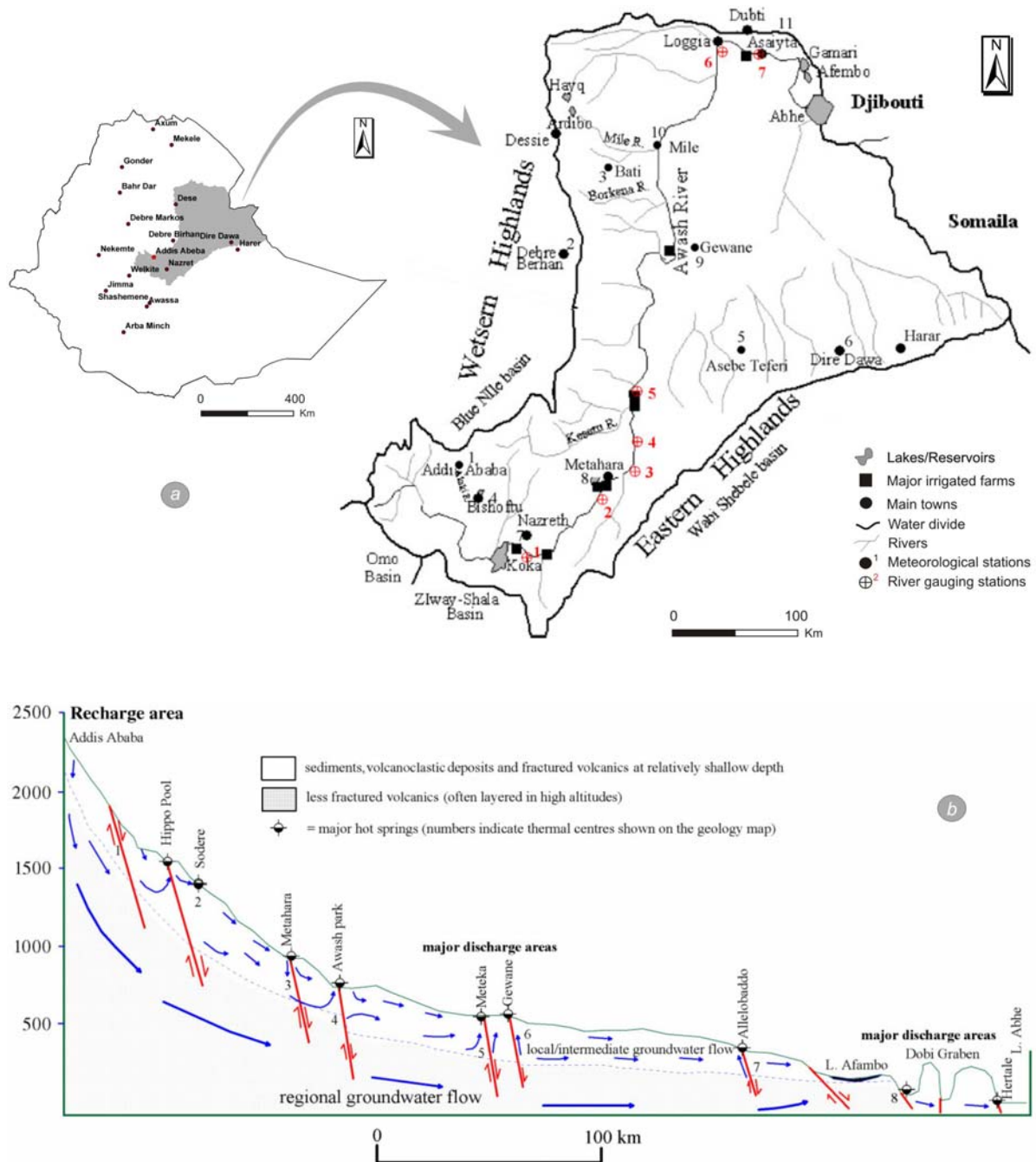


Fig 6.3: Awash drainage basin (a) Location map of Awash drainage basin, (b) Schematic section illustrating highland-rift groundwater flow and fault-controlled major springs, vertical exaggeration is 100 times the horizontal (after DT, 1973 and Ayenew et al., 2008).

To estimate the final risk level, in this case ranging from 0 to 10, the parameters are prioritized according to their influence on the object of interest (Tendaho Reservoir) with three approaches; namely *simple averaging AVE*, *pair wise comparison PWC* and *analytic hierarchy process AHP*. The risk level was classified into four classes; low (0 – 2), medium (3 – 5), high (6 – 8) and very high (9 – 10).

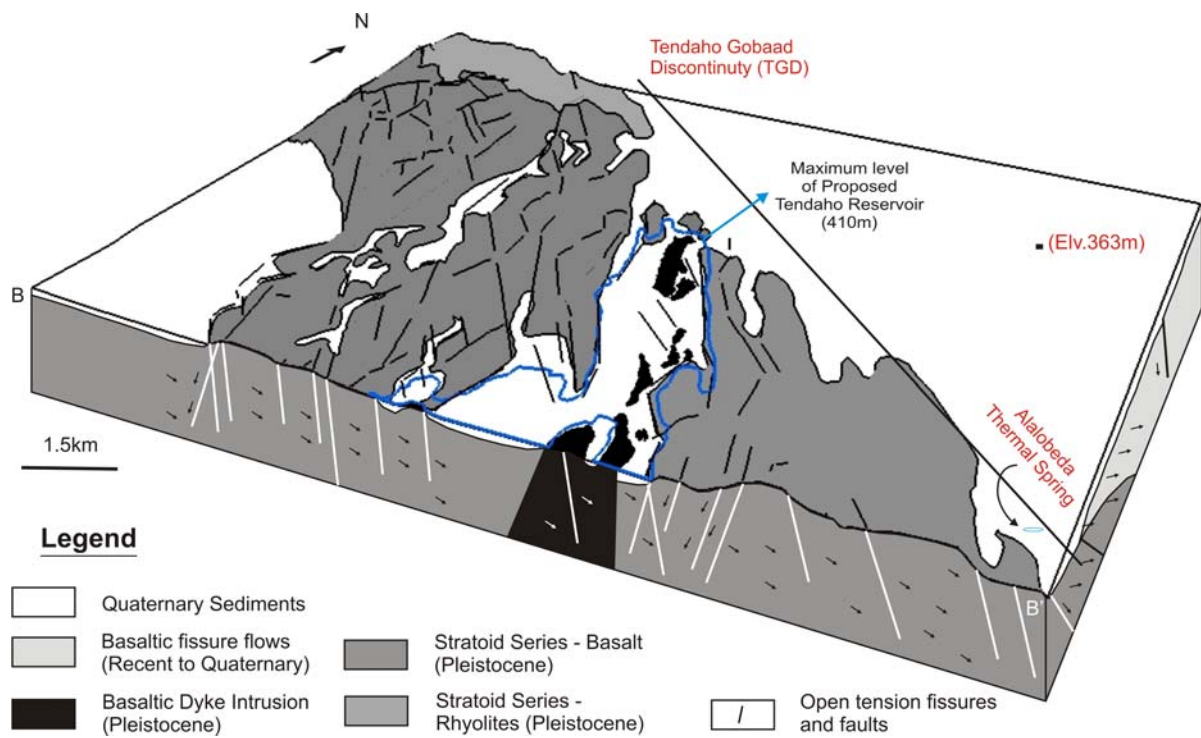


Fig 6.4: Conceptual Hydrogeological model of the Tendaho reservoir which is adapted from DT, 1973 and Ayenew et al., 2008 (Landsat ETM+ image with band combination 4-5-3 dragged on TIN model of 2x vertical exaggeration – see **Fig 4.9** for the location of the cross section).

Brittle tectonic structures which are located at a buffer distance of 2km from the proposed maximum level of the Tendaho reservoir were taken for the risk assessment of brittle tectonic structures – related to reservoir leakage. This assumption is considered to test the proposed brittle tectonic structures risk level for the reservoir leakage. A total of 168 brittle tectonic structures were selected which were partially and/or completely within this buffer zone. **Fig 6.5** shows the location of the selected tectonic structures for the risk assessment of brittle tectonic structures. Depending on the characteristics of the tectonic structures related to the above discussed parameters, particular classes were assigned (**Table 6.1**). Moreover, **Fig 6.6** shows the distribution of each parameter within the risk classes. According to the parameters distribution of the brittle tectonic structures, *Ed* parameter has near 50% whereas the remaining parameters are below 20% in the very high risk class. The *Th*, *G*, and *Ts* parameters have more than 60% in the high risk class and except the *Hp* parameter which is less than 5%, the remaining are around and above 20%. In the medium risk class, the *Trr* and *Cci* parameters have above 60% and the rest parameters are around and below 30% except the *Ex* parameter which is above 40%. The maximum percentage in the low risk class is from *Ps* parameter (40%), and the other parameters are below and around 30%. Within all class the average distribution of the *P* parameter is around 25%.

Table 6.1: Assessment of the risk level for the parameters.

Parameters		Risk level and classes			
		Class 1	Class 2	Class 3	Class 4
		Low	Medium	High	Very high
		0 – 2	3 – 5	6 – 8	9 – 10
Tectonic	Tectonic Status (Ts)	No indication of activity at all	There is no active tectonic processes at a closer distance	Tectonic activity is at closer distance including high earthquake epicenters, rifting axis	The structure itself is an Active Fault
	Tectonic Regime (Trr)	Contractional – Thrust and strike slip fault	Transitional – Oblique strike slip fault	Extensional – Normal faults	
	Past/previous Tectonic Histories (Th)	Negative – Closed up	Positive – Slightly Opened	Positive – Moderately Opened	Positive – Widely Opened
	Areal Extent (Ex)	< 500m	500 – 1000m	1000 – 2000m	> 2000m
	Cross cut Index (Cci)	I (Isolated structure)	T (the structure end at another structure)	Cross cut only one time (X')	Cross cut by more than one time (X'')
External	Geology (G)	Impermeable	Medium Permeable	High Permeable	Very high Permeable
	Proximity (P)	Very far (1000 – 2000m)	Far (500 – 1000m)	Near (0 - 500m)	Very near (< 0m)
	Relative Position (Ps)	Left side of the reservoir	Center of the reservoir	Right side of the reservoir	
	Elevation Difference (Ed)	150 – 230m	70 – 150m	0 – 70m	< 0
	Hydraulic Pressure (Hp)	Low (<10m)	Medium (10 - 20m)	High (20 – 30m)	Very high (>30m)

6.3.1 Simple weighting (Average)

Here, it was assumed that all parameters have equal contribution to the risk level of the brittle tectonic structures – related to reservoir leakage except the *Proximity P* which was taken as the most important parameter for the risk assessment. As it was discussed in the previous section, the maximum risk level for each parameter is 10. The risk level of the brittle tectonic structures was analyzed with equation 6.1 and 6.2 (simple weighting – Average) where the nine parameters are averaged and multiplied by *P* parameter.

$$RL[AVE] = \frac{P_{Priority} \cdot (P_1 + P_2 \dots + P_n)}{(P_{1=max} + P_{2=max} + \dots + P_{n-max})} \dots\dots\dots (6.1)$$

$$RL[AVE] = \frac{P \cdot (Trr + Ex + Cci + Th + G + Ts + Ps + Ed + Hp)}{90} \dots\dots\dots (6.2)$$

The risk level was compared by changing the value of the class within the same class; minimum, average and maximum (see **Fig 6.7**). The result shows that the mean values of the risk level in different classes constantly increases as the class value of the parameters increase from minimum to maximum within the class.

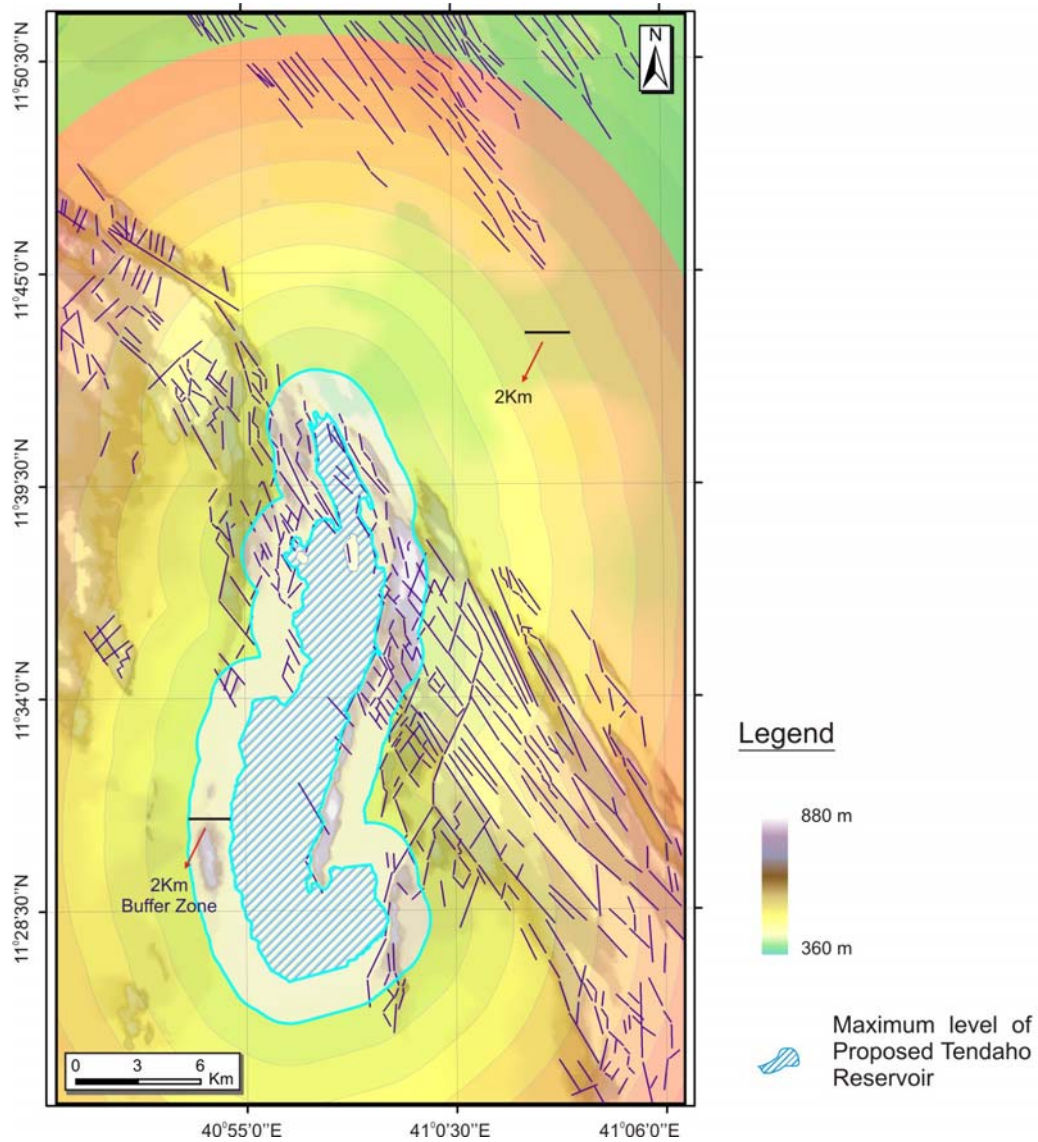


Fig 6.5: Location map of the selected brittle tectonic structures (2km buffer zone from the proposed maximum level of Tendaho Reservoir). See **Appendix A-9** for higher resolution.

Moreover, Mathematica 6.1 software was used to assess the possible risk level of brittle tectonic structures – related to reservoir leakage by varying the value of the parameter. **Fig 6.8** and **Fig 6.9** show the data plot and Mathematica analysis results with equation 6.3 versus 6.2, respectively. **Fig 6.10** shows the results of the brittle tectonic risk assessment – related to reservoir leakage.

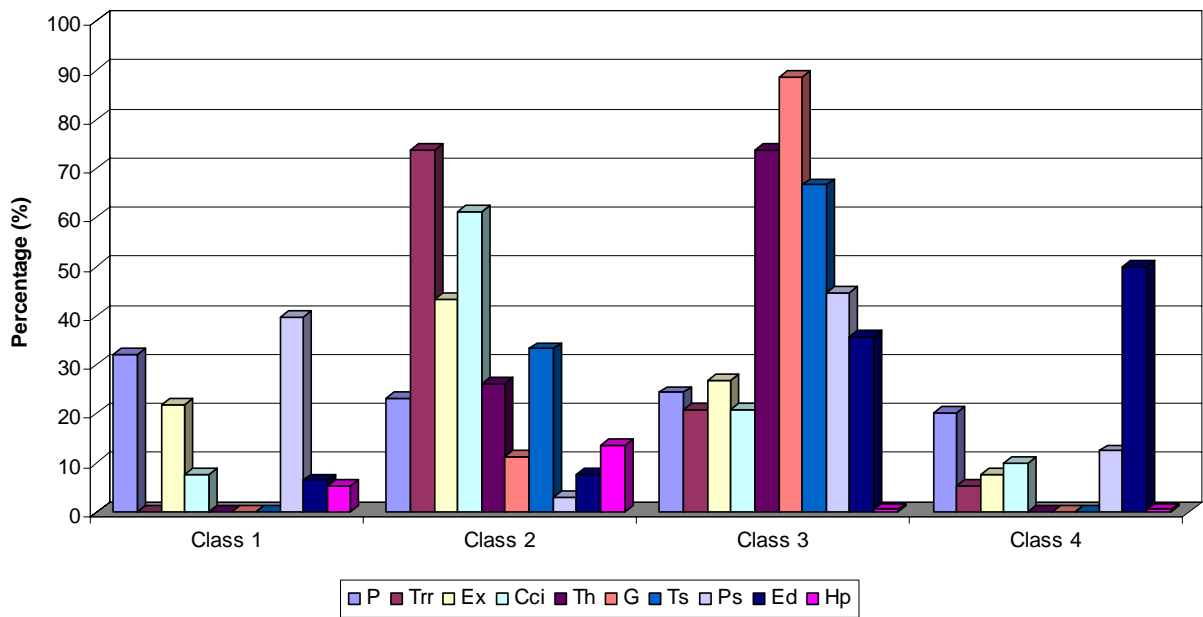


Fig 6.6: Key Parameter distribution (%) in the different risk level classes (See **Appendix B-2** for the data).

$$RL_o[AVE] = \frac{(Trr + Ex + Cci + Th + G + Ts + Ps + Ed + Hp)}{9} \dots\dots\dots (6.3)$$

Where RL_o is the risk level of brittle tectonic structures towards the reservoir leakage without the consideration of P proximity parameter. This equation tells us the behavior of the brittle tectonic structures related to the reservoir leakage.

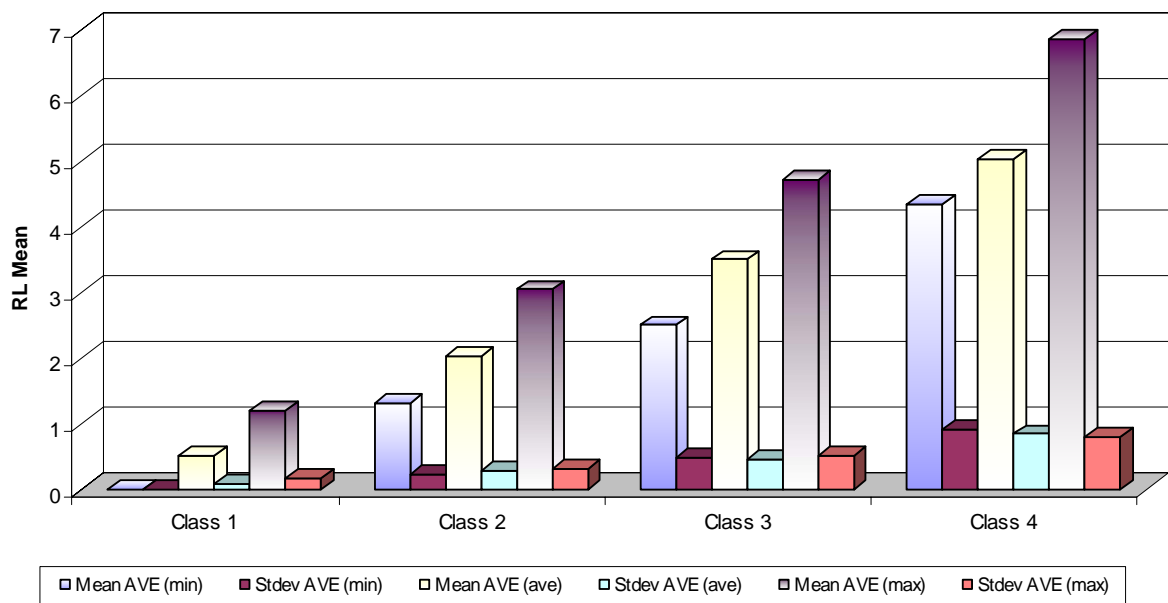


Fig 6.7: Mean and standard deviation of the risk level values of brittle tectonic structures – related to reservoir leakage by simple weighting (AVE) approach (See **Appendix B-2** for the data).

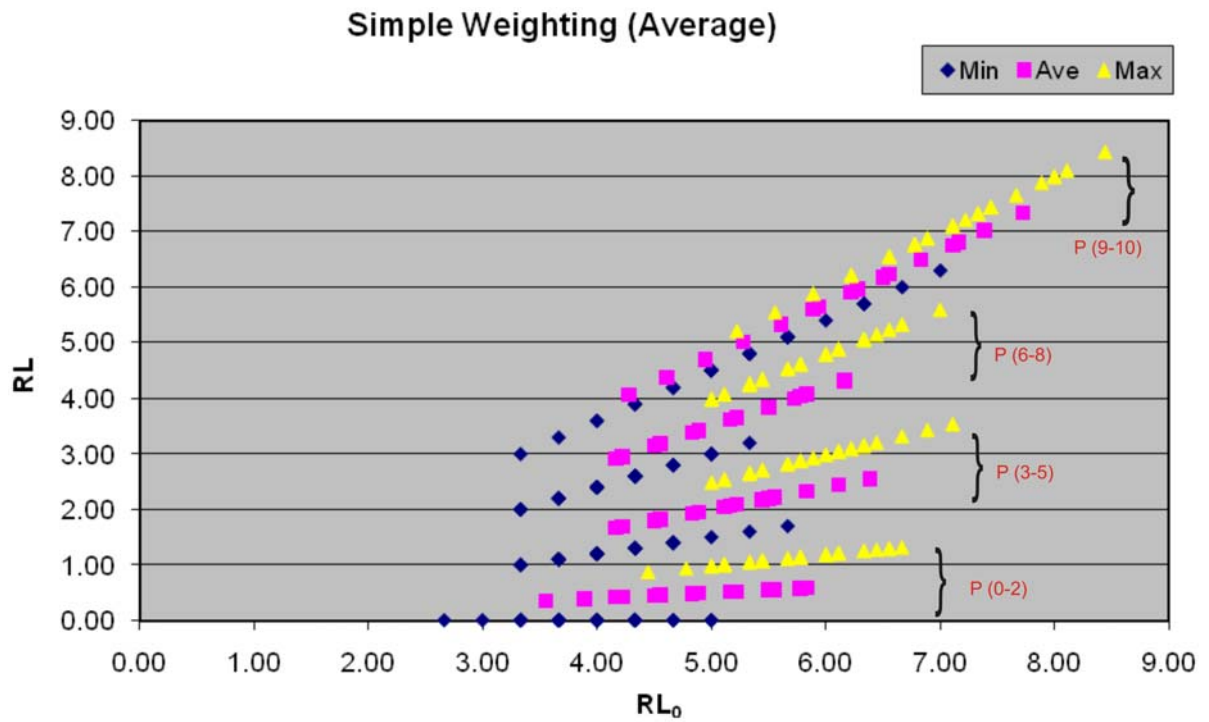


Fig 6.8: Plot of the risk level values of brittle tectonic structures – related to reservoir leakage by simple weighting (*AVE*) approach RL vs RL₀ (the blue rhombus – minimum, purple rectangle – average and yellow triangle – maximum values of the class parameter). See **Appendix B-2** for the data.

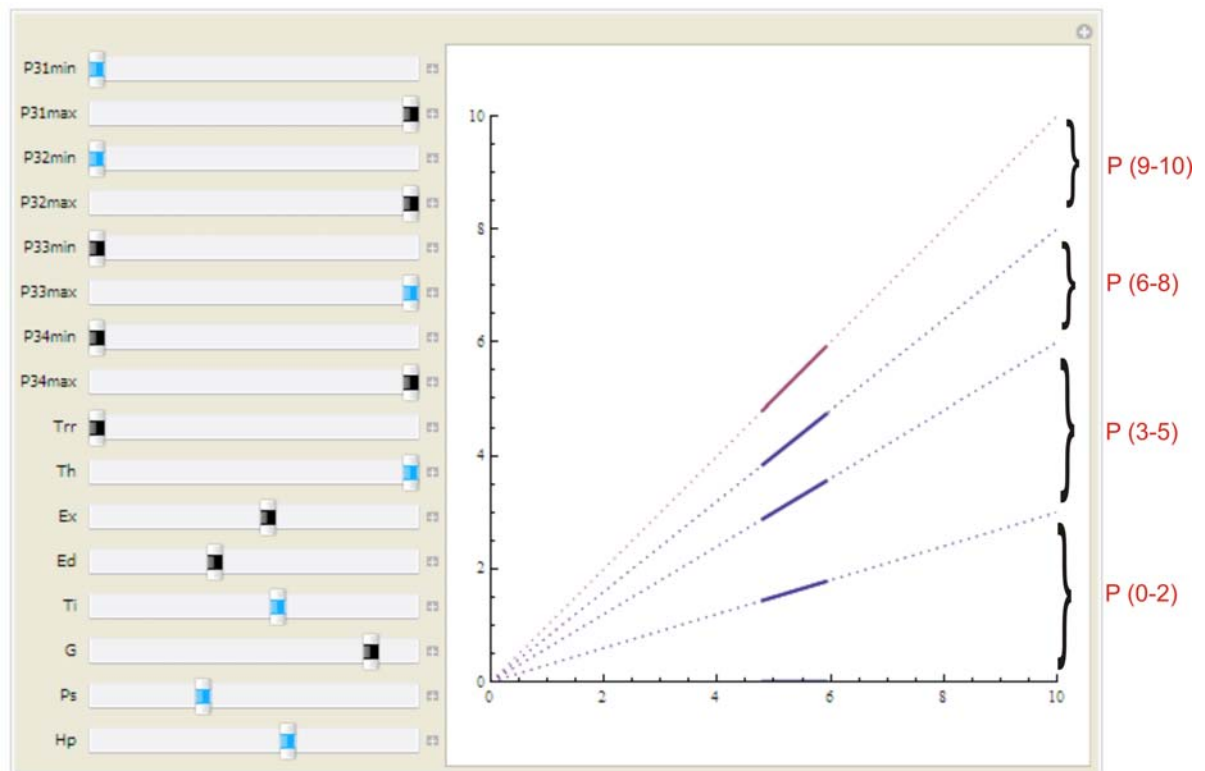


Fig 6.9: Assessment of the risk level of brittle tectonic structures – related to reservoir leakage by simple weighting (*AVE*) approach RL vs RL₀ (see **Appendix C-1** for the detail description of the equation and additional graph).

With the Mathematica analysis, it was possible to assess the risk level for any given values of the parameters and/or the influence of a single parameter on the risk level. By varying the value of the risk classes, it was found that the risk levels of the brittle tectonic structures were changed constantly from minimum to maximum values of the classes. The minimum values of the classes resulted with low and medium risk level except one structure which showed high risk level. When the medium values of the classes were taken, twelve brittle tectonic structures resulted with high risk level and the remaining other structures had similar risk level as of the minimum class values. Thirty (30) brittle tectonic structures resulted with high risk level and two with very high when the maximum value of the classes was taken for the analysis of the risk assessment of the brittle tectonic structures – related to reservoir leakage. The risk level of the brittle tectonic structures – related to reservoir leakage results are shown on **Fig 6.10**.

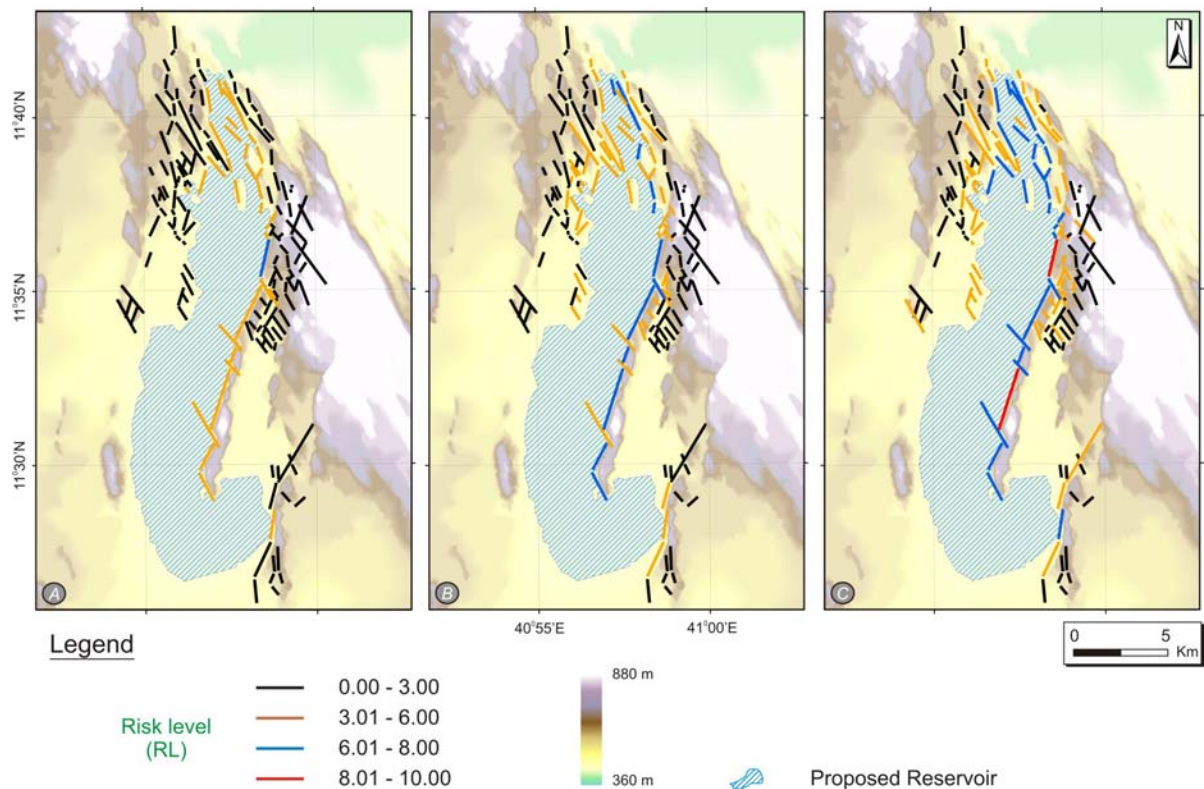


Fig 6.10: Risk level of brittle tectonic structures – related to reservoir leakage by simple weighting (*AVE*) approach: (a) minimum value of the class, (b) average value of the class and (c) maximum value of the class.

6.3.2 Pairwise Comparison (PWC)

Salustri, 2005 defines pairwise comparison as a kind of divide-and-conquer problem-solving method. It allows one to determine the relative order (ranking) of a group of items. This is

often used as part of a process of assigning weights to criteria in design concept development.

For the present study, the qualitative approach of pairwise comparison was used to analyze the risk level of brittle tectonic structures – related to reservoir leakage. The nine parameters (except *Proximity P*) were ranked based on the theoretical back ground of their influence on the risk level. As it is shown on **Table 6.2** each pair of the parameters were compared pairwise for one side of the triangle. The numbers of the parameter symbol were counted from the table and weighted. The total weight of the parameters must be 100%. In order to get the initial value, linear proportion was assumed between all the weights and solves the following equation:

$$100 = 8x + 7x + 6x + 5x + 4x + 3x + 2x + 1x + 0x$$

$$x = 2.77$$

The coefficients of the *Equation 6.3* (RL_{PWC}) were taken from weight value of the ranked parameters based on the qualitative approach of pairwise comparison. The average of the nine parameters was multiplied by the *Proximity P* parameter as it is shown at *Equation 6.3* (RL_{PWC}). The overall result was divided by 10 to get the maximum risk level value 10.

$$RL[PWC] = \frac{P \cdot (2.2Trr + 1.9Ex + 1.7Cci + 1.4Th + 1.1G + 0.8Ts + 0.5Ps + 0.3Ed + 0.1Hp)}{100} \quad (6.4)$$

Table 6.2: Pairwise comparison (*PWC*) of the risk parameters.

		Trr	Ex	Cci	Th	G	Ts	Ps	Ed	Hp	No Count	Weight
Tectonic Region	Trr	1	Trr	Trr	Trr	Trr	Trr	Trr	Trr	Trr	8	22
Areal Extention	Ex		1	Ex	Ex	Ex	Ex	Ex	Ex	Ex	7	19
Cross cut Index	Cci			1	Cci	Cci	Cci	Cci	Cci	Cci	6	17
Tectonic History	Th				1	Th	Th	Th	Th	Th	5	14
Geology	G					1	G	G	G	G	4	11
Tectonic Status	Ts						1	Ts	Ts	Ts	3	8
Relative Position	Ps							1	Ps	Ps	2	5
Elevation Difference	Ed								1	Ed	1	3
Hydraulic Pressure	Hp									1	0	1

The risk level was compared by changing the value of the class within the same class; minimum, average and maximum (see **Fig 6.11**). The result shows that the mean values of the risk level in different classes constantly increases as the class value of the parameters

increase from minimum to maximum within the class. **Fig 6.12** and **Fig 6.13** show the data plot and Mathematica analysis results with equation 6.5 verse 6.4, respectively. **Fig 6.14** shows the result of the brittle tectonic risk assessment – related to reservoir leakage.

$$RL_o[PWC] = \frac{(2.2Trr + 1.9Ex + 1.7Cci + 1.4Th + 1.1G + 0.8Ts + 0.5Ps + 0.3Ed + 0.1Hp)}{10} \quad (6.5)$$

Using the Pairwise Comparison (PWC) approaches, the risk level of the structures were analyzed with varying the value of the parameter classes. As it is shown on **Fig 6.14**, the minimum values of the classes resulted with low and medium risk level of the brittle tectonic structures except three structures which showed high risk level. When the medium values of the classes were taken, eight brittle tectonic structures resulted with high risk level and the remaining other structures had low and medium risk level. Four brittle tectonic structures resulted with very high risk level and twenty nine (29) structures with high risk level when the maximum value of the classes were taken for the analysis of the risk assessment of the brittle tectonic structures – related to reservoir leakage.

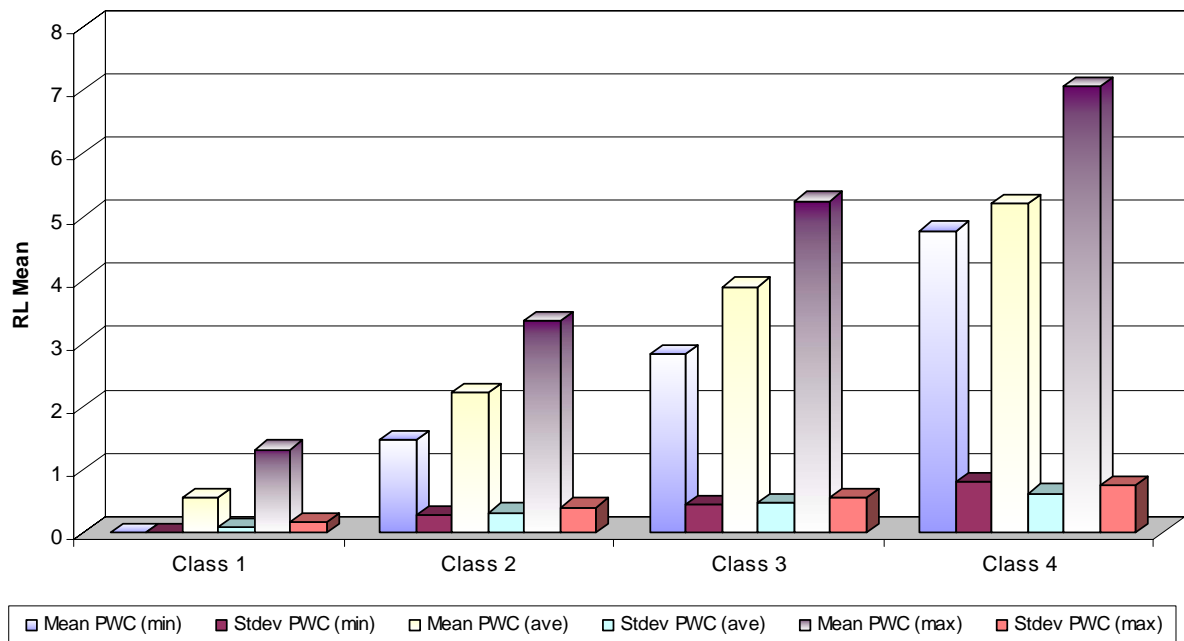


Fig 6.11: Mean and standard deviation of the risk level values of brittle tectonic structures – related to reservoir leakage by pairwise comparison (PWC) approach (See **Appendix B-2** for the data).

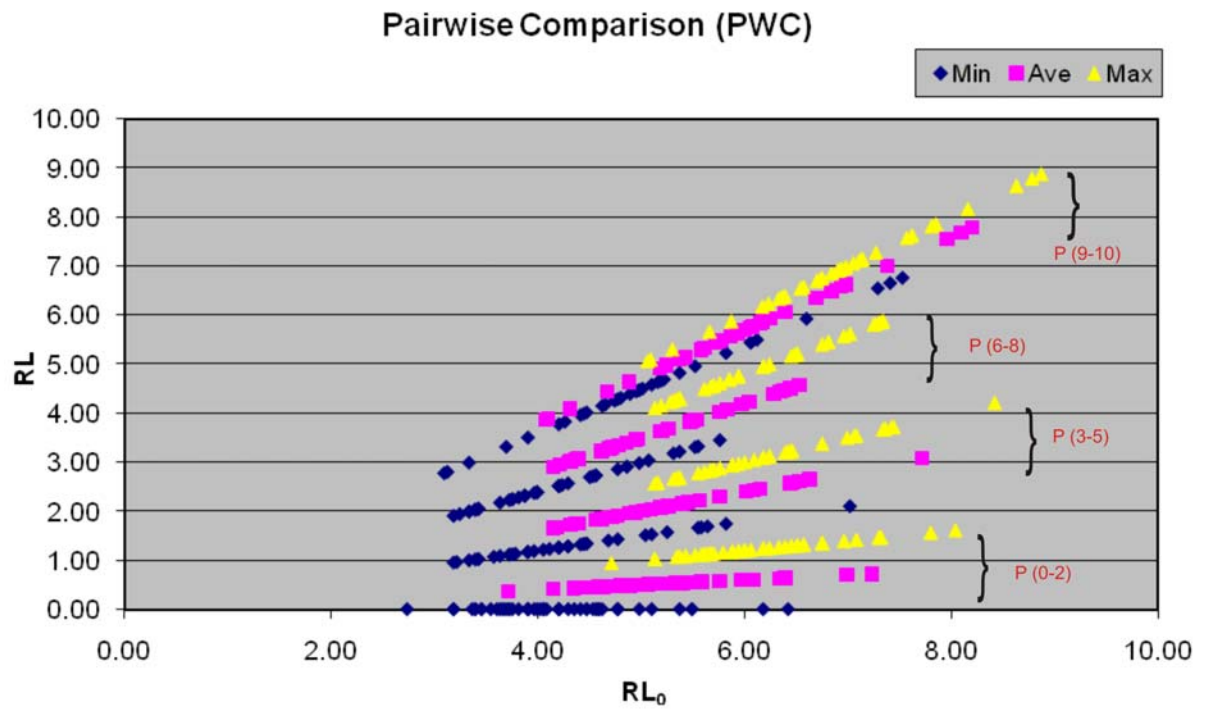


Fig 6.12: Plot of the risk level values of brittle tectonic structures – related to reservoir leakage by pairwise comparison (*PWC*) approach RL vs RL_0 (the blue rhombus – minimum, purple rectangle – average and yellow triangle – maximum values of the class parameter). See **Appendix B-2** for the data.

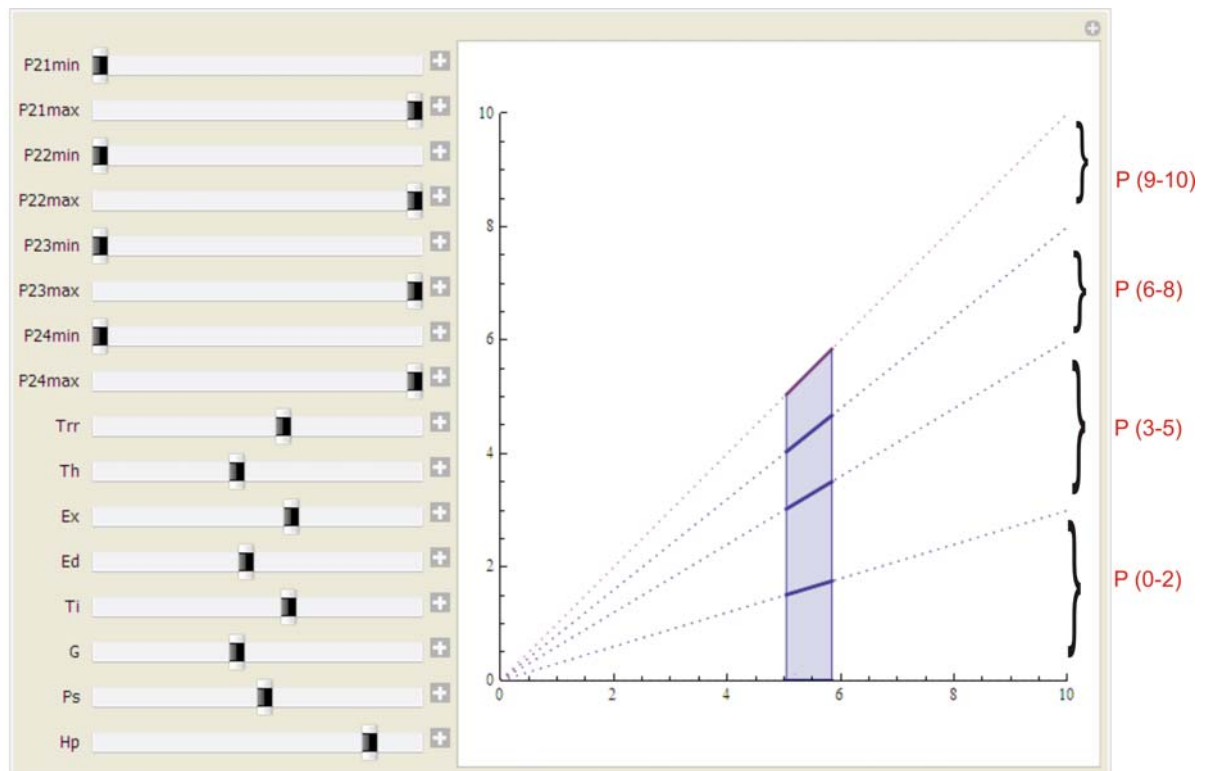


Fig 6.13: Assessment of the risk level of brittle tectonic structures – related to reservoir leakage by pairwise comparison (*PWC*) approach RL vs RL_0 (see **Appendix C-2** for the detail description of the equation and additional graph).

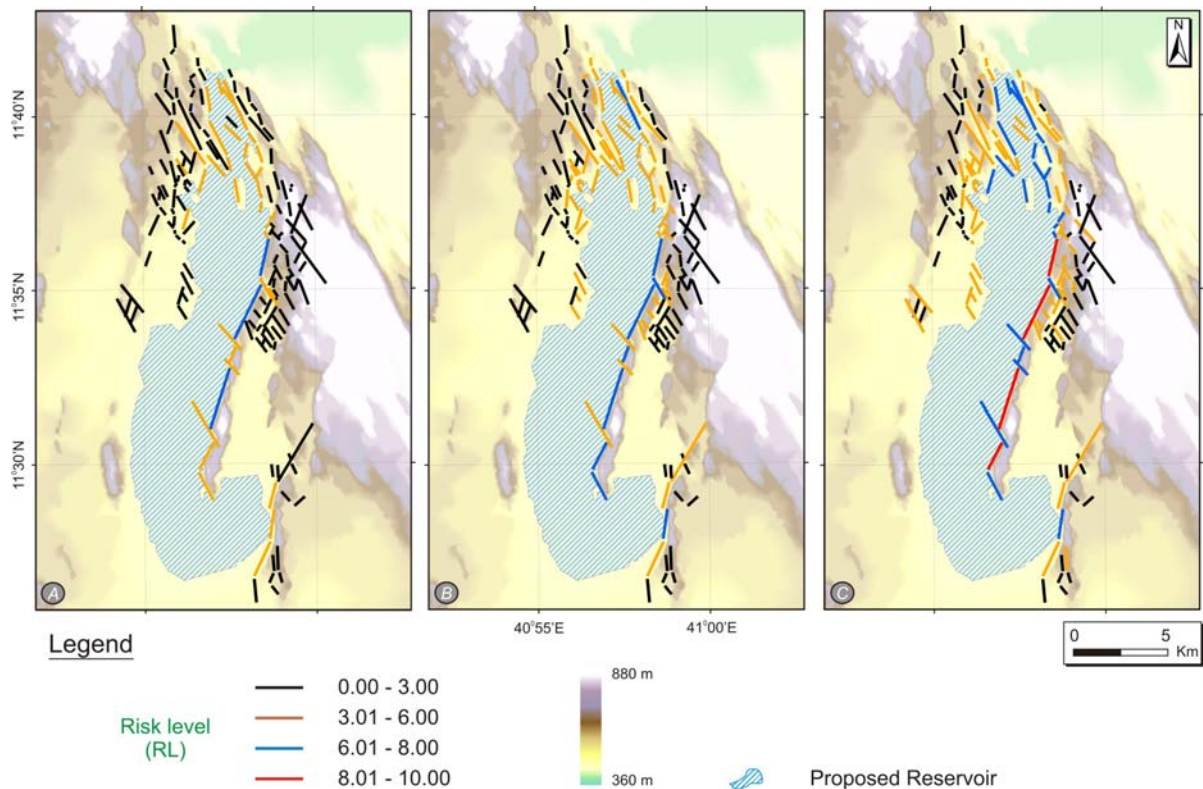


Fig 6.14: Risk level of brittle tectonic structures – related to reservoir leakage by pairwise comparison (PWC) approach: (a) minimum value of the class, (b) average value of the class and (c) maximum value of the class.

6.3.3 Analytical Hierarchical Process (AHP)

Teknomo, 2004 defines the *Analytic Hierarchy Process (AHP)* as *one of Multi Criteria decision making method that was originally developed by Prof. Thomas L. Saaty (Saaty, 1980)*. In short, it is a method to derive ratio scales from paired comparisons. AHP allow some small inconsistency in judgment because human is not always consistent. The major difference between the AHP and the previous pairwise comparison (PWC) method is AHP use semi-quantitative approach to compare the pairs of the parameters (see **Appendix B-5a** for the description of the fundamental scale of absolute numbers of Saaty, 1980, 2004a, 2004b). According to Saaty, 1980, 2004a and 2004b, the AHP based decision making method includes the following steps; *A Structuring the decision problem into a hierarchical model, B Making pair-wise comparison and obtaining the judgmental matrix, C Making local priorities and consistency comparisons and D Aggregation of priorities* (Woldearegay, 2005). **Table 6.3** summarizes the steps and result of the AHP.

For *Equation 6.6* (RL_{AHP}), the coefficients of the parameters were taken from the AHP result of less than 10% consistency ratio. The average of the nine parameters was multiplied by the

Proximity P parameter as it is shown at Equation 6.6 (RL_{AHP}). The overall result was divided by 10 to get the maximum risk level value 10.

Table 6.3: Analytic hierarchy process (AHP) of the risk parameters.

		Trr	Ex	Cci	Th	G	Ts	Ps	Ed	Hp	Weight
Tectonic Region	Trr	1	4	5	5	6	6	8	8	8	0.37
Areal Extention	Ex	1/4	1	3	3	4	4	5	5	6	0.19
Cross cut Index	Cci	1/5	1/3	1	3	3	3	4	4	5	0.13
Tectonic History	Ti	1/5	1/3	1/3	1	2	3	4	4	5	0.10
Geology	Th	1/6	1/4	1/3	1/2	1	2	2	3	3	0.07
Tectonic Status	G	1/6	1/4	1/3	1/3	1/2	1	2	2	3	0.05
Relative Position	Ts	1/8	1/5	1/4	1/4	1/2	1/2	1	2	2	0.04
Elevation Difference	Ps	1/8	1/5	1/4	1/4	1/3	1/2	1/2	1	2	0.03
Hydraulic Pressure	Hp	1/8	1/6	1/5	1/5	1/3	1/3	1/2	1/2	1	0.02

$$n = 9; \lambda_{max} = 9.92; CI = 0.11; CR = 0.079;$$

Where- n – number of parameters,

λ_{max} – highest eigenvalue,

CI – consistency index

$$CR = \frac{CI}{RI}$$

RI – Random consistency index (See **Appendix B-5b**)

and CR – consistency ratio

$$RL[AHP] = \frac{P \cdot (3.7Trr + 1.9Ex + 1.3Cci + Th + 0.7G + 0.5Ts + 0.4Ps + 0.3Ed + 0.2Hp)}{100} \quad (6.6)$$

The risk level was compared by changing the value of the class within the same class; minimum, average and maximum (see **Fig 6.15**). The result shows that the mean values of the risk level in different classes constantly increases as the class value of the parameters increase from minimum to maximum within the class.

Fig 6.16 and **Fig 6.17** show the data plot and Mathematica analysis results equation 6.7 verses 6.6, respectively. **Fig 6.18** shows the result of the brittle tectonic risk assessment – related to reservoir leakage.

$$RL_o[AHP] = \frac{(3.7Trr + 1.9Ex + 1.3Cci + Th + 0.7G + 0.5Ts + 0.4Ps + 0.3Ed + 0.2Hp)}{100} \quad (6.7)$$

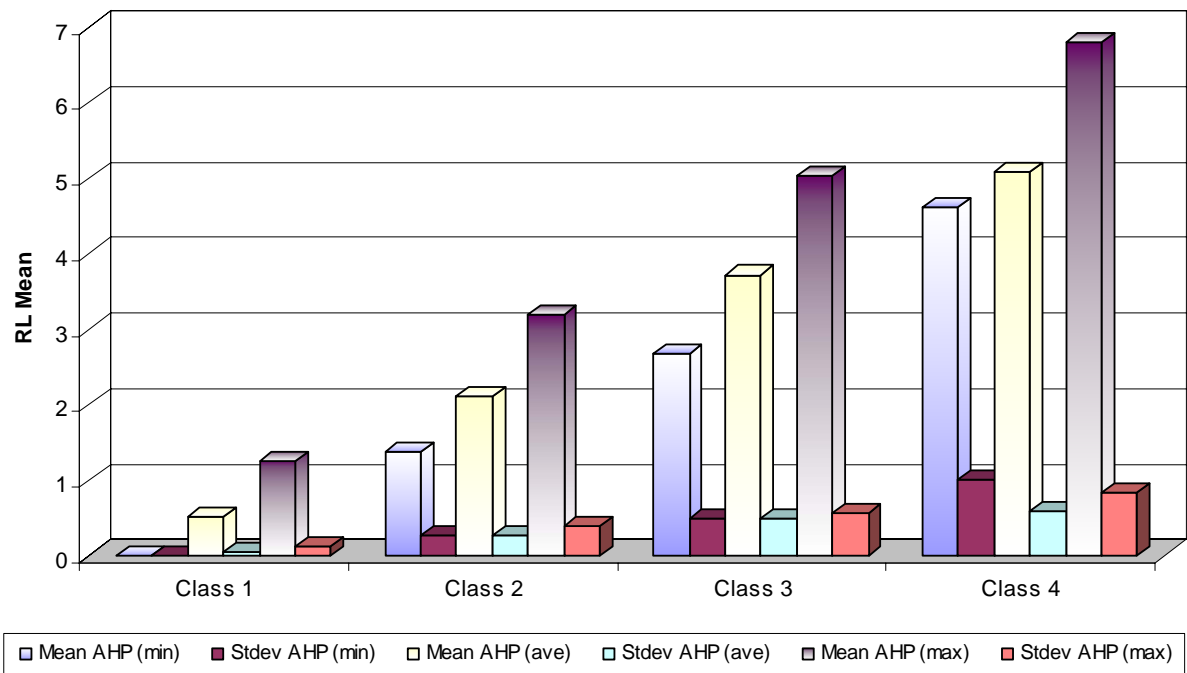


Fig 6.15: Mean and standard deviation of the risk level values of brittle tectonic structures – related to reservoir leakage by analytic hierarchy process (AHP) approach (See **Appendix B-2** for the data).

According to the Analytical Hierarchy Process (AHP) approaches, the risk levels of the structures were analyzed with varying the value of the parameter classes. As it is shown on **Fig 6.18**, the minimum values of the classes resulted with low and medium risk level of the brittle tectonic structures except three structures which showed high risk level.

When the medium values of the classes were taken, four brittle tectonic structures resulted with high risk level and the remaining other structures had low and medium risk level. Four brittle tectonic structures resulted with very high risk level and twenty eight structures with high risk level when the maximum value of the classes were taken for the analysis of the risk assessment of the brittle tectonic structures – related to reservoir leakage.

6.4 Risk Estimation

The Awash River flow/discharge rate was measured since 1962 at the Tendaho gauge station by the Ethiopian Ministry of Water Resources (WWDSE-WPCS-I, 2005). Based on the records of the last 40 years, the Awash River has a mean flow rate of $100\text{m}^3/\text{s}$ at the Tendaho dam site. The capacity of the proposed Tendaho reservoir is estimated as 1.8 billion m^3 with a maximum reservoir level of 410m above sea level.

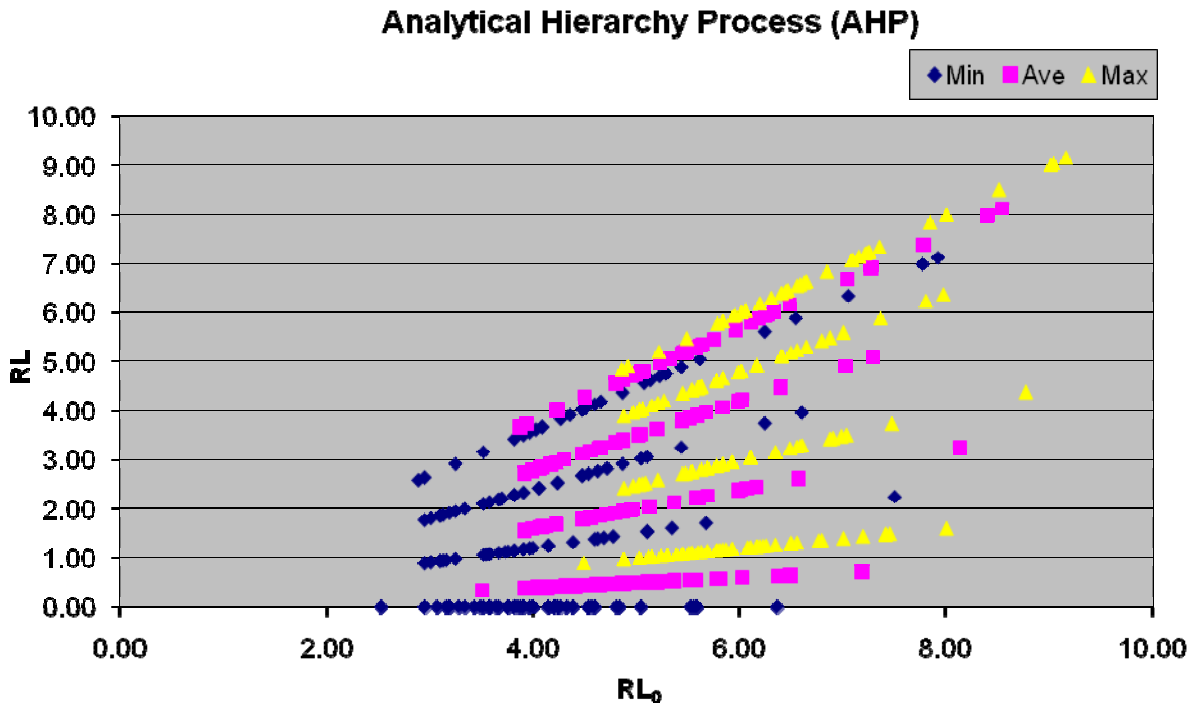


Fig 6.16: Plot of the risk level values of brittle tectonic structures – related to reservoir leakage by analytic hierarchy process (*AHP*) approach RL vs RL_0 (the blue rhombus – minimum, purple rectangle – average and yellow triangle – maximum values of the class parameter). See **Appendix B-2** for the data.

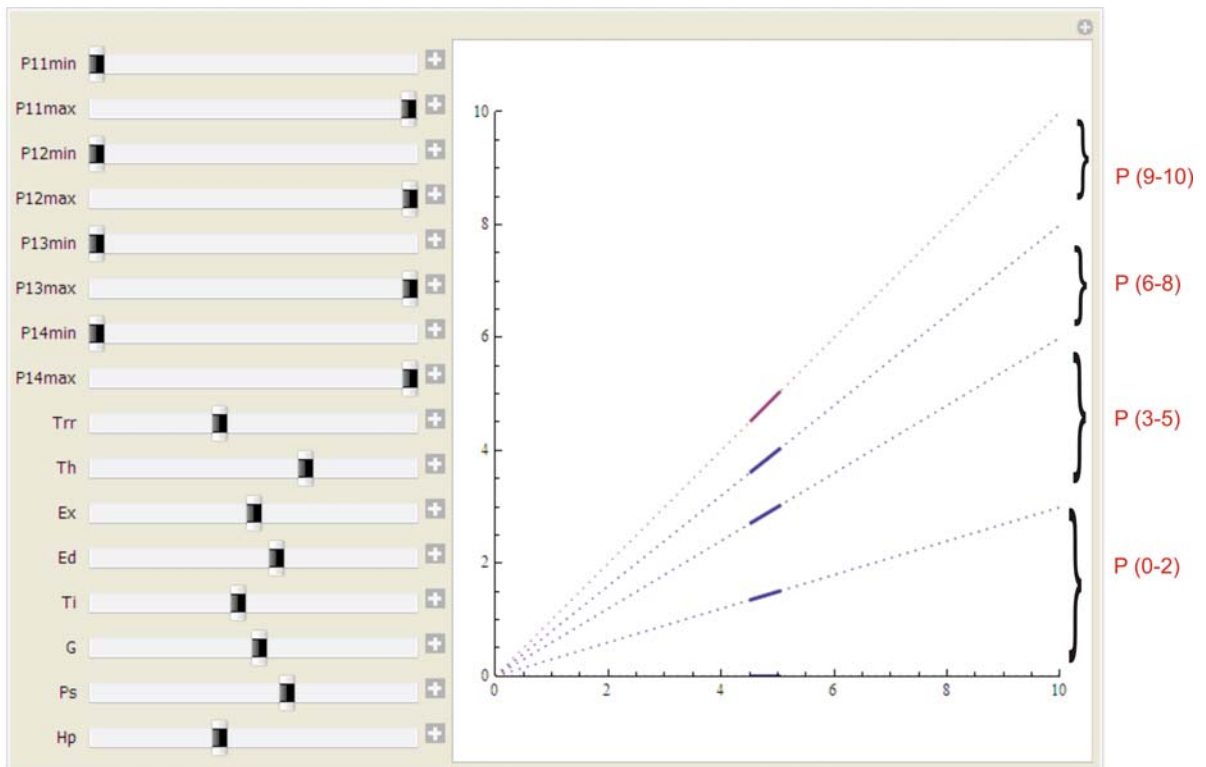


Fig 6.17: Assessment of the risk level of brittle tectonic structures – related to reservoir leakage by analytic hierarchy process (*AHP*) approach RL vs RL_0 (see **Appendix C-3** for the detail description of the equation and additional graph).

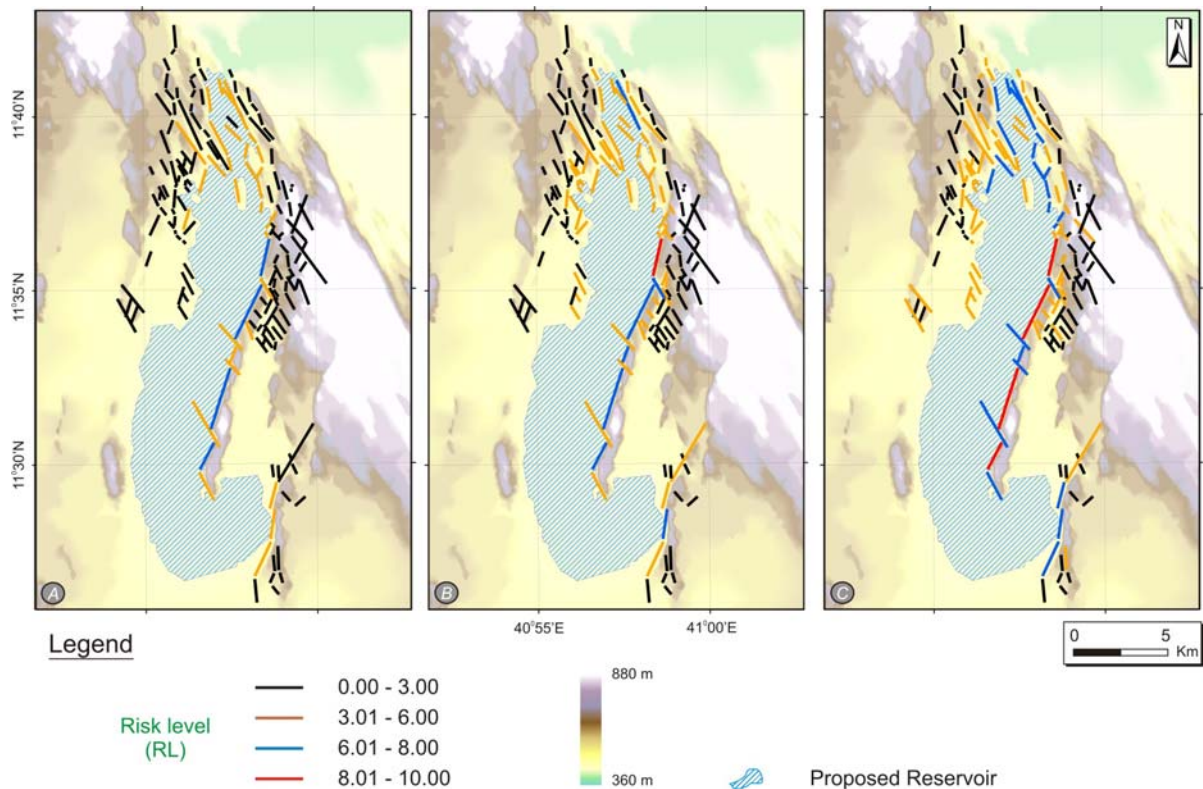


Fig 6.18: Risk level of brittle tectonic structures – related to reservoir leakage by analytic hierarchy process (AHP) approach: (a) minimum value of the class, (b) average value of the class and (c) maximum value of the class.

In this study, it is believed that there could be a potential reservoir leakage due to the unforeseen geological condition (the hydrogeological behavior of brittle tectonic structures) at the feasibility studies of the project.

Among the 168 brittle tectonic structures which are located at a distance of 2km buffer zone from the maximum level of proposed Tendaho reservoir, only 31 structures are selected for the risk estimation of reservoir leakage analysis. The structures are selected based on their risk level of the applied approaches (*AVE*, *PWC* and *AHP*) in the previous section. Structures with risk level greater than 6.01 in all approaches and intersected or completely included within the extent of maximum level of proposed Tendaho reservoir were used to estimate the worst and average scenarios of the brittle tectonic structures risk – related to reservoir leakage. **Fig 6.19** shows the location and distribution of the selected brittle tectonic structures for the risk estimation.

The project authorities of the Tendaho dam and irrigation project measured the permeability of the fractured basalt along the dam axis and on the reservoir ridge by pressure test (see **Appendix B-3** for the summary of the permeability test data). For the present study, the

maximum and medium values of the pressure test results were used for the estimation of the worst and average scenarios of the risk the reservoir leakage through the brittle tectonic structures, respectively. Equation 6.8 was applied for the risk estimation calculation of reservoir leakage.

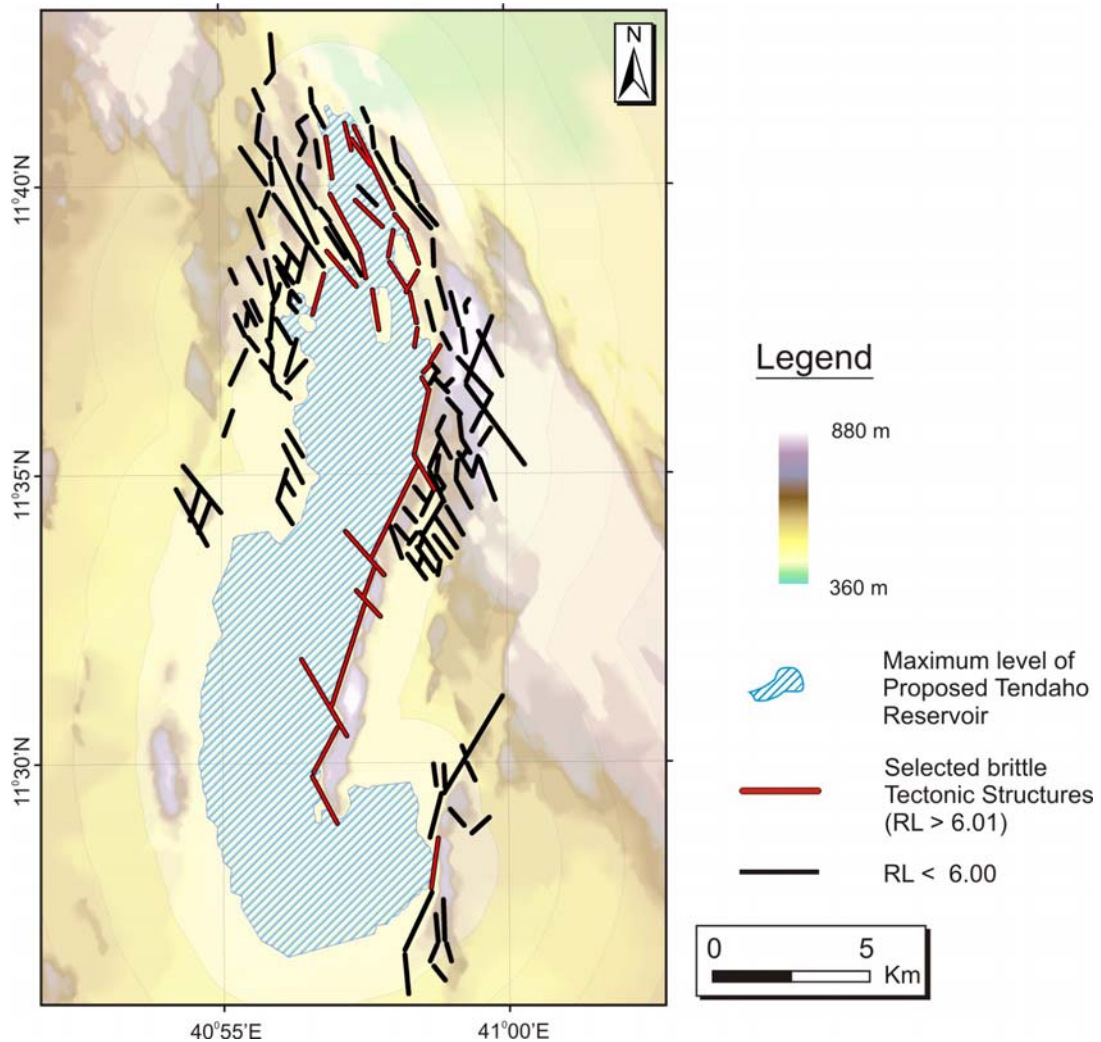


Fig 6.19: Selected brittle tectonic structures for the risk estimation of the reservoir leakage. See **Appendix A-10** for higher resolution.

The values of the actual pressures on the brittle tectonic structures were calculated from the average reservoir height above the structure (Equation 6.9). According to the estimation, there could be a potential leakage rate of $25.4\text{m}^3/\text{s}$ and $2.4\text{m}^3/\text{s}$ for the worst and average scenarios, respectively, from the proposed Tendaho reservoir through the brittle tectonic structures. Moreover, the worst and average scenarios of the risk estimation were checked for an ideal value of pressure test (100 and 10 Lugeon). **Table 6.4** summarizes the results of calculated reservoir leakage through the brittle tectonic structures.

$$\text{Lugeon Unit} = \text{Liter / meter / minute} * \frac{10 \text{ (bars)}}{\text{actual pressure (bars)}} \quad (6.8)$$

$$P_{\text{Actual}} = \rho gh \quad (6.9)$$

Where P_{Actual} – actual pressure, ρ – density of water, g – gravitational acceleration and h – average height of the water above the brittle tectonic structure

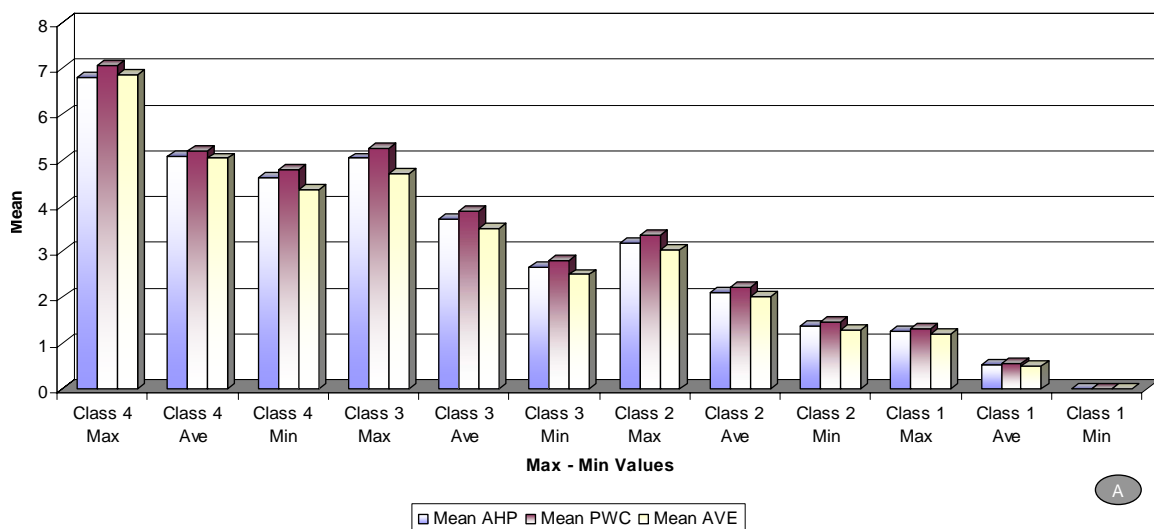
Table 6.4: Summary of risk estimation of proposed Tendaho reservoir leakage through the brittle tectonic structures for the worst and average scenarios.

	Id	Average RL	Length (m)	Average height (m)	Average Pressure (bar)	Worst Calculated leakage (L/min) 100 Lugeon	Average Calculated leakage (L/min) 10 Lugeon	Worst Calculated leakage (L/min) 316 Lugeon	Average Calculated leakage (L/min) 30 Lugeon
1	49	8	644	15	1.47	9467	947	29915	2840
2	51	7	1851	15	1.47	27216	2722	86004	8165
3	52	7	1124	15	1.47	16521	1652	52206	4956
4	53	7	2835	15	1.47	41681	4168	131713	12504
5	54	7	849	15	1.47	12480	1248	39438	3744
6	55	8	1615	5	0.49	7912	791	25002	2374
7	56	9	3384	15	1.47	49740	4974	157178	14922
8	57	8	923	15	1.47	13565	1356	42865	4069
9	58	9	3222	5	0.49	15789	1579	49894	4737
10	61	7	804	5	0.49	3940	394	12449	1182
11	72	8	2916	15	1.47	42871	4287	135473	12861
12	73	7	648	15	1.47	9526	953	30101	2858
13	74	6	483	5	0.49	2367	237	7479	710
14	75	7	853	15	1.47	12546	1255	39645	3764
15	76	7	995	15	1.47	14621	1462	46202	4386
16	77	7	382	5	0.49	1872	187	5915	562
17	78	7	975	15	1.47	14339	1434	45310	4302
18	79	7	585	15	1.47	8596	860	27163	2579
19	88	6	397	5	0.49	1945	195	6147	584
20	89	7	2038	15	1.47	29958	2996	94669	8988
21	91	7	877	35	3.43	30092	3009	95090	9028
22	99	7	1344	15	1.47	19752	1975	62418	5926
23	135	7	1329	15	1.47	19534	1953	61727	5860
24	140	6	735	15	1.47	10805	1080	34142	3241
25	145	7	1042	25	2.45	25520	2552	80644	7656
26	147	7	299	5	0.49	1465	147	4630	440
27	148	9	2045	15	1.47	30069	3007	95017	9021
28	153	7	318	5	0.49	1559	156	4926	468
29	154	6	385	15	1.47	5653	565	17864	1696
Total						481400	48140	1521225	144420
m³/s						8.02	0.80	25.35	2.41

Where Id – identification numbers for the brittle tectonic structures, $Average\ RL$ – the average risk level of brittle tectonic structures - related to reservoir leakage from AVE, PWC and AHP approaches, $Average\ Height$ – average reservoir height above the exposed location of the brittle tectonic structures and $Average\ Pressure$ – vertical hydraulic pressure due to the reservoir head

6.5 Discussion

GIS based risk assessment of geohazards is widely practiced by many countries and research groups. To predict the risk of spatially and temporally variable parameters of the geohazards, GIS based approaches are the state of art for the present risk assessment advancement. However, the accuracy of the risk level depends on the quality of the risk parameter description either in terms of qualitative or quantitative approaches. The present semi-quantitative descriptions of the risk parameters were examined by three approaches (*AVE*, *PWC* & *AHP*) as it was discussed in the previous sections. For comparison **Fig 6.20** shows the mean and standard deviations of the three used approaches. The mean values of the risk level and their standard deviation from the mean has higher and lower values, respectively by the *Pairwise comparison PWC* approach compared with the other two (*AVE* & *AHP*). This shows as such there is no big difference whether one considers a simple weighting or qualitative or semi-quantitative approaches. The map distribution of the brittle tectonic structures risk level – related to the reservoir leakage shows that structures which are closed to the proposed maximum level of the Tendaho reservoir, higher aerial extent, formed by the extensional tectonics and cross cut by other structures have high risk level. **Fig 6.21** shows the map distribution of the risk level result from the applied approaches. Risk level of the tectonic structures has higher values in the *PWC* approaches rather than the others.



The worst scenario of the reservoir leakage, which is based on the pressure test of the fracture geology, reduces the potential of the Awash River to fill the proposed Tendaho reservoir by 25%. These unexpected losses of water through the brittle tectonic structures directly affect the downstream irrigation project and may trigger seismotectonic hazard in the area. The average scenario of the brittle tectonic structures risks – related to the reservoir

leakage, is less than the expected/known water losses by evaporation (annual evaporation rate - 2078 mm/year – see **Appendix B-4** for the detail summary of evaporation data).

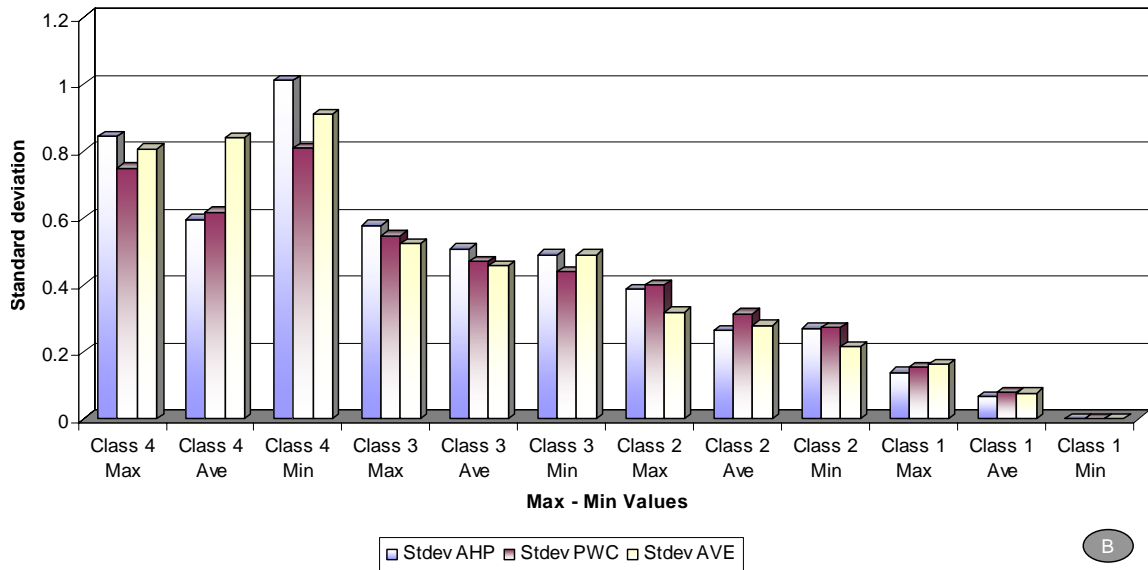


Fig 6.20: (a) Mean value and (b) Standard deviation of the risk level of brittle tectonic structures – related to reservoir leakage by AVE, PWC and AHP approaches.

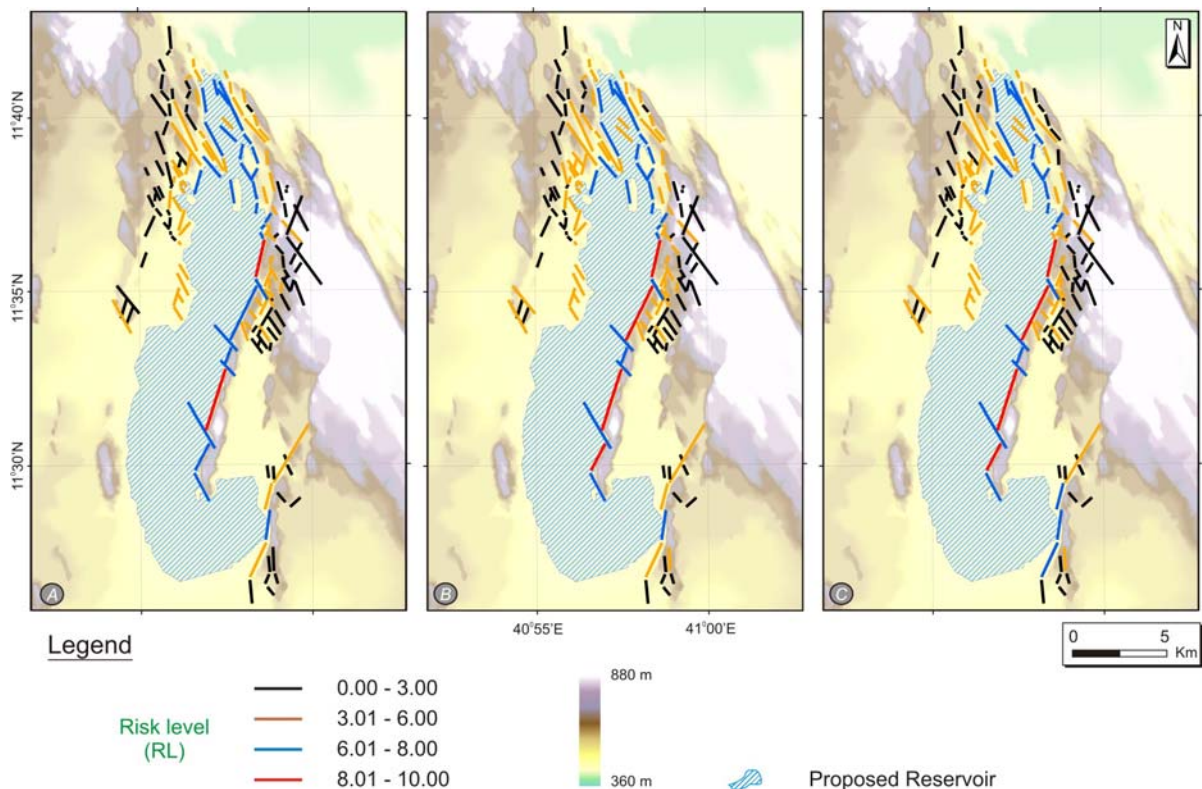


Fig 6.21: Compare the risk level of brittle tectonic structures – related to reservoir leakage from (a) Simple averaging AVE, (b) Pairwise comparison PWC and (c) Analytical hierarchy process AHP (maximum values of the classes are taken for the risk level analysis). See **Appendix A-11** for higher resolution.

Chapter Seven

Conclusion and Future Research Direction

7.1 Conclusion

To understand the tectonic situation and assess the tectonic related risks at the Tendaho reservoir and irrigation sites, different methodologies and data were used. Based on the results, the following conclusions are drawn:

- Dragging the Landsat ETM+ image and aerial photographs on the Triangular irregular network (TIN) model of 20 meter contour interval is more powerful to interpret geomorphologically defined tectonic structures visually than the Shuttle Radar Topographic Mission (SRTM) digital elevation model of 90 meter resolution.
- The Tendaho dam and irrigation site was subjected to a sequence of extensional tectonic processes in different direction. The Gesye graben which is located at the Tendaho Goba'ad discontinuity ridge (TGD) is formed during the propagation of the Main Ethiopian Rift (MER) system towards the Afar Depression. The graben is bisected by the basaltic dyke intrusion at the center and the younger Red Sea rift propagation structures crosscut the MER structures and Gesye graben too. The Main Ethiopian Rift structures are inter-fingered with the Red Sea Rift structures along the TGD (including the entire reservoir area) and recent extensional activities are concentrated within the Tendaho Graben along the NE-SW extension direction. Such past and active tectonic processes may dramatically increase the water conductivity of a rock mass and decrease the water tightness of the reservoir area.

- With a limited experience of active rifting events, the prediction of potential occurrence of the active rifting hazard could consider the theoretical background of the hazard nature/characteristic (like the Tendaho graben was opened by the Tendaho and Manda Hararo rift with a *constant spreading rate* and/or *violent rifting episodes*). Based on the discussed assumptions, active rifting hazard could happen with the average potential occurrence of 0.6% and 1.8% from the Manda Hararo and Tendaho rift, respectively during the life time of the project.
- In the previous studies (Knill, 2003; Price, 2009), the engineering properties of the earth material and mass fabric (discontinuity) of the different geological conditions were studied and fundamental knowledge was acquired. Keeping in mind the fundamental knowledge of the engineering properties of the extensional brittle tectonic structures, risk assessment approach of unforeseen geological conditions for the feasibility stage of the project was designed with selection and justification of key parameters. Brittle tectonic structures which are formed by extensional tectonic activities, younger, larger in their aerial extents, and cross cut by another tectonic structures have higher risk level to reservoir leakage. From the present risk assessment studies it is concluded that the GIS based approach of semi-quantitative risk assessment of the brittle tectonic structures – related to reservoir leakage can be used for *feasibility studies* of similar project site with some particular modification.
- From the present study it is found that the water tightness of Tendaho dam reservoir or irrigation scheme may not be much affected due to any future seismic activity, if any. Any future active rifting episodes may result into development of new rock fractures and may change existing rock fracture characteristics which may ultimately increase the water loss from the reservoir and irrigation scheme. It is expected that these additional water losses will be marginal and within the permissible limits. Moreover, seepage from reservoir is not simply dependent on the orientation and continuity of structural fractures but it also depends on the groundwater regime and the pre-existing permeability of the rocks in the reservoir flanks (Knill, 1971).

7.2 Future Research Direction

As Knill, 2003 said ‘understanding the past and present geological conditions of the given area help to minimize the unexpected risks on the proposed engineering structures or human

life due to the unforeseen geological conditions'. Interpretation of geological conditions like tectonic processes and structures can be further studied and simplified for the engineering and environmental applications. Besides, groundwater regime and permeability condition should also be studied in detail to work out the seepage potential of rocks in the reservoir area. As it is not always true that the reservoir water will recharge the subsurface water of the region, the flow in some conditions may be from the subsurface water towards the reservoir. For this the factors which influence the water leakage from the reservoir are; (i) Piezometric conditions in the reservoir's floor & flanks and (ii) Natural permeability of the floor and flank (Knill, 1971).

References

- Abbate, E., Passerini, P. & Zan, L. 1995. Strike-slip faults in a rift area: a transect in the Afar Triangle, East Africa. *Tectonophysics*, 241, 67-97.
- Abdelsalam, M.G., Robinson, C., El-Baz, F., Stern, R.J. 2000. Applications of orbital imaging radar for geologic studies in arid regions: The Saharan testimony. *Photogrammetric Engineering and Remote Sensing* 66, 717–726.
- Acocella, V., Abebe, B., Korme, T., & Barberi, F. 2008. Structure of Tendaho Graben and Manda Hararo Rift: Implications for the evolution of the southern Red Sea propagator in Central Afar. *Tectonics*, Vol. 27, No. 4, 17pp.
- Acton, G.D. & Stein, S. 1991. Block rotation and continental extension in Afar; a comparison to oceanic microplate systems. *Tectonics*, 10, 501-526.
- Acton, G.D., Tessema, A., Jackson, M. & Bilham, R. 2000. The tectonic and geomagnetic significance of paleomagnetic observations from volcanic rocks from central Afar, Africa. *Earth and Planetary Science Letters*, 180, 225–241.
- Afrouz, A.A. 1992. *Practical Handbook of Rock Mass Classification Systems and Modes of Ground Failure*. CRC Press, Inc., ISBN 0-8493-3711-9, pp.195, United States of America.
- Albert, Jim 1996. *An Introduction to Probability*. Document published was accessed on January, 2009 at: <http://www-math.bgsu.edu/~albert/m115/probability/outline.html>.
- Al-Saigh, N.H., Mohammed, Z.S., and Dahham, M.S. 1994. Detection of water leakage from dams by self-potential methods. *Engineering Geology*, 37, p115-121.
- Anbalagan, R. 1992a. Landslide hazard evaluation and zonation mapping in mountainous terrain. *Engineering Geology* Vol.32, No.4, pp.269–277.
- Anbalagan, R., Sharma,S., Raghuvanshi, T.K., (1992) “Rockmass Stability Evaluation using Modified SMR Approach” *Nati. Sympto. on Rock Mechanics*, 1992, pp.258 – 268
- Anbalagan, R., (1996) “Landslide hazard and risk assessment mapping of mountainous terrains- a case study from Kumaun Himalaya, India”. *Elsevier Science Publ., Eng.Geol.*43. Amesterdam, pp.237- 246.

- Angelier, J. 1994. Fault Slip Analysis and Palaeostress reconstruction. University of Bristol, UK, Pergamon Press.
- Aquater, 1996. Tendaho Geothermal Project Final Report – Volume I and II. Ethiopian Geological Survey, Addis Ababa, Ethiopia.
- Asfaw, L.M. 2007. Integrated Approach to the study of geohazards with the application in southern Afar. *Journal of African Earth Sciences*, Vol. 48, Iss. 2-3, pp. 237-244.
- Ayele, A. 1995. Earthquake catalogue of the Horn of Africa for the period 1960–93, Seism. Dept, Uppsala Univ., report 3–95, p. 32.
- Ayele, A., Jacques, Eric, Kassim, Mohammed, Kidane, Tesfaye, Omar, Ahmed, Tait, Stephen, Nercessian, Alexandre, Chabaliere, Jean-Bernard de, King, Geoffrey, 2007. The volcano-seismic crisis in Afar, Ethiopia, starting September 2005, *Earth Planet. Sci. Lett.*, 255, 177–187.
- Ayele, A., Nyblade, A.A., Langston, C.A., Cara, M., & Leveque, J-J. 2006. New evidence for Afro-Arabian plate separation in southern Afar. *The Geological Society of London, Special Publications*, 259, 133-141.
- Ayenew, Tenalem, Kebede, Seifu, Alemyahu, Tamiru 2008. Environmental isotopes and hydrochemical study applied to surface water and groundwater interaction in the Awash River basin. *Hydrological Processes*, 22, p1548-1563.
- Barberi, F., Ferrara, G., Santacroce, R. & Varet, J. 1975. Structural evolution of the Afar triple junction. In: A. Roesler (Editor), *Afar Depression of Ethiopia*. E. Schweizer, Stuttgart, Federal Republic of Germany, 38-54.
- Barton, N., Lien, R. and Lunde, J. 1974. Engineering classification of rock masses for the design of rock support. *Rock Mechanics* 6, 1974, pp. 189-236.
- Baynes, F.J., Fookes, P.G., & Kennedy, J.F. 2005. The total engineering geology approach applied to railways in the Pilbara, Western Australia. *Bull. Eng. Geol. Environ.* Vol. 64, pp. 67-94.
- BBC (British Broadcasting Corporation) news, 2007. Fears after volcano in Ethiopia. Press release, 15/08/2007. <http://news.bbc.co.uk/2/hi/africa/6948138.stm>.
- BBC (British Broadcasting Corporation) news, 2008. Ethiopia Volcano sets lare record. Press release, 5/13/2008. <http://news.bbc.co.uk/2/hi/africa/7711377.stm>.
- Beiniawski, Z.T. 1976. Rock mass classifications in rock engineering. *Proceedings Symposium Exploration Rock Engineering*, Johannesburg, pp. 97-106.
- Beyene, A. & Abdelsalam, M.G. 2005. Tectonics of the Afar Depression: A review and synthesis. *Journal of African Earth Sciences*, 41, 41-59.

- Beyene, A. 2004. Evolution of the Afar Depression from orbital optical and radar images, Ethiopia. Ph.D. Dissertation, University of Texas at Dallas, Richardson, p. 138.
- Bieniawski, Z.T. 1989. Engineering Rock Mass Classifications. Ed WILEY, New York, pp.252, United States of America.
- Bock, H. 2006. Common ground in engineering geology, soil mechanics and rock mechanics: past, present and future. Bull. Eng. Geol. Environ. Vol. 65, pp. 209-216.
- Buck, W. R., P. Einarsson, and B. Brandsdóttir 2006. Tectonic stress and magma chamber size as controls on dike propagation: Constraints from the 1975–1984 Krafla rifting episode, *J. Geophys. Res.*, 111, B12404, doi:10.1029/2005JB003879.
- Coates, D.F. 1963. Classification of Rock for Rock Mechanics. International Journal of Rock Mechanics and Mining Sciences & Geomechanics Abstracts, Vol.1, pp. 421-429.
- Courtillot, V. 1984. Episodic spreading and rift propagation; new paleomagnetic and geochronologic data from the Afar nascent passive margin. JGR. Journal of Geophysical Research. B, 89, 3315-3333.
- Crowe, Bruce M. 1986. Volcanic Hazard Assessment for Disposal of High-Level Radioactive Waste. Active Tectonics: Impact on Society, National Academic Press, Washington D.C., p266.
- Currey DT. 1973. Geomorphic, Geological and Groundwater Studies in the Awash Valley. Development of the Awash Valley Phase III, Tech. Rept. 4, UNDPjSFjETH25. Ministry of Water resources, unpublished report, Addis Ababa, Ethiopia.
- Deere, D.U. 1968. Geological consideration. In: K.G. Stagg and O.C. Zienkiewicz, Editors, *Rock Mechanics in Engineering Practice*, Wiley, London (1968).
- Ebinger, C.J. & Casey, M., 2001. Continental breakup in magmatic provinces: an Ethiopian example, *Geology*, **29**, 527–530.
- Ebinger, C.J. 2006. The Birth of an Ocean. Natural Environment Research Council, Planet Earth, p26-27, <http://www.nerc.ac.uk/publications/planetearth/2006/autumn/>.
- Ebinger, C.J., Keir, D., Ayele, A., Baker, E., Rowland, J., Wright, T. & Calais, E., 2006. Continued seismic and magmatic activity following the September 2005 rupture of the Dabbahu magmatic segment, Afar, *Eos Trans. AGU*, **87**(52), Fall Meet. Suppl., abstract T41B-1562.
- Ebinger, C.J., Keir, D., Ayele, A., Calais, E., Wright, T.J., Belachew, M., Hammond, J.O.S., Campbell, M.E., and Buck, W.R., 2008, Capturing magma intrusion and faulting process during continental rupture: Seismicity of the Dabbahu (Afar) rift: *Geophysical Journal International*, v. 174, p. 1138–1152, doi: 10.1111/j.1365–246X. 2008.03877.x.

- Engelder, T. 1985. Loading paths to joint propagation during a tectonic cycle: An example from the Appalachian Plateau, USA: *Journal of Structural Geology*, Vol.7, pp456-476.
- Ethiopian Electric power corporation (EEPSCO), 2004. Gilgel Gibe II Hydro electric power project Geotechnical report for tunnel alignment, Addis Ababa, Ethiopia.
- Ethiopian Electric Power Corporation (EEPSCO), 2007. Gilgel Gibe II Hydro-Electric Project site visit of May19 to May 21, 2007 report by ELC- TBM specialists.
- FAO/SOGREAH, 1965. Report on Survey of the Awash River Basin. Unpublished report, Addis Ababa, Ethiopia.
- Fault dynamics research group, 2007. The website was accessed on January 12, 2008 <http://fdrg.rhul.ac.uk/index.html>.
- Fekadu, N. 2006. Engineering Geological Studies for suitability of Construction Material and Foundation Condition Evaluation - with special emphasis on seepage studies – Tendaho Dam; Afar Region, Ethiopia. Masters Thesis, Addis Ababa University, Ethiopia, pp. 123.
- Fell, R., Ho, K.K.S, Lacasse, S., and Leroi, E. 2005. A framework for landslide risk assessment and management. *Landslide Risk Management*, proceedings of the international conference on landslide risk management, Vancouver, Canada, 31 May-3 June 2005, p3-25.
- Gibbs, A., & Partners 1975. Feasibility Study of the Lower Awash Valley. With association Hunting Technical Service Ltd. Comp., London, unpublished report.
- Gouin, P. 1979. Earthquake History of Ethiopia and the Horn of Africa. International Development Research Center, Ottawa, Ontario.
- Gresta, S., Patane, D., Daniel, A., Zan, L., Carletti, A., & Befekadu, O. 1997. Seismological Evidence of Active Faulting in the Tendaho Rift (Afar Triangle, Ethiopia). *Pure and Applied Geophysics*. Vol. 149, p357-374.
- Grinstead, Charles M. and Snell, J. Laurie 1997. *Introduction to Probability*, 2nd Edition. American Mathematical Society, p508.
- Gupta, R.P. 2004. *Remote Sensing Geology*. Springer, Berlin, Federal Republic of Germany (DEU), 2nd Edition, ISBN 3-5404-3185-3, pp.655, Germany.
- Halcrow, 1989. Master plan for the development of surface water resources in the Awash basin. Vol.4, Climate and Hydrology. Minister of Water Resources Library, Addis Ababa, Ethiopia, unpublished report.

- Halcrow, 1989. Master plan for the development of surface water resources in the Awash basin. Vol.8, Climate and Hydrology. Minister of Water Resources Library, Addis Ababa, Ethiopia, unpublished report.
- Hamling, I., Keir, D., Ayele, A., Calais, E., Ebinger, C., Lewi, E., Yirgu, G., and Wright, T. 2007. Continued dyking in the Dabbuhu Rift segment, Afar, Ethiopia, from radar interferometry. FRINGE 2007 Workshop, European Space Agency.
- Hancock, P.L. 1994. Continental Deformation. University of Bristol, UK, Pergamon Press.
- Hatcher, R.D. 1990. Structural Geology – Principles, Concepts, and Problems. Merrill Publishing Company, A Bell & Howell Information Company; Columbus, Toronto, London and Melbourne. ISBN 0-675-20626-X United States of America.
- Heister, Katja, Kleingeld, Pieter J., Keijzer, Thomas J.S., and Loch, J.P. Gustav 2005. A new laboratory set-up for measurements of electrical, hydraulic, and osmotic fluxes in clays. *Engineering geology*, 77, p295-303.
- Hoek, E. 1999. Putting number to geology – an engineer’s view. *Quarterly Journal of Engineering Geology*, Vol. 32, No. 1 (1-19).
- Hofstetter, R. & Beyth, M. 2003. The Afar Depression; interpretation of the 1960-2000 earthquakes. *Geophysical Journal International*, 155, 715-732.
- Hudson, J.A., & Priest, S.D. 1979. Discontinuities and rock mass geometry. *International Journal of Rock Mechanics and Mining Sciences & Geomechanics Abstracts*, Volume 16, Issue 6, December 1979, Pages 339-362.
- IAGE, 2000. Statutes of the International Association for the Engineering geology and the Environment. Statutes adopted by IAEG Council in Kyoto [1992], modified by the Council in Athens [1997] (article I - Name of the Association) and in Rio de Janeiro [2000] (article IV - Membership, and Article IX - Meetings of the Association).
- ITC (International Institute for Geo-Information Science and Earth Observatory, Netherlands), 2009. Distance Course in Multi-Hazard Risk Assessment. Last modified: Monday April 06, 09. http://www.itc.nl/education/courses/course_descriptions/C09-ESA-DED-01.aspx#nowhere.
- Kalkani, E.C. 1997. Geological conditions, seepage grouting, and evaluation of piezometer measurements in the abutment of earth dam. *Engineering Geology*, 46, p93-104.
- Kazmir V. 1973. Geological map of Ethiopia. Ministry of Mines, Energy and Water Resources, Geological Survey of Ethiopia, First edition, Addis Ababa.
- Kearey, P., & Vine, F.J. 1990. *Global Tectonics*. Blackwell Scientific Publications, ISBN 0-632-02425-9, pp. 302, Great Britain.

- Kebede, F., Kim, W.-Y. & Kulhanek, O. 1989. Dynamic source parameters of the March–May 1969 Serdo earthquakes in Central Afar, Ethiopia, deduced from teleseismic body waves, *J. geophys. Res.*, 94, 5603–5614.
- Keir, D., Hamling, I. J., Ayele, A., Calais, E., Ebinger, C.J., Wright, T.J., Jacques, E., Mohamed, K., Hammond, J.O.S, Belachew, M., Baker, E., Rowland, J.V., Lewi, E., Bennati, L. 2009. Evidence for focused magmatic accretion at segment centers from lateral dike injections captured beneath the Red Sea rift in Afar. *Geology* 2009;37;59-62. doi:10.1130/G25147A.1.
- Kidane, T., Courtillot, V., Manighetti, I., Audin, L., Lahitte, P., Quidelleur, X., Gillot, P.Y., Gallet, Y., Carlot, J. & Haile, T. 2003. New paleomagnetic and geochronologic results from Ethiopian Afar: Block rotations linked to rift overlap and propagation and determination of ~ 2 Ma reference pole for stable Africa. *Journal of Geophysical Research*, 108, 1-32.
- Klügel, J.-U., Mualchin, L., and Panza, G.F. 2006. A scenario-based procedure for seismic risk analysis. *Engineering Geology*, 88, p1-22.
- Knill, J.D 1971. Assessment of Reservoir Feasibility. *Quaternary Journal of Engineering Geology*, Vol.4, pp. 355-372.
- Knill, J.L. 2003. Core values: the first Hans-Cloos lecture. *Bulletin of Engineering Geology and the Environment* 62:1–34.
- Lahitte, P, Gillot, P., Kidane, T., Courtillot, V. & Bekele, A. 2003b. New age constraints on the timing of volcanism in central Afar, in the presence of propagating rifts. *Journal of Geophysical Research*, Vol.108, (B2), 2123, doi:10.1029/2001JB001689.
- Lahitte, P., Gillet, P.Y. & Courtillot, V. 2003a. Silicic central volcanoes as precursor to rift propagation: the Afar case. *Earth and Planetary Science Letters*, Vol. 207, pp. 103–116.
- Lane, R.G.T., 1974. Investigations of seismicity at dam/reservoir sites. *Engineering Geology*, 8: 95-98.
- Le Maitre, R.W. 2004. *Igneous Rocks – A Classification and Glossary of Terms*, 2nd Edition. Cambridge University Press, ISBN 0-521-66215-X, pp. 236, United Kingdom.
- Li, Ping, Lu, Wenxi, Long, Yuqiao, Yang, Zhongping, and Li, Jun 2007. Seepage analysis in a fractured rock mass: The upper reservoir of Pushihe pumped-storage power station in China. *Engineering Geology*, 97, p53-62.
- Long, R.E. 1974. Seismicity investigations at dam sites. *Engineering Geology*, 8: 199-212.

- MacDonald, Sir M. and Partners, May 1987, Kesem Irrigation Project Feasibility Study, Final Report.
- Mamo, S., Yokota S. 1998. Estimation of Koka Reservoir leakage paths by integrated hydrogeological and environmental stable isotope techniques. Proceedings of 8th Congress of Engineering Geology, 21 – 25 September Vancouver, Canada.
- Manighetti, I., Tapponnier, P., Courtillot, V., Gallet, Y., Jacques, E. & Gillot, P.Y. 2001. Strain transfer between disconnected, propagating rifts in Afar. *Journal of Geophysical Research* 106, 13, 613-665.
- Manighetti, I., Tapponnier, P., Gillot, P.Y., Jacques, E., Courtillot, V., Armijo, R., Ruegg, J.C., King, G. 1998. Propagation of rifting along the Arabia–Somalia plate boundary; into Afar. *Journal of Geophysical Research* 103, 4947–4974.
- Miall, Andrew D. 2002. An introduction to rift basins and their sediments. *Sedimentary Geology*, 147, 3-8.
- Moores, E.M., & Twiss, R.J. 1995. *Tectonics*. W.H. Freeman and Company. ISBN 0-7167-2437-5 United States of America.
- Olsen, K.H., and Morgen, P. (1995). Introduction: Progress in Understanding Continental Rifts, Part I, p3-26. *Continental Rift: Evolution, Structure, Tectonics*, Elsevier, ISBN 0-444-8956-3, p466.
- Paige, S. 1950. Application of geology to engineering practice. Berkeley Volume. Geological Society of America, Washington, DC, 327 pp.
- Palmstrom, A. 1996. Characterizing Rock Masses by the Rmi for Use in Practical Rock Engineering – Part1: The development of the Rock Mass index (RMi). *Journal of Tunnelling and Underground Space Technology*, Vol. 11, No. 2, pp. 175-188.
- Price, David G. 2009. *Engineering Geology – Principles and Practice*. Springer Verlag Berlin Heidelberg, ISBN 978-3-540-29249-4, Germany.
- Priest, S.D., & Hudson, J.A. 1976. Discontinuity spacings in rocks. *International Journal of Rock Mechanics and Mining Sciences & Geomechanics Abstracts*, Volume 13, Issue 5, May 1976, Pages 135-148.
- Priest, S.D., & Hudson, J.A. 1981. Estimation of discontinuity spacing and trace length using scanline surveys. *International Journal of Rock Mechanics and Mining Sciences & Geomechanics Abstracts*, Volume 18, Issue 3, June 1981, Pages 183-197.
- Priest, Stephen D. 1992. *Discontinuity Analysis for Rock Engineering*. Capman and Hall publications, p443.

- Redfield, T.F., Wheeler, W.H., & Often, M. 2003 A kinematic model for the development of the Afar depression and its paleogeographic implications. *Earth and Planetary Science Letters* Vol. 216, pp. 383–398.
- Rees, W.G. 2001. *Physical Principles of Remote Sensing*. Cambridge University Press, 2nd Edition, ISBN 0-521-66034-3, pp. 343, United Kingdom.
- Reuter, H.I., Nelson, A., & Jarvis, A. 2007. An evaluation of void-filling interpolation methods for SRTM data. *International Journal of Geographical Information Science*, Vol. 21, No. 9, pp.983–1008.
- Richards, J.A, & Jia, X. 2006. *Remote Sensing Digital Image Analysis*. Springer-Verlag Berlin Heidelberg, 4th Edition, ISBN 3-540-25128-6, pp. 439, Germany.
- Riedmüller, G., Brosch, F.J., Klima, K., & Medley, E.W. 2001. Engineering Geological Characterization of Brittle Faults and Classification of Fault Rocks. *Felsbau* Vol.19, No.4, pp.13-19.
- Rocha M. 1976. Alguns problemas relativos a Mecânica das Rochas dos materiais de baixa resistencia. *Geotecnia. Revista de Sociedade Portuguesa de Geotecnia*, No.18, pp. 3-27 (in portuguese).
- Romana, M., (1985). “New Adjustment Ratings for application of Bieniawski Classification to Slopes”. *Inte. Sympo. on the role of rock mechanics ISRM, Zacatecas*, pp. 49 – 53.
- Romanov, Douchko, Gabrovsek, Franci, and Dreybrodt, Wolfgang 2003. Dam sites in soluble rocks: a model of increasing leakage by dissolutional widening of fractures beneath a dam. *Engineering Geology*, 70, p17-35.
- Rowland, J.V., Baker, E., Ebinger, C.J., Keir, D., Kidane, T., Biggs, J., Hayward, N., & Wright, T.J. 2007. Fault growth at a nascent slow-spreading ridge: 2005 Dabbahu rifting episode, Afar. *International Journal of Geophysics*, 171, 1226-1246.
- Saaty TL (1980). *The Analytic Hierarchy Process*. New York: McGraw Hill, 350p.
- Saaty TL (2004a). Decision making – The Analytic Hierarchy and Network Processes (AHP/ANP). *Journal of Systems Science and Systems Engineering*, 13 (1), 1-34.
- Saaty TL (2004b). Fundamentals of the Analytic Network Processes – Dependence and feedback in decision making with a single network. *Journal of Systems Science and Systems Engineering*, 13 (2), 129-157.
- Salustri, Filippo A. 2005. Pairwise Comparison. The published document was accessed on November, 2008 from <http://deseng.ryerson.ca/~fil/t/pwisecomp.html>.

- Sanchez, M.A. Foyo, A., Tomillo, C., & Iriarte, E., 2007. Geological risk assessment of the area surrounding Altamira Cave: A proposed Natural Risk Index and Safety Factor for protection of prehistoric caves. *Engineering Geology*, Vol.97, pp180-200.
- Sengör, A.M.C., 1995. Sedimentation and tectonics of fossil rifts. In: Busby, C.J., Ingersoll, R.V. (Eds.), *Tectonics of Sedimentary Basins*. Blackwell, Oxford, pp. 53– 117.
- Sengör, A.M.C., Burke, K., 1978. Relative timing of rifting and volcanism on earth and its tectonic implications. *Geophysical Research Letters* 5, 419– 421.
- Sigmundsson, F. 1992. Tectonic implications of the 1989 Afar earthquake sequence. *Geophysical Research Letters*, 19, 877-880.
- Solomon, N., Pischinger, G.; Klima, K., Kieffer, D. S. 2008, Extensional Tectonics at Tendaho Dam and Irrigation Site, Afar Depression, Ethiopia. - in: *Journal of alpine geology* 49 (2008).
- SRTM Project Office, 2006. SRTM Version2, the mission to map the world. Website administrator E. Ramirez. Available from: < <http://www2.jpl.nasa.gov/srtm/> >.
- Suppe, J. 1985. *Principles of Structural Geology*. Prentice-Hall, Inc., Englewood Cliffs, New Jersey 07632. ISBN 0-13-710500-2 United States of America.
- Tapponnier, P., Armijo, R., Manighetti, I. & Courtillot, V. 1990. Bookshelf faulting and horizontal block rotations between overlapping rifts in southern Afar. *Geophysical Research Letters*, 17, 1-4.
- Tarback, E.J., & Lutgens, F.K. 1996. *Earth – An Introduction to Physical Geology*. Prentice Hall, Inc., 5th Edition, ISBN 0-13-371584-2, pp. 605, United States of America.
- Tefera, M., Chernet, T., Haro, W. 1996. Geological map of Ethiopia; scale 1:2,000,000. Ministry of Mines and Energy. Ethiopian Institute of Geological Surveys, Addis Ababa, Ethiopia (ETH).
- Teknomo, Kardi. (2006) Analytic Hierarchy Process (AHP) Tutorial. The document was accessed on November, 2008 from <http://people.revoledu.com/kardi/tutorial/ahp/>.
- Tesfaye, S. 2005. Fault population investigation and estimating magnitude of extension in Guma Graben, Central Afar, Ethiopia. *Journal of African Earth Sciences*. Vol. 41, pp 437-444.
- Tesfaye, S., Harding, D. J. & Kusky, T. M. 2003. Early continental breakup boundary and migration of the Afar triple junction, Ethiopia. *Geological Society of America Bulletin*, 115, 1053-1067.

- Thurmond, A., & Abdelsalam, M. 2005. Normal and strike slip faults interplay in the Tendaho Goba'ad Discontinuity, Afar Depression, Ethiopia. Geological Society of America Abstract Programs, Vol. 37, No. 3, p11.
- Thurmond, A., Abdelsalam, M. & Thurmond, J. 2006. Optical-Radar-DEM Remote Sensing Data Integration for Geological Mapping in the Afar Depression, Ethiopia. Journal of African Earth Sciences, 44, 119-134.
- Thurmond, A.K., Abdelsalam, M., Lemme, T. 2007. Normal and strike slip faults interplay in the Tendaho Graben, Afar Depression, Ethiopia. Submitted to Journal of the Geological Society.
- Turrini, M.C., Visintainer, P. 1998. Proposal of a method to define areas of landslide hazard and application to an area of the Dolomites, Italy. Engineering Geology 50, 250–256.
- Twiss, R.J., & Moores, E.M. 1992. Structural Geology. W.H. Freeman and Company, New York, ISBN 0-7167-2252-6, pp. 532, United States of America.
- Uemura, T., & Mizutani, S. 1984. Geological Structures. John Wiley and Sons, ISBN 0-471-90411-2, pp. 309, England.
- Unal, Bunyamin, Celik, Mehmet and Yıldırım, Turgut 2008. Evaluation of seepage problems of the Armag'ın Dam, Kırklareli, northwestern Turkey. Bulletin of Engineering Geology and the Environment, 67, p335-345.
- Unal, Bunyamin, Eren, Mucahit, and Yalcin, M.Gurhan 2007. Investigation of leakage at Ataturk dam and hydroelectric power plant by means of hydrometric measurements. Engineering Geology, 93, p45-63.
- UZBEK/ UZGIPROVODHOZ, 1985. Feasibility Study, Proposal and estimate of Cotton Development in 60th ha in the Lower Awash Valley Ethiopia, Addis Ababa, Ethiopia.
- Varet, J. 1978. Geologie de L'Afar central et meridional (Ethiopie et Republique de Djibouti) – Geology of central and southern Afar (Ethiopia and Djibouti Republic). Cent. Natl. Rech. Sci., Paris, France (FRA), Paris, France.
- Watters, R.J. 1989. Engineering Geology and Geotechnical Engineering. A.A Balkema, Rotterdam, ISBN 90-6191-878-2, the Netherlands.
- Wells, Donald L. and Coppersmith, Kevin J. 1994. New Empirical Relationships among Magnitude, Rupture Length, Rupture Width, Rupture Area, and Surface Displacement. Bulletin of the Seismological Society of America, Vol. 84, No. 4, pp. 974-1002.
- Wickham, G.E., Tiedemann, H.R., & Skinner, E.H. 1972. Support Determination based on Geologic Predictions. Proceedings Rapid Excavation Tunneling Conference, AIME, New York, pp. 43-64.

- Wilson, Stanely D. 1986. A discussion of the Bandwin hills reservoir failure. *Engineering Geology*, 24, p127-141.
- Woldearegay, Kifle 2005. Rainfall-triggered landslides in the northern highlands of Ethiopia: Characterization, GIS-based Prediction and Mitigation. PhD Thesis, Graz University of Technology, Austria.
- Wolfenden, E., Ebinger, C., Yirgu, G., Deino, A. & Ayalew, D. 2004. Evolution of the northern Main Ethiopian rift: birth of a triple junction. *Earth and Planetary Science Letters*, 224, 213-228.
- Wright, T., Ebinger, C.J., Biggs, J., Ayele, A., Yirgu, G., Kier, D., & Stork, A. 2006. Magma-maintained rift segmentation at continental rupture in the 2005 Afar dyking episode, *Nature*, 422, 291-294.
- Wu, Z., Barosh, P. J., Hua, D., Wu, Z., Peishenga, Y., Qishenga, L., Chunjinga, Z. 2002. Migrating pingos in the permafrost region of the Tibetan Plateau, China and their hazard along the Golmud–Lhasa railway. *Engineering Geology Journal*, Elsevier, 79, p267-287.
- WWDSE-WPCS(I) Water Work Design and Supervision Enterprise with Association in Water and Power Consultancy Service (India), 2005. Tendaho Dam and Irrigation Project – Main Report, Addis Ababa, Ethiopia.
- Yirgu, G., Ayele, A., Fisseha, S., Chernet T., & Damtew K. 2007. Fresh Volcanic activity during August 2007 in the Karbahi Graben, unpublished report posted at Afar Rift Consortium website. <http://www.see.leeds.ac.uk/afar/websitepages/news.htm>, Accessed on 05/11/2007.

List of Figures

Fig 1.1: Schematic illustration for verbal equation of *engineering geological behaviors of the ground* (Price, 2009): (a) Stages of tectonic processes 1 - 3 (b) & (c) tunneling and reservoir impoundment through different tectonic conditions, respectively. The graben drawing is taken from USGS.

Fig 1.2: Location map of Tendaho reservoir and irrigation site (the base map is clipped from 1:250,000 scale Serdo NC 37-4, 1972 topographic map).

Fig 1.3: Flow Chart of adopted research methodology.

Fig 1.4: The first 'a' and second 'b' field visit to Afar Depression, NE Ethiopia.

Fig 2.1: Satellite image (panchromatic image of Landsat Enhanced Thematic Mapper Plus) of Afar Depression, NE Ethiopia; Tenahdo Dam and Reservoir site is located at the center of the depression. Abbreviations: DA Dabbahu rifting, DB Danakil block, DO Dobi graben, EA Erta' Ale, ECB East Central Block GU Guma graben, IM Immino graben, KA Karbahri graben, MER Main Ethiopian Rift, TA Tat 'Ale, TG Tendaho graben, TGD Tendaho Goba'ad Discontinuity.

Fig 2.2: Tectonic map the Afar Depression (after Manighetti et al., 1998, 2001; Beyene & Abdelsalam, 2005). AAM Ayelu Amoissa; AL Alayata; AP Awsa plain; AS Asal; DD Dadar graben; DL Dallol; ECB East Central Block; EA Erta Ale; GB Ghoubbet; HA Herta Ale; GD Goba'ad; TA Tat Ale; MER Main Ethiopian Rift; MH Manda Hararo; MI Manda Inakir; SA Sabure; TGD Tendaho Goba'ad Discontinuity; TJ Tajura.

Fig 2.3: Geological Settings of the Afar Depression (after Varet, 1978; Acton et al., 1991; Beyene, 2004).

Fig 2.4: Seismicity in the Afar Depression during (a) the 1960 – 2000 (green circle) and (b) 2001 – 2009 (deep pink – see **Appendix B-1** for the data) (modified after Hofstetter and Beyth, 2003). Broad band stations are represented by a solid square. The dimensions of the circle are related to the magnitude of the earthquake and boxes are referred in the text as region I-VII. See **Appendix A-1** for higher resolution.

Fig 2.5: Recent Tectonic Activities at North of East Central Block ECB, Afar Depression. Shuttle Radar Tomography Mission (SRTM) elevation model (90m resolution) is used here as base map to locate the September, 2005 Dabbahu rifting episode (after Rowland, 2007); August, 2007 Karbahi rifting (report of the Afar Rift Consortium, 2007); and the February, 2008 ground uplift (documented during the second field studies time in Spring 2008).

Fig 2.6: After Thurmond, 2007; Schematic representation of major tectonic elements acting within the East Central Block (ECB): AB = Abana, AS = Asgura, B = Borwali, F = Finini, K=Kurub Koma, U=Unda Gamarri.

Fig 2.7: Flow chart for landslide risk assessment (ISSMGE, 2005).

Fig 3.1: Location map of the study area including the proposed maximum level of Tendaho Reservoir; the red rectangles show the locations of **Fig 3.2**, **3.3** and **3.4**.

Fig 3.2: (a) Aerial Photo at the center of a proposed maximum level of Tendaho Reservoir (b) lineaments and lithological boundaries are delineated with white and yellow lines, respectively, see **Fig 3.1** for the location.

Fig 3.3: Compare TIN and SRTM topographic models; (a) Triangular Irregular Network (TIN), (b) lineaments are delineated with white lines from the TIN topographic model, (c) Shuttle Radar Topographic Mission (3-arc,

90 meter resolution) and **(d)** lineaments are delineated with white lines from the SRTM topographic model, see **Fig 3.1** for the locations.

Fig 3.4: **(a)** Band combination (4-5-3) of Landsat ETM+ image, **(b)** lineaments and lithology boundaries are delineated with white and yellow lines, respectively from the Landsat ETM+ image, **(c)** Principal Component Analysis (PCA) image **(d)** lineaments and lithology boundary are delineated with white and yellow lines, respectively from PCA, **(e)** Intensity-Hue-Saturation (IHS) of band combination 2-1-2) image, and **(f)** lineaments are delineated with white lines from IHS, see **Fig 3.1** for the locations.

Fig 3.5: Panchromatic image (Band 8) of Landsat ETM+ with delineated lineaments (white color). **GR** Gayderu Ridge – NW to W of the proposed maximum level of Tendaho Reservoir; **GP** Gesye Plain – center of the proposed maximum level of Tendaho reservoir; **MR** Megenta Ridge – E to SE of the proposed maximum level of Tendaho Reservoir; and **TG** Tendaho Graben. See **Appendix A-2** for higher resolution.

Fig 3.6: Rose diagrams of lineaments at **(a)** Tendaho Graben TG, **(b)** Gayderu Ridge GR, **(c)** Gesye Plain GP and **(d)** Megenta Ridge MR, see **Fig 3.5** for the locations.

Fig 3.7: Distribution of lineaments length at Tendaho Graben (TG), Gayderu Ridge (GR), Gesye Plain (GP) and Megenta Ridge (MR).

Fig 3.8: Geological map of the proposed Tendaho Reservoir and its vicinity; Modified after Varet, 1978; Manighetti et al., 1998, 2001; & Thurmond et al., 2006 with the interpretation of Landsat ETM+ image, aerial photograph, SRTM and TIN model. See **Appendix A-5** for higher resolution.

Fig 3.9: Landsat ETM+ image (band combination 4-5-3) dragged on; **A** TIN model and **B** SRTM (2x vertical exaggeration) to compare the SRTM and TIN elevation models for visualization of morphologically defined structures and extraction of risk parameters (structural).

Fig 3.10: Lineament density zones using Kernel density analysis method (Arc GIS) with approximately 120 meter pixel size and 2 Km radius. The classification was normalized by dividing the class boundaries with the maximum value – 0.002692875 (<http://webhelp.esri.com/arcgisdesktop/9.1/index.cfm?id=2961&pid=2960&topicname=Density%20calculations>). See **Appendix A-3** for higher resolution.

Fig 4.1: Petrographic thin section analysis with polarized and 4x resolution: **(a)** LR 022/1, Fresh coarse grained plagioclase crystal with ground mass olivine, pyroxene and plagioclase – called fresh porphyritic basalt; **(b)** RR 032/1, Fine grained basalt with plagioclase (very fine), rich in feldspar and opaque minerals; **(c)** IC 023/1, Coarse grained sandstone with oolitic material, quartz and feldspar; and **(d)** RR 032/2 (0-2); Coarse grained Amygdaloidal basalt, mainly plagioclase, pyroxene, feldspar & secondary mineral growth - carbonate. For the location of the samples, see **Fig 4.2**.

Fig 4.2: Outcrop locations of faults, regional joint settings, scan line mapping; and sample location of rocks, water and filling materials. Where *IC* Irrigation Canal, *RR* Right Reservoir, *RDX* Right dam axis, *LR* Left Reservoir, *LDX* Left dam axis, *SLLR* Scanline Left reservoir, *SLIC* Scanline Irrigation canal, *SEM* Semera Fissure, *TG* Tendaho Graben and *SPRING* Alalobeda Thermal Spring. See **Appendix A-4** for higher resolution.

Fig 4.3: Regional joint sets of tectonic structures located at west of the proposed Tendaho Reservoir area; **(a)** great circle and **(b)** Pi-Plot.

Fig 4.4: Field mapping of LR 005 fault plane (LR left reservoir - **Fig 4.2**): **(a)** Landscape shows more than 800 m lateral extent and 40 m vertical displacement; **(b)** stretched boulder along the sliding plane. It can be used to estimate the magnitude of the applied tectonic stress in the area; **(c)** paleostress analysis of fault plane using Angelier and Pt Axes methods (Angelier, 1994).

Fig 4.5: Regional joint sets **(a & b)** and scanline mapping **(c & d)** of tectonic structures located within the proposed Tendaho Reservoir area and nearby the dam axis; **(a, c)** great circle and **(b, d)** Pi-Plot.

Fig 4.6: Regional joint sets of tectonic structures located east of the proposed Tendaho Reservoir area; **(a)** great circle and **(b)** Pi-Plot.

Fig 4.7: Regional joint sets **(a & b)** and scanline mapping **(c & d)** of tectonic structures located within the irrigation canal, 1.5km west of the Tendaho dam axis; **(a, c)** great circle and **(b, d)** Pi-Plot.

Fig 4.8: SEM 003, Extension fracture at the center of Tendaho Graben. **Fig 4.12** for the location of the site.

Fig 4.9: A Ground uplifted in February, 2008 by 1.5 m height with continued release of geothermal vapors along the active Tendaho Rift Axis (TG 001); and B new geothermal spot (TG 002, TG 003). See **Fig 4.2** for the location of the site.

Fig 4.10: Scanline Mapping of lacustrine deposit along irrigation canal: (a) photo shows scanline alignment and how to collect data of tectonic feature (dip direction, filling material and aperture width); (b) SLIC1 (Scanline Irrigation canal 1) between 10 – 20m and their discontinuity parameters.

Fig 4.11: Gesye Graben: A Photo shows the Tendaho Reservoir which lay at the center of the Gesye Graben, B Topographic profile of the graben from point B to B'. **Fig 4.12** shows the location of the profile BB'.

Fig 4.12: Tectonic structure of Gesye Graben: (a) Geological map of the Tendaho reservoir and its vicinity are presented with the stereonet projections of regional joint sets (black), fault planes (red), block rotation (blue) and fissure crack (green); (b) Geological cross sections along point AA' and BB' (borehole data are used from Aquater, 1996 and IPCC, 2005). See **Appendix A-5** for higher resolution.

Fig 4.13: Schematic Model of Extensional Tectonics at Tendaho Dam and Irrigation Site (20 m contour interval) (Solomon et. al, 2008). (1) Main Ethiopian Rift MER (Normal Fault and uplift by dyke intrusion); (2) Propagation of Red Sea Rift and stretching to NE - SW direction; and (3) Tendaho Rift (Normal fault, fissure cracks and uplift). See **Appendix A-6** for higher resolution.

Fig 5.1: Highly simplified end-member models of the causative or initiating mechanisms of continental rifting (Olsen and Morgen, 1995).

Fig 5.2: Geological Map of the Tendaho graben (after Thurmond, 2006). The purple rectangles indicate the inter-fingered MER and propagated Red sea rift structures. See **Appendix A-7** for higher resolution.

Fig 5.3: Radar interferometric image and aerial photograph of violent rifting episode of Dabbahu rifting – September, 2005 (Rowland, 2007). (a) Oblique aerial photograph of the vent area, viewed to the north. The photo was taken by Elizabeth Baker, Royal Holloway, University of London. (b) Initial subsidence during the major intrusive phase (blue area) inferred from satellite radar data (Wright *et al.* 2006) and the distribution of seismicity (Ebinger *et al.* 2006) associated with the post-intrusive phase (small black dots). (c) Zones of ground deformation due to magmatic injection. See **Appendix A-8** for higher resolution.

Fig 5.4: Linear relationship between the numbers of violent rifting episodes in the past and potential occurrence of active rifting episode during the life time of the Tendaho dam and irrigation project (%) – 50 years; *Blue line* – Manda Hararo Rift and *Red line* – Tendaho Rift.

Fig 5.5: Potential extents of the ground deformation zones by the active rifting episodes of Manda Hararo and Tendaho rifting at the Tendaho reservoir and irrigation site.

Fig 6.1: Risk assessment of natural hazards (geohazards) and geological conditions: (a) Asfaw, 2007; Chains of cause and effects for processes originating in the earth's interior (E.I.) or the solar-terrestrial (S-T) interaction. (b) Different geological conditions as a result of various geological processes can be source of risk for the object of interest.

Fig 6.2: Key parameters for the risk assessment of brittle tectonic structures – related to 'the proposed Tendaho Reservoir'.

Fig 6.3: Awash drainage basin (a) Location map of Awash drainage basin, (b) Schematic section illustrating highland-rift groundwater flow and fault-controlled major springs, vertical exaggeration is 100 times the horizontal (after DT, 1973 and Ayenew et al., 2008).

Fig 6.4: Conceptual Hydrogeological model of the Tendaho reservoir which is adapted from DT, 1973 and Ayenew et al., 2008 (Landsat ETM+ image with band combination 4-5-3 dragged on TIN model of 2x vertical exaggeration – see **Fig 4.9** for the location of the cross section).

Fig 6.5: Location map of the selected brittle tectonic structures (2km buffer zone from the proposed maximum level of Tendaho Reservoir). See **Appendix A-9** for higher resolution.

Fig 6.6: Key Parameter distribution (%) in the different risk level classes (See **Appendix B-2** for the data).

Fig 6.7: Mean and standard deviation of the risk level values of brittle tectonic structures – related to reservoir leakage by simple weighting (*AVE*) approach (See **Appendix B-2** for the data).

Fig 6.8: Plot of the risk level values of brittle tectonic structures – related to reservoir leakage by simple weighting (*AVE*) approach RL vs RL_0 (the blue rhombus – minimum, purple rectangle – average and yellow triangle – maximum values of the class parameter). See **Appendix B-2** for the data.

Fig 6.9: Assessment of the risk level of brittle tectonic structures – related to reservoir leakage by simple weighting (*AVE*) approach RL vs RL_0 (see **Appendix C-1** for the detail description of the equation and additional graph).

Fig 6.10: Risk level of brittle tectonic structures – related to reservoir leakage by simple weighting (*AVE*) approach: (a) minimum value of the class, (b) average value of the class and (c) maximum value of the class.

Fig 6.11: Mean and standard deviation of the risk level values of brittle tectonic structures – related to reservoir leakage by pairwise comparison (*PWC*) approach (See **Appendix B-2** for the data).

Fig 6.12: Plot of the risk level values of brittle tectonic structures – related to reservoir leakage by pairwise comparison (*PWC*) approach RL vs RL_0 (the blue rhombus – minimum, purple rectangle – average and yellow triangle – maximum values of the class parameter). See **Appendix B-2** for the data.

Fig 6.13: Assessment of the risk level of brittle tectonic structures – related to reservoir leakage by pairwise comparison (*PWC*) approach RL vs RL_0 (see **Appendix C-2** for the detail description of the equation and additional graph).

Fig 6.14: Risk level of brittle tectonic structures – related to reservoir leakage by pairwise comparison (*PWC*) approach: (a) minimum value of the class, (b) average value of the class and (c) maximum value of the class.

Fig 6.15: Mean and standard deviation of the risk level values of brittle tectonic structures – related to reservoir leakage by analytic hierarchy process (*AHP*) approach (See **Appendix B-2** for the data).

Fig 6.16: Plot of the risk level values of brittle tectonic structures – related to reservoir leakage by analytic hierarchy process (*AHP*) approach RL vs RL_0 (the blue rhombus – minimum, purple rectangle – average and yellow triangle – maximum values of the class parameter). See **Appendix B-2** for the data.

Fig 6.17: Assessment of the risk level of brittle tectonic structures – related to reservoir leakage by analytic hierarchy process (*AHP*) approach RL vs RL_0 (see **Appendix C-3** for the detail description of the equation and additional graph).

Fig 6.18: Risk level of brittle tectonic structures – related to reservoir leakage by analytic hierarchy process (*AHP*) approach: (a) minimum value of the class, (b) average value of the class and (c) maximum value of the class.

Fig 6.19: Selected brittle tectonic structures for the risk estimation of the reservoir leakage. See **Appendix A-10** for higher resolution.

Fig 6.20 (a) Mean value and (b) Standard deviation of the risk level of brittle tectonic structures – related to reservoir leakage by *AVE*, *PWC* and *AHP* approaches.

Fig 6.21: Compare the risk level of brittle tectonic structures – related to reservoir leakage from (a) *Simple averaging AVE*, (b) *Pairwise comparison PWC* and (c) *Analytical hierarchy process AHP* (maximum values of the classes are taken for the risk level analysis). See **Appendix A-11** for higher resolution.

List of Tables

Table 3.1: Summary of lineaments distribution at Tendaho Graben (TG), Gayderu Ridge (GR), Gesye Plain (GP) and Megenta Ridge (MR).

Table 4.1: Regional joint sets located west of the proposed Tendaho reservoir.

Table 4.2: Faults located west of the proposed Tendaho reservoir.

Table 4.3: Regional joint sets located within the proposed Tendaho reservoir and nearby the dam axis.

Table 4.4: Faults located within the proposed Tendaho reservoir.

Table 4.5: Scanline mapping of tectonic structures located within the proposed Tendaho reservoir.

Table 4.6: Regional joint sets located east of the proposed Tendaho reservoir.

Table 4.7: Faults located east of the proposed Tendaho reservoir.

Table 4.8: Scanline mapping of tectonic structures located within the irrigation canal, 1.5km west of the Tendaho dam axis.

Table 4.9: Regional joints sets located within the irrigation canal, 1.5km west of the Tendaho dam axis.

Table 5.1: Summary of the potential occurrence of Manda Hararo and Tendaho rifting in the lifetime of the Tendaho Dam and Irrigation scheme.

Table 6.1: Assessment of the risk level for the parameters.

Table 6.2: Pairwise comparison (*PWC*) of the risk parameters.

Table 6.3: Analytic hierarchy process (*AHP*) of the risk parameters.

Table 6.4: Summary of risk estimation of proposed Tendaho reservoir leakage through the brittle tectonic structures for the worst and average scenarios.

Appendices

Appendix

A

Under this appendix, maps and figures which were discussed in the main text are presented with higher resolution. The figures are:-

A-1: Fig 2.4a, b

A-2: Fig 3.5

A-3: Fig 3.10

A-4: Fig 4.2

A-5: Fig 4.12a, b

A-6: Fig 4.13

A-7: Fig 5.2

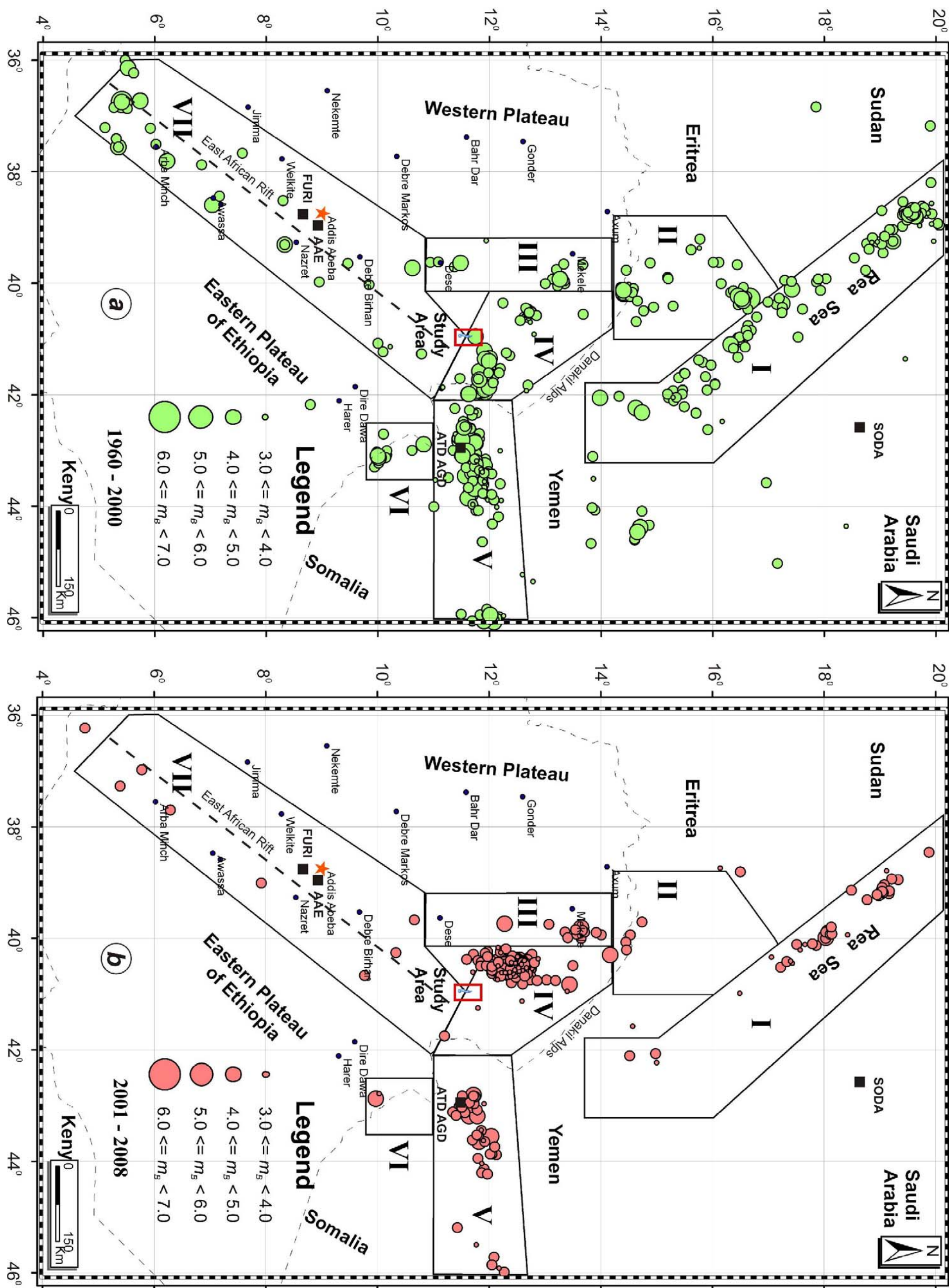
A-8: Fig 5.3b, c

A-9: Fig 6.5

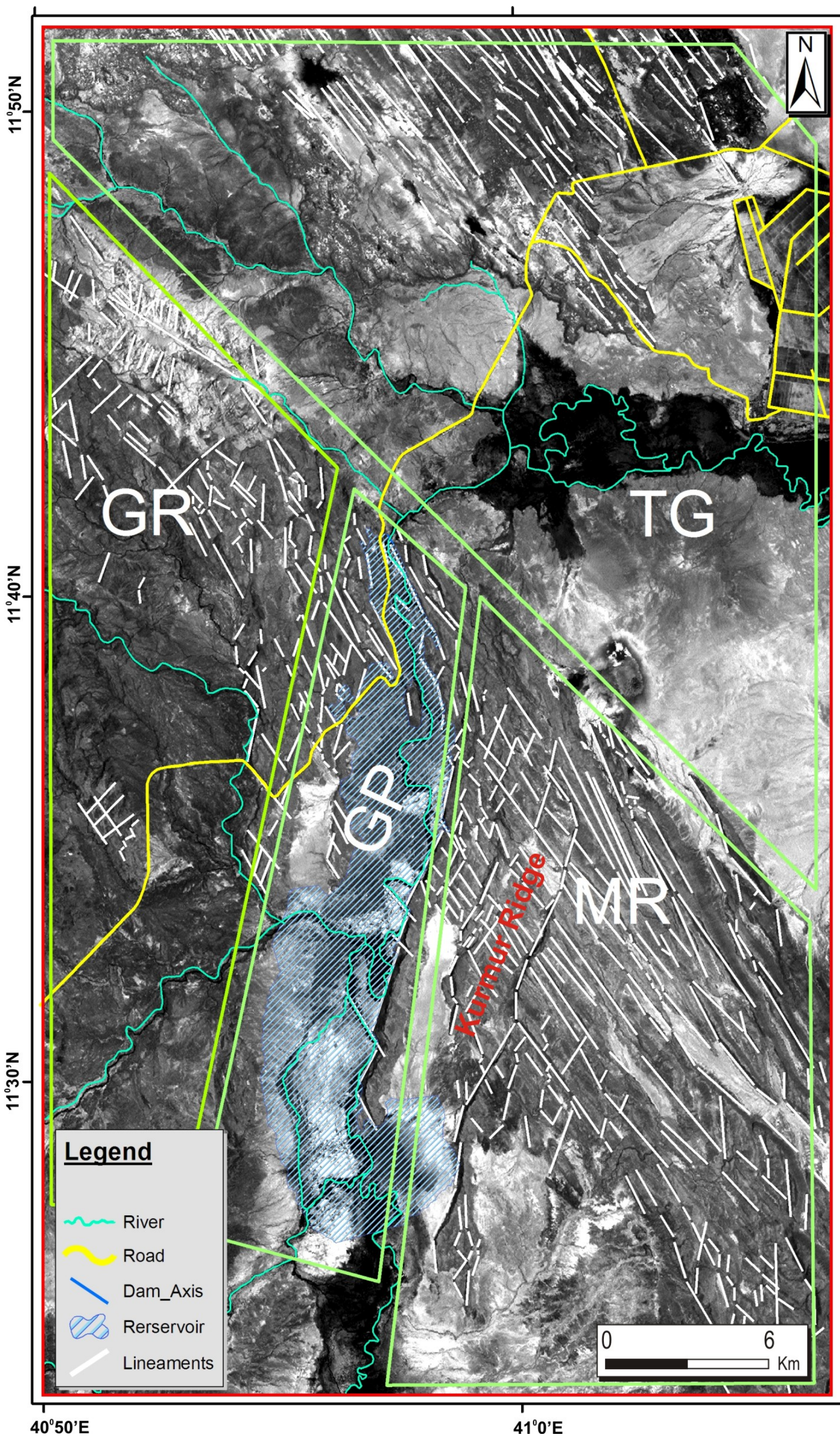
A-10: Fig 6.19

A-11: Fig 6.21a, b, c

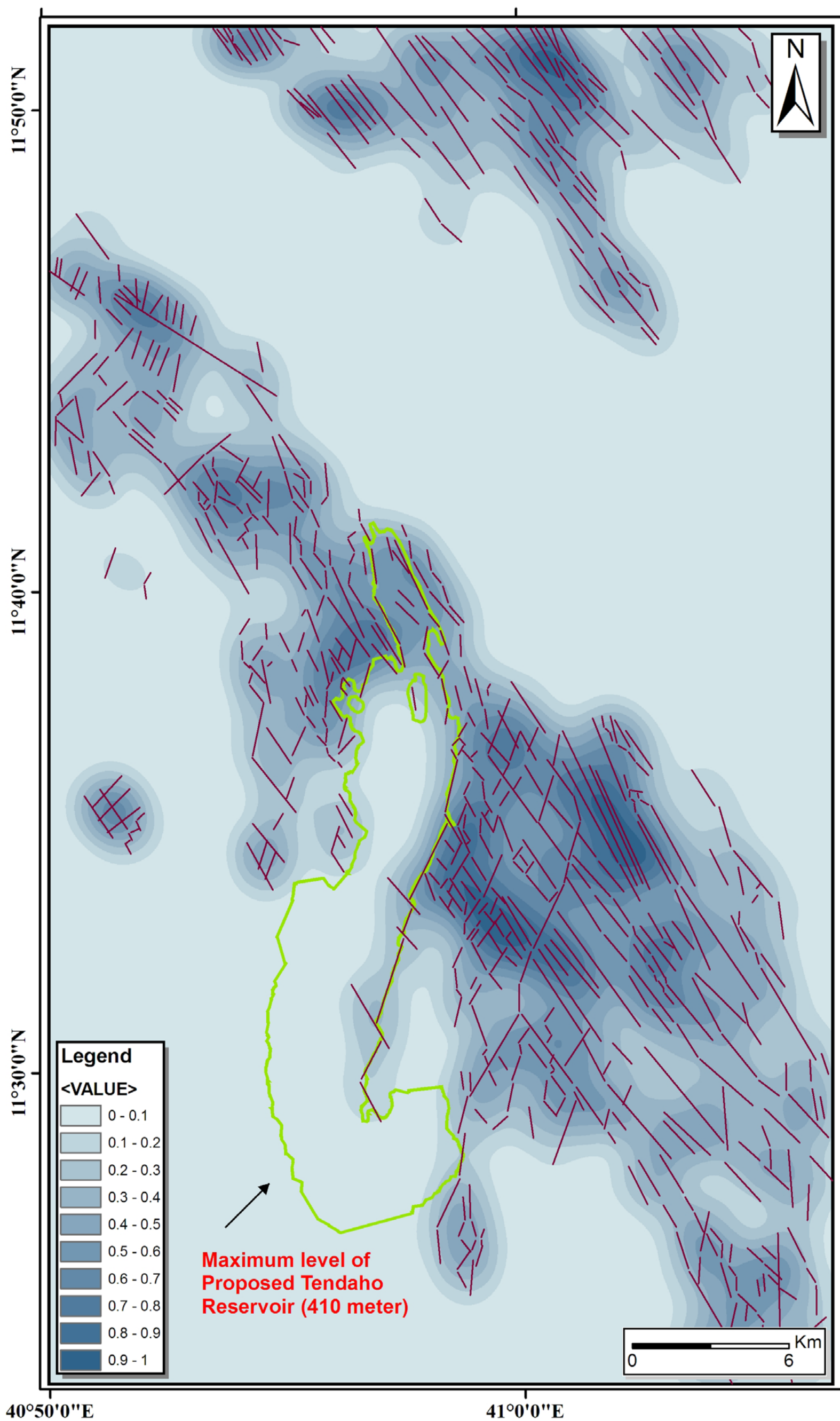
A-1: Fig 2.4



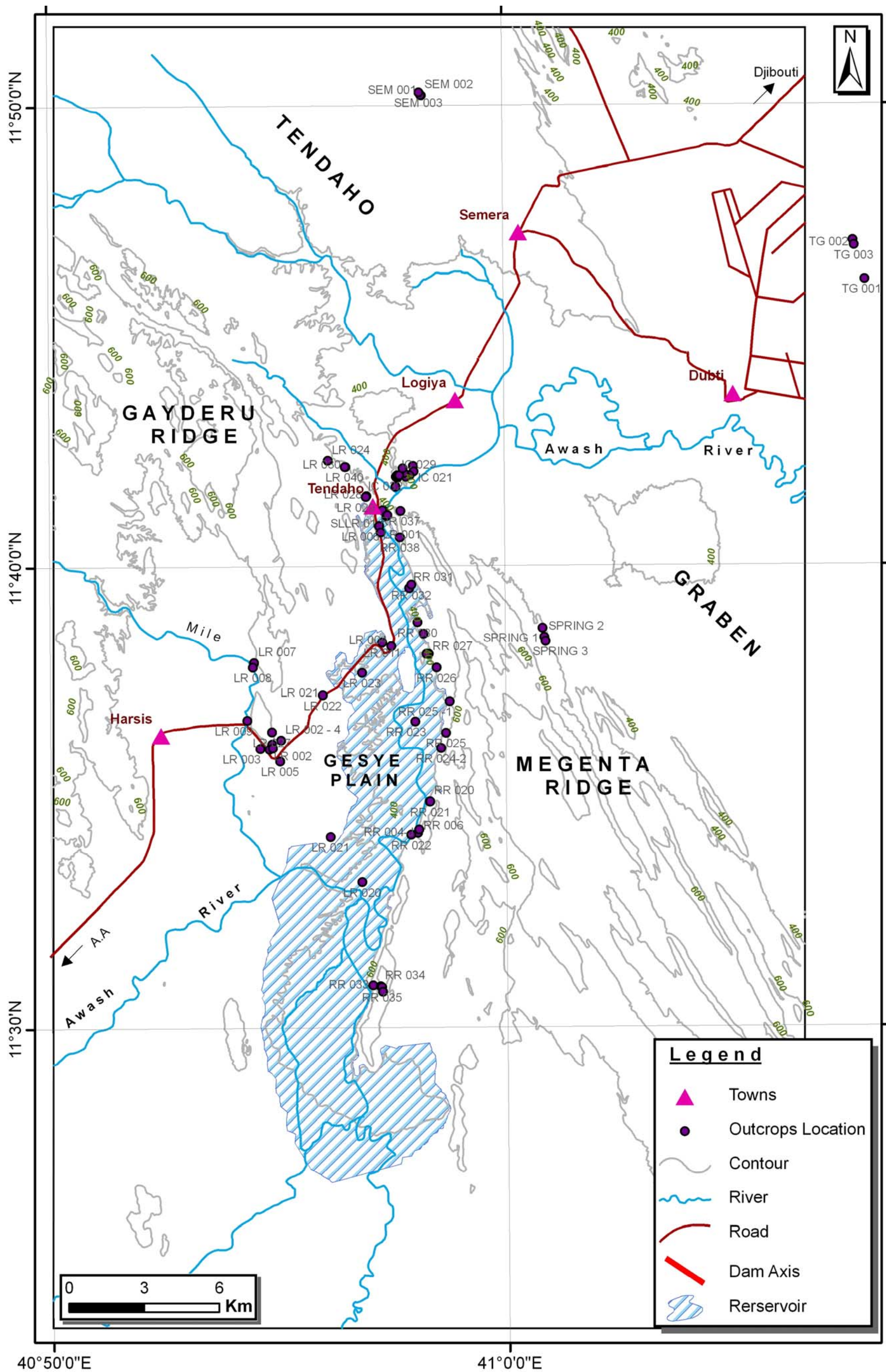
A-2: Fig 3.5



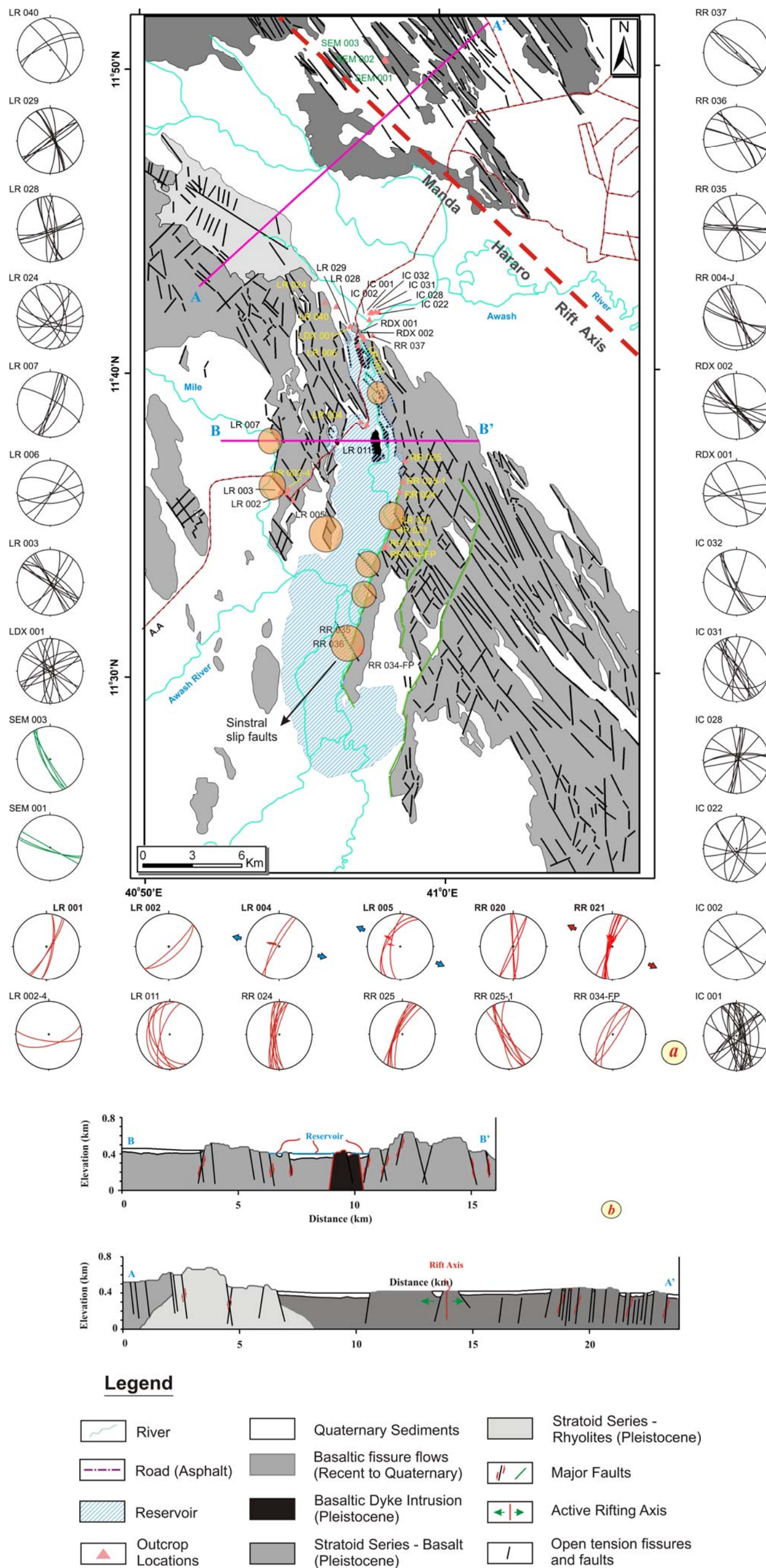
A-3: Fig 3.10



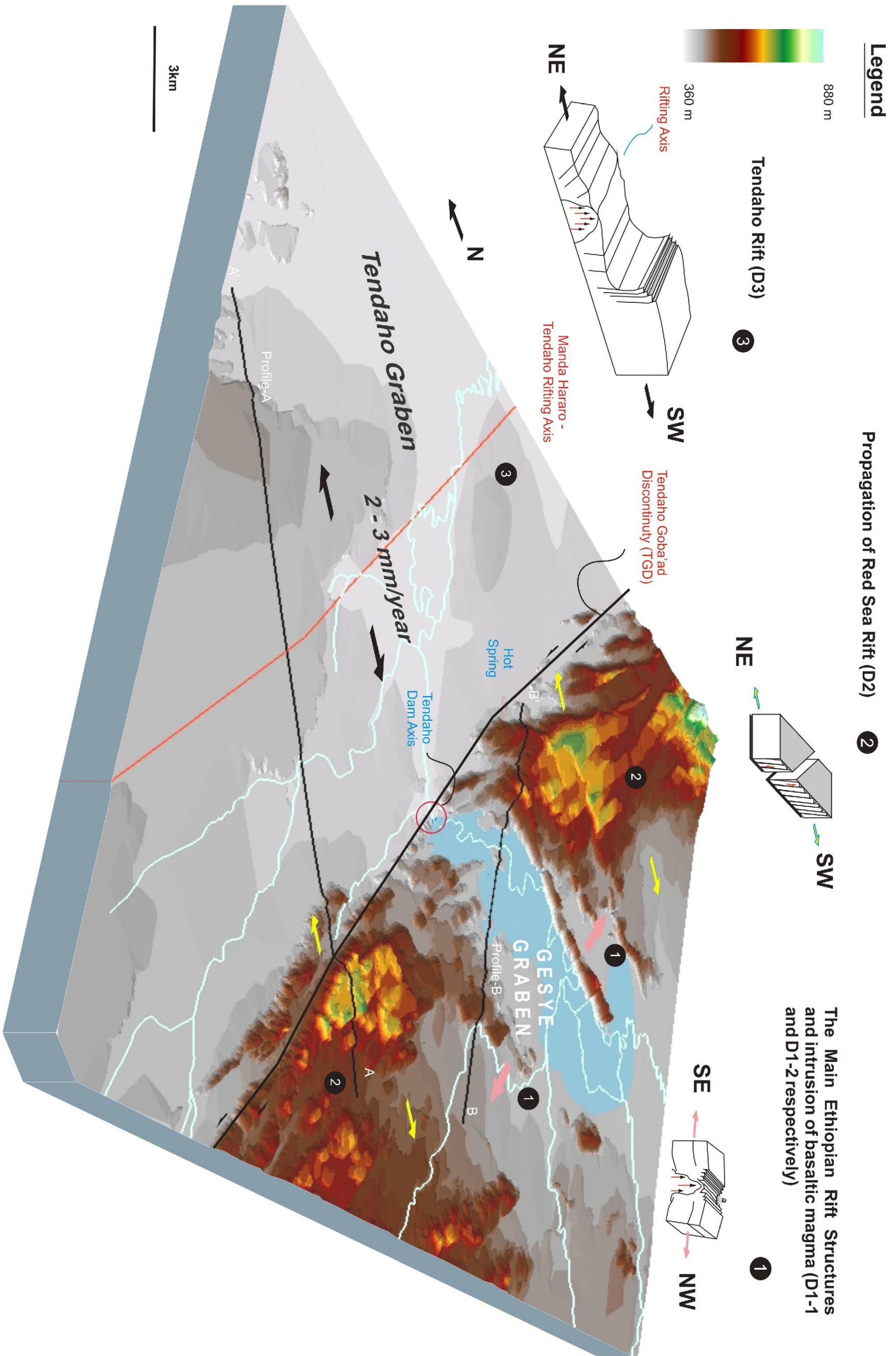
A-4: Fig 4.2



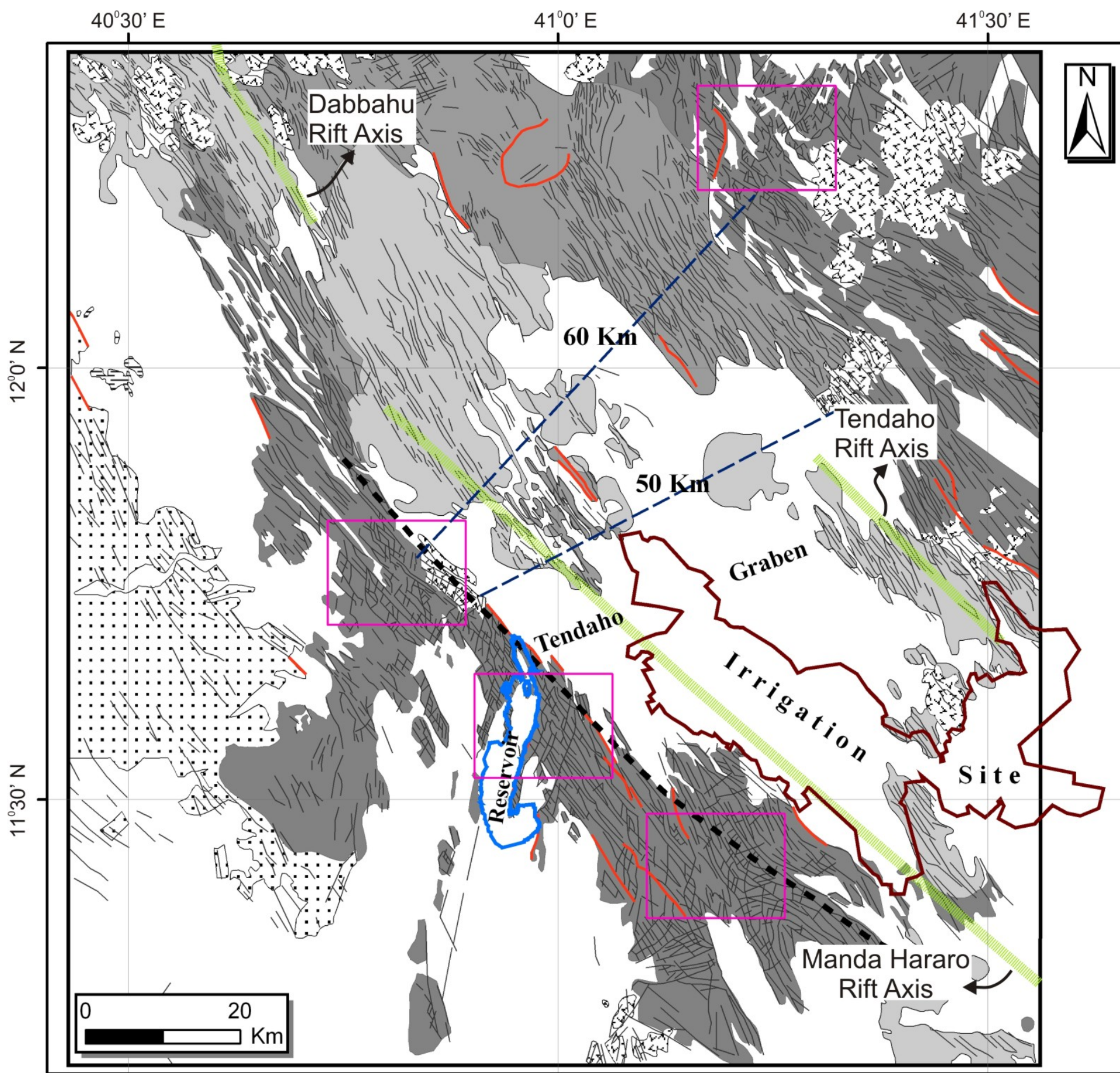
A-5: Fig 4.12




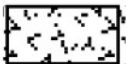


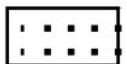


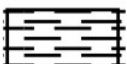



A-6: Fig 4.13



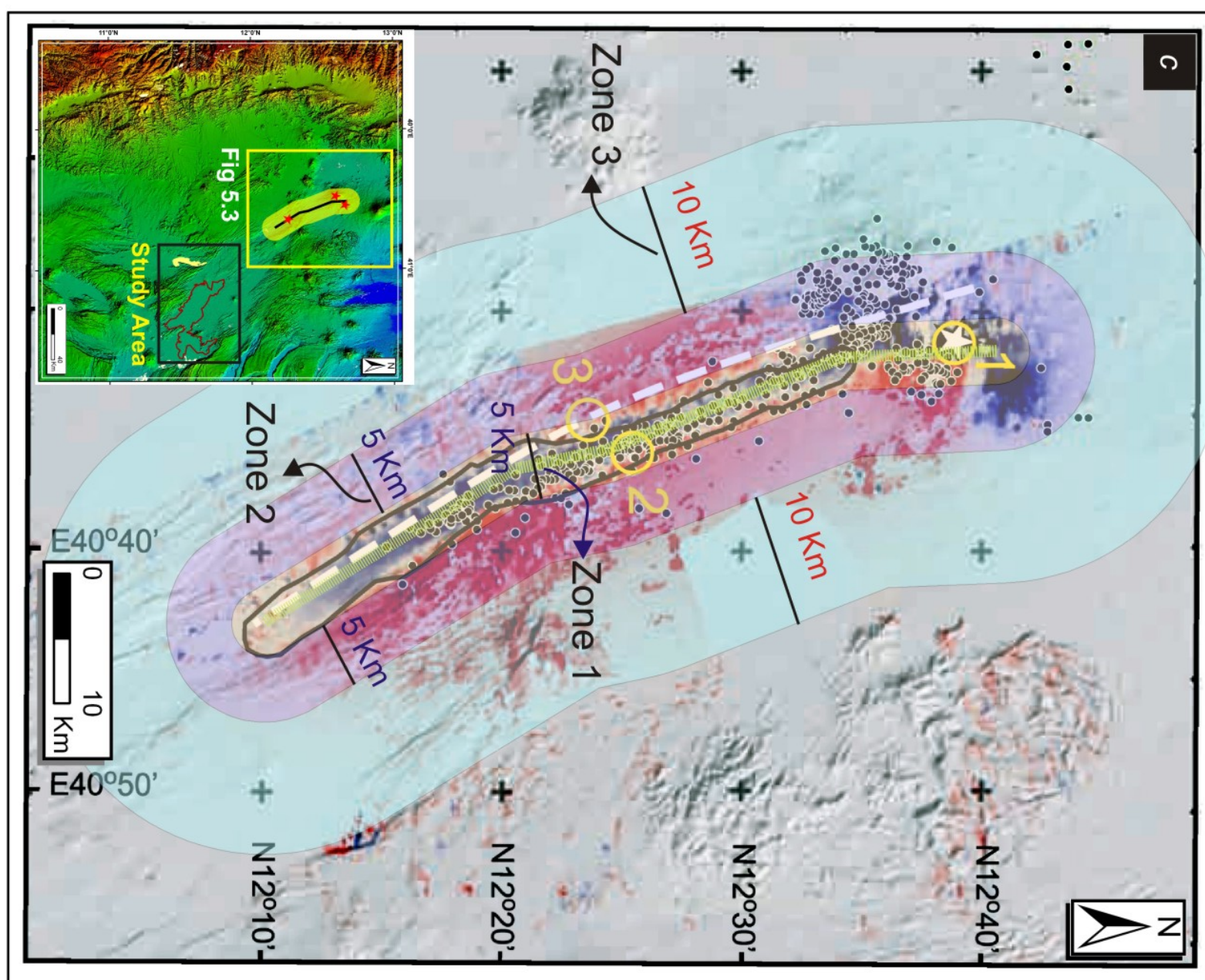
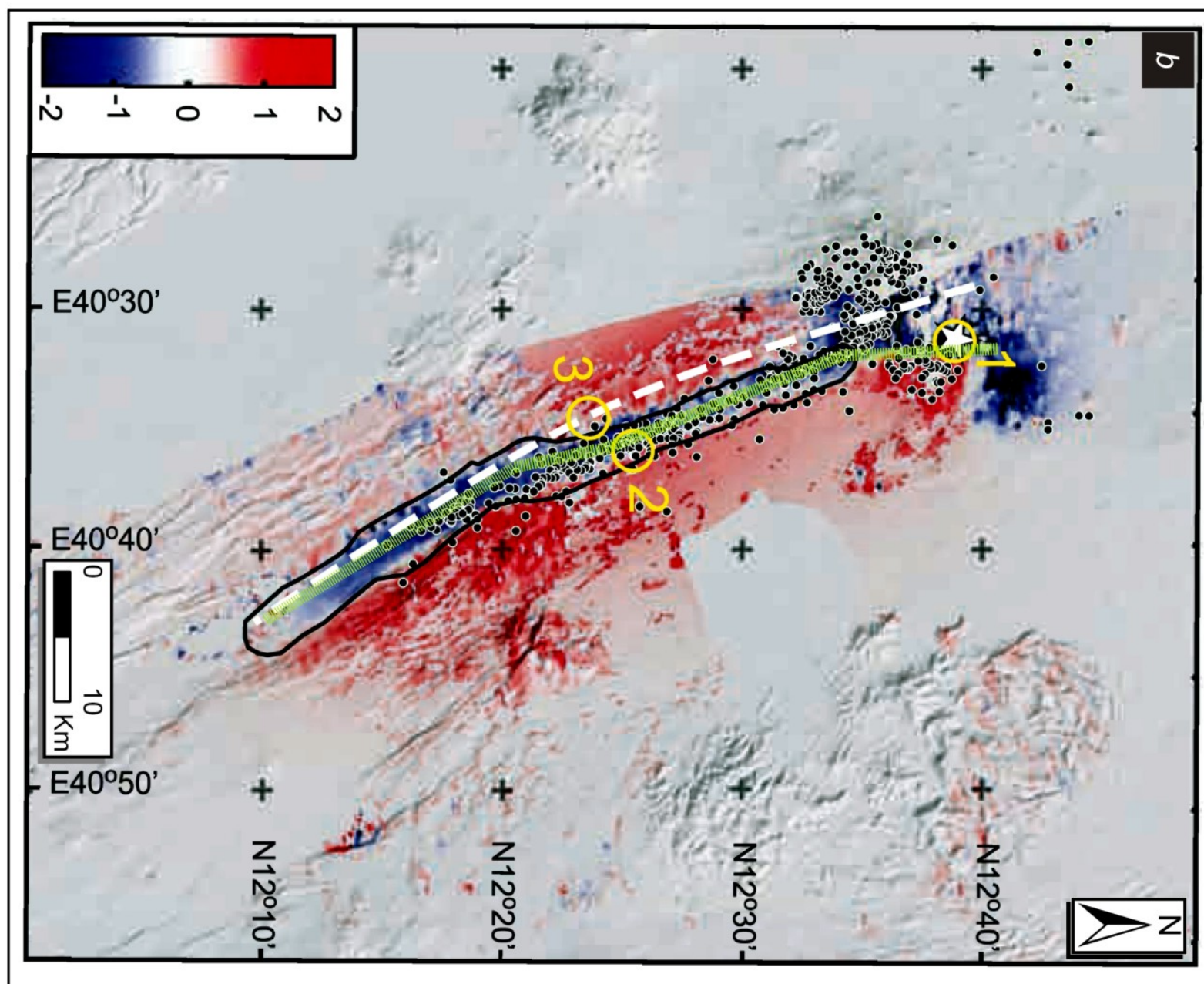
A-7: Fig 5.2



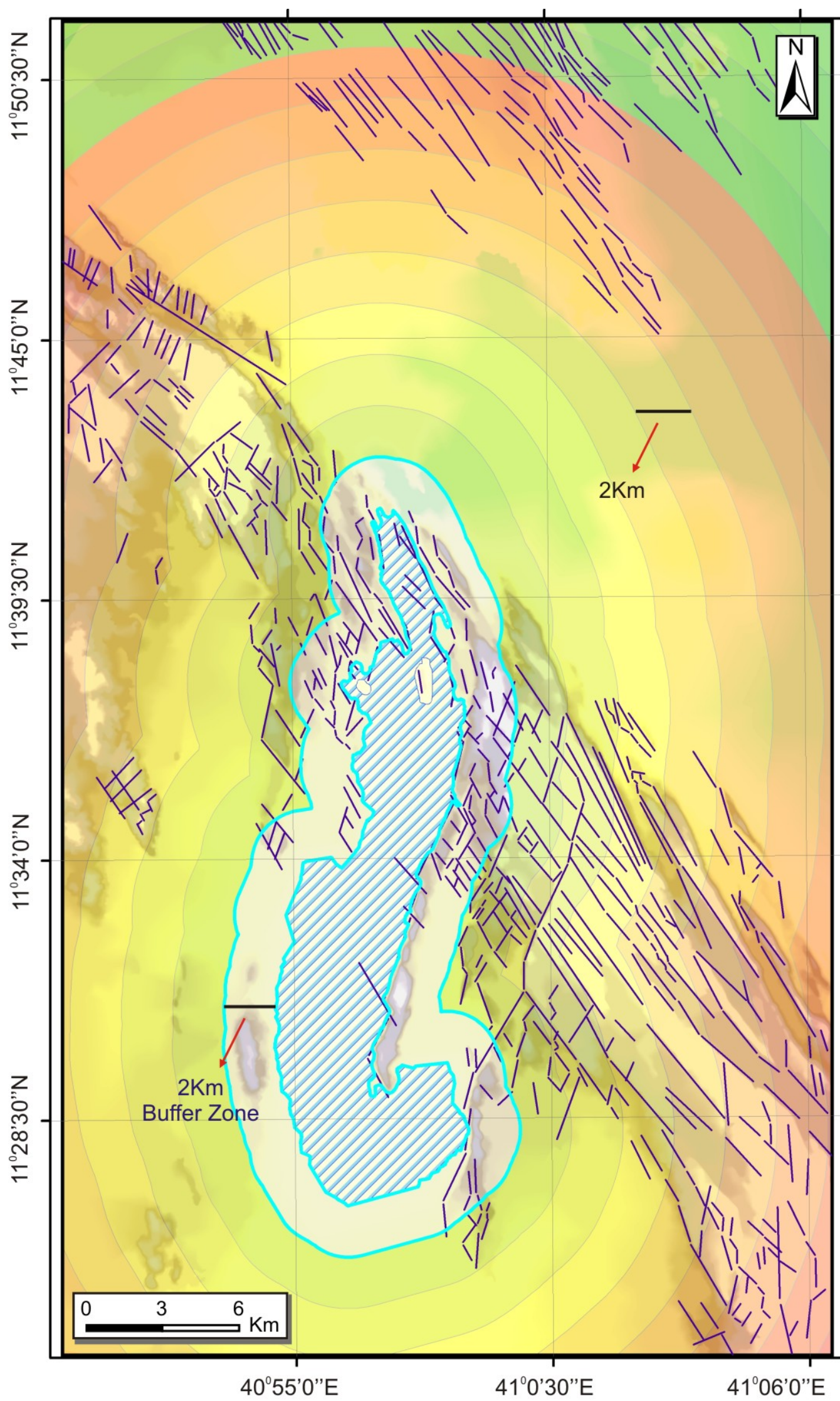
Legend

- | | | | | | |
|---|----------------------|---|--------------|---|------------------|
|  | Sediments |  | Rhyolites |  | Faults |
|  | Recent fissure flows |  | Dahla Basalt |  | Major Faults |
|  | Gulf Basalt |  | Granites |  | TGD |
|  | Stratoid Basalt | | |  | Active Rift axis |

A-8: Fig 5.3




A-9: Fig 6.5

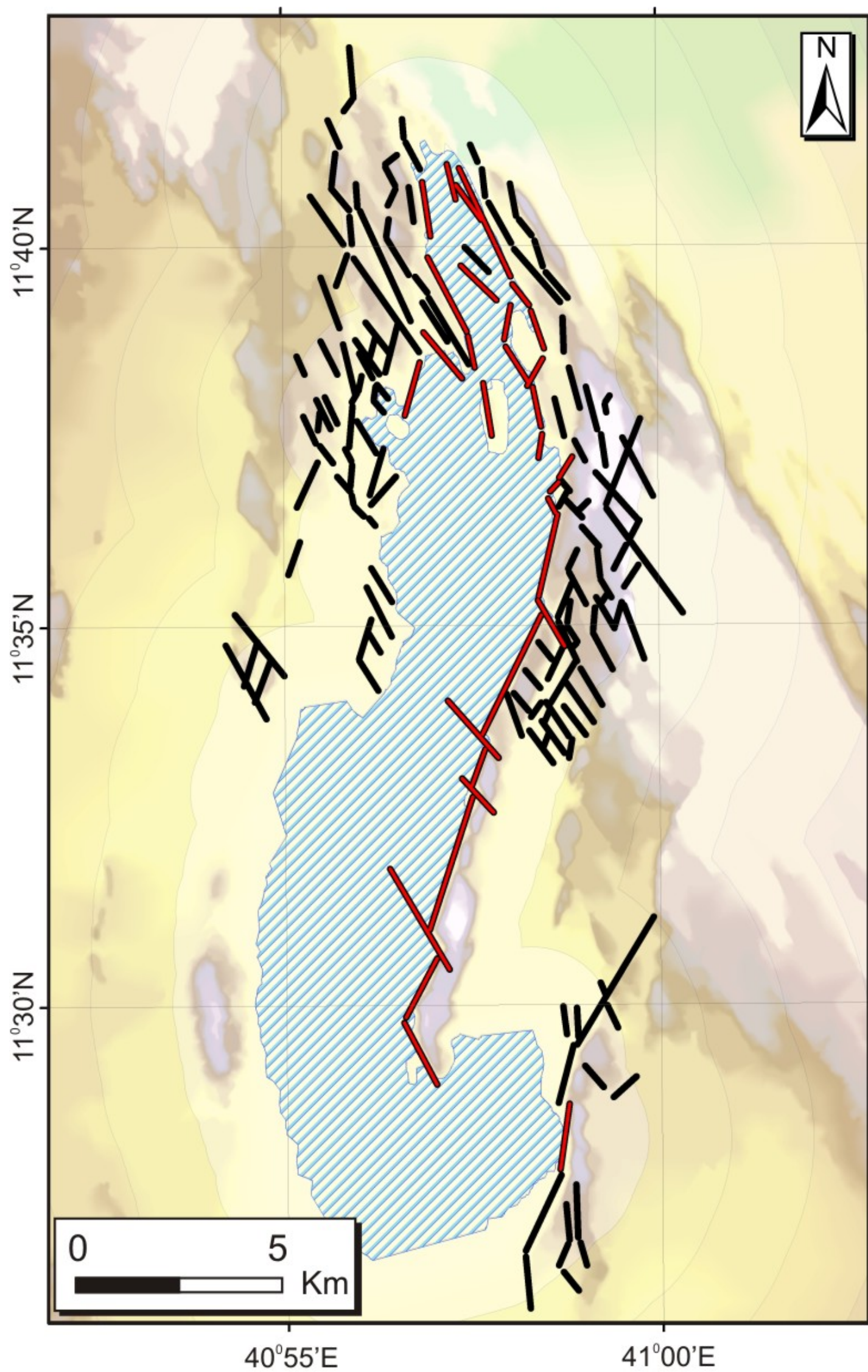


Legend






 Maximum level of Proposed Tendaho Reservoir

A-10: Fig 6.19

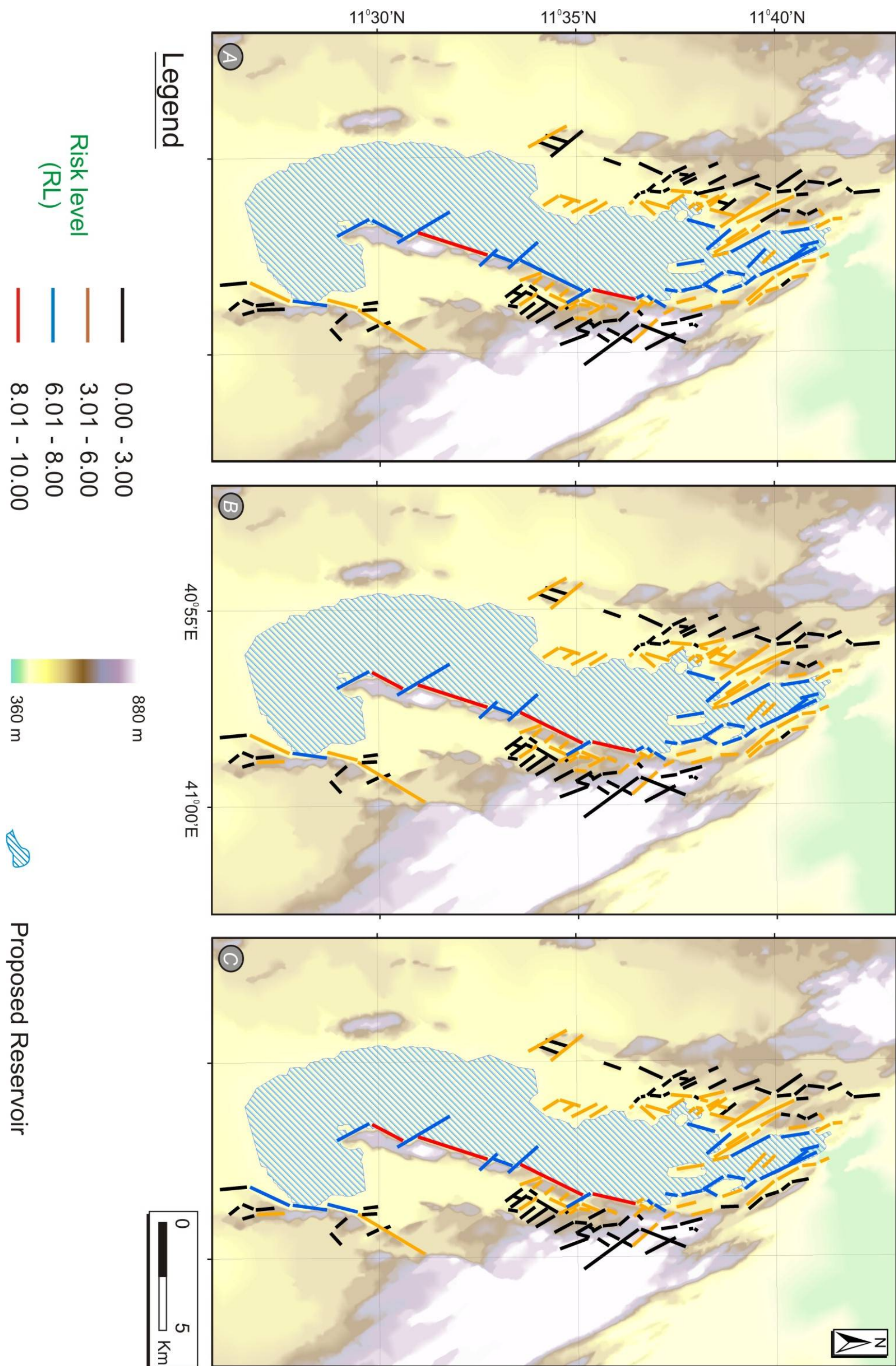


Legend



-  Maximum level of Proposed Tendaho Reservoir
-  Selected brittle Tectonic Structures (RL > 6.01)
-  RL < 6.00

A-11: Fig 6.21



Appendix

B

B-1: Earthquake Data from January 01, 2001 to February 28, 2009 (NEIC)¹.

YEA R	MONT H	DA Y	TIME_HHMM S	LATITUD E	LONGITUD E	MAGNITUD E	DEPT H (km)
2001	5	3	191544	18.49	39.14	4.40	10
2001	5	25	181414	18.03	40.00	4.60	10
2001	5	25	221822	18.03	39.99	5.30	10
2001	5	26	132959	18.03	39.89	4.50	10
2001	5	26	135348	18.14	39.92	4.20	10
2001	5	26	150236	18.13	39.80	4.10	10
2001	6	23	160746	19.02	39.21	4.90	10
2001	6	23	162956	18.99	39.23	4.50	10
2001	11	2	162345	11.79	43.19	5.20	4
2001	12	5	155237	12.67	40.53	4.00	10
2001	12	23	70733	12.18	45.92	3.80	10
2002	5	14	184928	12.59	41.13	3.90	10
2002	6	18	104416	14.52	42.11	4.40	10
2002	8	8	15033	14.01	39.94	4.40	10
2002	8	8	211712	13.65	40.00	4.90	10
2002	8	9	220843	11.82	43.65	5.20	10
2002	8	10	94542	12.13	43.88	4.90	10
2002	8	10	120120	13.92	39.90	4.30	10
2002	8	10	155602	13.65	39.81	5.70	10
2002	8	10	164556	13.71	39.89	4.60	10
2002	8	11	202938	12.02	43.87	4.30	10
2002	8	14	204925	13.41	39.99	4.40	10
2002	8	25	61237	13.67	39.86	4.30	10
2002	11	19	10958	11.91	44.14	4.50	10
2002	11	19	82410	11.87	44.04	4.00	10

¹ http://neic.usgs.gov/neis/epic/epic_global.html, accessed on March 19, 2009.

2002	11	20	34524	11.87	44.21	4.50	10
2002	12	1	111832	12.28	39.74	5.10	10
2003	1	1	233646	11.20	41.75	4.60	10
2003	4	8	161005	18.98	39.24	4.60	10
2003	6	10	71039	14.45	40.07	4.60	10
2003	6	10	182323	14.46	40.21	4.30	10
2003	8	18	200750	11.80	41.25	4.00	10
2004	1	3	231752	11.51	43.04	5.20	10
2004	1	4	946	11.64	43.19	5.40	10
2004	1	18	62701	10.66	39.67	4.60	10
2004	1	29	231937	17.86	40.13	4.50	10
2004	4	26	70501	18.05	39.86	4.60	10
2004	4	27	5840	5.39	37.27	4.10	10
2004	6	11	3944	13.07	39.75	4.50	10
2004	8	31	231606	14.74	39.71	4.20	10
2004	10	8	235720	12.09	45.72	4.20	10
2004	10	22	120012	14.17	40.30	5.50	10
2005	2	17	4943	19.03	39.13	4.60	10
2005	4	30	12333	11.86	43.45	4.60	10
2005	4	30	31111	11.90	43.63	3.80	10
2005	4	30	45441	11.86	43.44	3.50	10
2005	4	30	191336	11.41	43.18	4.10	10
2005	6	4	184035	12.75	40.69	4.50	10
2005	7	7	165757	6.29	37.70	4.70	10
2005	7	11	203612	12.21	40.26	3.70	27
2005	7	18	163143	12.73	40.75	4.50	10
2005	9	14	150746	12.49	40.42	4.70	10
2005	9	20	21760	12.42	40.47	4.80	10
2005	9	20	183828	12.57	40.60	4.40	10
2005	9	20	212338	12.71	40.53	5.40	10
2005	9	20	232707	12.77	40.29	4.60	10
2005	9	21	143	12.81	40.44	4.40	10
2005	9	21	42122	12.65	40.53	4.40	10
2005	9	21	71258	12.39	40.50	4.40	10
2005	9	21	84004	12.60	40.44	4.30	10
2005	9	21	101416	13.50	40.49	4.20	10
2005	9	21	103058	13.19	40.76	4.20	10
2005	9	21	103302	12.36	40.38	4.40	10
2005	9	21	115723	12.41	40.42	4.60	10
2005	9	21	133302	12.51	40.51	4.60	10
2005	9	21	145727	12.53	40.47	5.00	10
2005	9	21	165650	11.97	40.24	4.30	10
2005	9	21	184401	12.44	40.39	4.50	10
2005	9	21	200452	12.55	40.50	4.80	10
2005	9	21	210550	12.62	40.66	4.50	10
2005	9	21	222559	12.47	40.45	4.00	10

2005	9	21	233621	11.98	40.32	4.40	10
2005	9	21	234911	12.60	40.42	4.40	10
2005	9	22	13133	12.78	40.44	4.70	10
2005	9	22	13934	12.15	40.46	4.60	10
2005	9	22	15647	12.50	40.64	4.50	10
2005	9	22	31234	12.70	40.46	5.20	10
2005	9	22	41539	12.65	40.49	4.50	10
2005	9	22	42819	12.73	40.51	4.50	10
2005	9	22	52153	12.72	40.34	4.70	10
2005	9	22	60835	12.27	40.42	4.40	10
2005	9	22	71304	12.88	40.37	3.90	4
2005	9	22	101424	12.63	40.50	4.80	10
2005	9	22	115743	12.60	40.52	4.40	10
2005	9	22	121039	12.05	40.41	4.20	0
2005	9	22	135844	12.70	40.55	5.20	10
2005	9	22	144818	13.03	40.75	4.50	10
2005	9	22	155931	12.69	40.38	4.50	21
2005	9	22	160809	12.63	40.40	3.90	21
2005	9	22	175326	12.51	40.33	3.90	14
2005	9	22	180853	12.47	40.34	4.50	10
2005	9	22	195153	12.40	40.44	5.10	10
2005	9	22	222250	12.52	40.49	4.40	10
2005	9	23	5546	12.28	40.47	4.30	10
2005	9	23	45751	12.55	40.60	4.80	10
2005	9	23	70609	12.57	40.59	4.30	10
2005	9	23	91832	12.58	40.54	4.40	10
2005	9	23	94948	12.51	40.60	4.00	10
2005	9	23	180126	12.64	40.49	4.40	10
2005	9	23	180507	12.20	40.25	4.30	10
2005	9	23	202632	12.57	40.47	4.80	10
2005	9	23	235927	12.59	40.62	4.20	10
2005	9	24	10419	12.38	40.42	4.10	10
2005	9	24	30158	12.68	40.63	4.30	10
2005	9	24	30932	12.39	40.43	4.40	10
2005	9	24	32526	12.73	40.43	4.80	10
2005	9	24	33823	12.64	40.56	4.50	10
2005	9	24	34513	12.86	40.76	4.20	10
2005	9	24	35715	12.60	40.40	4.70	10
2005	9	24	40756	12.64	40.47	4.20	10
2005	9	24	41154	12.68	40.46	4.50	10
2005	9	24	42035	12.61	40.57	4.60	10
2005	9	24	45050	12.16	40.17	3.90	10
2005	9	24	45732	12.64	40.47	4.10	10
2005	9	24	50803	12.30	40.19	4.10	10
2005	9	24	51534	12.67	40.52	5.20	10
2005	9	24	53611	12.50	40.46	4.80	10

2005	9	24	54604	12.57	40.42	4.50	10
2005	9	24	54942	12.42	40.32	4.10	10
2005	9	24	61045	12.61	40.40	4.50	10
2005	9	24	61446	12.29	40.45	4.70	10
2005	9	24	62804	12.67	40.49	4.60	10
2005	9	24	63247	12.69	40.64	4.30	10
2005	9	24	63819	12.54	40.59	3.90	10
2005	9	24	64517	12.60	40.58	4.00	10
2005	9	24	65440	12.41	40.32	4.20	10
2005	9	24	65828	12.57	40.57	5.30	10
2005	9	24	70615	12.53	40.53	3.90	10
2005	9	24	73608	12.62	40.53	5.20	10
2005	9	24	81152	12.45	40.55	4.40	10
2005	9	24	82049	12.54	40.39	5.10	10
2005	9	24	84137	12.62	40.57	4.30	10
2005	9	24	85221	12.69	40.52	4.60	10
2005	9	24	91716	12.51	40.36	4.80	10
2005	9	24	95344	12.35	40.45	4.70	10
2005	9	24	180849	12.43	40.46	4.40	10
2005	9	24	192403	12.47	40.63	5.50	11
2005	9	24	212549	11.80	40.40	4.30	10
2005	9	24	221522	12.30	40.66	4.50	10
2005	9	24	221737	12.48	40.70	4.40	10
2005	9	24	223148	12.10	40.47	4.40	10
2005	9	24	223825	11.86	40.43	4.30	10
2005	9	24	230520	12.39	40.66	4.80	10
2005	9	24	232249	12.39	40.58	4.70	10
2005	9	25	3729	12.45	40.60	5.00	10
2005	9	25	10016	11.60	40.38	4.10	10
2005	9	25	11059	12.26	40.51	4.90	10
2005	9	25	11131	12.42	40.46	4.60	10
2005	9	25	11227	12.35	40.49	4.70	10
2005	9	25	12658	12.23	40.62	3.90	10
2005	9	25	13145	12.22	40.55	4.60	10
2005	9	25	14717	12.37	40.61	4.00	10
2005	9	25	23358	12.05	40.58	4.10	10
2005	9	25	34335	12.00	40.43	4.30	10
2005	9	25	35119	12.25	40.46	4.70	10
2005	9	25	41532	12.35	40.65	4.40	10
2005	9	25	42642	11.94	40.45	4.40	10
2005	9	25	51150	12.32	40.59	4.50	10
2005	9	25	53314	12.05	40.51	4.10	10
2005	9	25	60021	12.20	40.51	4.30	10
2005	9	25	63303	11.85	40.50	4.20	10
2005	9	25	63712	12.40	40.44	3.70	10
2005	9	25	64313	12.00	40.45	4.20	10

2005	9	25	64735	12.10	40.51	4.50	10
2005	9	25	73926	11.98	40.44	4.60	10
2005	9	25	81843	12.44	40.49	5.00	10
2005	9	25	82129	12.19	40.50	4.60	10
2005	9	25	82737	12.15	40.37	4.50	10
2005	9	25	83340	12.32	40.48	4.60	10
2005	9	25	84451	12.58	40.47	4.00	10
2005	9	25	85138	12.64	40.68	4.10	10
2005	9	25	85201	12.19	40.47	4.40	10
2005	9	25	90908	12.13	40.52	4.50	10
2005	9	25	90924	12.09	40.59	4.50	10
2005	9	25	91138	12.50	40.52	4.70	10
2005	9	25	91732	12.08	40.47	4.40	10
2005	9	25	93409	12.21	40.68	4.10	10
2005	9	25	100213	12.37	40.51	5.00	10
2005	9	25	100758	12.45	40.62	4.80	10
2005	9	25	101800	12.49	40.47	4.60	10
2005	9	25	103120	12.21	40.49	4.60	10
2005	9	25	104128	12.21	40.47	4.40	10
2005	9	25	112004	12.42	40.58	5.10	10
2005	9	25	133602	12.17	40.43	4.10	10
2005	9	25	150911	12.00	40.37	4.60	10
2005	9	25	162202	12.44	40.62	4.80	10
2005	9	25	171648	12.32	40.51	4.50	10
2005	9	25	192257	11.71	40.61	3.90	10
2005	9	25	194755	12.20	40.62	4.20	10
2005	9	25	194815	11.95	40.49	4.20	10
2005	9	25	225404	12.33	40.57	4.30	10
2005	9	26	25833	12.64	40.60	4.60	10
2005	9	26	93109	12.45	40.63	4.40	10
2005	9	26	93354	12.43	40.60	5.20	10
2005	9	26	132833	12.39	40.58	5.20	10
2005	9	26	153626	12.53	40.58	4.70	10
2005	9	26	172429	12.05	40.63	4.60	10
2005	9	26	203002	12.46	40.54	5.10	10
2005	9	26	212502	12.34	40.62	5.00	10
2005	9	26	235311	12.46	40.45	4.50	10
2005	9	27	4028	12.52	40.71	4.50	10
2005	9	27	4219	11.93	40.27	4.20	10
2005	9	27	101358	12.55	40.56	4.70	10
2005	9	27	111044	12.24	40.37	4.50	10
2005	9	27	161909	12.34	40.60	4.60	10
2005	9	27	200826	12.29	40.54	4.30	10
2005	9	27	202137	12.22	40.63	4.70	10
2005	9	27	204441	12.38	40.40	4.10	10
2005	9	28	2123	12.32	40.40	4.70	10

2005	9	28	33611	12.55	40.58	4.40	10
2005	9	28	74317	11.72	40.29	4.60	10
2005	9	28	161714	11.97	40.33	4.20	10
2005	9	28	163136	12.44	40.63	5.10	10
2005	9	29	115219	12.42	40.58	4.80	10
2005	9	29	204913	12.15	40.74	4.00	10
2005	10	1	41621	12.60	40.82	4.50	10
2005	10	2	232442	12.02	40.54	4.90	10
2005	10	4	41940	12.46	40.65	4.50	10
2005	11	5	2112	11.92	43.65	4.70	10
2005	11	6	121118	11.70	43.62	4.50	10
2005	11	11	135337	12.05	45.86	4.20	10
2005	12	2	91329	11.78	43.53	4.30	10
2005	12	2	94745	11.81	43.54	4.60	10
2006	1	31	133658	14.57	41.58	4.00	10
2006	2	9	101800	11.73	42.97	4.50	10
2006	2	18	92028	11.52	42.83	4.50	10
2006	2	21	112115	11.57	43.13	4.40	10
2006	2	21	115152	11.91	42.97	4.00	10
2006	4	10	133647	14.53	39.94	4.90	10
2006	4	26	103626	18.11	39.93	4.30	10
2006	6	17	143332	12.24	40.51	4.40	0
2006	6	17	144516	12.40	40.80	4.60	0
2006	6	17	154259	12.29	40.62	3.90	0
2006	6	17	162041	12.31	40.54	4.50	0
2006	6	17	165311	12.24	40.53	4.30	0
2006	7	2	234505	19.33	38.95	4.70	0
2006	7	4	55158	7.92	39.01	4.50	0
2006	8	7	165634	11.43	45.19	4.70	0
2006	9	13	63919	11.79	43.08	4.70	0
2006	10	1	15351	17.57	40.21	3.70	0
2006	10	1	62349	17.06	40.34	3.90	0
2006	10	18	10917	19.09	39.14	3.80	0
2006	10	19	141404	13.55	39.85	4.10	0
2006	11	1	223121	5.78	36.98	4.40	0
2006	12	7	115823	12.27	45.99	4.90	0
2006	12	21	90746	12.04	43.55	5.00	0
2006	12	21	91150	11.97	44.23	4.50	0
2007	1	4	91331	19.12	38.79	3.80	0
2007	1	8	144406	15.00	42.23	4.00	0
2007	1	8	150320	16.50	38.81	4.10	0
2007	1	9	72912	14.98	42.07	4.10	0
2007	2	22	175054	10.03	42.79	3.90	0
2007	2	26	84859	9.97	42.88	5.00	0
2007	4	9	143854	12.10	43.74	4.30	0
2007	4	16	174119	18.77	39.31	4.40	0

2007	4	17	85014	19.04	39.09	4.10	0
2007	4	28	2543	12.05	43.87	4.60	0
2007	5	17	2138	9.77	40.67	4.40	0
2007	7	8	183130	10.33	40.26	4.10	0
2007	7	17	63841	13.40	40.95	3.90	0
2007	7	24	181704	19.21	38.94	4.30	0
2007	10	2	90632	13.44	40.83	5.00	0
2007	11	4	210618	13.36	39.89	4.50	0
2007	11	6	234406	13.57	39.93	4.40	0
2007	11	11	212142	12.15	40.69	4.70	0
2007	11	23	1837	16.49	40.99	4.00	0
2007	12	15	45937	19.16	39.20	4.50	0
2007	12	20	151343	17.51	40.11	4.10	0
2007	12	23	51802	4.76	36.23	4.60	0
2008	2	20	163121	19.88	38.46	4.20	0
2008	3	1	145352	11.80	43.95	4.50	0
2008	3	28	214440	19.08	39.04	4.20	0
2008	4	25	21340	16.14	38.74	4.00	0
2008	4	29	659	11.68	42.99	5.00	0
2008	4	29	10731	11.72	42.81	5.00	0
2008	4	29	14748	11.65	42.95	4.30	0
2008	4	29	15025	11.72	42.83	4.10	0
2008	4	29	23317	11.75	42.84	4.50	0
2008	4	29	170451	11.51	43.03	4.10	0
2008	4	29	224128	11.35	43.12	4.40	0
2008	8	19	53558	11.77	45.50	4.00	0
2008	9	18	214222	18.42	39.94	3.80	0
2008	9	20	45051	17.79	40.10	4.20	0
2008	10	17	94041	12.39	40.61	4.40	0
2008	10	17	102610	12.16	40.50	3.90	0
2008	10	17	105716	12.34	40.65	4.80	0
2008	10	17	130609	12.46	40.57	3.90	0
2008	10	17	154522	12.38	40.55	4.30	0
2008	10	17	202425	12.15	40.49	4.50	0
2008	10	18	125712	12.38	40.69	4.00	0
2008	11	5	50522.69	17.66	40.11	3.9	10
2008	12	31	215448.05	17.33	40.42	4.2	10
2008	12	31	215618.18	17.43	40.45	4.0	10
2008	12	31	221437.60	17.40	40.41	3.8	10
2009	1	1	13921.90	17.22	40.52	4.6	10
2009	2	5	173358.22	19.06	39.18	4.6	10
2009	2	5	213613.81	19.17	39.15	4.8	10
2009	2	6	32756.12	19.04	39.16	4.5	10
2009	2	11	35626.90	18.95	39.22	4.2	10

B-2: Risk parameters and level for the average value of the class.

ID	P	Trr	Ex	Cci	Th	G	Ts	Ps	Ed	Hp	RL1	RL2	RL3	RL4	RL5	RL6
1	7.0	4.0	4.0	4.0	7.0	7.0	4.0	1.0	9.5	0.0	3.15	4.50	3.13	4.48	3.31	4.73
2	7.0	4.0	7.0	1.0	7.0	7.0	4.0	1.0	9.5	0.0	3.15	4.50	3.26	4.66	3.35	4.79
3	7.0	4.0	4.0	1.0	7.0	7.0	4.0	1.0	9.5	0.0	2.92	4.17	2.86	4.09	2.95	4.22
4	7.0	4.0	4.0	4.0	7.0	7.0	4.0	1.0	9.5	0.0	3.15	4.50	3.13	4.48	3.31	4.73
5	4.0	7.0	7.0	9.5	4.0	7.0	4.0	1.0	9.5	0.0	2.18	5.44	2.63	6.57	2.59	6.47
6	7.0	4.0	1.0	4.0	7.0	7.0	4.0	1.0	9.5	0.0	2.92	4.17	2.73	3.91	2.91	4.16
7	4.0	4.0	1.0	4.0	7.0	7.0	4.0	1.0	9.5	0.0	1.67	4.17	1.56	3.91	1.66	4.16
8	1.0	4.0	9.5	9.5	7.0	7.0	7.0	7.0	1.0	0.0	0.58	5.78	0.64	6.37	0.70	6.99
9	1.0	7.0	4.0	7.0	4.0	7.0	7.0	7.0	1.0	0.0	0.49	4.89	0.58	5.81	0.58	5.76
10	1.0	7.0	1.0	7.0	4.0	7.0	7.0	7.0	1.0	0.0	0.46	4.56	0.52	5.24	0.52	5.19
11	1.0	7.0	4.0	4.0	4.0	7.0	7.0	7.0	4.0	0.0	0.49	4.89	0.55	5.51	0.53	5.34
12	1.0	4.0	4.0	1.0	7.0	7.0	4.0	7.0	7.0	0.0	0.46	4.56	0.43	4.25	0.44	4.44
13	1.0	4.0	4.0	1.0	7.0	7.0	4.0	7.0	4.0	0.0	0.42	4.22	0.42	4.16	0.44	4.35
14	1.0	4.0	4.0	4.0	7.0	7.0	4.0	7.0	9.5	0.0	0.52	5.17	0.47	4.72	0.50	5.03
15	4.0	4.0	4.0	1.0	7.0	4.0	4.0	7.0	9.5	0.0	1.80	4.50	1.65	4.12	1.67	4.19
16	1.0	4.0	1.0	7.0	7.0	7.0	4.0	7.0	9.5	0.0	0.52	5.17	0.45	4.54	0.50	4.97
17	1.0	4.0	4.0	4.0	7.0	7.0	4.0	7.0	9.5	0.0	0.52	5.17	0.47	4.72	0.50	5.03
18	4.0	4.0	4.0	4.0	7.0	7.0	4.0	7.0	7.0	0.0	1.96	4.89	1.86	4.64	1.98	4.95
19	1.0	7.0	4.0	4.0	4.0	7.0	4.0	7.0	9.5	0.0	0.52	5.17	0.55	5.53	0.53	5.27
20	4.0	4.0	7.0	4.0	7.0	7.0	4.0	7.0	4.0	0.0	1.96	4.89	2.05	5.12	2.17	5.43
21	1.0	4.0	4.0	4.0	7.0	7.0	4.0	7.0	7.0	0.0	0.49	4.89	0.46	4.64	0.50	4.95
22	1.0	7.0	1.0	4.0	4.0	7.0	4.0	7.0	7.0	0.0	0.46	4.56	0.49	4.88	0.46	4.62
23	1.0	4.0	4.0	4.0	7.0	7.0	4.0	7.0	9.5	0.0	0.52	5.17	0.47	4.72	0.50	5.03
24	1.0	7.0	7.0	4.0	4.0	7.0	4.0	7.0	7.0	0.0	0.52	5.22	0.60	6.02	0.58	5.76
25	4.0	7.0	1.0	4.0	4.0	7.0	4.0	7.0	9.5	0.0	1.93	4.83	1.98	4.96	1.88	4.70
26	4.0	4.0	4.0	4.0	7.0	7.0	4.0	7.0	9.5	0.0	2.07	5.17	1.89	4.72	2.01	5.03
27	1.0	4.0	4.0	7.0	7.0	7.0	4.0	7.0	9.5	0.0	0.55	5.50	0.51	5.11	0.55	5.54
28	4.0	4.0	7.0	9.5	7.0	7.0	4.0	7.0	9.5	0.0	2.44	6.11	2.40	6.00	2.61	6.53
29	1.0	7.0	1.0	4.0	4.0	7.0	4.0	7.0	9.5	0.0	0.48	4.83	0.50	4.96	0.47	4.70
30	1.0	7.0	1.0	4.0	4.0	7.0	4.0	7.0	9.5	0.0	0.48	4.83	0.50	4.96	0.47	4.70
31	1.0	7.0	7.0	7.0	4.0	7.0	4.0	7.0	9.5	0.0	0.58	5.83	0.65	6.49	0.63	6.35
32	4.0	7.0	4.0	7.0	4.0	7.0	7.0	7.0	9.5	0.0	2.33	5.83	2.43	6.07	2.41	6.02
33	7.0	4.0	7.0	7.0	7.0	7.0	7.0	7.0	9.5	0.0	4.32	6.17	4.08	5.83	4.44	6.35
34	7.0	7.0	4.0	4.0	4.0	7.0	7.0	7.0	9.5	0.0	3.85	5.50	3.97	5.68	3.85	5.51
35	4.0	7.0	4.0	4.0	4.0	7.0	7.0	7.0	7.0	0.0	2.09	5.22	2.24	5.60	2.17	5.43
36	4.0	4.0	4.0	4.0	7.0	7.0	7.0	7.0	7.0	0.0	2.09	5.22	1.92	4.79	2.08	5.19
37	1.0	4.0	7.0	4.0	7.0	7.0	7.0	7.0	7.0	0.0	0.56	5.56	0.54	5.36	0.58	5.76
38	1.0	4.0	4.0	4.0	7.0	7.0	7.0	7.0	7.0	0.0	0.52	5.22	0.48	4.79	0.52	5.19
39	4.0	4.0	4.0	4.0	7.0	7.0	7.0	7.0	7.0	0.0	2.09	5.22	1.92	4.79	2.08	5.19
40	1.0	4.0	4.0	4.0	7.0	7.0	7.0	7.0	7.0	0.0	0.52	5.22	0.48	4.79	0.52	5.19
41	1.0	4.0	1.0	4.0	7.0	7.0	7.0	7.0	4.0	0.0	0.46	4.56	0.41	4.13	0.45	4.53
42	1.0	4.0	4.0	1.0	7.0	7.0	7.0	7.0	4.0	0.0	0.46	4.56	0.43	4.31	0.46	4.59
43	1.0	4.0	4.0	4.0	7.0	7.0	7.0	7.0	7.0	0.0	0.52	5.22	0.48	4.79	0.52	5.19
44	4.0	4.0	4.0	4.0	7.0	7.0	7.0	7.0	4.0	0.0	1.96	4.89	1.88	4.70	2.04	5.10
45	1.0	4.0	7.0	4.0	7.0	7.0	7.0	7.0	1.0	0.0	0.49	4.89	0.52	5.18	0.56	5.58
46	4.0	4.0	7.0	7.0	7.0	7.0	7.0	7.0	1.0	0.0	2.09	5.22	2.23	5.57	2.44	6.09
47	1.0	7.0	9.5	9.5	4.0	7.0	7.0	7.0	1.0	0.0	0.58	5.78	0.72	7.18	0.72	7.23
48	1.0	4.0	7.0	7.0	7.0	7.0	7.0	7.0	1.0	0.0	0.52	5.22	0.56	5.57	0.61	6.09
49	9.5	4.0	7.0	9.5	7.0	7.0	7.0	9.5	9.5	4.0	6.81	7.17	6.01	6.33	6.59	6.94
50	7.0	7.0	7.0	4.0	4.0	7.0	4.0	7.0	7.0	0.0	3.66	5.22	4.21	6.02	4.03	5.76

51	9.5	4.0	7.0	7.0	7.0	4.0	4.0	9.5	7.0	4.0	5.65	5.94	5.29	5.57	5.57	5.87
52	9.5	4.0	7.0	7.0	7.0	4.0	4.0	9.5	4.0	4.0	5.33	5.61	5.21	5.48	5.49	5.78
53	9.5	4.0	9.5	7.0	7.0	4.0	4.0	9.5	4.0	4.0	5.59	5.89	5.66	5.96	5.94	6.25
54	9.5	4.0	7.0	9.5	7.0	7.0	4.0	9.5	9.5	4.0	6.49	6.83	5.87	6.18	6.36	6.70
55	9.5	9.5	7.0	9.5	4.0	7.0	4.0	9.5	7.0	1.0	6.18	6.50	7.39	7.78	7.01	7.38
56	9.5	9.5	9.5	9.5	4.0	7.0	4.0	9.5	9.5	4.0	7.02	7.39	7.97	8.39	7.56	7.96
57	9.5	9.5	4.0	9.5	4.0	7.0	4.0	9.5	7.0	4.0	6.18	6.50	6.91	7.27	6.50	6.84
58	9.5	9.5	9.5	9.5	4.0	7.0	7.0	9.5	7.0	1.0	6.76	7.11	7.98	8.41	7.69	8.10
59	1.0	4.0	7.0	4.0	7.0	7.0	4.0	7.0	9.5	0.0	0.55	5.50	0.53	5.29	0.56	5.60
60	7.0	9.5	9.5	4.0	4.0	4.0	4.0	7.0	9.5	0.0	4.01	5.72	5.10	7.29	4.57	6.53
61	9.5	9.5	7.0	4.0	4.0	7.0	4.0	7.0	9.5	1.0	5.59	5.89	6.69	7.04	6.08	6.40
62	7.0	9.5	7.0	4.0	4.0	7.0	4.0	7.0	9.5	0.0	4.04	5.78	4.91	7.02	4.47	6.39
63	4.0	9.5	9.5	9.5	4.0	7.0	4.0	7.0	7.0	0.0	2.56	6.39	3.25	8.14	3.09	7.72
64	4.0	4.0	4.0	4.0	7.0	4.0	4.0	7.0	9.5	0.0	1.93	4.83	1.80	4.51	1.88	4.70
65	4.0	4.0	4.0	4.0	7.0	7.0	7.0	7.0	7.0	0.0	2.09	5.22	1.92	4.79	2.08	5.19
66	4.0	4.0	1.0	4.0	7.0	4.0	7.0	7.0	9.5	0.0	1.93	4.83	1.63	4.09	1.75	4.37
67	4.0	4.0	4.0	4.0	7.0	7.0	7.0	7.0	9.5	0.0	2.20	5.50	1.95	4.87	2.11	5.27
68	4.0	4.0	4.0	4.0	7.0	7.0	7.0	7.0	9.5	0.0	2.20	5.50	1.95	4.87	2.11	5.27
69	7.0	4.0	7.0	4.0	7.0	7.0	7.0	7.0	9.5	0.0	4.08	5.83	3.80	5.44	4.08	5.84
70	7.0	4.0	7.0	4.0	7.0	7.0	7.0	7.0	9.5	0.0	4.08	5.83	3.80	5.44	4.08	5.84
71	7.0	4.0	4.0	4.0	7.0	7.0	7.0	7.0	9.5	0.0	3.85	5.50	3.41	4.87	3.69	5.27
72	9.5	4.0	9.5	7.0	7.0	7.0	7.0	9.5	9.5	4.0	6.81	7.17	6.16	6.48	6.64	6.99
73	9.5	4.0	4.0	4.0	7.0	7.0	7.0	9.5	9.5	4.0	5.91	6.22	4.79	5.05	5.16	5.43
74	9.5	4.0	4.0	4.0	7.0	7.0	7.0	9.5	9.5	1.0	5.59	5.89	4.74	4.99	5.13	5.40
75	9.5	7.0	4.0	7.0	4.0	7.0	7.0	9.5	9.5	4.0	6.23	6.56	5.93	6.25	5.87	6.18
76	9.5	4.0	4.0	7.0	7.0	4.0	7.0	9.5	9.5	4.0	5.91	6.22	4.96	5.23	5.33	5.61
77	9.5	7.0	4.0	7.0	4.0	7.0	7.0	9.5	7.0	1.0	5.65	5.94	5.80	6.11	5.77	6.08
78	9.5	4.0	4.0	7.0	7.0	7.0	7.0	9.5	9.5	4.0	6.23	6.56	5.16	5.44	5.64	5.94
79	9.5	4.0	4.0	7.0	7.0	7.0	7.0	9.5	9.5	4.0	6.23	6.56	5.16	5.44	5.64	5.94
80	4.0	4.0	4.0	4.0	7.0	7.0	7.0	7.0	7.0	0.0	2.09	5.22	1.92	4.79	2.08	5.19
81	1.0	4.0	1.0	4.0	7.0	7.0	7.0	7.0	1.0	0.0	0.42	4.22	0.40	4.04	0.44	4.44
82	1.0	7.0	1.0	4.0	4.0	7.0	7.0	7.0	1.0	0.0	0.42	4.22	0.49	4.85	0.47	4.68
83	1.0	4.0	4.0	4.0	7.0	7.0	7.0	7.0	1.0	0.0	0.46	4.56	0.46	4.61	0.50	5.01
84	7.0	4.0	4.0	4.0	7.0	7.0	7.0	7.0	7.0	0.0	3.66	5.22	3.35	4.79	3.63	5.19
85	4.0	4.0	7.0	4.0	7.0	7.0	7.0	7.0	7.0	0.0	2.22	5.56	2.14	5.36	2.30	5.76
86	1.0	4.0	7.0	4.0	7.0	7.0	7.0	7.0	1.0	0.0	0.49	4.89	0.52	5.18	0.56	5.58
87	7.0	4.0	1.0	4.0	7.0	4.0	7.0	7.0	9.5	0.0	3.38	4.83	2.86	4.09	3.06	4.37
88	9.5	4.0	7.0	1.0	7.0	7.0	7.0	4.0	9.5	1.0	5.01	5.28	4.70	4.95	4.93	5.19
89	9.5	4.0	9.5	4.0	7.0	7.0	7.0	1.0	9.5	4.0	5.59	5.89	5.46	5.75	5.75	6.05
90	9.5	4.0	4.0	4.0	7.0	4.0	7.0	1.0	9.5	4.0	4.70	4.94	4.27	4.50	4.44	4.68
91	9.5	4.0	4.0	7.0	7.0	7.0	7.0	4.0	9.5	9.5	6.23	6.56	5.06	5.33	5.43	5.72
92	7.0	4.0	1.0	4.0	7.0	7.0	7.0	1.0	7.0	0.0	2.96	4.22	2.79	3.98	3.02	4.32
93	4.0	4.0	4.0	4.0	7.0	7.0	7.0	1.0	7.0	0.0	1.82	4.56	1.82	4.55	1.96	4.89
94	4.0	7.0	1.0	4.0	4.0	7.0	7.0	1.0	7.0	0.0	1.69	4.22	1.92	4.79	1.82	4.56
95	7.0	4.0	1.0	4.0	7.0	7.0	7.0	1.0	9.5	0.0	3.15	4.50	2.84	4.06	3.08	4.40
96	7.0	4.0	4.0	4.0	7.0	7.0	7.0	1.0	9.5	0.0	3.38	4.83	3.24	4.63	3.48	4.97
97	1.0	4.0	7.0	4.0	7.0	7.0	7.0	1.0	9.5	0.0	0.52	5.17	0.52	5.20	0.55	5.54
98	1.0	7.0	1.0	4.0	4.0	7.0	7.0	1.0	9.5	0.0	0.45	4.50	0.49	4.87	0.46	4.64
99	9.5	7.0	7.0	7.0	4.0	4.0	7.0	1.0	9.5	4.0	5.33	5.61	5.95	6.27	5.70	6.00
100	7.0	4.0	9.5	7.0	7.0	7.0	7.0	1.0	7.0	0.0	3.85	5.50	4.19	5.99	4.51	6.45
101	4.0	4.0	4.0	7.0	7.0	7.0	7.0	1.0	7.0	0.0	1.96	4.89	1.98	4.94	2.16	5.40
102	7.0	4.0	7.0	7.0	7.0	7.0	7.0	1.0	7.0	0.0	3.66	5.22	3.86	5.51	4.18	5.97
103	1.0	7.0	4.0	1.0	4.0	7.0	4.0	1.0	7.0	0.0	0.39	3.89	0.48	4.82	0.44	4.38
104	1.0	7.0	7.0	4.0	4.0	7.0	4.0	1.0	7.0	0.0	0.46	4.56	0.58	5.78	0.55	5.46

105	1.0	7.0	7.0	9.5	4.0	7.0	4.0	1.0	7.0	0.0	0.52	5.17	0.65	6.50	0.64	6.40
106	1.0	7.0	7.0	9.5	4.0	7.0	4.0	1.0	7.0	0.0	0.52	5.17	0.65	6.50	0.64	6.40
107	4.0	4.0	7.0	9.5	7.0	7.0	4.0	1.0	7.0	0.0	2.07	5.17	2.27	5.69	2.46	6.16
108	4.0	4.0	9.5	9.5	7.0	7.0	4.0	1.0	7.0	0.0	2.18	5.44	2.46	6.16	2.65	6.63
109	7.0	4.0	7.0	7.0	7.0	7.0	7.0	1.0	9.5	0.0	3.85	5.50	3.91	5.59	4.23	6.05
110	4.0	7.0	1.0	9.5	4.0	7.0	7.0	1.0	9.5	0.0	2.04	5.11	2.23	5.58	2.23	5.57
111	1.0	4.0	4.0	4.0	7.0	7.0	7.0	1.0	7.0	0.0	0.46	4.56	0.46	4.55	0.49	4.89
112	1.0	4.0	1.0	4.0	7.0	7.0	4.0	1.0	9.5	0.0	0.42	4.17	0.39	3.91	0.42	4.16
113	1.0	4.0	1.0	4.0	7.0	7.0	4.0	1.0	9.5	0.0	0.42	4.17	0.39	3.91	0.42	4.16
114	7.0	7.0	4.0	4.0	4.0	7.0	7.0	1.0	9.5	0.0	3.38	4.83	3.80	5.44	3.64	5.21
115	7.0	7.0	7.0	7.0	4.0	7.0	7.0	1.0	9.5	0.0	3.85	5.50	4.48	6.40	4.40	6.29
116	1.0	4.0	4.0	1.0	7.0	7.0	7.0	1.0	7.0	0.0	0.42	4.22	0.42	4.16	0.44	4.38
117	1.0	4.0	4.0	4.0	7.0	7.0	4.0	1.0	7.0	0.0	0.42	4.22	0.44	4.40	0.47	4.65
118	1.0	4.0	4.0	4.0	7.0	7.0	4.0	1.0	9.5	0.0	0.45	4.50	0.45	4.48	0.47	4.73
119	1.0	7.0	1.0	7.0	4.0	7.0	7.0	1.0	7.0	0.0	0.46	4.56	0.52	5.18	0.51	5.07
120	4.0	4.0	4.0	4.0	7.0	7.0	7.0	1.0	7.0	0.0	1.82	4.56	1.82	4.55	1.96	4.89
121	4.0	4.0	4.0	4.0	7.0	7.0	7.0	1.0	7.0	0.0	1.82	4.56	1.82	4.55	1.96	4.89
122	7.0	4.0	4.0	4.0	7.0	7.0	7.0	1.0	9.5	0.0	3.38	4.83	3.24	4.63	3.48	4.97
123	4.0	4.0	1.0	4.0	7.0	7.0	7.0	1.0	9.5	0.0	1.80	4.50	1.62	4.06	1.76	4.40
124	4.0	4.0	4.0	4.0	7.0	7.0	4.0	1.0	9.5	0.0	1.80	4.50	1.79	4.48	1.89	4.73
125	7.0	4.0	1.0	4.0	7.0	7.0	7.0	1.0	9.5	0.0	3.15	4.50	2.84	4.06	3.08	4.40
126	4.0	4.0	1.0	4.0	7.0	7.0	7.0	1.0	9.5	0.0	1.80	4.50	1.62	4.06	1.76	4.40
127	7.0	4.0	4.0	4.0	7.0	7.0	7.0	1.0	9.5	0.0	3.38	4.83	3.24	4.63	3.48	4.97
128	1.0	4.0	7.0	4.0	7.0	7.0	7.0	1.0	7.0	0.0	0.49	4.89	0.51	5.12	0.55	5.46
129	1.0	4.0	4.0	4.0	7.0	7.0	7.0	1.0	7.0	0.0	0.46	4.56	0.46	4.55	0.49	4.89
130	4.0	4.0	9.5	7.0	7.0	7.0	7.0	1.0	7.0	0.0	2.20	5.50	2.39	5.99	2.58	6.45
131	1.0	4.0	7.0	7.0	7.0	7.0	7.0	1.0	7.0	0.0	0.52	5.22	0.55	5.51	0.60	5.97
132	1.0	4.0	4.0	7.0	7.0	7.0	7.0	1.0	7.0	0.0	0.49	4.89	0.49	4.94	0.54	5.40
133	1.0	4.0	4.0	4.0	7.0	7.0	7.0	1.0	7.0	0.0	0.46	4.56	0.46	4.55	0.49	4.89
134	1.0	4.0	4.0	4.0	7.0	7.0	7.0	1.0	4.0	0.0	0.42	4.22	0.45	4.46	0.48	4.80
135	9.5	4.0	7.0	7.0	7.0	4.0	7.0	1.0	9.5	4.0	5.33	5.61	5.18	5.46	5.47	5.76
136	4.0	4.0	1.0	4.0	7.0	7.0	7.0	1.0	7.0	0.0	1.69	4.22	1.59	3.98	1.73	4.32
137	1.0	4.0	4.0	4.0	7.0	7.0	7.0	1.0	7.0	0.0	0.46	4.56	0.46	4.55	0.49	4.89
138	7.0	4.0	7.0	4.0	7.0	7.0	7.0	1.0	9.5	0.0	3.62	5.17	3.64	5.20	3.87	5.54
139	7.0	4.0	7.0	4.0	7.0	7.0	7.0	1.0	9.5	0.0	3.62	5.17	3.64	5.20	3.87	5.54
140	9.5	4.0	7.0	4.0	7.0	4.0	7.0	1.0	9.5	4.0	5.01	5.28	4.81	5.07	4.98	5.25
141	4.0	4.0	7.0	4.0	7.0	7.0	7.0	1.0	7.0	0.0	1.96	4.89	2.05	5.12	2.18	5.46
142	7.0	4.0	1.0	4.0	7.0	7.0	7.0	1.0	9.5	0.0	3.15	4.50	2.84	4.06	3.08	4.40
143	7.0	4.0	4.0	1.0	7.0	7.0	7.0	1.0	7.0	0.0	2.96	4.22	2.91	4.16	3.07	4.38
144	9.5	4.0	7.0	1.0	7.0	4.0	7.0	4.0	9.5	4.0	5.01	5.28	4.56	4.80	4.64	4.89
145	9.5	4.0	7.0	7.0	7.0	4.0	7.0	4.0	9.5	7.0	5.96	6.28	5.35	5.64	5.64	5.94
146	9.5	4.0	4.0	1.0	7.0	4.0	7.0	4.0	9.5	4.0	4.70	4.94	4.01	4.23	4.10	4.32
147	9.5	7.0	4.0	7.0	4.0	7.0	7.0	9.5	9.5	1.0	5.91	6.22	5.88	6.19	5.84	6.15
148	9.5	9.5	9.5	9.5	4.0	7.0	7.0	9.5	9.5	4.0	7.34	7.72	8.11	8.54	7.79	8.20
149	7.0	4.0	1.0	4.0	7.0	7.0	7.0	7.0	9.5	0.0	3.62	5.17	3.01	4.30	3.29	4.70
150	7.0	4.0	4.0	4.0	7.0	7.0	7.0	7.0	7.0	0.0	3.66	5.22	3.35	4.79	3.63	5.19
151	4.0	7.0	1.0	4.0	4.0	7.0	7.0	7.0	4.0	0.0	1.82	4.56	1.98	4.94	1.91	4.77
152	7.0	4.0	4.0	4.0	7.0	7.0	7.0	7.0	7.0	0.0	3.66	5.22	3.35	4.79	3.63	5.19
153	9.5	7.0	1.0	7.0	4.0	7.0	7.0	9.5	9.5	1.0	5.59	5.89	5.33	5.62	5.30	5.58
154	9.5	4.0	1.0	7.0	7.0	7.0	7.0	9.5	9.5	4.0	5.91	6.22	4.62	4.87	5.10	5.37
155	7.0	7.0	1.0	4.0	4.0	7.0	7.0	7.0	7.0	0.0	3.42	4.89	3.52	5.03	3.40	4.86
156	7.0	4.0	4.0	4.0	7.0	7.0	7.0	7.0	7.0	0.0	3.66	5.22	3.35	4.79	3.63	5.19
157	7.0	4.0	1.0	4.0	7.0	7.0	7.0	7.0	7.0	0.0	3.42	4.89	2.95	4.22	3.23	4.62
158	4.0	4.0	1.0	4.0	7.0	7.0	7.0	7.0	7.0	0.0	1.96	4.89	1.69	4.22	1.85	4.62

159	1.0	4.0	7.0	4.0	7.0	7.0	4.0	7.0	7.0	0.0	0.52	5.22	0.52	5.21	0.55	5.52
160	7.0	4.0	4.0	4.0	7.0	7.0	4.0	7.0	4.0	0.0	3.19	4.56	3.19	4.55	3.40	4.86
161	7.0	4.0	4.0	4.0	7.0	7.0	4.0	7.0	4.0	0.0	3.19	4.56	3.19	4.55	3.40	4.86
162	7.0	4.0	4.0	4.0	7.0	7.0	4.0	7.0	7.0	0.0	3.42	4.89	3.25	4.64	3.47	4.95
163	9.5	4.0	1.0	4.0	7.0	4.0	7.0	1.0	9.5	4.0	4.38	4.61	3.73	3.93	3.90	4.11
164	9.5	4.0	1.0	4.0	7.0	4.0	7.0	1.0	9.5	1.0	4.06	4.28	3.67	3.87	3.87	4.08
165	7.0	4.0	4.0	7.0	7.0	7.0	7.0	1.0	9.5	0.0	3.62	5.17	3.51	5.02	3.83	5.48
166	7.0	7.0	1.0	4.0	4.0	4.0	7.0	1.0	9.5	0.0	2.92	4.17	3.26	4.66	3.01	4.31
167	4.0	4.0	7.0	4.0	7.0	7.0	7.0	1.0	7.0	0.0	1.96	4.89	2.05	5.12	2.18	5.46
168	1.0	4.0	1.0	1.0	7.0	7.0	7.0	1.0	4.0	0.0	0.36	3.56	0.35	3.50	0.37	3.72

ID Identity number; P Proximity; Trr Tectonic Region; Ex Aerial Extent; Cci Termination Index; Th Tectonic History; G Geology; Ts Tectonic Status; Ps Relative Position; Ed Elevation Difference; Hp Hydraulic Pression; RL1 Risk Level using simple weighting method; RL2 Risk Level using simple weight method without the consideration of Proximity parameter; RL3 Risk Level using AHP method; RL4 Risk Level using AHP method without the consideration of Proximity parameter; RL5 Risk Level using PWC method; and RL6 Risk Level using PWC method without the consideration of Proximity parameter.

B-3: Water Pressure test and Rock Quality Designation (Fekadu, 2005).

Bore hole number	Location	Elevation (m.a.l)	Test conducted depth (m)	RQD (%)			Permeability (Lugeon) Average	Remarks on Permeability **
				Min.	Max	Average		
Abutment Section								
BH-TT2	Left Abutment	421.73	23.75-28.57	36	65	50.5	245	Very High
BH-TT2	Left Abutment		43.75-48.57	36	66	51	3.68	Low
BH-TT2	Left Abutment		54.3-59.25	37	61	49	135	Very High
BH-TT2	Left Abutment		61.05-64.05	42	87	64.5	331.67	Very High
BH-TT2	Left Abutment		66.1-70	20	90	59.5	24.73	Medium
BH-TE	Right Abutment	410.339	21.5-25.8	-	-	50	316	Very High
BH-TE	Right Abutment		44.85-49.70	-	-	72	3.85	Low
BH-TE	Right Abutment		50.7-55.7	-	-	72	89.5	Very High
BH-TE	Right Abutment		56.7-61.2	13	72	42.5	33.01	High
BH-TE	Right Abutment		64.85-70	13	30	21.5	168.16	Very High
River Section								
BH-TC	Left Bank	374.41	23.75-28.57	42	90	66	1.8	Impervious
BH-TC	Left Bank		29.75-34.75	42	67	54.5	1.75	Impervious
BH-TC	Left Bank		36-40			67	1.82	Impervious
BH-TD	Left Bank	374.15	23.75-28.57	25	66	45.5	0.39	Impervious
BH-TD	Left Bank		29.39-33.15	25	25	25	0.53	Impervious
BH-TD	Left Bank		37.2-42.2	24	66	45	3.14	Low
BH-TD	Left Bank		46.0-51.15	62	64	63	0.97	Impervious
BH-TD	Left Bank		66-70	11	63	37	4.11	Low
BH-TC1	Left Bank	377.791	24-29.2			72	2.16	Impervious
BH-TC1	Left Bank		32.6-36.2	22	83	52.5	0	Impervious
BH-TC1	Left Bank		36.2-40	83		83	5.26	Low
BH-TF	Right Bank	377.652	39-44	45	91	68	0.31	Impervious
BH-TF	Right Bank		61-65	37	56	46.5	4.29	Low
River section falling head test		-	On alluvial deposit <10			-	18	Medium
** 0-3 Lugeon impervious, 3-10 Lugeon low permeability, 10-30 Lugeon medium permeability, 30-60 Lugeon high permeability, and > 60 Lugeon very high permeability								

B-4: Historical monthly flow of the Awash river at the Tendaho dam site (1962 – 2002).

Year	Historical Monthly flow at Tendaho (MMC) the data from (1962 to 1964) is Awash Dubti station data from Sogreah (1965)												Annual
	Jan	Feb	Mar	Apr	May	Jun	Jul	Aug	Sep	Oct	Nov	Dec	
1962	105.61	102.59	123.77	103.12	81.14	44.28	77.77	520.35	340.81	244.98	127.71	92.34	1964.48
1963	117.77	49.52	57.15	238.76	320.00	130.86	161.73	397.57	571.17	213.74	125.42	109.80	2493.09
1964	129.46	107.02	93.31	183.49	121.97	86.54	592.99	1158.03	685.20	313.09	145.00	387.00	4003.09
1965	92.65	70.93	109.43	201.85	105.76	54.79	80.51	329.90	245.01	185.62	153.96	115.75	1746.16
1966	103.61	153.18	146.96	166.46	110.95	85.33	100.47	274.61	293.86	238.14	125.97	89.10	1888.64
1967	68.26	97.96	68.29	151.78	215.92	59.40	204.51	642.96	208.88	332.73	340.01	167.59	2558.29
1968	108.17	232.65	174.50	303.22	148.34	118.74	558.03	578.27	383.10	202.47	129.09	110.53	3047.11
1969	266.36	218.67	225.71	211.20	200.57	200.57	135.23	572.91	332.54	242.76	121.71	77.26	2805.49
1970	139.46	84.86	373.89	117.14	100.94	67.19	358.48	1040.13	510.80	299.46	122.39	72.55	3287.29
1971	63.77	42.95	41.48	59.74	80.63	49.24	87.11	455.86	482.98	282.22	157.16	85.15	1888.29
1972	87.00	262.00	122.10	200.23	178.07	124.48	164.33	216.17	194.64	148.12	75.90	52.35	1825.39
1973	47.00	33.44	17.40	13.78	32.99	9.30	184.77	1430.55	242.93	185.06	98.22	56.67	2352.11
1974	39.08	27.14	761.84	94.70	60.90	59.27	492.70	1015.10	570.01	248.27	128.98	76.94	3574.93
1975	89.48	97.29	67.63	253.76	107.30	48.94	289.08	709.40	1254.88	600.48	196.38	115.08	3829.70
1976	143.16	124.53	142.40	175.74	179.58	137.76	114.24	315.35	221.64	184.53	160.92	113.46	2013.31
1977	79.11	72.35	61.69	236.46	187.31	56.63	124.96	531.00	291.63	682.27	362.17	173.28	2858.86
1978	127.16	425.49	284.60	188.72	183.56	67.82	471.26	393.92	201.98	169.22	143.55	126.15	2783.43
1979	281.71	118.64	566.00	198.77	148.97	33.18	163.72	718.34	345.18	363.95	157.96	141.18	3237.60
1980	82.84	86.55	60.38	79.90	41.97	18.49	114.71	659.33	285.38	226.68	88.43	46.74	1791.40
1981	16.91	9.88	517.46	270.54	114.37	54.26	135.53	354.04	332.21	222.68	158.56	112.27	2298.71
1982	88.44	64.98	173.89	205.84	166.90	40.72	51.13	132.86	137.34	545.26	551.47	167.91	2326.74
1983	111.92	140.81	113.40	265.91	189.78	131.92	99.03	194.37	210.37	233.76	155.96	124.92	1972.21
1984	106.65	84.82	67.64	43.64	131.21	40.94	57.58	57.80	116.51	73.52	44.58	107.28	932.17
1985	56.96	47.04	55.44	260.14	188.62	79.15	124.60	255.47	526.46	260.27	133.24	108.06	2095.45
1986	82.86	199.81	218.90	284.41	136.78	120.36	216.79	344.68	283.23	190.51	134.83	86.86	2300.02
1987	53.02	32.82	537.36	431.02	135.86	149.67	77.42	281.62	150.00	114.96	68.69	69.28	2101.72
1988	2.26	63.11	20.55	392.44	130.00	80.00	193.00	97.00	446.67	142.88	138.19	76.34	1782.43
1989	66.42	39.09	58.99	303.06	33.23	44.09	66.46	138.33	138.58	175.36	112.07	84.91	1260.59
1990	51.90	369.53	194.55	480.10	217.71	87.69	86.39	98.99	113.02	187.27	120.84	78.58	2086.55
1991	46.22	47.12	164.07	100.17	81.88	56.13	77.63	363.02	177.55	266.75	148.07	68.68	1597.28
1992	77.18	122.41	102.36	108.12	88.14	41.83	109.37	527.62	345.00	623.77	244.86	100.74	2491.39
1993	135.47	233.34	151.92	270.10	98.51	236.87	243.72	271.00	420.45	328.27	284.12	144.96	2818.73
1994	78.98	42.91	116.48	193.00	130.00	80.00	193.00	483.00	345.00	260.00	156.00	227.56	2305.93
1995	91.00	105.00	172.00	193.00	130.00	80.00	147.00	483.00	345.00	260.00	156.00	122.00	2284.00
1996	91.00	19.10	62.72	31.64	130.00	44.69	19.45	537.37	227.31	113.93	156.00	122.00	1555.22
1997	33.28	32.69	119.80	139.57	56.13	58.17	93.11	191.71	67.66	319.64	281.73	61.43	1454.92
1998	87.78	63.90	177.29	32.47	3.40	87.17	439.16	1155.12	848.77	281.72	52.61	213.08	3383.75
1999	119.76	79.23	134.05	63.19	34.48	25.38	352.72	499.15	482.82	225.47	160.96	179.82	2357.02
2000	101.82	59.59	48.14	25.28	67.47	18.62	192.00	483.00	345.00	260.00	156.00	1878.91	2385.98
2001	47.93	32.25	170.50	161.93	233.58	171.63	299.89	576.73	365.99	182.09	21.46	122.00	2385.98
2002	40.32	39.19	192.11	510.33	231.17	164.53	137.98	353.46	64.88	33.06	2.22	325.69	2094.94
mean	91.70	105.76	172.39	193.77	130.15	80.19	192.44	483.88	345.18	260.12	156.08	122.81	2334.48
STD	53.47	91.82	160.91	119.37	66.24	51.99	143.90	311.05	221.99	137.11	96.51	67.83	678.03
CV	0.58	0.87	0.93	0.62	0.51	0.65	0.75	0.64	0.64	0.53	0.62	0.55	0.29

B-5a: The fundamental scale of absolute numbers (Saaty, 1980, 2004a, 2004b).

Intensity of important	Definition	Explanation
1	Equal importance	Two activities contribute equally to the objective
3	Moderate importance	Experience and judgement slightly favour one activity over the other
5	Strong importance	Experience and judgement strongly favour one activity over the other
7	Very strong or demonstrated importance	An activity is favoured very strongly over another; its dominance demonstrated in practice
9	Extreme importance	The evidence favouring one activity over another is of the highest possible order of affirmation
2, 4, 6, 8	For compromise between the above values	A reasonable assumption; sometimes one needs to interpolate a compromise judgement numerically because there is no good word to describe it
Reciprocals of the above judgments	If activity i has one of the above nonzero numbers assigned to it when compared with activity j, then j has the reciprocal value when compared with i.	A comparison mandated by choosing the smaller element as the unit to estimate the large one as a multiple of that unit.

B-5b: Random consistency indices (RI) of random reciprocal matrices of order n (Saaty, 1980, 2004a, 2004b).

n	1	2	3	4	5	6	7	8	9	10	11	12	13	14	15
RI	0.0	0.0	0.58	0.90	1.12	1.24	1.32	1.41	1.45	1.49	1.51	1.48	1.56	1.57	1.59

Appendix

C

Under this appendix, mathematica equation which was used to analyze the possible risk level of the brittle tectonic structures related to reservoir leakage by simple weighting (AVE), pairwise comparison (PWC) and analytic hierarchy processing (AHP) methods are explained here.

Mathematica is a computational software program used in scientific, engineering, and mathematical fields and other areas of technical computing. It was originally conceived by Stephen Wolfram and is developed by Wolfram Research of Champaign, Illinois¹.

C-1: Simple weighting method (AVE)

```
Clear[P,Ts,Trr,Th,Ex,Ti,G,Ps,Ed,Hp,RL3,RL3Full,RL12, RL13, RL21, RL22,
RL23,RL31minFull,RL31maxFull,RL31min,RL31max,RL32min,RL32max,RL33min,RL33max,RL34min,RL34max,RL3
1Full,P31min,P31max,P32min,P32max,P33min,P33max,P34min,P34max];
```

```
Manipulate[
```

```
RL31minFull[x_?NumberQ]:=P31min*x;
```

```
RL31maxFull[x_?NumberQ]:=P31max*x;
```

```
RL31min[Ts_?NumberQ]:=P31min*(Trr+Ex+Ti+Th+G+Ts+Ps+Ed+Hp)/90;
```

```
RL31max[Ts_?NumberQ]:=P31max*(Trr+Ex+Ti+Th+G+Ts+Ps+Ed+Hp)/90;
```

```
RL32minFull[x_?NumberQ]:=P32min*x;
```

```
RL32maxFull[x_?NumberQ]:=P32max*x;
```

```
RL32min[Ts_?NumberQ]:=P32min*(Trr+Ex+Ti+Th+G+Ts+Ps+Ed+Hp)/90;
```

```
RL32max[Ts_?NumberQ]:=P32max*(Trr+Ex+Ti+Th+G+Ts+Ps+Ed+Hp)/90;
```

```
RL33minFull[x_?NumberQ]:=P33min*x;
```

```
RL33maxFull[x_?NumberQ]:=P33max*x;
```

```
RL33min[Ts_?NumberQ]:=P33min*(Trr+Ex+Ti+Th+G+Ts+Ps+Ed+Hp)/90;
```

```
RL33max[Ts_?NumberQ]:=P33max*(Trr+Ex+Ti+Th+G+Ts+Ps+Ed+Hp)/90;
```

¹ <http://en.wikipedia.org/wiki/Mathematica>, accessed on December 15, 2009.

```

RL34minFull[x_?NumberQ]:=P34min*x;
RL34maxFull[x_?NumberQ]:=P34max*x;

```

```

RL34min[Ts_?NumberQ]:=P34min*(Trr+Ex+Ti+Th+G+Ts+Ps+Ed+Hp)/90;
RL34max[Ts_?NumberQ]:=P34max*(Trr+Ex+Ti+Th+G+Ts+Ps+Ed+Hp)/90;

```

```

RL3[Ts_?NumberQ]:=(Trr+Ex+Ti+Th+G+Ts+Ps+Ed+Hp)/9;
RL3Full[x_?NumberQ]:=10*x;

```

```

plot1=Show[

```

```

{ParametricPlot[{{RL3Full[x],RL31minFull[x]},{RL3Full[x],RL31maxFull[x]}},{x,0,1},PlotRange->{{0,10},{0,10}},PlotStyle->{Dotted,Dotted}},

```

```

{ParametricPlot[{{RL3[Ts],RL31min[Ts]},{RL3[Ts],RL31max[Ts]}},{Ts,0,10},PlotRange->{{0,10},{0,10}},PlotStyle->{Thick,Thick}},

```

```

{ParametricPlot[{{RL3Full[x],RL32minFull[x]},{RL3Full[x],RL32maxFull[x]}},{x,0,1},PlotRange->{{0,10},{0,10}},PlotStyle->{Dotted,Dotted}},

```

```

{ParametricPlot[{{RL3[Ts],RL32min[Ts]},{RL3[Ts],RL32max[Ts]}},{Ts,0,10},PlotRange->{{0,10},{0,10}},PlotStyle->{Thick,Thick}},

```

```

{ParametricPlot[{{RL3Full[x],RL33minFull[x]},{RL3Full[x],RL33maxFull[x]}},{x,0,1},PlotRange->{{0,10},{0,10}},PlotStyle->{Dotted,Dotted}},

```

```

{ParametricPlot[{{RL3[Ts],RL33min[Ts]},{RL3[Ts],RL33max[Ts]}},{Ts,0,10},PlotRange->{{0,10},{0,10}},PlotStyle->{Thick,Thick}},

```

```

{ParametricPlot[{{RL3Full[x],RL34minFull[x]},{RL3Full[x],RL34maxFull[x]}},{x,0,1},PlotRange->{{0,10},{0,10}},PlotStyle->{Dotted,Dotted}},

```

```

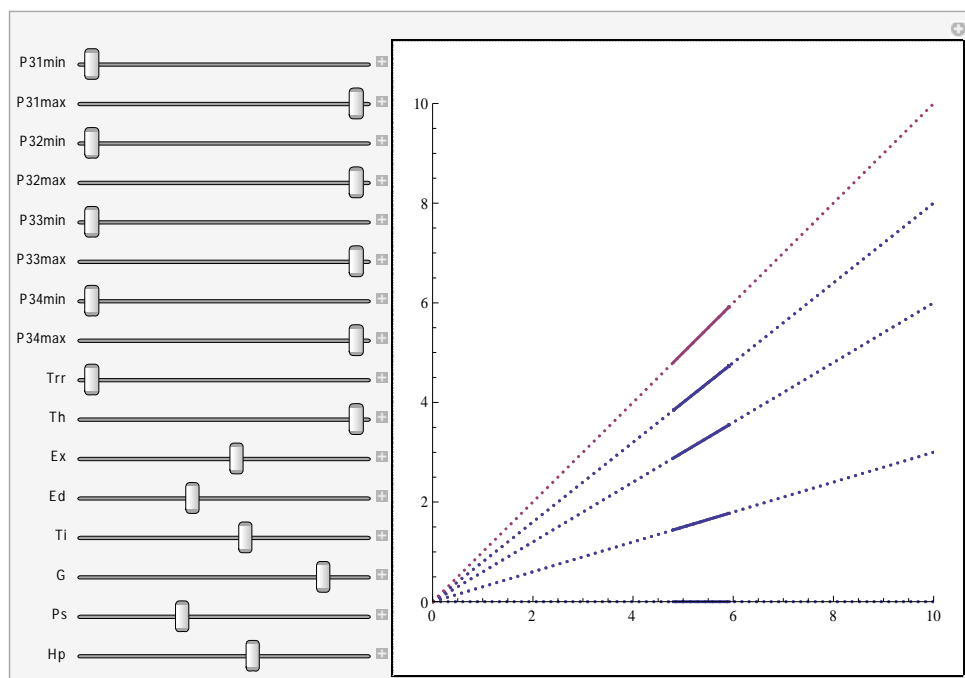
{ParametricPlot[{{RL3[Ts],RL34min[Ts]},{RL3[Ts],RL34max[Ts]}},{Ts,0,10},PlotRange->{{0,10},{0,10}},PlotStyle->{Thick,Thick}}
}],

```

```

{P31min,0,3},{P31max,P31min,3},{P32min,3,6},{P32max,P32min,6},{P33min,6,8},{P33max,P33min,8},{P34min,8,10},
{P34max,P34min,10},{Trr,0,10},{Th,0,10},{Ex,0,10},{Ed,0,10},{Ti,0,10},{G,0,10},{Ps,0,10},{Hp,0,10}}

```



```
Clear[P,Ts,Trr,Th,Ex,Dip,Ti,G,Ps,Hp,RL3,RL3Full,RL12, RL13, RL21, RL22,
RL23,RL31minFull,RL31maxFull,RL31min,RL31max,RL32min,RL32max,RL33min,RL33max,RL34min,RL34max,RL3
1Full,P31min,P31max,P32min,P32max,P33min,P33max,P34min,P34max, RL31, P33];
```

```
Manipulate[
```

```
RL33minFull[x_?NumberQ]:=P33min*x;
RL33maxFull[x_?NumberQ]:=P33max*x;
```

```
RL33min[Ts_?NumberQ]:=P33min*(Trr+Ex+Ti+Th+G+Ts+Ps+Ed+Hp)/90;
RL33max[Ts_?NumberQ]:=P33max*(Trr+Ex+Ti+Th+G+Ts+Ps+Ed+Hp)/90;
```

```
RL31[Ts_?NumberQ,P23_?NumberQ]:=P33*(Trr+Ex+Ti+Th+G+Ts+Ps+Ed+Hp)/90;
```

```
RL3[Ts_?NumberQ]:=(Trr+Ex+Ti+Th+G+Ts+Ps+Ed+Hp)/9;
RL3Full[x_?NumberQ]:=10*x;
```

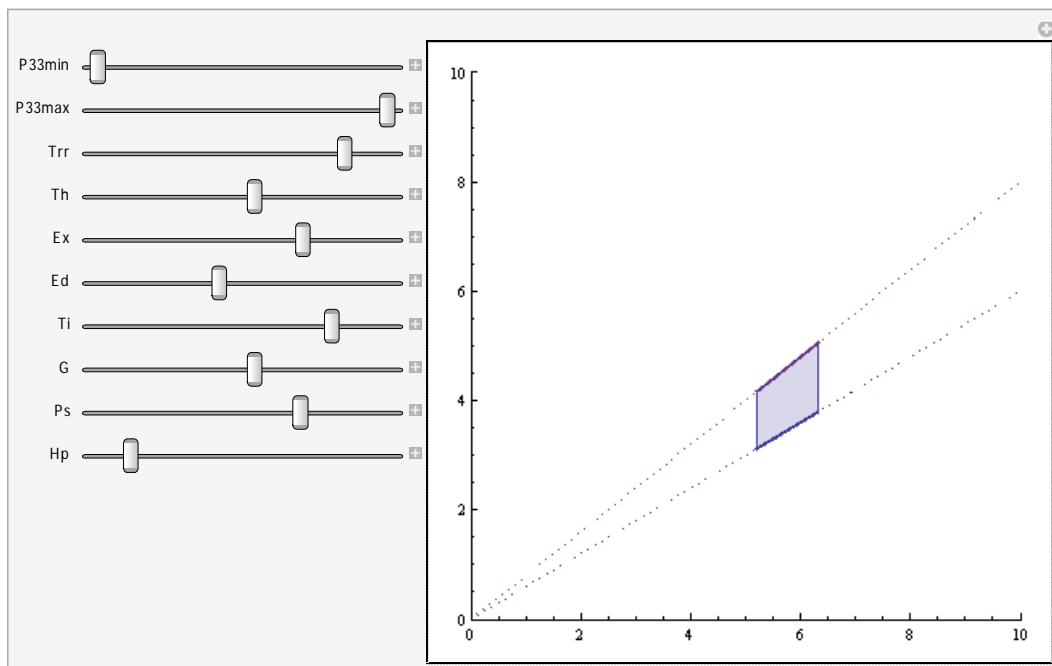
```
plot1=Show[{
```

```
{ParametricPlot[{{RL3Full[x],RL33minFull[x]},{RL3Full[x],RL33maxFull[x]}},{x,0,1},PlotRange->{{0,10},{0,10}},Pl
otStyle->{Dotted,Dotted}]},
```

```
{ParametricPlot[{{RL3[Ts],RL33min[Ts]},{RL3[Ts],RL33max[Ts]}},{Ts,0,10},PlotRange->{{0,10},{0,10}},PlotStyle->{
Thick,Thick}]},
```

```
{ParametricPlot[{{RL3[Ts],RL31[Ts,P33]},{Ts,0,10},{P33,6,8},Mesh->
0,MeshStyle->Orange,PlotRange->{{0,10},{0,10}}]}
}],
```

```
{P33min,6,8},{P33max,P33min,8},{Trr,0,10},{Th,0,10},{Ex,0,10},{Ed,0,10},{Ti,0,10},{G,0,10},{Ps,0,10},{Hp,0,10}]
```



C-2: Pairwise comparison (PWC)

```
Clear[P,Ts,Trr,Th,Ex,Ti,G,Ps,Ed,Hp,RL2,RL2Full,RL12, RL13, RL21, RL22,
RL23,RL21minFull,RL21maxFull,RL21min,RL21max,RL22min,RL22max,RL23min,RL23max,RL24min,RL24max,RL2
1Full,P21min,P21max,P22min,P22max,P23min,P23max,P24min,P24max, P21, P22, P23, P24, RL22, RL23, RL24];
```

```
Manipulate[
```

```
RL21minFull[x_?NumberQ]:=P21min*x;
```

$$RL21_{\max Full}[x_?NumberQ]:=P21_{\max}*x;$$

$$RL21[Ts_?NumberQ,P21_?NumberQ]:=P21*(2.2*Trr+1.9*Ex+1.7*Ti+1.4*Th+1.1*G+0.8*Ts+0.5*Ps+0.3*Ed+0.1*Hp)/100;$$

$$RL21_{\min}[Ts_?NumberQ]:=P21_{\min}*(2.2*Trr+1.9*Ex+1.7*Ti+1.4*Th+1.1*G+0.8*Ts+0.5*Ps+0.3*Ed+0.1*Hp)/100;$$

$$RL21_{\max}[Ts_?NumberQ]:=P21_{\max}*(2.2*Trr+1.9*Ex+1.7*Ti+1.4*Th+1.1*G+0.8*Ts+0.5*Ps+0.3*Ed+0.1*Hp)/100;$$

$$RL22_{\min Full}[x_?NumberQ]:=P22_{\min}*x;$$

$$RL22_{\max Full}[x_?NumberQ]:=P22_{\max}*x;$$

$$RL22[Ts_?NumberQ,P22_?NumberQ]:=P22*(2.2*Trr+1.9*Ex+1.7*Ti+1.4*Th+1.1*G+0.8*Ts+0.5*Ps+0.3*Ed+0.1*Hp)/100;$$

$$RL22_{\min}[Ts_?NumberQ]:=P22_{\min}*(2.2*Trr+1.9*Ex+1.7*Ti+1.4*Th+1.1*G+0.8*Ts+0.5*Ps+0.3*Ed+0.1*Hp)/100;$$

$$RL22_{\max}[Ts_?NumberQ]:=P22_{\max}*(2.2*Trr+1.9*Ex+1.7*Ti+1.4*Th+1.1*G+0.8*Ts+0.5*Ps+0.3*Ed+0.1*Hp)/100;$$

$$RL23_{\min Full}[x_?NumberQ]:=P23_{\min}*x;$$

$$RL23_{\max Full}[x_?NumberQ]:=P23_{\max}*x;$$

$$RL23[Ts_?NumberQ,P23_?NumberQ]:=P23*(2.2*Trr+1.9*Ex+1.7*Ti+1.4*Th+1.1*G+0.8*Ts+0.5*Ps+0.3*Ed+0.1*Hp)/100;$$

$$RL23_{\min}[Ts_?NumberQ]:=P23_{\min}*(2.2*Trr+1.9*Ex+1.7*Ti+1.4*Th+1.1*G+0.8*Ts+0.5*Ps+0.3*Ed+0.1*Hp)/100;$$

$$RL23_{\max}[Ts_?NumberQ]:=P23_{\max}*(2.2*Trr+1.9*Ex+1.7*Ti+1.4*Th+1.1*G+0.8*Ts+0.5*Ps+0.3*Ed+0.1*Hp)/100;$$

$$RL24_{\min Full}[x_?NumberQ]:=P24_{\min}*x;$$

$$RL24_{\max Full}[x_?NumberQ]:=P24_{\max}*x;$$

$$RL24[Ts_?NumberQ,P24_?NumberQ]:=P24*(2.2*Trr+1.9*Ex+1.7*Ti+1.4*Th+1.1*G+0.8*Ts+0.5*Ps+0.3*Ed+0.1*Hp)/100;$$

$$RL24_{\min}[Ts_?NumberQ]:=P24_{\min}*(2.2*Trr+1.9*Ex+1.7*Ti+1.4*Th+1.1*G+0.8*Ts+0.5*Ps+0.3*Ed+0.1*Hp)/100;$$

$$RL24_{\max}[Ts_?NumberQ]:=P24_{\max}*(2.2*Trr+1.9*Ex+1.7*Ti+1.4*Th+1.1*G+0.8*Ts+0.5*Ps+0.3*Ed+0.1*Hp)/100;$$

$$RL2[Ts_?NumberQ]:=(2.2*Trr+1.9*Ex+1.7*Ti+1.4*Th+1.1*G+0.8*Ts+0.5*Ps+0.3*Ed+0.1*Hp)/10;$$

$$RL2_{Full}[x_?NumberQ]:=10*x;$$

plot1=Show[{

{ParametricPlot[{{RL2Full[x],RL21minFull[x]},{RL2Full[x],RL21maxFull[x]}},{x,0,1},PlotRange->{{0,10},{0,10}},PlotStyle->{Dotted,Dotted}],

{ParametricPlot[{{RL2[Ts],RL21min[Ts]},{RL2[Ts],RL21max[Ts]}},{Ts,0,10},PlotRange->{{0,10},{0,10}},PlotStyle->{Thick,Thick}],

{ParametricPlot[{{RL2[Ts],RL21[Ts,P21]},{Ts,0,10},{P21,0,3},Mesh->0,MeshStyle->Orange,PlotRange->{{0,10},{0,10}}],

{ParametricPlot[{{RL2Full[x],RL22minFull[x]},{RL2Full[x],RL22maxFull[x]}},{x,0,1},PlotRange->{{0,10},{0,10}},PlotStyle->{Dotted,Dotted}],

{ParametricPlot[{{RL2[Ts],RL22min[Ts]},{RL2[Ts],RL22max[Ts]}},{Ts,0,10},PlotRange->{{0,10},{0,10}},PlotStyle->{Thick,Thick}],

{ParametricPlot[{{RL2[Ts],RL22[Ts,P22]},{Ts,0,10},{P22,3,6},Mesh->0,MeshStyle->Orange,PlotRange->{{0,10},{0,10}}],

{ParametricPlot[{{RL2Full[x],RL23minFull[x]},{RL2Full[x],RL23maxFull[x]}},{x,0,1},PlotRange->{{0,10},{0,10}},PlotStyle->{Dotted,Dotted}],

{ParametricPlot[{{RL2[Ts],RL23min[Ts]},{RL2[Ts],RL23max[Ts]}},{Ts,0,10},PlotRange->{{0,10},{0,10}},PlotStyle->{Thick,Thick}],

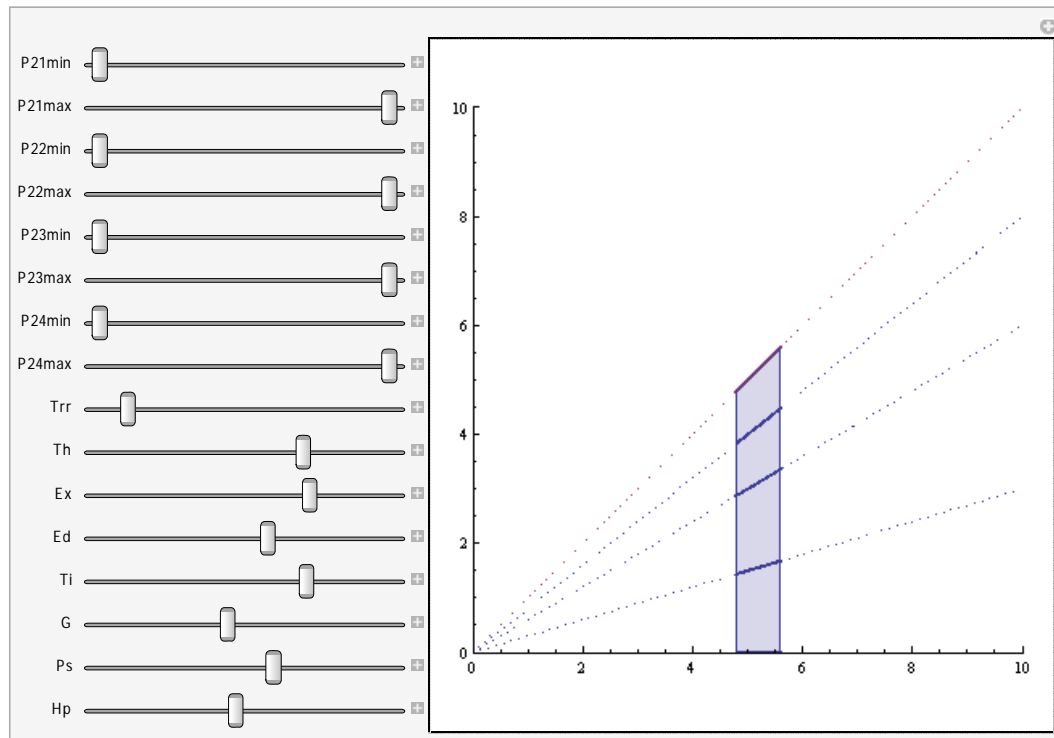
{ParametricPlot[{{RL2[Ts],RL23[Ts,P23]},{Ts,0,10},{P23,6,8},Mesh->0,MeshStyle->Orange,PlotRange->{{0,10},{0,10}}],

```
{ParametricPlot[{{RL2Full[x],RL24minFull[x]},{RL2Full[x],RL24maxFull[x]}},{x,0,1},PlotRange->{{0,10},{0,10}},PlotStyle->{Dotted,Dotted}]},
```

```
{ParametricPlot[{{RL2[Ts],RL24min[Ts]},{RL2[Ts],RL24max[Ts]}},{Ts,0,10},PlotRange->{{0,10},{0,10}},PlotStyle->{Thick,Thick}]},
```

```
{ParametricPlot[{{RL2[Ts],RL24[Ts,P24]},{Ts,0,10},{P24,8,10},Mesh->0,MeshStyle->Orange,PlotRange->{{0,10},{0,10}}}],
```

```
{P21min,0,3},{P21max,P21min,3},{P22min,3,6},{P22max,P22min,6},{P23min,6,8},{P23max,P23min,8},{P24min,8,10},{P24max,P24min,10},{Trr,0,10},{Th,0,10},{Ex,0,10},{Ed,0,10},{Ti,0,10},{G,0,10},{Ps,0,10},{Hp,0,10}}
```



```
Clear[P,Ts,Trr,Th,Ex,Ti,G,Ps,Ed,Hp,RL3,RL3Full,RL12, RL13, RL21, RL22, RL23,RL31minFull,RL31maxFull,RL31min,RL31max,RL32min,RL32max,RL33min,RL33max,RL34min,RL34max,RL31Full,P31min,P31max,P32min,P32max,P33min,P33max,P34min,P34max, P23];
```

```
Manipulate[
```

```
RL23minFull[x_?NumberQ]:=P23min*x;  
RL23maxFull[x_?NumberQ]:=P23max*x;
```

```
RL21[Ts_?NumberQ,P23_?NumberQ]:=P23*(2.2*Trr+1.9*Ex+1.7*Ti+1.4*Th+1.1*G+0.8*Ts+0.5*Ps+0.3*Ed+0.1*Hp)/100;
```

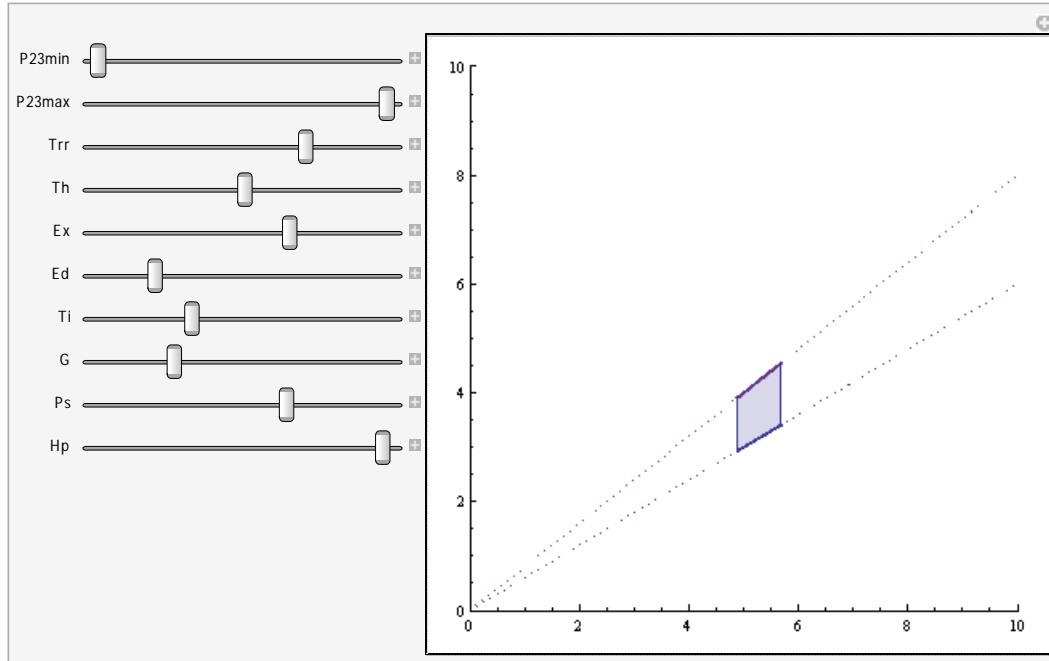
```
RL23min[Ts_?NumberQ]:=P23min*(2.2*Trr+1.9*Ex+1.7*Ti+1.4*Th+1.1*G+0.8*Ts+0.5*Ps+0.3*Ed+0.1*Hp)/100;  
RL23max[Ts_?NumberQ]:=P23max*(2.2*Trr+1.9*Ex+1.7*Ti+1.4*Th+1.1*G+0.8*Ts+0.5*Ps+0.3*Ed+0.1*Hp)/100;
```

```
RL2[Ts_?NumberQ]:=(2.2*Trr+1.9*Ex+1.7*Ti+1.4*Th+1.1*G+0.8*Ts+0.5*Ps+0.3*Ed+0.1*Hp)/10;  
RL2Full[x_?NumberQ]:=10*x;
```

```
plot1=Show[{
```

```
{ParametricPlot[{{RL2Full[x],RL23minFull[x]},{RL2Full[x],RL23maxFull[x]}},{x,0,1},PlotRange->{{0,10},{0,10}},PlotStyle->{Dotted,Dotted}]},
```

```
{ParametricPlot[{{RL2[Ts],RL23min[Ts]},{RL2[Ts],RL23max[Ts]}},{Ts,0,10},PlotRange->{{0,10},{0,10}},PlotStyle->{Thick,Thick}},
{ParametricPlot[{{RL2[Ts],RL21[Ts,P23]},{Ts,0,10}},{P23,6,8},Mesh->0,MeshStyle->Orange,PlotRange->{{0,10},{0,10}}]}],
{P23min,6,8},{P23max,P23min,8},{Trr,0,10},{Th,0,10},{Ex,0,10},{Ed,0,10},{Ti,0,10},{G,0,10},{Ps,0,10},{Hp,0,10}]
```



C-3: Analytic hierarchy processing (AHP)

```
Clear[P,Ts,Trr,Th,Ex,Ti,G,Ps,Ed,Hp,RL11,RL12, RL13, RL21, RL22,
RL23,RL11minFull,RL11maxFull,RL11min,RL11max,RL21Full,P1min,P1max,P1];
P1min=6;
P1max=8;
Manipulate[
RL11minFull[x_?NumberQ]:=P1min*x;
RL11maxFull[x_?NumberQ]:=P1max*x;
RL11min[Ts_?NumberQ]:=P1min*(3.7*Trr+1.9*Ex+1.3*Ti+Th+0.7*G+0.5*Ts+0.4*Ps+0.3*Ed+0.2*Hp)/100;
RL11max[Ts_?NumberQ]:=P1max*(3.7*Trr+1.9*Ex+1.3*Ti+Th+0.7*G+0.5*Ts+0.4*Ps+0.3*Ed+0.2*Hp)/100;
RL11[Ts_?NumberQ,P1_?NumberQ]:=P1*(3.7*Trr+1.9*Ex+1.3*Ti+Th+0.7*G+0.5*Ts+0.4*Ps+0.3*Ed+0.2*Hp)/100;

RL12[Ts_?NumberQ]:=P*(2.2*Trr+1.9*Ex+1.7*Ti+1.4*Th+1.1*G+0.8*Ts+0.5*Ps+0.3*Ed+0.1*Hp)/100;
RL13[Ts_?NumberQ]:=P*(Trr+Ex+Ti+Th+G+Ts+Ps+Ed+Hp)/90;

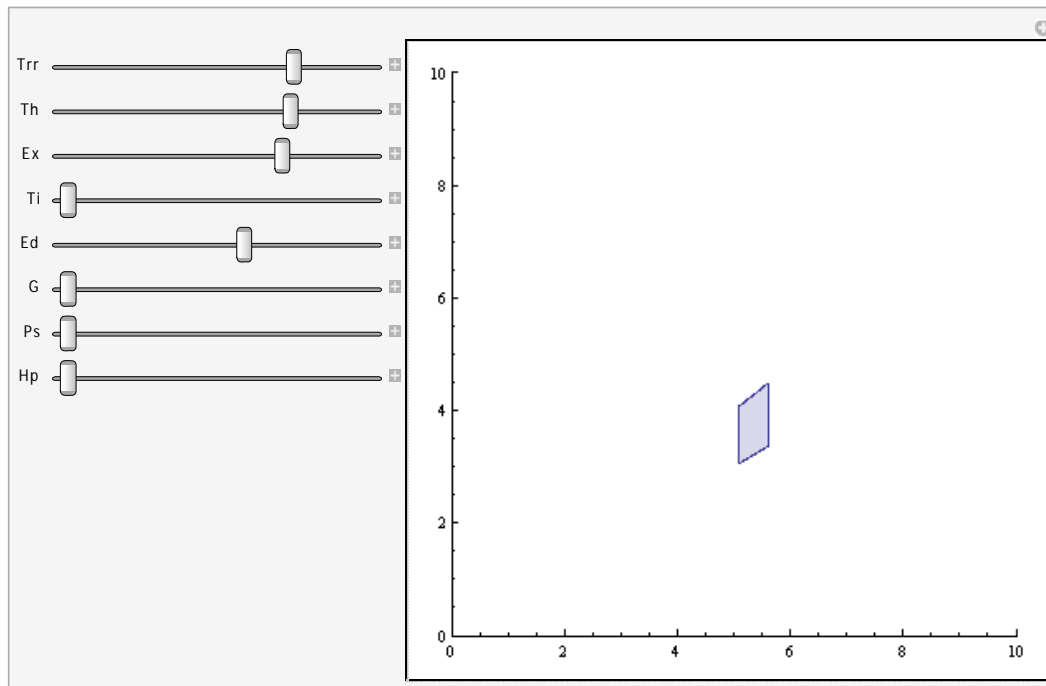
RL21[Ts_?NumberQ]:=(3.7*Trr+1.9*Ex+1.3*Ti+Th+0.7*G+0.5*Ts+0.4*Ps+0.3*Ed+0.2*Hp)/10;
RL21Full[x_?NumberQ]:=10*x;
RL22[Ts_?NumberQ]:=(2.2*Trr+1.9*Ex+1.7*Ti+1.4*Th+1.1*G+0.8*Ts+0.5*Ps+0.3*Ed+0.1*Hp)/10;
RL23[Ts_?NumberQ]:=(Trr+Ex+Ti+Th+G+Ts+Ps+Ed+Hp)/9;

plot1=Show[

{ParametricPlot[{{RL21Full[x],RL11minFull[x]},{RL21Full[x],RL11maxFull[x]}},{x,0,1},PlotRange->{{0,10},{0,10}},
PlotStyle->{Dotted,Dotted}}],

{ParametricPlot[{{RL21[Ts],RL11min[Ts]},{RL21[Ts],RL11max[Ts]}},{Ts,0,10},PlotRange->{{0,10},{0,10}},PlotStyle
->{Thick,Thick}},
{ParametricPlot[{{RL21[Ts],RL11[Ts,P1]},{Ts,0,10}},{P1,6,8},Mesh->0,MeshStyle->Orange,PlotRange->{{0,10},{0,10}}]}],
}],
```

{Trr,0,10},{Th,0,10},{Ex,0,10},{Ti,0,10},{Ed,0,10},{G,0,10},{Ps,0,10},{Hp,0,10}]



```
Clear[P,Ts,Trr,Th,Ex,Ti,G,Ps,Ed,Hp,RL11,RL12, RL13, RL21, RL22,
RL23,RL11minFull,RL11maxFull,RL11min,RL11max,RL12min,RL12max,RL13min,RL13max,RL14min,RL14max,RL2
1Full,P11min,P11max,P12min,P12max,P13min,P13max,P14min,P14max];
```

Manipulate[

```
RL11minFull[x_?NumberQ]:=P11min*x;
RL11maxFull[x_?NumberQ]:=P11max*x;
```

```
RL11min[Ts_?NumberQ]:=P11min*(3.7*Trr+1.9*Ex+1.3*Ti+Th+0.7*G+0.5*Ts+0.4*Ps+0.3*Ed+0.2*Hp)/100;
RL11max[Ts_?NumberQ]:=P11max*(3.7*Trr+1.9*Ex+1.3*Ti+Th+0.7*G+0.5*Ts+0.4*Ps+0.3*Ed+0.2*Hp)/100;
```

```
RL12minFull[x_?NumberQ]:=P12min*x;
RL12maxFull[x_?NumberQ]:=P12max*x;
```

```
RL12min[Ts_?NumberQ]:=P12min*(3.7*Trr+1.9*Ex+1.3*Ti+Th+0.7*G+0.5*Ts+0.4*Ps+0.3*Ed+0.2*Hp)/100;
RL12max[Ts_?NumberQ]:=P12max*(3.7*Trr+1.9*Ex+1.3*Ti+Th+0.7*G+0.5*Ts+0.4*Ps+0.3*Ed+0.2*Hp)/100;
```

```
RL13minFull[x_?NumberQ]:=P13min*x;
RL13maxFull[x_?NumberQ]:=P13max*x;
```

```
RL13min[Ts_?NumberQ]:=P13min*(3.7*Trr+1.9*Ex+1.3*Ti+Th+0.7*G+0.5*Ts+0.4*Ps+0.3*Ed+0.2*Hp)/100;
RL13max[Ts_?NumberQ]:=P13max*(3.7*Trr+1.9*Ex+1.3*Ti+Th+0.7*G+0.5*Ts+0.4*Ps+0.3*Ed+0.2*Hp)/100;
```

```
RL14minFull[x_?NumberQ]:=P14min*x;
RL14maxFull[x_?NumberQ]:=P14max*x;
```

```
RL14min[Ts_?NumberQ]:=P14min*(3.7*Trr+1.9*Ex+1.3*Ti+Th+0.7*G+0.5*Ts+0.4*Ps+0.3*Ed+0.2*Hp)/100;
RL14max[Ts_?NumberQ]:=P14max*(3.7*Trr+1.9*Ex+1.3*Ti+Th+0.7*G+0.5*Ts+0.4*Ps+0.3*Ed+0.2*Hp)/100;
```

```
RL1[Ts_?NumberQ]:=(3.7*Trr+1.9*Ex+1.3*Ti+Th+0.7*G+0.5*Ts+0.4*Ps+0.3*Ed+0.2*Hp)/10;
RL1Full[x_?NumberQ]:=10*x;
```

```
plot1=Show[{
```

```
{ParametricPlot[{{RL1Full[x],RL11minFull[x]},{RL1Full[x],RL11maxFull[x]}},{x,0,1},PlotRange->{{0,10},{0,10}},Plot
tStyle->{Dotted,Dotted}],
```

```
{ParametricPlot[{{RL1[Ts],RL11min[Ts]},{RL1[Ts],RL11max[Ts]}},{Ts,0,10},PlotRange->{{0,10},{0,10}},PlotStyle->{
Thick,Thick}],
```

```
{ParametricPlot[{{RL1Full[x],RL12minFull[x]},{RL1Full[x],RL12maxFull[x]}},{x,0,1},PlotRange->{{0,10},{0,10}},PlotStyle->{Dotted,Dotted}]},
```

```
{ParametricPlot[{{RL1[Ts],RL12min[Ts]},{RL1[Ts],RL12max[Ts]}},{Ts,0,10},PlotRange->{{0,10},{0,10}},PlotStyle->{Thick,Thick}]},
```

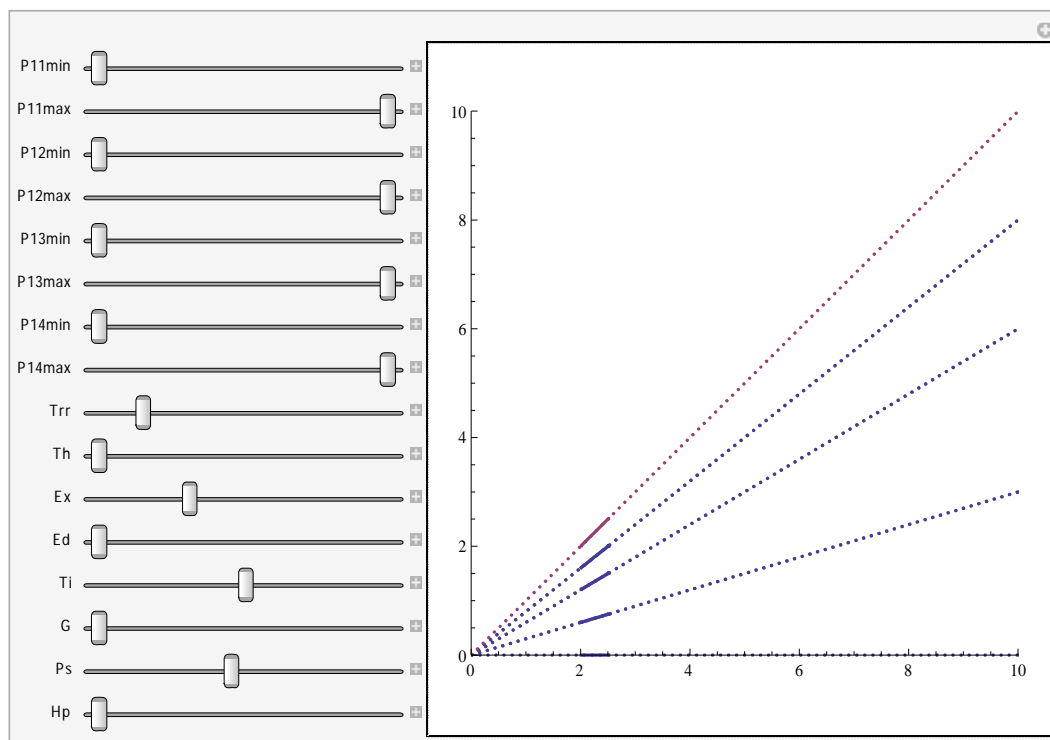
```
{ParametricPlot[{{RL1Full[x],RL13minFull[x]},{RL1Full[x],RL13maxFull[x]}},{x,0,1},PlotRange->{{0,10},{0,10}},PlotStyle->{Dotted,Dotted}]},
```

```
{ParametricPlot[{{RL1[Ts],RL13min[Ts]},{RL1[Ts],RL13max[Ts]}},{Ts,0,10},PlotRange->{{0,10},{0,10}},PlotStyle->{Thick,Thick}]},
```

```
{ParametricPlot[{{RL1Full[x],RL14minFull[x]},{RL1Full[x],RL14maxFull[x]}},{x,0,1},PlotRange->{{0,10},{0,10}},PlotStyle->{Dotted,Dotted}]},
```

```
{ParametricPlot[{{RL1[Ts],RL14min[Ts]},{RL1[Ts],RL14max[Ts]}},{Ts,0,10},PlotRange->{{0,10},{0,10}},PlotStyle->{Thick,Thick}]},
}],
```

```
{P11min,0,3},{P11max,P11min,3},{P12min,3,6},{P12max,P12min,6},{P13min,6,8},{P13max,P13min,8},{P14min,8,10},
{P14max,P14min,10},{Trr,0,10},{Th,0,10},{Ex,0,10},{Ed,0,10},{Ti,0,10},{G,0,10},{Ps,0,10},{Hp,0,10}}
```



```
Clear[P,Ts,Trr,Th,Ex,Ti,G,Ps,Ed,Hp,RL11,RL12,RL13,RL21,RL22,
RL23,RL11minFull,RL11maxFull,RL11min,RL11max,RL21Full,P13min,P13max,P1];
P13min=6;
P13max=8;
Manipulate[
RL11minFull[x_?NumberQ]:=P13min*x;
RL11maxFull[x_?NumberQ]:=P13max*x;
RL11min[Ts_?NumberQ]:=P1min*(3.7*Trr+1.9*Ex+1.3*Ti+Th+0.7*G+0.5*Ts+0.4*Ps+0.3*Ed+0.2*Hp)/100;
RL11max[Ts_?NumberQ]:=P1max*(3.7*Trr+1.9*Ex+1.3*Ti+Th+0.7*G+0.5*Ts+0.4*Ps+0.3*Ed+0.2*Hp)/100;

RL11[Ts_?NumberQ,P1_?NumberQ]:=P1*(3.7*Trr+1.9*Ex+1.3*Ti+Th+0.7*G+0.5*Ts+0.4*Ps+0.3*Ed+0.2*Hp)/100;

RL12[Ts_?NumberQ]:=P*(2.2*Trr+1.9*Ex+1.7*Ti+1.4*Th+1.1*G+0.8*Ts+0.5*Ps+0.3*Ed+0.1*Hp)/100;
RL13[Ts_?NumberQ]:=P*(Trr+Ex+Dip+Ti+Th+G+Ts+Ps+Hp)/90;
```



```

RL21[Ts_?NumberQ]:=(3.7*Trr+1.9*Ex+1.3*Ti+Th+0.7*G+0.5*Ts+0.4*Ps+0.3*Ed+0.2*Hp)/10;
RL21Full[x_?NumberQ]:=10*x;
RL22[Ts_?NumberQ]:=(2.2*Trr+1.9*Ex+1.7*Ti+1.4*Th+1.1*G+0.8*Ts+0.5*Ps+0.3*Ed+0.1*Hp)/10;
RL23[Ts_?NumberQ]:=(Trr+Ex+Ti+Th+G+Ts+Ps+Ed+Hp)/9;

```

```
plot1=Show[
```

```
{ParametricPlot[{ {RL21Full[x],RL11minFull[x]},{RL21Full[x],RL11maxFull[x]}},{x,0,1},PlotRange->{{0,10},{0,10}},
PlotStyle->{Dotted,Dotted}]},
```

```
{ParametricPlot[{ {RL21[Ts],RL11min[Ts]},{RL21[Ts],RL11max[Ts]}},{Ts,0,10},PlotRange->{{0,10},{0,10}},PlotStyle
->{Thick,Thick}]},
```

```
{ParametricPlot[{RL21[Ts],RL11[Ts,P1]},{Ts,0,10},{P1,6,8},Mesh->
0,MeshStyle->Orange,PlotRange->{{0,10},{0,10}}]
}],
```

```
{Trr,0,10},{Th,0,10},{Ex,0,10},{Ed,0,10},{Ti,0,10},{G,0,10},{Ps,0,10},{Hp,0,10}]
```

